



**The epigenetic differences between  
neurofibromas and malignant peripheral nerve  
sheath tumours**

A thesis submitted to the University College London (UCL) for the  
degree of  
Doctor of Philosophy

*By*

*Tarek Abdelaziz Hasan Shemais*

*April 2015*

I, Tarek A. H. Shemais, confirm that the work presented in this thesis is my own. Where information has been derived from other sources, I confirm that this has been indicated in the thesis.

*Tarek A. H. Shemais*

*April 2015*

## Abstract

Malignant peripheral nerve sheath tumours (MPNSTs) are rare soft tissue sarcomas, which can arise *de novo* in a peripheral nerve or from a neurofibroma. The molecular mechanisms leading to progression of neurofibroma to MPNST remain largely unknown.

In this thesis, I examined the role played by microRNAs (miRNAs) in the pathogenesis of MPNSTs from neurofibromas. I analysed miRNA microarray expression profiles from 10 MPNSTs and 10 neurofibromas and identified sixteen differentially expressed miRNAs; fourteen were downregulated and two upregulated in MPNSTs. One of these, miR-29c, was confirmed as downregulated in MPNSTs by qRT-PCR. Its expression was also shown to be relatively low in other sarcomas and low-grade tumours. *In vitro* functional studies revealed miR-29c inhibits cell migration following its ectopic expression in MPNST-derived sNF96.2 cells.

Using *in silico* prediction analyses, I identified extracellular matrix (ECM) genes *COL1A1*, *COL1A2*, *COL4A1*, *COL4A2*, *COL5A2*, *COL21A1* and *MMP2* as well as *TGFB3* and DNA methyltransferases *DNMT3A* and *DNMT3B* as potential targets of miR-29c. I demonstrated direct inhibition of these genes and partial inhibition of MMP9 via an indirect mechanism in miR-29c-transfected sNF96.2 cells. *DNMT3B* mRNA expression was higher in MPNSTs vs neurofibromas and inversely correlated with miR-29c expression.

Using previous methylome and microarray data, I identified *CDKN2A*, *WT1*, and *S100B* as possible targets for epigenetic regulation in MPNSTs. I demonstrated hypermethylation of these genes' regulatory regions in MPNSTs by pyrosequencing and, in a larger cohort of 80 MPNSTs and 80 neurofibromas archival samples, I revealed increased levels of *WT1* and *S100B* gene methylation in high-grade MPNSTs compared to low-grade MPNSTs and neurofibromas. *S100B* protein expression by immunohistochemistry was also shown to be downregulated in MPNSTs compared to neurofibromas and its expression inversely correlated with *S100B* gene methylation. Furthermore, introduction of *S100B* cDNA using an adenoviral expression vector resulted in reduced proliferation of sNF96.2 cells.

My results suggest miR-29c may function as a tumour suppressor in MPNSTs by targeting ECM genes as well as DNA methyltransferases and *TGFB3*. *S100B* was also identified as a potential tumour suppressor whose expression is epigenetically regulated in MPNSTs. These findings lead to a better understanding of MPNST pathogenesis and identify *S100B* and miR-29c as potential targets for future intervention in MPNST patients.

## Acknowledgments

I would like to thank my supervisor Professor Adrienne Flanagan for her kind supervision and guidance throughout this project. She provided me with invaluable guidance and inspiration. I am indebted to her for her time and patience. Without her guidance, I would never have got to the end.

I would like to thank Professor Stephan Beck, my second supervisor for his guidance and academic support through my project.

I am extremely grateful and forever indebted to Dr Nick Henriquez for his patience and time, thank you for showing me the joy in scientific endeavour.

I am extremely grateful and indebted to Dr Rajai Al-Jehani for all her valuable scientific advice and critical appraisal of the manuscript as well as her sincere guidance and encouragement.

I would like to show my deep thanks to Dr Nischalan Pillay and who generously helped me and provided a lot of support. I would also like to thank Dr Andy Feber, Dr Nadège Presneau, Dr Malihe Eskandarpour, and Mr Fitim Berisha for their endless help throughout the entire project.

Many thanks to Mr Rakesh Chandar-Nair who have provided valuable advices and moral support.

Last but not least, thank you to Nesrin, my wife, for her help, inspiration and support.

## **Publications**

**(Resulting in part from the work presented in this thesis)**

- 1- MicroRNA profiling of peripheral nerve sheath tumours identifies miR-29c as a tumour suppressor gene involved in tumour progression. N Presneau, M Eskandarpour, T Shemais, S Henderson, D Halai, R Tirabosco and A M Flanagan. *British Journal of Cancer* (2013) 108, 964–972.
- 2- S100B is regulated by DNA methylation in peripheral nerve sheath tumours (in preparation).

---

## Table of contents

Abstract.....	3
Acknowledgments.....	5
Publications.....	6
Table of contents .....	7
List of figures.....	16
List of tables.....	22
List of abbreviations .....	24
1. Introduction .....	28
1.1. Neurofibromatosis Type 1.....	28
1.1.1. History of Neurofibromatosis Type 1 .....	29
1.1.2. Clinical diagnosis of Neurofibromatosis type 1.....	30
1.1.3. Genetics of Neurofibromatosis type 1 .....	33
1.1.4. Other RAS/MAPK pathway dysregulation (RASopathies).....	37
1.2. Pathology of Neurofibroma .....	40
1.2.1. Gross pathology of neurofibromas .....	41
1.2.2. Microscopy of neurofibromas .....	44

---

1.3.	Malignant Peripheral Nerve Sheath Tumours.....	46
1.3.1.	Grading of MPNST.....	47
1.3.2.	Diagnosis and management of MPNST.....	48
1.3.3.	Pathology of Malignant Peripheral Nerve Sheath Tumours ..	51
1.4.	S100B as a marker of nerve sheath tumours .....	56
1.5.	Management of neurofibromatosis type 1 .....	58
1.5.1.	Neurofibroma variants and likelihood of malignant transformation .....	58
1.5.2.	Neurological problems .....	59
1.5.3.	Cognitive problems and behavioural difficulties .....	61
1.5.4.	Optic pathway gliomas.....	61
1.5.5.	Orthopaedic problems.....	62
1.5.6.	Cardiovascular abnormalities in neurofibromatosis type 1 ....	62
1.5.7.	Glomus tumours.....	63
1.6.	Malignant transformation of neurofibroma to MPNST.....	64
1.6.1.	Genetic mechanisms .....	64
1.6.2.	Epigenetic mechanisms .....	68
1.7.	Aims .....	83

---

2.	Materials and methods.....	84
2.1.	Clinical samples.....	84
2.2.	Cell Lines.....	91
2.2.1.	MPNST-derived cell line sNF96.2.....	91
2.2.1.	Other cell lines.....	91
2.3.	RNA extraction from frozen cells sections and cell lines.....	92
2.3.1.	MiRNeasy Mini Kit (Qiagen).....	92
2.4.	cDNA synthesis.....	94
2.5.	Quantitative Reverse Transcription polymerase chain reaction (qRT-PCR).....	96
2.5.1.	Quantitative PCR with double-stranded DNA-binding dyes as reporters (SYBR Green assay) to test gene expression.....	96
2.5.2.	Fluorescent reporter probe methods (Quantitation of microRNA by TaqMan assay).....	99
2.6.	Cell culture.....	100
2.6.1.	Thawing cells from liquid nitrogen.....	100
2.6.2.	Cell maintenance.....	100
2.6.3.	Cell trypsinisation.....	101

---

2.6.4.	Freezing cells in liquid nitrogen.....	101
2.6.5.	Trypan blue cell viability assay.....	101
2.6.6.	Live cell imaging using IncuCyte (Growth curve) .....	102
2.6.7.	MTS cell viability assay.....	103
2.6.8.	Cell migration analysis .....	104
2.7.	MiRNA microarray expression profiling .....	105
2.7.1.	Sample preparation.....	105
2.7.2.	miRNA microarray hybridization and scanning .....	107
2.7.3.	miRNA microarray data analysis.....	107
2.8.	MicroRNA mimics transfection of sNF96.2 cells .....	108
2.9.	DNA methylation detection .....	109
2.9.1.	Genomic DNA extraction.....	109
2.9.2.	Bisulphite treatment of DNA.....	112
2.9.3.	PCR and pyrosequencing of bisulphite treated and control samples .....	113
2.10.	5-aza-2'-deoxycytidine treatment of sNF96.2 MPNST cells.....	116
2.11.	Protein isolation and Western blot analysis .....	117
2.12.	Gelatin Zymography .....	118

---

2.13.	Sequencing of <i>NF1</i> gene .....	119
2.14.	Immunohistochemistry (IHC) .....	120
2.14.1.	Slide staining.....	120
2.14.2.	Immunohistochemistry scoring.....	120
2.15.	<i>S100B</i> expression cloning .....	122
2.15.1.	PCR cloning strategy .....	122
2.15.2.	Restriction enzyme digestion .....	127
2.15.3.	Plasmid Ligation.....	128
2.15.4.	Bacterial transformation .....	129
2.15.5.	Plasmid purification.....	130
2.15.6.	Agarose gel electrophoresis.....	132
2.15.7.	DNA extraction from agarose gel .....	133
2.15.8.	Lentivirus production .....	134
2.15.9.	Lentivirus titration.....	135
2.15.10.	Infection of sNF96.2 cells with Lentivirus .....	136
2.16.	Statistical analysis .....	137
3.	Role of miR-29c in the progression of neurofibroma to MPNST.....	138

---

3.1.	Introduction.....	138
3.2.	Aims .....	141
3.3.	Results.....	142
3.3.1.	miRNA microarrays demonstrate down-regulation of miR-29 family in MPNSTs versus neurofibromas .....	142
3.3.2.	Confirmation of decreased miR-29c expression in MPNSTs versus neurofibromas by qRT-PCR .....	145
3.3.3.	<i>NF1</i> mRNA expressed at low levels in MPNSTs and neurofibromas .....	146
3.3.4.	miR-29c expression in different types of sarcomas and low-grade tumours .....	149
3.3.5.	<i>In vitro</i> studies on the MPNST- derived sNF96.2 cell line ...	151
3.3.6.	<i>In silico</i> prediction of miR-29c targets implicated in migration... ..	159
3.3.7.	miR-29c targets collagen matrix genes .....	163
3.3.8.	miR-29c directly influenced MMP2 but indirectly inhibits MMP9 activity .....	165
3.3.9.	miR-29c partially inhibits MMP9 activity through influencing <i>TGFB3</i> .....	167

---

3.3.10.	Suppression of <i>ROBO1</i> expression by miR-29c .....	172
3.4.	Summary of results.....	175
4.	Relationship between miR-29c and DNMT3A and 3B.....	178
4.1.	Introduction.....	178
4.2.	Aims .....	180
4.3.	Results.....	181
4.3.1.	<i>DNMT3B</i> mRNA expression is higher in MPNSTs compared to neurofibromas and inversely correlates with miR-29c expression.....	181
4.3.2.	miR-29c inhibits <i>DNMT3A</i> and <i>DNMT3B</i> expression in sNF96.2 cells .....	187
4.3.3.	Identification of candidate genes that may be targets for DNMTs in MPNSTs and Neurofibromas.....	189
4.3.4.	Hypermethylation of <i>CDKN2A</i> , <i>WT1</i> and <i>S100B</i> is frequent in MPNSTs compared to neurofibromas in human samples .....	192
4.3.5.	Increased expression of <i>WT1</i> and <i>S100B</i> in 5-aza-dC-treated sNF96.2 cells .....	201
4.3.6.	<i>S100B</i> and <i>WT1</i> DNA methylation is frequent in high grade MPNST as compared with low grade MPNST and Neurofibromas ....	206
4.4.	Summary of Results .....	217

---

5. Analysis of <i>S100B</i> and <i>WT1</i> candidates as potential tumour regulators in nerve sheath tumours .....	219
5.1. Introduction.....	219
5.2. Aims .....	222
5.3. Results.....	223
5.3.1. <i>S100B</i> mRNA expression is low in MPNST compared to neurofibromas and inversely correlated with DNA methylation. ....	223
5.3.2. <i>S100</i> IHC staining inversely correlates with CpG methylation ..	229
5.3.3. Cloning of <i>S100B</i> into lentivirus expression vector .....	235
5.3.1. Re-expression of <i>S100B</i> in sNF96.2 MPNST cells causes reduced cell proliferation .....	238
5.3.2. <i>S100B</i> gene methylation unaltered by miR-29c expression in sNF96.2 cells .....	244
5.4. Summary of results.....	246
6. Discussion.....	248
6.1. Role of miR-29c in the progression of neurofibroma to MPNST	248
6.2. Relationship between miR-29c and DNA methyltransferases 3A and 3B .....	261

6.3.	S100B as a potential tumour regulator in nerve sheath tumours	275
7.	Future work .....	283
8.	Reference list .....	285

---

## List of figures

Figure 1-1: Multiple benign neurofibromas.....	31
Figure 1-2: Café au lait macules .....	32
Figure 1-3: Iris Lisch nodules.....	32
Figure 1-4: Loss of NF1 expression leads to activation of RAS, dysregulation of cell growth and tumourigenesis.....	34
Figure 1-5: Localised neurofibroma, macroscopic .....	41
Figure 1-6: Diffuse neurofibroma, macroscopic .....	42
Figure 1-7: Plexiform neurofibroma, macroscopic.....	43
Figure 1-8: Classic neurofibroma histology.....	45
Figure 1-9: Atypical neurofibroma histology .....	45
Figure 1-10: Malignant Peripheral Nerve Sheath Tumour, macroscopic.....	51
Figure 1-11: Malignant Peripheral Nerve Sheath Tumour.....	52
Figure 1-12: Triton tumour .....	53
Figure 1-13: Glandular MPNST.....	54
Figure 1-14: Epithelioid MPNST.....	55
Figure 2-1: pENTR 4 dual selection entry vector map .....	125
Figure 2-2: pLenti PGK PuroDEST destination vector map .....	126

---

Figure 3-1: miRNA expression profiling of neurofibromas and MPNSTs by microarray analysis .....	144
Figure 3-2: Downregulation of miR-29c expression in MPNSTs compared to neurofibromas demonstrated by qRT-PCR.....	146
Figure 3-3: Low levels of <i>NF1</i> mRNA expression in neurofibromas and MPNSTs .....	148
Figure 3-4: miR-29c expression in neurofibromas and MPNSTs compared with other sarcomas and low-grade tumours. ....	150
Figure 3-5: Single nucleotide deletion in the <i>NF1</i> gene of sNF96.2.....	152
Figure 3-6: Increased miR-29c expression following transfection of sNF96.2 cells.....	154
Figure 3-7: sNF96.2 Cell proliferation following miR-29c transfection.....	156
Figure 3-8: miR-29c transfection inhibits sNF96.2 cell migration .....	158
Figure 3-9: Extracellular matrix genes are highly expressed in MPNSTs compared to neurofibromas .....	162
Figure 3-10: Down-regulation of collagen gene expression in miR-29c transfected sNF96.2 cells .....	164
Figure 3-11: MMP2 and MMP9 activity & expression in miR-29c transfected sNF96.2 cells .....	167
Figure 3-12: Downregulation of <i>TGFB3</i> mRNA is induced by miR-29c.....	169

---

Figure 3-13: Down-regulation of <i>TGFB3</i> mRNA expression partially inhibits MMP9 and MMP2 activity .....	171
Figure 3-14: Downregulation of <i>ROBO1</i> expression following transfection of sNF96.2 cells with miR-29c .....	174
Figure 4-1: No significant difference in <i>DNMT3A</i> mRNA expression between MPNSTs and neurofibromas.....	183
Figure 4-2: <i>DNMT3B</i> mRNA expression is significantly higher in the MPNSTs compared neurofibromas .....	184
Figure 4-3: No correlation between miR-29c and <i>DNMT3A</i> mRNA expression in MPNSTs and neurofibromas .....	185
Figure 4-4: Inverse correlation between miR-29c and <i>DNMT3B</i> expression in MPNSTs and neurofibromas.....	186
Figure 4-5: Down-regulation of <i>DNMT3A</i> and <i>DNMT3B</i> mRNA expression in miR-29c-transfected sNF96.2 cells .....	189
Figure 4-6: <i>CDKN2A</i> gene as depicted by ensemble showing location of the regulatory feature area (transcription factor binding site), which was examined by pyrosequencing. The zoom box shows the DNA sequence within this area and location of the 7 CpG sites which are highlighted in red. ....	193
Figure 4-7: <i>WT1</i> gene as depicted by ensemble showing location of the regulatory feature area (open chromatin), which was examined by	

---

pyrosequencing. The zoom box shows the DNA sequence within this area and location of the 5 CpG sites which are highlighted in red. ....	194
Figure 4-8: <i>S100B</i> gene as depicted by ensemble showing location of the regulatory feature area (enhancer), which was examined by pyrosequencing. The zoom box shows the DNA sequence within this area and location of the 6 CpG sites which are highlighted in red.....	195
Figure 4-9: Methylation analysis of <i>CDKN2A</i> in Neurofibromas and MPNSTs .....	197
Figure 4-10: Methylation analysis of <i>WT1</i> in Neurofibromas and MPNSTs	198
Figure 4-11: Methylation analysis of <i>S100B</i> in Neurofibromas and MPNSTs .....	199
Figure 4-12: Decreased <i>S100B</i> gene methylation in 5-aza-dC-treated sNF96.2 cells .....	203
Figure 4-13: Increased expression of <i>WT1</i> and <i>S100B</i> mRNA in 5-aza-dC treated sNF96.2 cells .....	206
Figure 4-14: Hypermethylation of <i>S100B</i> in MPNSTs vs Neurofibromas ...	210
Figure 4-15: Hypermethylation of <i>WT1</i> in MPNSTs vs Neurofibromas .....	212
Figure 4-16: Hypermethylation of <i>S100B</i> with increasing grade of MPNST	214
Figure 4-17: Hypermethylation of <i>WT1</i> with increasing grade of MPNST ..	216

---

Figure 5-1: <i>WT1</i> mRNA expression shows no significant difference between MPNSTs and neurofibromas.....	225
Figure 5-2: <i>WT1</i> mRNA expression does not correlate with the level of <i>WT1</i> gene methylation.....	226
Figure 5-3: <i>S100B</i> mRNA expression is significantly lower in MPNSTs compared to neurofibromas .....	227
Figure 5-4: <i>S100B</i> mRNA expression inversely correlates with level of <i>S100B</i> gene methylation.....	228
Figure 5-5: <i>S100B</i> gene methylation level versus protein expression pattern in NFs and MPNSTs .....	232
Figure 5-6: <i>S100B</i> protein expression inversely correlates with level of <i>S100B</i> gene methylation.....	233
Figure 5-7: <i>S100B</i> protein expression in MPNSTs and NFs .....	234
Figure 5-8: <i>S100B</i> mRNA & protein expression following transduction of sNF96.2 cells with <i>S100B</i> expression vector .....	237
Figure 5-9: Incucyte imaging of lentivirus transduced sNF96.2 cells .....	239
Figure 5-10: Decreased proliferation of <i>S100B</i> expressing sNF96.2 cells .	240
Figure 5-11: Decreased viability of <i>S100B</i> expressing sNF96.2 cells .....	241
Figure 5-12: Cell motility rate unaltered in <i>S100B</i> expressing sNF96.2 cells .....	243

Figure 5-13: *S100B* gene methylation unaltered by miR-29c expression in  
sNF96.2 cells ..... 245

## List of tables

Table 1-1: National Institutes of Health diagnostic criteria of neurofibromatosis type 1 .....	30
Table 2-1: Neurofibroma (fresh frozen).....	86
Table 2-2: MPNST (fresh frozen) .....	86
Table 2-3: Archival neurofibromas (continued on next page).....	87
Table 2-4: Archival MPNSTs (continued on next page) .....	89
Table 2-5: List of primer sequences used for direct sequencing <i>NF1</i> gene .	91
Table 2-6: List of primer sequences used for qRT-PCR .....	98
Table 2-7: List of primer sequences used for pyrosequencing.....	115
Table 2-8: List of primers sequences used for Lentiviral titration .....	136
Table 3-1: Gene ontology analysis for miR-29c predicted target genes identified extracellular matrix genes as the top category. ....	160
Table 3-2: Description of selected predicted target genes relevant to migration and invasion in three different <i>in silico</i> databases (TargetScan, PicTar, and MiRanda) .....	161
Table 4-1: Genes which are differentially methylated and differentially expressed in MPNSTs compared to neurofibromas.....	191

---

Table 4-2: Hypermethylation of <i>CDKN2A</i> , <i>WT1</i> , and <i>S100B</i> in MPNSTs vs Neurofibromas .....	200
Table 4-3: <i>S100B</i> DNA methylation is significantly higher in MPNSTs compared to neurofibromas .....	209
Table 4-4: <i>WT1</i> gene methylation level is significantly higher in MPNSTs compared to neurofibromas .....	211
Table 4-5: <i>S100B</i> is significantly hypermethylated in high grade MPNSTs compared to lower grades .....	213
Table 4-6: <i>WT1</i> is significantly hypermethylated in high grade MPNSTs compared to lower grades .....	215
Table 5-1: <i>S100B</i> gene methylation level and protein staining score in Neurofibromas and MPNSTs .....	231

## List of abbreviations

5-aza-dC	5-aza-2'deoxyctidine
A	Adenine
AKT	V-akt murine thymoma viral oncogene homolog 1
AML	Acute myeloid leukaemia
ATP	Adenosine triphosphate
BCL2	B-Cell CLL/Lymphoma 2 protein family
bp	Base pair
BSA	Bovine serum albumin
C	Cytosine
CALMs	Café au lait macules
cAMP	Cyclic adenosine monophosphate
CBL	Cbl proto-oncogene, E3 ubiquitin protein ligase
CDH1	Cadherin 1, type 1
CDK4	Cyclin-dependent kinase 4
CDKN2A	Cyclin-dependent kinase inhibitor 2A
cDNA	Complementary DNA
CEACAM6	Carcinoembryonic antigen-related cell adhesion molecule 6
CGI	Cytosine Guanine (linear dinucleotide) islands
CO <sub>2</sub>	Carbon dioxide
COL1A1	Collagen, type I, alpha 1
COL1A2	Collagen, type I, alpha 2
COL21A1	Collagen, type XXI, alpha 1
COL4A1	Collagen, type IV, alpha 1
COL4A2	Collagen, type IV, alpha 2
COL5A2	Collagen, type V, alpha 2
CpG	Cytosine Guanine (linear dinucleotide)
CST6	Cystatin 6
Ct	Threshold cycle
CXCL12	Chemokine (C-X-C motif) ligand 12
CXCR4	Chemokine (C-X-C motif) receptor 4
d	Day
dCt	Delta threshold cycle
ddH <sub>2</sub> O	Double distilled water
DMEM	Dulbecco's modified Eagle medium
DMSO	Dimethylsulfoxide
DNA	Deoxyribonucleic acid
DNase	Deoxyribonuclease
DNMT1	DNA (cytosine-5-)-methyltransferase 1
DNMT3A	DNA (cytosine-5-)-methyltransferase 3 alpha
DNMT3B	DNA (cytosine-5-)-methyltransferase 3 beta
Dnmt3L	DNA (cytosine-5-)-methyltransferase 3-like
dNTP	Deoxyribonucleotide triphosphate
E2F7	E2F transcription factor 7
E2F8	E2F transcription factor 8
ECG	Electrocardiography
ECM	Extracellular matrix
EDTA	Ethylenediamine tetraacetic acid
EED	Polycomb protein EED
EFNA3	Ephrin-A3
EGF	Epidermal growth factor
EGFR	Epidermal growth factor receptor

---

EMT	Epithelial-mesenchymal transition
ERK	Extracellular signal-regulated kinase
ESR1	Estrogen receptor 1
EV	Empty vector
EVI2A	Ecotropic viral integration site 2A
EVI2B	Ecotropic viral integration site 2B
FBS	Foetal bovine serum
FISH	Fluorescent in situ hybridisation
FNCLCC	French Federation of Cancer Centres
Foxr2	Fork head box R2
G	Guanine
GAPDH	Glyceraldehyde 3-phosphate dehydrogenase
GDP	Guanosine diphosphate
GEM	Gene expression microarray
GNA11	Guanine nucleotide binding protein , alpha 11
GPCR	G protein-coupled receptor
GRb2	Growth factor receptor-bound protein 2
GTP	Guanosine triphosphate
GTPase	Guanosine triphosphatase
h	Hour
H&E	Haematoxylin and eosin staining
HEK293T	Human embryonic kidney cell line 293T
HMG2A	High-mobility group AT-hook 2
hMLH1	Human mutL homolog 1
hMSH2	Human mutS homolog 2
hMSH6	Human mutS homolog 6
HPF	High-power fields
H-RAS	Harvey Rat Sarcoma Viral Oncogene
HRP	Horseradish peroxidase
HT1080	Fibrosarcoma cell line
IHC	Immunohistochemistry DMEM
K -RAS	Kirsten rat sarcoma viral oncogene homolog
kDa	Kilodalton
L	Litre
LB	Lysogeny broth
let-7a	MicroRNA Let-7
LOH	Loss of heterozygosity
MAPK	Mitogen activated protein kinase
MBDs	Methyl-binding domain proteins
Mcl-1	Myeloid cell leukaemia sequence 1
MCS	Multiple cloning site
MDM2	Mouse double minute 2 homolog (E3 ubiquitin-protein ligase)
MDM4	Mdm4 p53 binding protein homolog
MDS	Myelodysplastic syndrome (myelodysplasia)
MeDIP	Methylated DNA immunoprecipitation
MeDIP-seq	Methylated DNA immunoprecipitation and high-throughput sequencing
MEK	Mitogen activated extracellular signal-regulated kinase
MET	Met proto-oncogene (hepatocyte growth factor receptor)
mg	Milligram
miRNA	Micro ribonucleic acid
ml	Millilitre
mM	Millimolar
mm	Millimetre
MMP2	Matrix metalloproteinase 2
MMP3	Matrix metalloproteinase 3

---

MMP9	Matrix metalloproteinase 9
MMR	Mismatch repair
MPNST	Malignant peripheral nerve sheath tumours
MRI	Magnetic resonance imaging
mRNA	Messenger ribonucleic acid
MSP	Methylation specific polymerase chain reaction
mTOR	Mammalian target of Rapamycin
MUC1	Mucin 1, cell surface associated
MYB	V-myb avian myeloblastosis viral oncogene homolog
MYCN	Neuroblastoma derived v-myc myelocytomatosis viral oncogene
NCBI	National Centre for Biotechnology Information
NCI	National Cancer Institute
NF	Neurofibroma
<i>NF1</i>	Neurofibromin 1 gene (Italic font)
NF1	Neurofibromin 1 protein (non Italic font)
ng	Nanogram
nM	Nanomolar
nmol	Nanomole
N-RAS	Neuroblastoma RAS viral (v-RAS) oncogene homolog
NS	Noonan syndrome
NSCLC	Non-small cell lung cancer
nt(s)	Nucleotide(s)
NTC	Non template control
O/N	Over night
OMGP	Oligodendrocyte Myelin Glycoprotein
OPG	Optic pathway gliomas
p	P-value
P16INK4A	Cyclin-dependent kinase inhibitor 2A
p53	Tumour protein p53
PAGE	Polyacrylamide gel electrophoresis
PBS	Phosphate buffered saline
PBS-T	Phosphate buffered saline with Tween 20
PCR	Polymerase chain reaction
PDCD4	Programmed cell death protein 4
PGK	Phosphoglycerate kinase
pH	Potential of hydrogen
PI3K	Phosphatidylinositol-4,5-bisphosphate 3-kinase
PIP3	Phosphatidylinositol-3,4,5-tris phosphate
PITA	Probability of interaction by target accessibility
pmol	Picomole
PNST	Peripheral nerve sheath tumour
PPi	Pyrophosphate
PRC2	Polycomb repressive complex 2
PTEN	Phosphatase and tensin homolog
PTPN11	Protein tyrosine phosphatase, non-receptor type 11
PVDF	Polyvinylidene fluoride
qPCR	Quantitative polymerase chain reaction
qRT-PCR	Reverse-transcriptase quantitative polymerase chain reaction
Rac	RAS-related C3 botulinum toxin substrate
RAF1	V-raf-1 murine leukaemia viral oncogene homolog 1
RB	Retinoblastoma protein 1
RIPA	Radioimmunoprecipitation assay
RNA	Ribonucleic acid
RNase	Ribonuclease
RNU66	Small nucleolar RNA, H/ACA box 66
RTK	Receptor tyrosine kinase

---

s	Second
SD	Standard deviation
S100	S100 calcium binding protein
SCNN1A	Sodium channel, non-voltage-gated 1 alpha subunit
SDS	Sodium dodecyl sulfate
SHC	Src homology 2 domain containing
SHOC2	Soc-2 suppressor of clear homolog (C. elegans)
shRNA	Short hairpin RNA
siRNA	Short interfering RNA
sNF96.2	Human malignant peripheral nerve sheath tumour cell line
SNP	Single nucleotide polymorphism
SOC	Super Optimal broth with catabolite repression
SOCS6	Suppressor of cytokine signaling 6
SOS1	Son of sevenless homolog 1
SPRED1	Sprouty-related, EVH1 domain containing 1
Src	V-src avian sarcoma (Schmidt-Ruppin A-2) viral oncogene homolog
STS	Soft tissue sarcomas
SUZ12	Polycomb protein SUZ12
T	Thymine
TGFB	Transforming growth factor beta
TBS	Tris buffered saline solution
TBST	Tris buffered saline solution with tween 20
TFF3	trefoil factor 3
TKR	Tyrosine kinase receptor
TMA	Tissue microarray
TP53	Tumour Protein p53 gene
U	Uracil
U/ml	Unit/millilitre
U/ $\mu$ l	Unit/microlitre
UCL	University College London
UTR	Untranslated region
UV	Ultra violet
WIBR	Wolfson Institute for Biomedical Research
Wnt	Wingless-type MMTV integration site
WST	Water soluble tetrazolium salt
WT1	Wilms' Tumour 1
$\Delta$ Ct	Delta (difference) of threshold cycles
$\Delta\Delta$ Ct	Comparative Ct method
$\mu$ g	Microgram
$\mu$ l	Microlitre
$\mu$ m	Micrometre
$\mu$ M	Micromolar

# 1. Introduction

## 1.1. Neurofibromatosis Type 1

Neurofibromatosis type 1 (von Recklinghausen neurofibromatosis) is a common, familial autosomally dominant neurocutaneous disorder, affecting approximately one in 3000 individuals (Friedman 1999). Neurofibromatosis type 1 is caused by monoallelic inactivation of the tumour suppressor gene neurofibromin 1 located on chromosome 17q11.2 (Wallace et al. 1990; Cawthon et al. 1990). A “second hit” of the *NF1* gene leads to biallelic inactivation is crucial to the development of certain manifestations, such as neurofibromas and café au lait macules (Jouhilahti et al., 2011). Adult heterozygotes always show some signs of the disease, therefore penetrance is said to be 100% in adults. Some patients may have café au lait spots, axillary skin freckles, and iris Lisch nodules, whereas others may have life-threatening benign tumours involving the spinal cord or malignant sarcomas of an extremity reflecting the variable expressivity of the disease (Nussbaum et al. 2007). Examples are depicted and described further in section 1.1.2.

Individuals with neurofibromatosis type 1 have a further risk of developing malignant peripheral nerve sheath tumours (MPNSTs). There are two types of MPNST, sporadic MPNST and neurofibromatosis type 1-associated MPNST. Neurofibromatosis type 1-associated MPNST is a malignant tumour arising from a pre-existing benign neurofibroma in neurofibromatosis type 1

patients, however sporadic MPNST occurs sporadically in patients with no known risk factors. MPNSTs are very difficult to detect, metastasise widely and usually have poor prognosis (Ferner & Gutmann, 2002).

Approximately one-fourth to one-half of MPNSTs develop in patients with neurofibromatosis type 1 (Weiss & Goldblum 2007), and individuals with neurofibromatosis type 1 have an 8%–13% lifetime risk of developing neurofibromatosis type 1-associated MPNST (most commonly in individuals aged 20–35 years) (Evans et al. 2002). The five year survival from diagnosis of MPNST is 21% for patients with neurofibromatosis type 1 compared to 42% for patients developing sporadic MPNST (Evans et al. 2002).

### **1.1.1. History of Neurofibromatosis Type 1**

In 1882, Friedrich Daniel von Recklinghausen described the disorder that we nowadays call neurofibromatosis type 1; hence also named von Recklinghausen disease. However, more accurately the disorder's first characterisation was earlier in 1849 by Robert William Smith, although Smith described the disorder originated from connective tissue not the nerves (Smith 1989; Reynolds et al. 2003; Brosius 2010). In 1956, a study by Crowe, Schull, & Neel described in detail various manifestations of neurofibromatosis type 1 (Crowe FW & Schull WJ 1956). In 1982, Riccardi classified the different neurofibromatosis disorders where Neurofibromatosis type 1 and 2 were described in details (Riccardi 1982). In 1987, the National Institutes of Health (NIH) consensus development

conference suggested the diagnostic criteria for neurofibromatosis type 1 (Stumpf et al. 1988) These criteria are listed in (Table 1-1) and will be discussed in detail in the next section.

### 1.1.2. Clinical diagnosis of Neurofibromatosis type 1

Neurofibromatosis type 1 is diagnosed clinically using a set of criteria formulated by the National Institutes of Health consensus development conference (Stumpf et al. 1988); (Table 1-1). These criteria can diagnose about 50% of patients by the first year of life, 97% of patients by the age of 8 years old, and 100% of patients by the age of 20 years (Abramowicz & Gos 2014; DeBella et al. 2000).

**Table 1-1: National Institutes of Health diagnostic criteria of neurofibromatosis type 1**

**Two or more of the following are required for the diagnosis**

Six or more café au lait macules over 5 mm in greatest diameter in prepubertal individuals and over 15 mm in greatest diameter in postpubertal individuals
Two or more neurofibromas of any type or one plexiform neurofibroma
Freckling in the axillary or inguinal regions (Crowe's sign)
Optic glioma
Two or more Lisch nodules
A distinctive osseous lesion such as sphenoid dysplasia or thinning of long bone cortex with or without pseudoarthrosis
A first-degree relative (parent, sibling, or offspring) with neurofibromatosis type 1 by the above criteria

The most frequent clinical features are neurofibromas (Figure 1-1), café au lait macules (Figure 1-2), intertriginous freckling, iris Lisch nodules (Figure 1-3), and learning disabilities; however optic glioma, malignant peripheral nerve sheath tumours, and characteristic bone lesions can also be present.



**Figure 1-1: Multiple benign neurofibromas**

Numerous subcutaneous neurofibromas, some are marked with arrows, in a patient with neurofibromatosis type 1. Retrieved from Jett & Friedman (2010).



**Figure 1-2: Café au lait macules**

Café au lait macules (CALMs) in the trunk of an 11-year-old child with neurofibromatosis type 1. Retrieved from Purkait et al. (2011).



**Figure 1-3: Iris Lisch nodules**

Multiple small, oval, yellow-brown papules (Lisch nodules) in the iris. Retrieved from Adams et al. (2011).

### **1.1.3. Genetics of Neurofibromatosis type 1**

#### **1.1.3.1. *NF1* Gene**

Neurofibromatosis type 1 is caused by germline mutations of the tumour suppressor *NF1*. The *NF1* gene is one of the largest human genes and spans ~350 kb of 17q11.2, contains 60 exons, of which 3 are alternatively spliced, and encodes a 12 kb mRNA transcript. (Cichowski & Jacks 2001; Upadhyaya 2008).

The *NF1* encoded protein, neurofibromin, is a large multi-domain protein (2,839 amino acids; 319 kDa) that activates RAS-GTPase; and functions as negative regulator of RAS proteins (Figure 1-4) (Leondaritis et al. 2009; Dasgupta 2003; DeClue et al. 1992). Loss of *NF1* function causes constitutive activation of RAS and its associated cascade of signaling pathways, promoting cell growth and proliferation (RAS–mitogen-activated protein kinase–extracellular signal–regulated kinase (RAS-MAPK-ERK) and phosphatidyl inositol 3-kinase (PI3K-AKT-mTOR) in human neurofibromas and MPNST-derived cell lines (Sherman et al. 2000; Cichowski & Jacks 2001; Leondaritis et al. 2009).

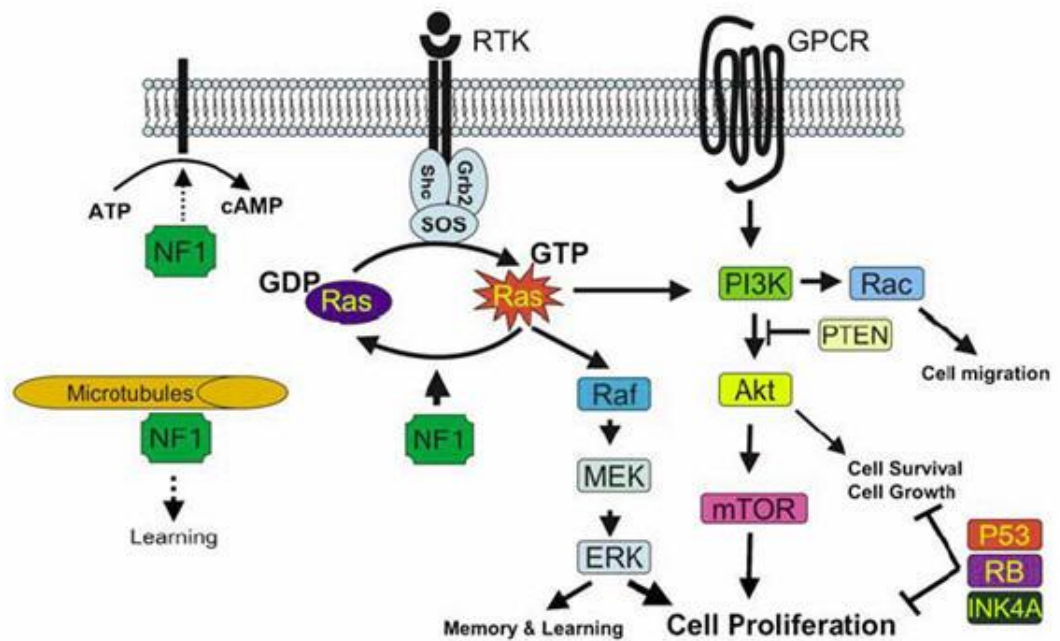


**Figure 1-4: Loss of *NF1* expression leads to activation of RAS, dysregulation of cell growth and tumourigenesis**  
 Retrieved from Le & Parada (2007).

### 1.1.3.2. Germline mutational spectrum of *NF1*

About 1300 different inherited mutations of *NF1* gene have been reported (<http://www.hgmd.org>). For unknown reasons, the germline mutation rate for the *NF1* gene is some 10-fold higher than that observed in most other comparable inherited disease genes, and *de novo* mutations are present in almost half of neurofibromatosis type 1 cases (Huson et al. 1988; Evans et al. 2010). These mutations vary in size from deletions of more than a megabase to a single base pair substitution. Examination of these germline mutations demonstrated that 80% are predicted to be truncating mutations, with about 30% of these truncating mutation expected to result in RNA splicing abnormalities (Ars et al. 2000).

Post-zygotic *NF1* mutations causes mosaic neurofibromatosis type 1 and usually have a milder clinical picture depending on the proportion and type of affected tissues. Mosaic neurofibromatosis type 1 can be either localised or generalised with clinical features varying from a narrow strip to one quadrant and occasionally to one half of the body, therefore called segmental neurofibromatosis type 1 (Ruggieri & Huson 2001; Kehrer-Sawatzki & Cooper 2008).

Germline mosaicism is very rare in patients with neurofibromatosis type 1 due to the fact that very few families have been reported with two or more affected child born to unaffected parents (Lázaro et al. 1994; Bottillo et al. 2010; Trevisson et al. 2013). Molecular analysis is essential to confirm the germline mosaicism diagnosis as cases of two or more siblings with non-

identical (*de novo*) mutations have been reported (Upadhyaya et al. 2003). Molecular analysis of fathers of cases who originated from germline mosaicism detected an *NF1* mutation in 10% to 17% of spermatozoa (Bottillo et al. 2010). Trevisson et al. (2013) have also reported *NF1* germline mosaicism in the maternal germline (Trevisson et al. 2013).

### **1.1.3.3. Molecular diagnosis of neurofibromatosis type 1**

A diagnosis of neurofibromatosis type 1 is mainly made on the clinical phenotype. However, the identification of an *NF1* mutation and hence understanding the impact of the *NF1* gene may direct the overall clinical assessment of patients (Griffiths et al. 2007). The available mutation detection protocols reliably diagnose 95% of neurofibromatosis type 1 patients (Messiaen et al. 2000). Negative results for *NF1* mutations largely exclude the diagnosis neurofibromatosis type 1, eliminate the need and expense of specialist follow up, and can reassure the patient. Mutational analysis is useful for diagnostic confirmation in individuals who do not fulfil diagnostic criteria or when prenatal diagnosis is desired (Hirbe & Gutmann 2014). The *NF1* mutation analysis has been found to be cost effective when taking in consideration all the costs of health care (Tsang et al. 2012)

#### **1.1.4. Other RAS/MAPK pathway dysregulation (RASopathies)**

Having described neurofibromatosis in some detail, it is important to recognise that this disease belongs to a group of RAS/MAPK pathway dysregulation syndromes (RASopathies) which share characteristic facial features, cardiac abnormalities, cutaneous abnormalities, growth deficit, neurocognitive disorders, and predisposition to malignancies (Zenker 2011). RASopathies comprise neurofibromatosis type 1, Noonan syndrome, Leopard syndrome, Legius syndrome and Costello syndrome (Zenker 2011). Although not the main focus of this thesis, each of the other RASopathies is described briefly below.

##### **1.1.4.1. Noonan syndrome**

Noonan syndrome (NS) is an autosomal dominant, multisystem disorder with 1 in 1000–2500 prevalence (Mendez & Opitz 1985). It is typically characterised by broad forehead, ocular hypertelorism, ptosis (drooping of the upper eyelid), pulmonary valve stenosis, short stature, mild intellectual disability, undescended testes, and skeletal malformations (Romano et al. 2010).

Understanding of the molecular genetics underlying Noonan syndrome has increased in the past decade, enabling the study of the pathophysiological mechanisms causing the varied medical and developmental features of the disorder.

Seven genes have been shown to cause Noonan syndrome: *PTPN11* (Tartaglia et al. 2001), *K-RAS* (Schubbert et al. 2006), *N-RAS* (Cirstea et al. 2010), *SOS1* (Roberts et al. 2007; Tartaglia et al. 2007), *SHOC2* (Mendez & Opitz 1985), *CBL* (Martinelli et al. 2010) and *RAF1* (Pandit et al. 2007; Razzaque et al. 2007).

#### **1.1.4.2. Leopard syndrome**

Leopard syndrome (LS) is a rare autosomal dominant disorder with a similar phenotype to NS, including a “Noonan-like” appearance as well as multiple **L**entigines, **E**CG abnormalities, **O**cular hypertelorism, **P**ulmonary valve stenosis, **A**bnormal genitalia, **R**etardation of growth, and **D**eafness (acronym **LEOPARD**) (Tidyman & Rauen 2009). LS is a very rare disorder; by the year 2008 only 200 patients have been recorded worldwide however the real incidence of LS has not been assessed (Sarkozy et al. 2008). LS and NS are allelic disorders, caused by different heterozygous missense mutations in the same genes, *PTPN11* (Digilio et al. 2002; Legius et al. 2002) and *RAF1* (Pandit et al. 2007). This common genetic defect between LS and NS probably explains the phenotypic similarities between the two diseases.

#### **1.1.4.3. Legius syndrome**

Unlike NS and LS, Legius syndrome is an autosomal dominant disorder that shares many phenotypic features with neurofibromatosis type 1. Individuals may have café au lait maculae, axillary freckling, mild neurocognitive impairment, and macrocephaly. However, the phenotypic features common

in neurofibromatosis type 1 such as neurofibromas, iris Lisch nodules and central nervous system tumours are lacking (Brems et al. 2007). Legius syndrome is caused by heterozygous mutations in *SPRED1* (Brems et al. 2007). *SPRED1* gene, encodes SPRED1, which is a member of the SPROUTY/SPRED family of proteins. SPRED1 functions as negative regulator of RAS by inhibiting phosphorylation of Raf (Wakioka et al. 2001). Neurofibromatosis type 1-like features encountered in Legius syndrome can be explained that neurofibromin is a SPRED1 interacting protein and SPRED1 binding to neurofibromin stimulates localisation of neurofibromin in the plasma membrane which in turn down-regulates RAS-GTP levels (Stowe et al. 2012).

#### **1.1.4.4. Costello syndrome**

Costello syndrome is a very rare disorder characterised by dysmorphic craniofacial features, cardiac, musculoskeletal and ectodermal abnormalities, failure to thrive and neurocognitive delay (Rauen 2007). The real incidence of Costello has not been assessed. Individuals with Costello syndrome are at increased risk of developing neoplasms, both benign and malignant (Tidyman & Rauen 2009). Heterozygous germline mutations in *H-RAS* cause Costello syndrome (Aoki et al. 2005) and explain the overlap in clinical features with the above diseases.

## 1.2. Pathology of Neurofibroma

Neurofibromas are benign peripheral nerve tumours that may occur either as solitary lesions unrelated to a genetic syndrome (i.e. sporadic) or as multiple lesions in association with neurofibromatosis type 1. The main neoplastic cellular components of neurofibroma are Schwann cells, which are characterised cytologically by wavy nuclear contours and S100 protein expression (Weiss et al. 1983; Chaubal et al. 1994; Perry et al. 2001). Neurofibromas' cellular component also contain a mixture of non-neoplastic cells, including fibroblasts, perineural cells, endothelial cells, smooth muscle cells, pericytes, mast cells, lymphocytes and nerve axons (Gray et al. 1990; Hirose et al. 2003; Fine et al. 2004). In addition, a population of CD34 positive cells of unclear histogenesis are present (Carroll 2012; Weiss & Nickoloff 1993).

Neurofibromas have three different subtypes based on architectural growth patterns: localised (nodular, discrete), diffuse, and plexiform. However mainly plexiform and diffuse neurofibromas are significant precursors of MPNST. Despite the fact that all neurofibromas have a risk of transformation to MPNST, neurofibromas that transform are usually deeply located. Plexiform neurofibromas have much greater risk of developing MPNST (Weiss & Goldblum 2007).

## 1.2.1. Gross pathology of neurofibromas

### 1.2.1.1. Localised neurofibroma

The localised neurofibroma is the most common form of neurofibroma, and occurs sporadically in the majority of cases. The majority of neurofibromas (90%) occur sporadically, however only 10% were proven to be associated with neurofibromatosis type 1. Localised neurofibromas are well-circumscribed nodules but without a capsule (Figure 1-5). Localised neurofibromas usually occur in the dermis or soft tissue, however it may also involve a major nerve (intranural subtype), and result typically in fusiform expansion of the nerve trunk (Huson et al. 1988).



**Figure 1-5: Localised neurofibroma, macroscopic**

The tumour is well circumscribed and has a homogenous fleshy cut surface.

Retrieved from:

[http://www.humpath.com/IMG/jpg\\_jpg\\_localized\\_neurofibroma\\_08\\_NF1\\_2.jpg](http://www.humpath.com/IMG/jpg_jpg_localized_neurofibroma_08_NF1_2.jpg).

### 1.2.1.2. Diffuse neurofibroma

Diffuse neurofibroma is an uncommon form of neurofibroma that occurs primarily in children and young adults. Diffuse neurofibroma is an ill-defined infiltrative lesion (Figure 1-6) and tends to involve the skin and subcutaneous tissues. It produces localised thickening and induration of the skin. Diffuse neurofibroma may occur in the skin, in the soft tissue, or in the viscera. The most commonly involved visceral organ is the gastrointestinal tract (Hochberg et al. 1974).

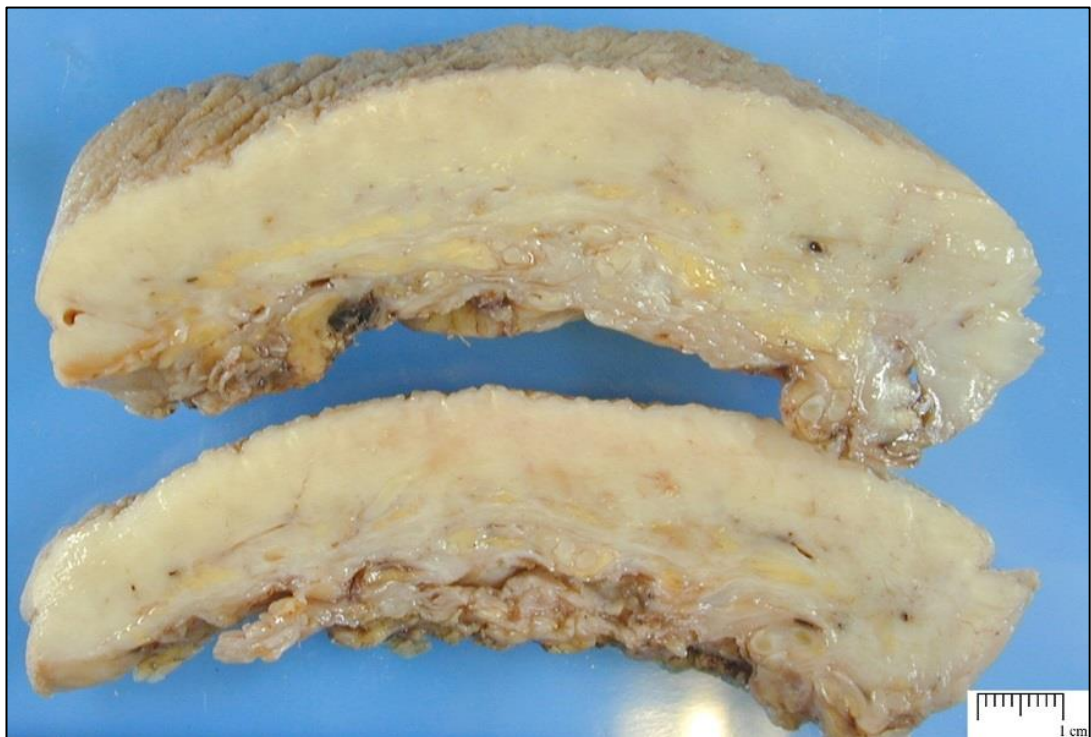


**Figure 1-6: Diffuse neurofibroma, macroscopic**

Diffuse cutaneous neurofibroma infiltrating the dermis which is thickened and firm.  
Retrieved from: <http://www.humpath.com/spip.php?article3900>.

### 1.2.1.3. Plexiform neurofibroma

Plexiform neurofibroma is the least common variant of neurofibromas and it occurs almost exclusively in neurofibromatosis type 1 patients. Plexiform neurofibromas occur in 30 - 40% of neurofibromatosis type 1 patients develop in early childhood, and they are often multiple large lesions that grow along major nerve trunk of large nerves, expanding and distorting the nerves, acquiring a plexiform architecture (Figure 1-7). It is usually characterised by the involvement of numerous adjacent nerve fascicles or multiple components of a nerve plexus (McCarron & Goldblum 1998; Weiss & Goldblum 2007; Huson et al. 1988). Plexiform neurofibroma has a potential for malignant transformation (details in section 1.6).



**Figure 1-7: Plexiform neurofibroma, macroscopic**

The tumour involves multiple nerves with multinodular appearance. Retrieved from: <http://www.humpath.com/spip.php?article3900>.

## 1.2.2. Microscopy of neurofibromas

Microscopically, solitary and plexiform neurofibroma shares common histological features. They both have a variable hypocellular, myxomatous background (Figure 1-8). Fine collagen fibres are also present at a variable density. The cellular component is composed of a mixture of neoplastic Schwann cells and a variety of non-neoplastic cells (including fibroblasts, perineural cells, endothelial cells, smooth muscle cells, pericytes, mast cells, lymphocytes and nerve axons). Immunohistochemical staining is typically positive for S100, CD34, calretinin and Factor XIIIa (Gray et al. 1990; Hirose et al. 2003; Fine et al. 2004).

When neurofibromas show a low level of cytological atypia and areas of increased cellularity fascicle formation and even occasional numbers of mitotic figures they are referred to as atypical neurofibroma (Figure 1-9) and this variant has to be distinguished from low-grade MPNST (Yamaguchi et al. 2003). Atypical neurofibroma may be precursors of MPNST and are usually encountered in patients with neurofibromatosis type 1. Differentiating atypical neurofibroma from low-grade MPNST is difficult, however, low-grade MPNST microscopically shows more generalised nuclear atypia with increased cellularity and low levels of mitotic activity (Weiss & Goldblum 2007).

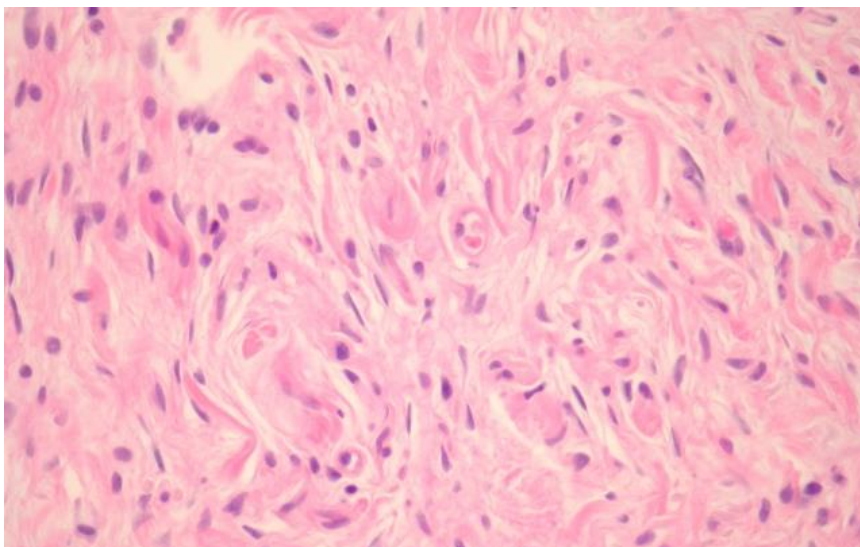


**Figure 1-8: Classic neurofibroma histology**

Hypocellular tumour with myxoid stroma and collagen strands. Retrieved from: <http://dermnetnz.org/pathology/neurofibroma-path.html>.

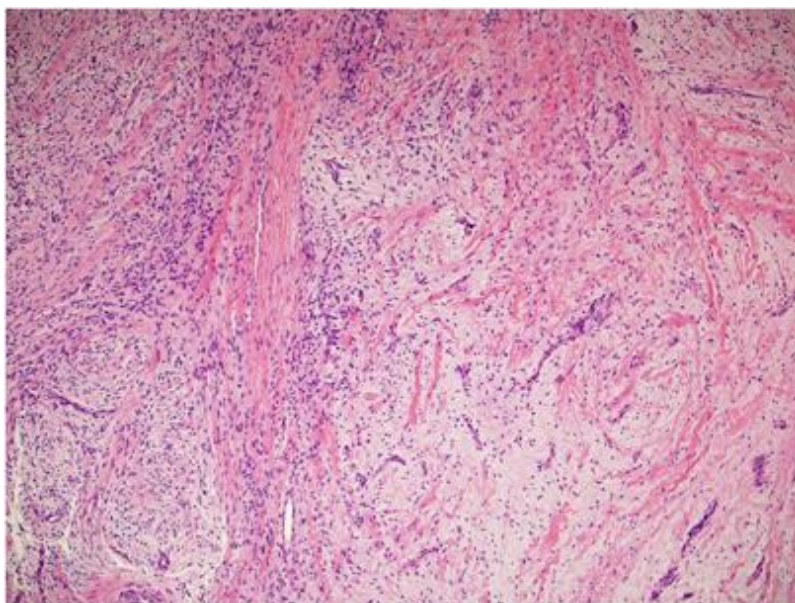


**Figure 1-9: Atypical neurofibroma histology**

Hypocellular tumour with myxoid stroma and collagen strands with mild atypia consisting of mild hypercellularity and hyperchromasia. Retrieved from: Babovic-Vuksanovic et al. (2012).

## 1.3. Malignant Peripheral Nerve Sheath Tumours

Malignant Peripheral Nerve Sheath Tumour (MPNST) is a malignant tumour arising from a peripheral nerve or from a pre-existing benign neurofibroma. MPNST display Schwann cell differentiation by histologic or immunohistochemical features. MPNST arise from a pre-existing benign neurofibroma in neurofibromatosis type 1 patient is called neurofibromatosis type 1-associated MPNST. However, MPNST that occur in a patient with no known risk factors is called sporadic MPNST. Other historical synonymous terms used previously to describe MPNST include malignant schwannoma, neurogenic sarcoma and neurofibrosarcoma (Evans et al. 2002).

Neurofibromatosis type 1 has a risk of developing MPNST; where about one-fourth to one-half of MPNSTs develop in patients with neurofibromatosis type 1 (Weiss & Goldblum 2007). The life time risk for neurofibromatosis type 1 patient to develop MPNST is 8%–13% (Most commonly in individuals aged 20–35 years) (Evans et al. 2002). MPNST patients with neurofibromatosis type 1 have bad prognosis compared to sporadic MPNST; where the five year survival from diagnosis of MPNST is 21% for patients with neurofibromatosis type 1 compared to 42% for patients developing sporadic MPNST (Evans et al. 2002). It is very difficult to detect MPNSTs early, and it is usually metastasise widely and have a poor prognosis (Ferner & Gutmann 2002).

### **1.3.1. Grading of MPNST**

The grading system used for MPNST grading is the same grading system for other soft tissue sarcomas (STS). Grading is important because it guides patient management. The two most commonly used grading systems are the National Cancer Institute (NCI) system and the French Federation of Cancer Centres Sarcoma Group (FNCLCC) system. The NCI system applies a combination of histological type, pleomorphism, cellularity and mitotic rate for attributing grade 1 to 3. MPNSTs categorized as grade 1 tumours when they had the appearance of neurofibroma except mitoses were present (< six mitoses per 10 HPF) and the tumour was composed of areas of high cellularity. MPNSTs are categorised as either grade 2 or grade 3 according to the amount of tumour necrosis, where 15% necrosis is considered the threshold for differentiating grade 2 from grade 3 tumours. The FNCLCC is a score based system that obtained by evaluating three parameters: tumour differentiation, mitotic rate and the amount of tumour necrosis. A score is assigned separately to individual parameter and the grade is obtained by summing the three assigned scores. Differentiation is scored from 1 to 3 where 1 is well differentiated; 2 is well defined histogenetic type; and 3 is poorly differentiated. Mitotic rate is scored from 1 to 3 where 1 for mitotic count of 0-9 / 10 high-power fields (HPF), 2 for mitotic count of 10-19 / 10 HPF and 3 for mitotic count of 20 / 10 HPF or more. Necrosis is scored from 0-2 where 0 means no necrosis, 1 means 50% necrosis or more and 2 means more than 50% necrosis. Grading depends on the sum of all the

above score as grade 1 is given for total score of 2 or 3, grade 2 is given for total score 4 or 5 and grade 3 is given for total score 6, 7 or 8 (Guillou et al. 1997; Trojani et al. 1984; Coindre 2006). It is usually difficult to distinguish low-grade MPNST from neurofibromas with varying degrees of atypia (Yamaguchi et al. 2003).

### **1.3.2. Diagnosis and management of MPNST**

Careful clinical monitoring is required for individuals who have a personal or family history of cancer, after radiotherapy, optic pathway glioma, multiple subcutaneous neurofibromas, whole gene deletion, or neurofibromatosis neuropathy; These group might have an increased risk of developing MPNST (De Raedt et al. 2003; Khosrotehrani et al. 2005; Ferner & Gutmann 2002). Urgent expert opinion (from specialist neurofibromatosis clinics or soft tissue tumour units) is needed if neurofibromatosis type 1 patients develop any of the following in association with a subcutaneous or plexiform neurofibroma: persistent pain lasting for longer than a month or pain that disturbs sleep; new or unexplained neurological deficit or sphincter disturbance; alteration in the texture of a neurofibroma from soft to hard; and rapid increase in the size of a neurofibroma (Ferner & Gutmann 2002). Fluorodeoxyglucose positron emission tomography allows the visualisation and quantification of glucose metabolism in cells and is a useful diagnostic tool in differentiating benign plexiform neurofibromas from MPNST (Ferner et al. 2000).

Any sarcoma involves a major nerve, without definite line of differentiation or arising from benign neurofibroma would have been accepted by most authors to be categorised as MPNST (Allison et al. 2005; Weiss & Goldblum 2007). Additionally, any spindle cell tumour in neurofibromatosis type 1 patient should be considered as MPNST until proved otherwise (Weiss & Goldblum 2007).

Schwann cell differentiation and Immunohistochemical finding of partial S100 expression must be present for the diagnosis of MPNST specially for those that more difficult to classify and unrelated to major nerves (Weiss & Goldblum 2007). Some MPNSTs (malignant triton tumour) may show heterologous differentiation e.g., bone, cartilage, skeletal muscles, smooth muscle, angiosarcoma and even well-formed glands (Brown et al. 1992; Ducatman & Scheithauer 1984; Rodriguez et al. 2007). A different, uncommon subtype of MPNST that raises a totally separate differential diagnosis is portrayed by a prevalence of extensive epithelioid cells, i.e. epithelioid MPNST (DiCarlo et al. 1986; Laskin et al. 1991; Lodding et al. 1986). These tumours are more common in superficial sites and as opposed to ordinary MPNSTs, express S100 protein unequivocally and normally, diffusely (Laskin et al. 1991). For obscure reasons, the immense dominant part of MPNST emerging inside prior schwannoma (an exceptionally uncommon occasion) are of epithelioid sort (McMenamin & Fletcher 2001). The differential diagnosis of epithelioid MPNST includes melanoma, clear cell sarcoma, epithelioid sarcoma, and carcinoma. Absence of representation

of melanocytic markers (e.g., MelanA, HMB45, MITF) is exceptionally useful in the differentiation of epithelioid MPNST from melanoma and clear cell sarcoma, and loss of cytokeratin expression recognises them from carcinoma and epithelioid sarcoma (Carter et al. 2012; Hollmann & Hornick 2011).

The treatment for MPNST is primarily surgical, although radiotherapy can be employed in pre-operative, intraoperative, and post-operative settings (Yang et al. 1998). Surgical treatment aims for complete removal of the lesion with tumour free margins (Ferner & Gutmann 2002). Adjuvant radiotherapy has a role in treating high-grade lesions or post-operative for incompletely excised tumours. Chemotherapy offers little benefit to patients with MPNST (Angelov et al. 1998). With the recent advances in molecular genetics, there is a hope for targeted therapy to be discovered (Ferner & Gutmann 2002). New agents targeting RAS-RAF-MAPK/ERK kinase-extracellular signal-regulated kinase pathway, may prove effective against MPNST in neurofibromatosis type 1. One of those drugs is farnesyl transferase, which blocks the ability of RAS to reach membrane and hence its activation (Cox 2001). Inhibitors or RAS downstream targets are developed for clinical trials such as MAPK/ERK kinase (Ferner & Gutmann 2002). Ifosfamide and doxorubicin are administered as palliative therapy in patients with metastatic disease and to reduce the size of tumour with the aim of making it amenable to surgery (Ferner & Gutmann 2002). A study by Wojtkowiak et al. showed that combination of farnesyl transferase inhibitors and lovastatin induce apoptosis

in neurofibromatosis type 1 associated MPNST cell lines with low or no detectable toxicity (Wojtkowiak et al. 2008).

### 1.3.3. Pathology of Malignant Peripheral Nerve Sheath Tumours

#### 1.3.3.1. Gross pathology of Malignant Peripheral Nerve Sheath Tumour

Malignant Peripheral Nerve Sheath Tumour is usually a fusiform mass and their gross appearance is similar to other soft-tissue sarcomas. They are usually large (10-15 cm in greatest dimension and infrequently less than 5 cm) with heterogeneous cut surface, tan white and foci of necrosis and haemorrhage (Figure 1-10).



**Figure 1-10: Malignant Peripheral Nerve Sheath Tumour, macroscopic**  
Malignant Peripheral Nerve Sheath Tumour mass, homogeneous with areas of haemorrhage and necrosis. Retrieved from: <http://www.humpath.com/spip.php?article15440>.

### 1.3.3.2. Microscopic features of MPNST

MPNSTs (Figure 1-11) are cellular tumours composed of spindled, pleomorphic cells with areas of haemorrhage and necrosis. In some cases, MPNST often displays extensive pleomorphism, simulating a high-grade undifferentiated pleomorphic sarcoma.

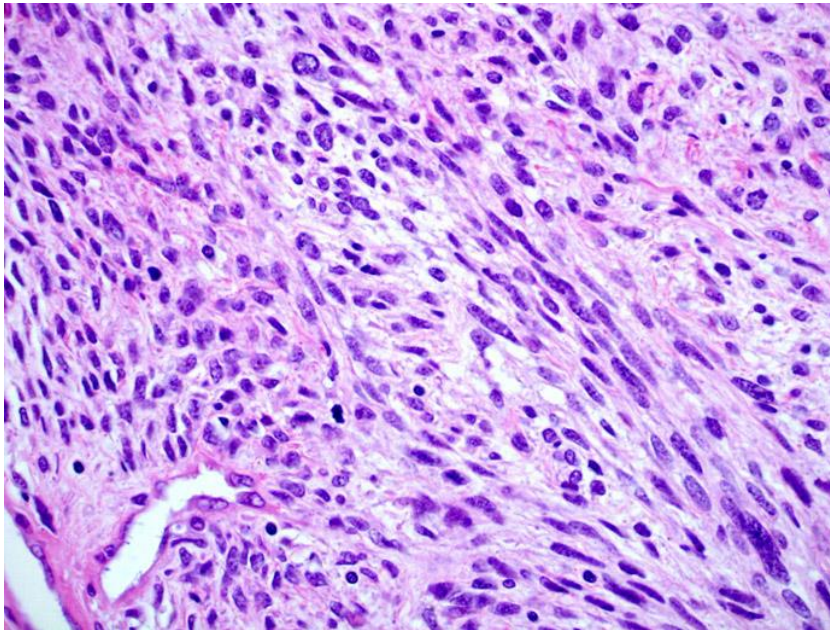


**Figure 1-11: Malignant Peripheral Nerve Sheath Tumour**

Cellular tumour composed of spindled, pleomorphic cells. Retrieved from: [http://www.sarcomaimages.com/index.php?v=Malignant-Peripheral-Nerve-on-Sheath-Tumour-\(MPNST\)](http://www.sarcomaimages.com/index.php?v=Malignant-Peripheral-Nerve-on-Sheath-Tumour-(MPNST)).

### 1.3.3.3. Malignant Triton tumour

Malignant Triton tumour refers to the presence of skeletal muscle differentiation in an MPNST. These tumours are rare (accounts for about 5% of all MPNSTs) and often occur in the setting of neurofibromatosis type 1 (Tripathy et al. 2010; Brooks 1999). Histologically, the defining feature is the presence of variable number of rhabdomyoblasts with abundant eosinophilic cytoplasm (Figure 1-12). Differentiation into cartilage or bone is also common, whereas liposarcomatous differentiation is very rare. Where the five year survival from diagnosis of MPNST is 21% for patients with neurofibromatosis type 1, 42% for patients developing sporadic MPNST (Evans et al. 2002), malignant triton tumour showed five-year survival rates of 26% (Tripathy et al. 2010; Yakulis et al. 1996).

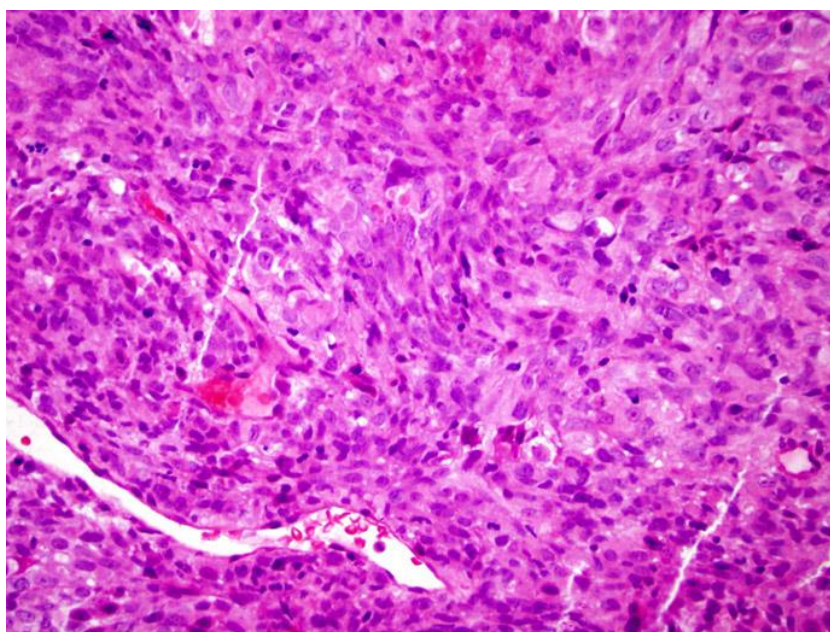


**Figure 1-12: Triton tumour**

MPNST with rhabdomyoblasts with abundant eosinophilic cytoplasm

Retrieved from: <http://www.sarcomaimages.com/sub.php?v=malignant-peripheral-nerve-sheath-tumor-with-rabdomyoblastic-differentiation-triton-tumor>.

#### 1.3.3.4. Glandular MPNST

Glandular MPNST is a rare subtype of MPNST. Histologically, it shows scattered well-differentiated glands in a background of spindle cells. The glands are lined with cuboidal epithelium containing mucin (Figure 1-13). MPNST with epithelial glandular structures is very rare and usually occurs in neurofibromatosis type 1 (Woodruff & Christensen 1993).

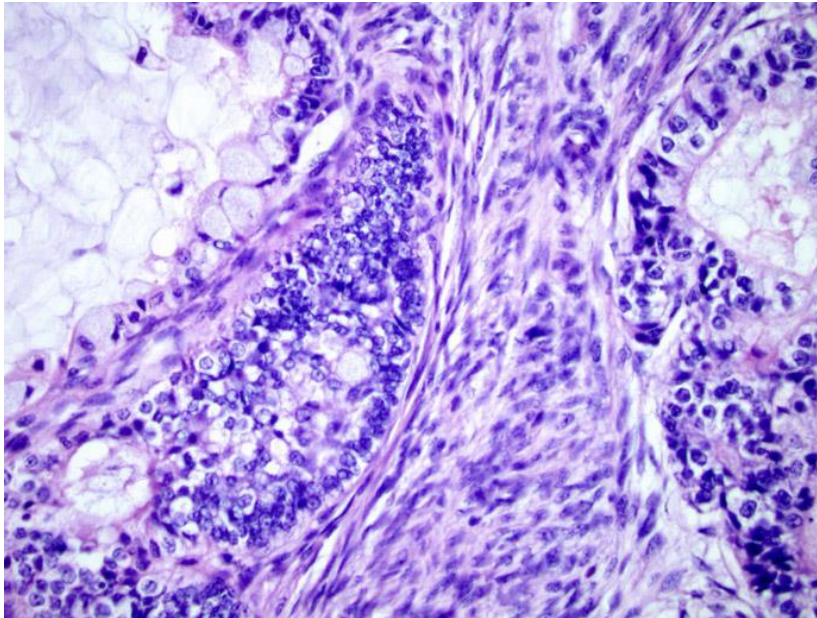


**Figure 1-13: Glandular MPNST**

MPNST containing well differentiated glandular element. Retrieved from:  
<http://www.sarcomaimages.com/sub.php?v=mpnst-with-glandular-elements&p=malignant-peripheral-nerve-sheath-tumor-mpnst>.

### 1.3.3.5. Epithelioid MPNST

Epithelioid MPNST is a rare variant of MPNST (less than 5% of all MPNSTs). It contains epithelioid cells with abundant eosinophilic cytoplasm (Figure 1-14). A greater percentage of epithelioid MPNSTs than conventional MPNST show S100 positivity (Perry et al. 2002).

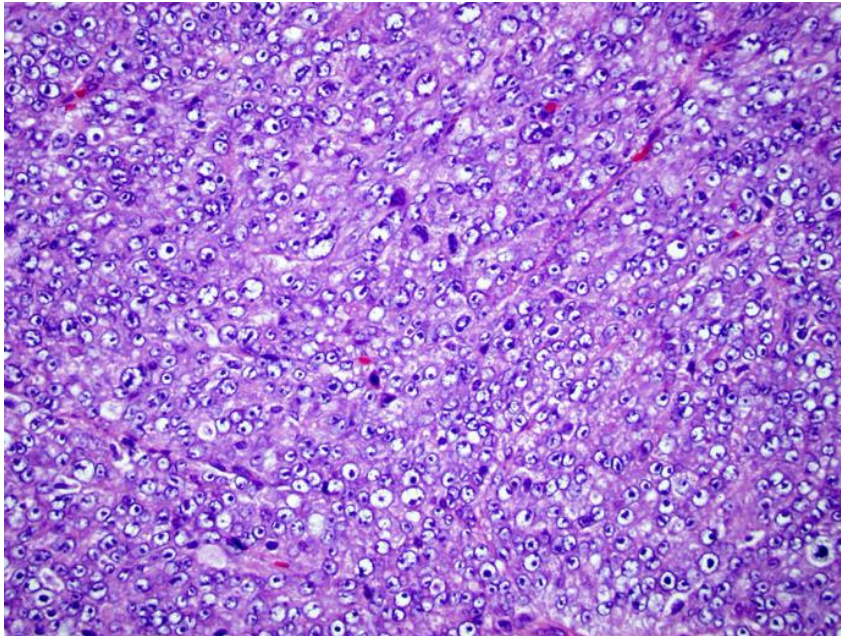


**Figure 1-14: Epithelioid MPNST**

Contains epithelioid cells with abundant eosinophilic cytoplasm. Retrieved from: <http://www.sarcomaimages.com/sub.php?v=epithelioid-mpnst&p=malignant-peripheral-nerve-sheath-tumor-mpnst>.

## **1.4. S100B as a marker of nerve sheath tumours**

S100 protein-immunoreactivity in formalin-fixed paraffin-embedded material was first suggested as a diagnostic tool for tumour diagnosis in 1982 by Nakajima et al. (Nakajima et al. 1982). They showed that S100 was expressed in the cells of eosinophilic granuloma, Langerhans cell histiocytosis as well as in interdigitating reticulum cells sarcoma in the lymph node, spleen and thymus (Nakajima et al. 1982). Subsequently, further studies identified the expression of S100 in different types of sarcomas including rhabdomyosarcoma, Ewing sarcoma, and synovial sarcoma (Coindre et al. 1988; Shimada et al. 1988; Fisher & Schofield 1991).

The S100 proteins family consist of twenty-one known human members (Zimmer et al. 2013). They are small proteins of molecular weight between 9 kDa and 14 kDa (Marenholz et al. 2004; Donato 2003). S100 proteins have been shown to regulate different cellular functions using a calcium-dependent mechanism, they have also been shown to have a potential role in tumour formation and metastasis (Böni et al. 1997; Petersson et al. 2009; Keijser et al. 2006; Maelandsmo et al. 1997).

One particular variant, S100B, is most abundant in neural tissue and it is commonly used by pathologists as a marker to indicate glia cell and Schwann cell differentiation (Hachem et al. 2005). S100B function is through

intracellular and extracellular mechanisms and depending on its concentration, secreted S100B exerts either cytotropic or cytotoxic effects (Astrand et al. 2013). Some studies in the literature have discussed the expression of S100B protein in MPNST. For instance, Lévy et al. studied *S100B* mRNA expression in 14 neurofibromas and 9 MPNSTs using real-time quantitative RT-PCR. Their results showed that *S100B* mRNA is significantly downregulated in MPNST as compared to neurofibromas (Lévy et al. 2004). Nonaka et al. studied S100B expression in 86 neurofibromas and 77 MPNSTs using immunohistochemistry. Their results showed that S100B was stained diffusely in all neurofibroma, but its reaction was observed only in 30% of MPNSTs in a focal fashion (Nonaka et al. 2008). Karamchandani et al. studied S100B expression in 55 neurofibromas and 78 MPNSTs using immunohistochemistry. Their results showed that S100B was stained diffusely in 52 out of 55 neurofibroma, but its reaction was observed only in 15 out of 78 MPNSTs (Karamchandani et al. 2012).

There appears to be some alteration in expression correlated with tumorigenic transformation, but strikingly I have not found any study investigating S100B regulation and function in MPNST.

## **1.5. Management of neurofibromatosis type 1**

When neurofibromatosis type 1 is diagnosed, it has been recommended that they are referred to a specialised clinic that includes geneticists, paediatricians, neurologists and/or dermatologists (Ferner 2007). The management is determined by the age of the patient: specific monitoring of disease manifestations aiming to detect severe disease complications such as malignant peripheral nerve sheath tumours (MPNST) is important.

### **1.5.1. Neurofibroma variants and likelihood of malignant transformation**

As discussed, neurofibromas are generally benign peripheral nerve sheath tumours and can be dermal (cutaneous), subcutaneous or plexiform. Dermal neurofibromas develop from the terminal branches of peripheral nerves and can be classified as focal/discrete or diffuse (Riccardi 2007). There have been no reports of focal or diffuse lesions undergoing malignant change but they often catch on clothing and cause cosmetic problems, transient stinging, itching and when numerous can cause major disfigurement and psychological stress (Riccardi 1981).

Subcutaneous neurofibromas, in contrast, develop within a peripheral nerve and are surrounded by the perineurium (Riccardi 2007). Maunter et al.

(2008) observed association of MPNSTs with subcutaneous, but not cutaneous, neurofibromas (Mautner et al. 2008).

Plexiform neurofibromas cause significant morbidity because they can grow along a nerve and may involve multiple nerves and form a plexus (Korf 1999; Tucker et al. 2005). The lesions can be nodular, and multiple discrete tumours may develop on nerve trunks. Plexiform neurofibromas can infiltrate soft tissue causing hypertrophy, or infiltrate bone in some cases (Korf 1999). The growth rate is variable and may be rapid, especially in adolescence, followed by periods of inactivity. Surgical removal of benign plexiform neurofibromas is usually very difficult due to encroachment of the tumour on surrounding structures and nerves. In addition, due to its inherent vascular nature severe haemorrhage may occur, especially with facial plexiform neurofibromas. Expert advice from experienced soft tissue tumour or plastic surgeons is essential before removal of facial plexiform neurofibromas (Ferner 2007).

### **1.5.2. Neurological problems**

One of the important medical complications of neurofibromatosis type 1 is neurological dysfunction, which can include acute or progressive sensory disturbance, lack of coordination or sphincter disturbance and motor deficit, which might be the result of an intracranial lesion or spinal cord compression. Headaches on waking, morning vomiting and altered consciousness are

suggestive of raised intracranial pressure and constitute a neurological emergency (Ferner 2007).

Neurological complications develop from tumours and malformations, including aqueduct stenosis; a narrowing of the aqueduct of Sylvius which blocks the flow of cerebrospinal fluid (CSF) in the ventricular system leading to hydrocephalus (Créange et al. 1999), skull deformities due to sphenoid wing dysplasia leads to pulsating exophthalmos as the temporal lobe herniates into the orbit (Korf 1992), severe scoliosis deforms the spine and can result in spinal cord compression and respiratory compromise (Korf 1992). Neurological manifestations are the consequence of pressure on peripheral, spinal nerves or the spinal cord. Epilepsy occurs in approximately 6–7% of neurofibromatosis type 1 individuals and it is usually mild, and is likely to be related to an underlying cortical dysgenesis (Vivarelli et al. 2003). Sudden neurological deficit should be evaluated promptly for cerebrovascular disease. Cerebrovascular diseases include carotid artery stenosis or occlusion, cerebral haemorrhage or aneurysms. Treatment of cerebrovascular abnormalities in individuals with neurofibromatosis type 1 is identical to that in other patients and may include both surgical and medical options (Friedman et al. 2002).

### **1.5.3. Cognitive problems and behavioural difficulties**

Cognitive impairment is amongst the most common neurological complications in neurofibromatosis type 1 individuals and usually presents with the patient having a low average IQ; however severe intellectual impairment (IQ < 70) is rare (Ferner et al. 1996; North et al. 1997; Ozonoff 1999).

Approximately 70% of neurofibromatosis type 1 patients have learning problems or neuropsychological problems. Behavioural problems, sleep disturbance and impaired socialisation may also be found in neurofibromatosis type 1 patients (H. Johnson et al. 2005)

### **1.5.4. Optic pathway gliomas**

The most common astrocytic (glial) tumours affecting about 15% of children with neurofibromatosis type 1 are gliomas involving the optic pathway (Optic pathway gliomas, OPG) (Listernick et al. 1997).

Children with neurofibromatosis type 1-associated OPG generally have impaired visual acuity, visual field loss, abnormal colour vision, pupillary abnormalities, squint, pale optic disc, proptosis, and hypothalamic dysfunction. The majority of symptomatic OPG are children under 7 years; however older individuals rarely require medical intervention (Listernick et al. 2004; Listernick et al. 1997).

### **1.5.5. Orthopaedic problems**

Bone lesions in individuals with neurofibromatosis type 1 include short stature, bowing of the long bones particularly tibial pseudoarthrosis (a false joint), dystrophic scoliosis, and sphenoid wing dysplasia (Friedman 2002). Pathologic fractures often occur due to cortical bone thinning. Surgery is needed and sometimes amputation is required. Pseudoarthrosis results from repeated fractures and defective healing (Alwan et al. 2007).

Neurofibromatosis type 1 children should undergo yearly assessment of the spine aiming for early detection of scoliosis which affects 10% to 26% of neurofibromatosis type 1 patients (Dulai et al. 2007). Scoliosis is either idiopathic or dystrophic, dystrophic scoliosis is more severe and is marked by rapid progression, distortion of the vertebral bodies and ribs and the need for early spinal fusion (Yilmaz et al. 2007; Akbarnia et al. 1992).

### **1.5.6. Cardiovascular abnormalities in neurofibromatosis type 1**

Cardiovascular manifestations of neurofibromatosis type 1 include congenital heart disease, especially pulmonary stenosis, vasculopathy, and hypertension (Friedman et al. 2002).

At diagnosis, a careful examination of the heart should be undertaken with auscultation and blood pressure measurement and if murmur is present, the

child should be evaluated by a cardiologist for a cardiology opinion and echocardiography (Friedman et al. 2002).

### **1.5.7. Glomus tumours**

Glomus bodies are small, encapsulated arteriovenous anastomoses in the dermis, commonly occur in the fingertips. The glomus tumour is usually solitary but multiple lesions have been observed in neurofibromatosis type 1 individuals. The lesion is located most frequently under the fingernail and presents with pain, cold sensitivity, and localised tenderness. Glomus tumour symptoms should be differentiated from those caused by subcutaneous neurofibromas and the treatment is local excision of the tumour. Despite it is a rare condition, it should be recognised as an integral component of the neurofibromatosis type 1 spectrum of disease (Brems et al. 2009).

## 1.6. Malignant transformation of neurofibroma to MPNST

Individuals with neurofibromatosis type 1 have an 8%–13% lifetime risk of developing MPNST (Evans et al. 2002). Most MPNSTs arise in plexiform neurofibroma. Cutaneous and subcutaneous neurofibromas have lower risk of malignant transformation with subcutaneous neurofibromas carry a relatively high risk of malignant transformation than cutaneous neurofibroma (Riccardi 2007; Tucker et al. 2005).

### 1.6.1. Genetic mechanisms

The molecular mechanisms which lead to malignant progression of neurofibromas to MPNST are largely unknown (Dasgupta 2003), although some genetic events have been implicated in this process.

*TP53* mutations have been reported in some MPNSTs but not in neurofibromas (Upadhyaya et al. 2008; Birindelli et al. 2001; Verdijk et al. 2010; Legius et al. 1994; Menon et al. 1990). Upadhyaya et al. used DNA from 20 tumours and found evidence for loss of heterozygosity (LOH) across the *TP53* region in 11 samples, with novel *TP53* point mutations were also identified in four tumours (Upadhyaya et al. 2008). Holtkamp et al. detected *TP53* mutation in only 11% of MPNST and this was associated with high-grade tumours. In addition metastasis was linked to *TP53* Pro (72) polymorphism (Holtkamp et al. 2007). However, Lothe and colleagues have

analysed 16 MPNSTs (11 patients with neurofibromatosis type 1 and 5 sporadic cases) for mutations in the coding sequence of the *TP53* gene (exons 2–11) and found none of their MPNSTs harboured mutations (Lothe et al. 2001). Verdijk et al. tested *TP53* mutations in 72 MPNST tumours and detected *TP53* mutations in 24% of the tumours tested (Verdijk et al. 2010). From all the above, I can conclude that the extent of *TP53* mutation in human MPNST samples is variable.

In animal models, a mice with cis-linked *Nf1* and *Trp53* null mutations (cis-*Nf1*<sup>+/-</sup>;*Trp53*<sup>+/-</sup> mice) develop *de novo* MPNSTs (not on top of neurofibroma) (Cichowski et al. 1999).

Using MPNST-derived cell lines Fang et al. showed that not only the cycle regulators in *Rb1*-cyclin D1 and the p53 pathways but also the cyclin activators of CDKs and inhibitory proteins such as p16 are involved in their uncontrolled proliferation (Fang et al. 2009). *P16*<sup>INK4A</sup> (*CDKN2A*) inactivation is identified using immunohistochemistry in 50% of malignant peripheral nerve sheath tumours (Nielsen et al. 1999). Kourea et al. detected *P16*<sup>INK4A</sup> deletions in 4 out of 8 patients with MPNSTs studied but no deletion detected in neurofibromas (Kourea et al. 1999). Perry et al. studied the genetic changes in MPNST compared to benign nerve sheath tumours and detected p16 deletions in 75% of MPNSTs, but not in benign nerve sheath tumours (Perry et al. 2002).

Gregorian et al. showed that K-RAS activation in combination with a single *Pten* allele deletion prompted 100% penetrable development of neurofibroma lesions and resulting progression to MPNST. Vially, loss or decrease in PTEN expression was found in all murine MPNSTs and in most of human neurofibromatosis type 1-related MPNST lesions, recommending that PTEN dose and its controlled signaling pathways are critical for change of neurofibromas to MPNST (Gregorian et al. 2009).

In another study, Keng et al. created transgenic mice that lack both *Pten* and *Nf1* in Schwann cells and found that that complete loss of *Pten* accelerated neurofibroma development and led to the development of higher grade MPNSTs in the context of *Nf1* loss compared to the control (WT) mice. They also showed that genetic analysis of human MPNSTs also showed downregulation of PTEN expression (Keng et al. 2012).

Alterations of gene expression have been identified through a variety of different genome-wide analyses using different platform technologies including gene expression microarray (Henderson et al. 2005; Miller et al. 2006; Subramanian et al. 2010), microRNA (miRNA) array (Subramanian et al. 2010; Itani et al. 2012; Masliah-Planchon et al. 2013) or methylome analysis (Feber et al. 2011). Mo et al. (2013) showed that the chemokine receptor CXCR4 and its ligand, CXCL12, promote MPNST growth by stimulating cyclin D1 expression and cell-cycle progression through PI3-kinase (PI3K) and  $\beta$ -catenin signalling (Mo et al. 2013).

Rahrmann et al. compared human data sets and identified many cooperating mutations that are enriched in Wnt/ $\beta$ -catenin, PI3K-AKT-mTOR, and growth factor receptor signaling pathways. They also showed that Foxr2 (encoding fork head box R2) is involved in MPNST growth maintenance (Rahrmann et al. 2013).

Recently, *SUZ12* has been suggested to have a role in malignant progression of neurofibroma to MPNST where Zhang et al. performed targeted sequencing on 50 MPNST cases. They found that 16 MPNST cases have *SUZ12* mutation however none of the neurofibroma cases was mutant for *SUZ12* (M. Zhang et al. 2014). Lee et al. identified highly frequent loss of function somatic mutations in Polycomb repressive complex 2 (PRC2) components (*SUZ12* and *EED*) in MPNSTs but not in neurofibromas (Lee et al. 2014). In another report De Raedet et al. described that *SUZ12* function as tumour suppressor by cooperating with RAS activation pathway and has a role in MPNST progression (De Raedt et al. 2014).

All the above observations suggest that progression of neurofibroma to MPNST may require many cooperating genomic alterations. In part due to this complexity, the process of MPNST pathogenesis is still poorly understood, this is exacerbated because of its complex histopathological characteristics (Upadhyaya 2011; Sedani et al. 2012).

## **1.6.2. Epigenetic mechanisms**

Epigenetics is defined as “the field of research study of heritable modifications which able to influence gene expression in a stable manner without altering the DNA sequence” (Russo et al. 1996; Bird 2007). These modifications include histone modifications, miRNA post-transcriptional regulation and DNA methylation (Russo et al. 1996; Bird 2007). Epigenetic modifications are as important in cancer development as genetic changes (Baylin & Ohm 2006; Issa 2004; Jones & Baylin 2007; Plass et al. 2013).

As I discussed in the previous section (1.6.1) that progression of neurofibroma to MPNST may require many cooperating genomic alterations. In addition, the process of MPNST pathogenesis is still poorly understood, so I sought for epigenetic alterations that might have a role in the development and progression of nerve sheath tumours.

### **1.6.2.1. MicroRNAs**

#### **1.6.2.1.1. History and biogenesis of miRNAs**

MicroRNAs (miRNAs) are small (20 - 23 nucleotides) non-coding RNAs. MiRNAs are generally highly conserved among species (Lagos-Quintana et al. 2003). MicroRNAs are involved in fine-tuning gene expression networks controlling a wide range of biological and pathological processes. MicroRNAs can influence a wide variety of biological processes, including development, cell proliferation, differentiation and cell death (Schickel et al. 2008).

MicroRNAs regulate gene expression by hybridising to complementary target mRNAs, resulting in either translation inhibition or mRNA degradation (Ambros 2001; Bartel 2004). Guo et al. showed that the effect of miRNA is mostly on lowering mRNA level and lowered mRNA levels account for  $\geq 84\%$  of the decreased protein production in mammalian cells (Guo et al. 2010).

The first miRNA discovered was lin-4 in 1993 by Victor Ambros and colleagues in a study on *Caenorhabditis elegans* (*C. elegans*). They discovered that lin-14 was able to be regulated by a short RNA product from lin-4, a gene that transcribed a 61 nucleotide precursor that matured to a 22 nucleotide mature RNA which contained sequences partially complementary to multiple sequences in the 3' UTR of the lin-14 mRNA. This complementarity was sufficient and necessary to inhibit the translation of lin-14 mRNA (Lee et al. 1993). Seven years later the Ruvkin laboratory discovered another miRNA, let-7. They showed that let-7 directs the latter stages of *C. elegans* development in a similar manner to lin-4; let-7 represses lin-41, lin-14, lin-42, lin-28 and daf-12 mRNA during transitions in developmental stages (Reinhart et al. 2000).

### 1.6.2.1.2. MicroRNAs and Cancer

Like other developmental regulators, miRNAs have been shown to be involved in cancer. Early in miRNA research, Calin et al. (2002) detected a frequent deletion of miRNA genes miR-15 and miR-16 in 65% of B-cell chronic lymphocytic leukaemia patients (Calin et al. 2002). The link between miRNA dysregulated expression and cancer risk has since been demonstrated in different types of cancer. Breast cancer risk is found to be correlated the deregulation of miR-125b, miR-145, miR-21, and miR-155 expression (Iorio et al. 2005). In addition, lung cancer patients poor survival is correlated with up-regulation of miR-155 and downregulation of let-7a (Yanaihara et al. 2006). Recently, Que et al. demonstrated a link between glioma poor prognosis and decreased expression of miR-637 and showed an increase in glioma cell growth and invasion with decreased expression of miR-637 (Que et al. 2015). In the diagnosis of the origin of metastatic tumour, miRNAs can be suggested to be accurately used for identification of tumour tissue origin and help in classification of the poorly differentiated cancers (Rosenfeld et al. 2008).

A miRNA can act as a tumour suppressor when its functional loss can cause the malignant transformation of a normal cell. MicroRNAs with proven tumour suppressor functions are miR-15, miR-16, miR-29 family, and let-7 (Cimmino et al. 2005; S. M. Johnson et al. 2005; Mott et al. 2007). Cimmino et al. showed that miR-15 and miR-16 induce apoptosis by targeting BCL2 in BCL2-overexpressing chronic lymphocytic leukaemia (Cimmino et al. 2005).

Johnson et al. showed that let-7 regulate RAS genes in lung cancer by targeting let-60/RAS 3' UTR, furthermore, let-7 expression is lower in lung tumours compared to normal lung tissue, while RAS protein is significantly higher in lung tumours (S. M. Johnson et al. 2005). Mott et al. identified that miR-29 family targets Mcl-1 mRNA and miR-29b was downregulated in malignant cells which is consistent with the upregulation of Mcl-1 protein (Mott et al. 2007). miR-29b was also found to be regulating angiogenesis, invasion, and metastasis of hepatocellular carcinoma partly through MMP2 suppression (Fang et al. 2011). In addition, miR-155 has shown a tumour suppressor role in acute cell leukaemia through induction of apoptosis and suggested that miR-155 can be used as a target for therapy in future (Alizadeh et al. 2014). miR-145 was downregulated in a stepwise way in non-tumourous gastric mucosa, primary gastric cancers, and their secondary metastases. In addition, ectopic expression of miR-145 suppresses gastric cancer cell migration and invasion (Gao et al. 2013). Decreased expression of miR-637 stimulated increase in glioma cell growth and invasion through targeting RAC-alpha serine/threonine-protein kinase (Akt1) protein (Que et al. 2015). In hepatocellular carcinoma, miR-7 inhibits tumorigenesis and metastasis through targeting PIK3CD, mTOR, and p70S6K (Fang et al. 2012). Wang et al. showed that miR-194 acts as a tumour suppressor in colorectal cancer by regulating the MAP4K4/c-Jun/MDM2 signaling pathway and can serve as a target for colorectal cancer prevention and therapy (Wang et al. 2015).

Some other miRNAs, such as miR-21 and miR-155, act as oncogenes in different types of cancer (Kluiver et al. 2005; Chan et al. 2005; Medina et al. 2010; Valeri et al. 2010). Chan et al. showed that miR-21 acts as an anti-apoptotic factor in human glioblastoma (Chan et al. 2005). miR-21 overexpression caused a pre-B malignant lymphoid like phenotype, while inactivation of miR-21 in the same model caused apoptosis and tumour suppression (Medina et al. 2010). miR-155 is highly expressed in Hodgkin's, primary mediastinal and diffuse large B cell lymphomas (Kluiver et al. 2005). In colorectal cancer miR-155 repress the expression of the core MMR proteins, hMSH2, hMSH6, and hMLH1, inducing a mutator phenotype, and subsequently interferes with the process of mismatch repair (Valeri et al. 2010). In colorectal Cancer miR-301a, which is upregulated, was found to function as an oncogene and promote cell growth and Invasion through targeting SOCS6 (Suppressor of cytokine signaling 6) protein (Fang et al. 2015).

### 1.6.2.1.3. MicroRNA and nerve sheath tumours

The role of miRNAs in the development of peripheral nerve sheath tumours in the context of neurofibromatosis type 1 has rarely been discussed. In 2010, Subramanian et al. published a report on miRNA expression profiling for 482 known and predicted human miRNA on 23 peripheral nerve sheath tumours (6 MPNSTs, 11 neurofibromas, and 6 schwannomas). Not all of the tumours were obtained from patients with neurofibromatosis type 1. Five miRNAs (miR-214, miR-377, miR-409-3p, miR-487b, and miR-99b) were relatively up-regulated and five miRNAs (miR-517, miR-34a, miR-29a, miR-30e-5p, and miR-27a) were downregulated in MPNST compared to neurofibromas (Subramanian et al. 2010). In addition, gene expression profiling performed on the same samples showed that the majority of MPNSTs selected for miRNA profiling in this study showed the gene signature for p53 inactivation. Because p53 is a transcription factor and miR-34a is one of the known direct transcriptional targets of p53, they selected miR-34a for further functional characterisation. Forced expression of either p53 or its direct transcriptional target miR-34a in the MPNST-14 cell line induced apoptosis in these MPNST cells, thereby demonstrating that the expression of p53 mediates its effect through its target miR-34a. They also showed that the effect of miR-34a on apoptosis is mediated through targeting MYCN, E2F, and CDK4 whereas the expression of these genes in suppressed in miR-34a transfected MPNST cells. Subramanian et al. also showed that overexpressing wild-type p53 in the MPNST cell line caused a

significant increase in the levels of miR-34a, miR-34b, miR-34c, miR-638, miR-373\*, miR-492, miR-126, miR-140, miR-491, and miR-296; confirming that in MPNST, miR-34a expression is dependent on p53 activation status (Subramanian et al. 2010).

Lee et al. exploited the findings from the functional studies of Subramanian et al., employing a computational systems biology approach, identified a regulatory network which involves E2F7/E2F8 transcription factors in several cell cycle related gene modules. They hypothesised that the interactions between E2F7/E2F8 and gene modules in the network are probably indirect since their expression levels are all increased after miR-34a overexpression. They concluded that the biological activities associated with p53/miR-34a that are commonly observed in cancers, including MPNST may also be mediated through the imbalance of the E2F transcription factor activities. This raises the possibility of modulating the interactions between miR-34a and *E2F* transcription factor family in cancer treatment (Lee et al. 2012).

The loss of NF1 function is usually by bi-allelic inactivation that is classically brought about by a inactivation mutation of one allele followed by a second hit of inactivation mutation of the second wild-type allele in the tumour tissue (Berger et al. 2011). Chai et al. (2010) hypothesised that one of the two hits needed for the loss of function might result from silencing by a miRNA. There is good evidence that other tumour suppressor genes, including p53, can be silenced by a similar mechanism (Swarbrick et al. 2010). Chai et al performed a comparison between the neurofibromatosis type 1-associated

MPNST cell line (ST88-14) versus sporadic MPNST cell line (STS26T). Results showed that the oncogenic miRNAs, miR-10b, miR-155, and miR-335, exhibited selective higher expression in ST88-14. However, expression of let-7 family members, let-7a-f, known to target RAS, was significantly lower in ST88-14 than in STS26T cells. They also tested the expression level of miR-10b in human samples and showed that the expression level of miR-10b was significantly higher in comparison to benign neurofibromas in the setting of neurofibromatosis type 1 but not in sporadic MPNSTs, while let-7a and let-7b were significantly lower in both neurofibromatosis type 1 MPNSTs and sporadic MPNSTs. In addition, the expression level of miR-10b was significantly higher in neurofibromatosis type 1 MPNSTs than in sporadic MPNSTs although slightly elevated. However, insignificant expression levels of miR-335 and miR-155 were observed in neurofibromatosis type 1 MPNSTs compared with in sporadic MPNSTs. To summarise, the expression of miR-10b is higher in neurofibromatosis type 1 MPNST samples and cell lines compared to sporadic MPNSTs. Next, Chai et al. (2010) investigated the functional significance of the deregulated miRNAs observed from the previous experiment by transfecting ST88-14 cells with antisense inhibitors (miR-10b, miR-155, and miR-335), mimic enhancers let-7a, or with negative controls. Results showed that inhibiting miR-10b expression in ST8814 cells significantly decreased cell proliferation, migration, and invasion (Chai et al. 2010).

A tumour suppressor role is suggested for miR-204, which is downregulated in MPNST human samples and cell line. Restoration of miR-204 in MPNST cell lines *In vitro*, significantly suppressed cell proliferation migration and invasion. In addition, further *in vivo* study showed that Restoration of miR-204 expression in STS26T suppressed tumour growth and malignant progression. They reported that these functions for miR-204 are through inhibition of RAS signalling by targeting *HMGA2* (Gong et al. 2012).

On that other hand, an oncogenic role is suggested for miR-210 through targeting ephrin-A3 (*EFNA3*) which has been proved to be a target of miR-210. *In vitro* overexpression of miR-210 in MPNST cell line increased cellular viability, colony formation, S phase percentage, and invasiveness of MPNST cells. However, suppression of miR-210 expression decreased proliferation and invasion of MPNST cells (Z. Wang et al. 2013).

Itani et al. (2012) examined the miRNA expression profile of six MPNSTs with those of six neurofibromas. Results showed that miR-21, miR-135b, miR-152, miR-130b, miR-92, and miR-15b were upregulated in MPNST compared to neurofibromas, whereas the expression levels of miR-125b, miR-127, and miR-302d were downregulated in MPNST compared to neurofibromas. They focused their research on miR-21 and found that transfection of miR-21 inhibitor significantly increased caspase activity, suppressed cell growth, and upregulated protein level of PDCD4, indicating that miR-21 inhibitor could induce cell apoptosis of MPNST cells (Itani et al. 2012).

Another study analysed miRNAs expression in a large panel of dermal and plexiform neurofibromas and MPNSTs. Of those that the most significantly downregulated miRNAs in MPNST relative to neurofibroma were miR-139-5p, miR-150, miR-338-3p, miR-195, miR-146a, miR-95, let7b, miR-186, miR885-5p and miR-200c. However, there were also a number of upregulated miRNAs in MPNST relative to neurofibroma including miR-301a, miR-301b, miR-9, miR-19a, miR-106b, miR-135a and miR-10b (Masliah-Planchon et al. 2013).

From the above it can be concluded that miRNA expression in nerve sheath tumour has been studied in few studies, which show different expression profiles. These discrepancy in results can be explained by differences in the methodologies used (different miRNA expression platform) or to the use of different groups of patients based on differences in *NF1* diagnostic criteria.

## **1.6.2.2. DNA methylation**

### **1.6.2.2.1. Regulation of gene expression through**

#### **DNA methylation**

DNA methylation is a covalent modification of the cytosine ring at the 5' position of a CpG dinucleotide, where a methyl group is added on the carbon 5 of that ring using S-adenosyl methionine as a methyl donor. In the DNA replication process, transfer of methyl group reaction is catalysed by DNA methyltransferases (DNMTs) present at the replication fork during the S-phase (Klose & Bird 2006).

The usual targets of DNA methylation in mammals, CpG dinucleotides, are scattered throughout the genome (Glass et al. 2007). Recently, abundant DNA methylation in non-CpG contexts has been described at a genome-wide level in stem cells and some other mammalian cells; however CpG dinucleotides remain the primary site for DNA methylation in mammals (Lister et al. 2009; Pinney 2014).

CpG islands (CGIs) are areas of the genome where a high concentration of these CpG dinucleotides are found (Illingworth & Bird 2009). The average CGI is about 1000 base pairs and approximately 50% of genes have one or more CpG islands in the 5' promoter region. In a non-neoplastic differentiated cell, CpG loci are highly methylated genome-wide; except for the promoter

CGIs, which are generally not methylated (Jones 2012; Illingworth & Bird 2009).

One of the mechanism of silencing by DNA methylation is through direct inhibition of transcription factors binding to their target sites using the methyl-binding domain (MBDs) proteins (Klose & Bird 2006). The second possible mechanism is that methyl-CpG binding proteins (MBPs), that one family of proteins that recognise methyl-CpG and cause repressive effect on methylated DNA (Kass et al. 1997; Qu et al. 2013).

Ball et al. observed a pattern of low promoter methylation coupled with high gene body methylation in highly expressed genes and confirmed that gene body methylation in highly expressed genes is a consistent phenomenon over the entire genome (Ball et al. 2009). One of the most commonly cited features of cancer DNA methylation concerns directional hypomethylation of DNA satellite repeats (Ehrlich 2002; Wilson et al. 2007).

#### **1.6.2.2.2. DNA methyltransferases (DNMTs)**

In mammals, DNA is methylated by a group of enzymes called DNMT1, DNMT3A, and DNMT3B. A further protein in this family lacks catalytic activity and is called DNMT3L (DNA methyltransferase 3-like). I will discuss each of these important methylation regulators here in the context of cancer and MPNST.

DNMT1 is responsible for maintenance of methylation and is therefore called the “maintenance methyltransferase.” DNMT1 prefers to target the hemimethylated DNA (with methylation of only one DNA strand) 10 fold more than the unmethylated strand. The function of DNMT1 in the cell is to keep the DNA methylation status stable throughout cell division (Jones & Liang 2009), whereas DNMT3A and DNMT3B methylate previously unmethylated DNA in the mammalian cell, hence called *de novo* methyltransferases (Okano et al. 1999).

#### **1.6.2.2.3. DNA methylation and neurofibroma/MPNST**

Tumour development is a result of the activation of oncogenic and/or inactivation of tumour suppressor pathways. The hypermethylation of the promoters of tumour suppressor genes and the hypomethylation of the promoters of oncogenes have been shown to represent a distinct molecular pathway leading to cellular malignant transformation. DNA methylation silences a tumour suppressor gene in an equivalent manner to silencing the expression of genes through genetic changes (Baylin & Ohm 2006; Issa 2004; Jones & Baylin 2007). The role of aberrant DNA methylation in the development and progression of human cancer has been studied in several tumours including breast, lung and colorectal cancers (Barault et al. 2008; Ordway et al. 2007; Vaissière et al. 2010) .

In the past 30 years, there was much improvement in the technology to investigate DNA methylation. The first generation of methylation detection assays employed the digestion of genomic DNA with a methylation-sensitive restriction enzyme followed by either Southern blot analysis or PCR (Singer-Sam et al. 1990) but these techniques have some limitations leading to the generation of false positive results due to incomplete digestion.

A second generation of techniques uses bisulfite treatment of genomic DNA to convert unmethylated cytosines to uracils, while methylated cytosine residues will remain intact (Frommer et al. 1992). The bisulfite converted DNA can then be analysed either by methylation-specific PCR (MSP) or bisulfite sequencing. In MSP, PCR amplification was performed with primers that anneal specifically with either the converted methylated or converted unmethylated sequence (Herman et al. 1996). In contrast, in bisulfite sequencing the PCR reaction is undertaken by primers that do not themselves cover any CpG dinucleotides sites in the original genomic DNA (Frommer et al. 1992; Clark et al. 1994; Clark et al. 2006). A quantitative bisulfite sequencing method is called pyrosequencing, which produce quantifiable signals per each CpG being measured. Pyrosequencing has the disadvantage of allowing evaluation of only short regions (average 150 bp) per amplicon (Tost & Gut 2007; Shanmuganathan et al. 2013). One of the recent approaches to test regional DNA methylation changes at a genome-wide scale is MeDIP sequencing which is based on the chromatin immunoprecipitation of methylated fragments (Weber et al. 2005). With this method,

methylated DNA is enriched from an initial DNA sample through immunoprecipitation with an anti-methylcytosine antibody (MeDIP). DNA samples enriched for methylated DNA are then hybridised to microarray chips (MeDIP-Chip) for identification of the locations with DNA methylation (Shanmuganathan et al. 2013; Weber et al. 2005).

Feber et al. (2010) compared the methylome profile of neurofibromas and MPNSTs from patients with neurofibromatosis type 1 using a sequencing-based comparative methylome analysis by MeDIP-seq. Results showed that there were no significant global hypomethylation in MPNST; this is different from what has been reported for other tumour types (Zhang et al. 2012; Baylin & Ohm 2006; Issa 2004). However, satellite repeats showed a highly significant ( $p < 0.001$ ) directional difference DNA methylation, suggesting these repeats represent the main target for hypomethylation in MPNST (Feber et al. 2011).

## 1.7. Aims

At present, there are no available markers either immunohistochemical, genetic or epigenetic to make this distinguish benign neurofibroma from MPNST. Therefore, from a clinical diagnostic and management perspective, one of the immediate needs is to identify molecular alterations that drive and/or are associated with this progression of this disease to use as candidate prognostic biomarkers for subsequent validation in clinical trials.

In this thesis, the difference in miRNA expression between neurofibroma and MPNST will be tested with the aim of discovering if miRNAs have a role in transformation for neurofibroma to MPNST. In addition, the differences in DNA methylation between neurofibroma and MPNST based on the methylome analysis performed previously by my colleagues will be assessed (Feber et al. 2011). The relation between miRNA expression and DNA methylation in nerve sheath tumours will be assessed.

## 2. Materials and methods

### 2.1. Clinical samples

All research using human tissue samples complied with standards laid down by the Central Office for Research Ethics Committees (COREC) and was approved by the relevant ethics committees under the study number (REC 07/Q0506/8). All human tissue was handled as recommended by the Human Tissue Act 2004.

Fresh frozen tissue samples from 10 neurofibromas and 10 MPNSTs were obtained from the Royal National Orthopaedic Hospital Stanmore, UK and 3 samples were kindly provided by Dr Fredrik Mertens from Lund University Hospital in Sweden. Details of the fresh frozen tissue samples used for this study are given in Table 2-1 and Table 2-2. The fresh frozen neurofibromas and MPNSTs were all from patients with neurofibromatosis 1.

35 cases of soft tissue sarcomas were also obtained from the National Orthopaedic Hospital, Stanmore. These were comprised of 4 neurofibromas, 3 MPNSTs, 4 liposarcomas, 4 osteosarcomas, 4 synovial sarcomas, 4 rhabdomyosarcomas, 3 solitary fibrous tumours, 3 fibromatosis desmoid type, 2 chondromas and 2 chondroblastomas.

Formalin fixed paraffin embedded (FFPE) tissue samples from 80 neurofibromas and 80 MPNSTs were obtained from the histopathology

archives of the Royal National Orthopaedic Hospital, Stanmore, UK. Blocks with no evidence of tissue necrosis and minimal calcification were chosen dating from 2000 to 2010. Details of the FFPE neurofibromas and MPNSTs used are given in Table 2-3 and Table 2-4 respectively.

All human tissue samples were sectioned and reviewed by a pathologist following H&E staining. Diagnosis and grading of samples was carried out in accordance with the World Health Organization (WHO) (Kleihues et al. 2002; Fletcher & Unni 2002). All MPNSTs used in this study met with one of the following inclusion criteria:

- The tumour arose from a peripheral nerve.
- The tumour arose from a benign nerve sheath tumour (neurofibroma).
- The tumour displayed histologic features of Schwann cell differentiation.
- The tumour arose in a patient with neurofibromatosis type 1 and showed the same histological features of most MPNSTs.

**Table 2-1: Neurofibroma (fresh frozen)**

Sample No.	Atypia	Classification	Aetiology
1	No	Plexiform	NF1
2	No	Plexiform	NF1
3	No	Plexiform	NF1
4	No	Plexiform	NF1
5	No	Plexiform	NF1
6	No	Plexiform	NF1
7	No	Plexiform	NF1
8	No	Plexiform	NF1
9	No	Plexiform	NF1
10	No	Plexiform	NF1

Key: NF1= neurofibromatosis type 1.

**Table 2-2: MPNST (fresh frozen)**

Sample No.	Grade	Differentiation	Aetiology
1	3	No	NF1
2	3	No	NF1
3	3	No	NF1
4	3	No	NF1
5	3	No	NF1
6	3	No	NF1
7	3	No	NF1
8	3	No	NF1
9	3	No	NF1
10	3	No	NF1

Key: NF1= neurofibromatosis type 1.

**Table 2-3: Archival neurofibromas (continued on next page)**

No.	Atypia	Classification	Aetiology	Presentation	Site	Age	Gender
1	-	N	S	P	buttock	70	M
2	-	N	S	P	forearm	22	F
3	Yes	Plexiform	NF1	P	finger		
4	-	Plexiform	NF1	R	popliteal fossa	24	M
5	-	N	S	P	cutaneous	37	F
6	Yes	N	NF1	R	multiple	47	F
7	-	N	NF1	R	arm	57	M
8	-	Plexiform	NF1	P	tibia	13	M
9	-	N	S	P	cutaneous	40	F
10	-	N	NF1	R	arm-neck	22	M
11	-	N	NF1	R	abdominal wall	27	M
12	-	N	S	P	arm	46	F
13	-	N	S	P	leg	18	F
14	-	N	S	P	buttock	29	M
15	-	N	NF1	P	cutaneous	89	F
16	Yes	N	NF1	P	leg	51	F
17	-	Plexiform	NF1	P	leg	15	
18	-	N	S	P	cutaneous		F
19	-	N	S	P	abdominal wall		M
20	-	N	S	P	arm		M
21	-	N	S	P	buttock		F
22	-	N	S	P	cutaneous		F
23	-	N	S	P	cutaneous		F
24	-	N	S	P	leg		F
25	-	N	S	P	arm		F
26	-	N	S	P	buttock		M
27	-	N	S	P	cutaneous	46	F
28	-	N	S	P	cutaneous		M
29	-	N	S	P	buttock		F
30	-	N	S	P			M
31	-	N	S	P	cutaneous		M
32	-	N	S	P	forearm		F
33	-	N	S	P			F
34	-	N	S	P	cutaneous		M
35	-	N	S	P	buttock		F
36	-	N	S	P	cutaneous		F
37	-	N	S	P	arm		M
38	-	N	S	P	arm		M
39	-	N	S	P		38	M
40	-	N	S	P	leg		M

Key: -= none; N= nodular; S= sporadic; NF1= constitutional *NF1* gene mutation; P= primary; R= recurrence; Blank box= unknown

**Table 2-3: Archival neurofibromas (continued)**

No.	Atypia	Classification	Aetiology	Presentation	Site	Age	Gender
41	Yes	Plexiform	NF1	P	cutaneous		M
42	-	N	NF1	P	cutaneous		F
43	-	N	NF1	P	arm		F
44	-	Plexiform	NF1	P	arm		M
45	-	N	S	P	buttock		F
46	Yes	Plexiform	NF1	P	arm		M
47	-	N	S	P	cutaneous		F
48	-	Plexiform	NF1	P	leg		M
49	-	N	S	P	cutaneous		F
50	-	N	S	P			F
51	-	N	NF1	P	buttock		F
52	-	Plexiform	NF1	P	arm		F
53	-	N	S	P	leg		M
54	-	Plexiform	NF1	P	cutaneous		M
55	Yes	Plexiform	NF1	P	abdominal wall		M
56	-	N	S	P	cutaneous		M
57	-	N	S	P			F
58	-	N	S	P	arm		M
59	-	N	S	P	cutaneous		M
60	-	N	S	P			M
61	-	N	S	P	ulnar nerve		M
62	-	Plexiform	NF1	P			M
63	-	No	S	P	forearm		M
64	-	Plexiform	NF1	P			M
65	-	N	S	P			M
66	-	Plexiform	NF1	P			F
67	-	N	S	P	cutaneous		F
68	-	Plexiform	NF1	P	cutaneous		M
69	-	N	NF1	P	cutaneous		
70	-	Plexiform	NF1	P			M
71	-	N	S	P			F
72	-	N	S	P	arm		F
73	-	N	S	P			F
74	-	N	S	P	leg		M
75	-	N	S	P	cutaneous		M
76	-	N	S	P			M
77	-	N	S	P			F
78	-	Plexiform	NF1	P	cutaneous		F
79	-	N	S	P			F
80	-	N	NF1	P	Lumbar	29	M

Key: -= none; N= nodular; S= sporadic; NF1= constitutional *NF1* gene mutation; P= primary; R= recurrence; Blank box= unknown

**Table 2-4: Archival MPNSTs (continued on next page)**

No.	Grade	Differentiation	Aetiolo gy	Presentation	Site	Age	Sex
1	1	-	S	R	leg	54	F
2	1	-	S	P	thigh	64	F
3	1	-	S	P	arm	15	F
4	1	-	S	P	paraspinal (lumbar)	23	F
5	2	-	S	R	brachial plexus	38	F
6	2	Epithelioid	S	P	elbow	69	M
7	2	-	S	P	thigh	24	F
8	2	-	S	P	shoulder	63	M
9	2	-	S	P	big toe	56	F
10	2	-	S	P	paraspinal (lumbar)	16	M
11	2	-	S	P	thigh	60	F
12	2	-	S	P	paraspinal (cervical)	34	M
13	2	-	S	P	forearm	12	M
14	2	-	S	P	leg	64	F
15	2	-	NF1	P	leg	28	F
16	2	-	S	R	shoulder	31	F
17	2	-	NF1	R	paraspinal (lumbar)	43	F
18	2	-	S	P	forearm	73	F
19	2	-	S	P	forearm	25	M
20	2	-	S	P	buttock	19	F
21	2	Trition	S	P	thigh	52	F
22	2	Trition	S	R	buttock	16	M
23	2	-	NF1	P	thigh	43	F
24	2	-	NF1	P	brachial plexus	12	M
25	3	Trition	S	P	thigh	35	M
26	3	-	S	P	thigh	62	M
27	3	-	S	R	arm	21	F
28	3	-	S	P	thigh	73	M
29	3	-	S	P	arm	5	F
30	3	Trition	S	P	pelvis	24	F
31	3	Osteosarcomatous	S	P	thigh	72	M
32	3	-	S	R	leg	44	F
33	3	-	S	P	brachial plexus	37	M
34	3	-	S	R	paraspinal (lumbar)	71	M
35	3	-	S	P	brachial plexus	50	M
36	3	-	NF1	P	sacrum	19	F
37	3	-	S	P	iliac fossa /abdominal wall	25	F
38	3	-	NF1	R	buttock	32	M
39	3	Trition	S	P	thigh	78	M
40	3	-	S	P	thigh	52	M

Key: -= none; S= sporadic; NF1= constitutional NF1 gene mutation; P= primary; R= recurrence; Blank box= unknown

**Table 2-4: Archival MPNSTs (continued)**

No.	Grade	Differentiation	Aetiology	Presentation	Site	Age	Sex
41	3	No	S	P	arm	64	M
42	3	No	S	R	paraspinal (lumbar)	18	M
43	3	No	S	R	paraspinal (thoracic)	27	M
44	3	No	S	R	arm	62	F
45	3	No	NF1	R	leg	20	F
46	3	No	NF1	P	arm	61	F
47	3	Epithelioid	NF1	R	thigh	63	F
48	3	No	NF1	P	brachial plexus	35	F
49	3	No	NF1	P	pelvis	54	F
50	3	No	S		knee	23	M
51	3	No	S	R	knee	NK	M
52	3	No	S	R	pelvis	30	F
53	3	No	NF1	R	back	58	M
54	3	No	S	R	chest wall	94	F
55	3	No	S	R	paraspinal (lumbar)	16	M
56	3	No	S	R	paraspinal lumbar	25	M
57	3	No	S	R	chest wall	61	F
58	3	Trition	S	P	chest wall	58	F
59	3	No	S	P	forearm	52	F
60	3	No	S	P	wrist	84	F
61	3	Trition	S	R	thigh	62	M
62	3	No	NF1	P	buttock	49	M
63	3	No	S	P	arm	52	F
64	3	No	S	R	arm	78	F
65	3	No	NF1	P	leg	49	F
66	3	No	S	P	chest wall	46	M
67	3	No	S	P	forearm	68	F
68	3	Trition	S	R	thigh	30	M
69	3	No	S	P	popliteal fossa	48	F
70	3	No	S	P	paraspinal	57	F
71	3	No	S	P	arm (brachial plexus)	60	F
72	3	No	S	P	thigh	36	M
73	3	No	S	R	leg	44	F
74	3	No	S	P	arm	27	F
75	3	No	S	P	buttock	36	F
76	3	No	NF1	P	thigh	26	F
77	3	Trition	S	P	paraspinal	41	M
78	3	No	S	P	thigh	43	M
79	3	No	S	P	thigh	72	M
80	3	Epithelioid	S	Re-existence	brachial plexus	34	M

Key: -= none; S= sporadic; NF1= constitutional NF1 gene mutation; P= primary;  
R= recurrence; Blank box= unknown

## 2.2. Cell Lines

### 2.2.1. MPNST-derived cell line sNF96.2

The human MPNST-derived cell line sNF96.2 was kindly provided by Dr Abhijit Guha from The Hospital for Sick Children, Toronto, Ontario, Canada. The cell line was originally derived from a nerve tissue-associated recurrent mass diagnosed as MPNST in a neurofibromatosis type 1 patient. The cell line is karyotypically abnormal with complete LOH (no detection of the remaining *NF1* allele) and a mutation in exon 21 (3683delC) of the identified *NF1* germline causing a frameshift which leads to a premature stop codon (Perrin et al. 2007). The reported germline mutation in exon 21 (3683delC) and loss of the remaining wild-type (WT) allele in the cell line were confirmed before use in my study. The presence/absence was compared to HT1080 WT for *NF1* (Table 2-5 for primers sequences).

**Table 2-5: List of primer sequences used for direct sequencing *NF1* gene**

Primer Name	Primer Sequence (5' -> 3')
NF1-exon21-Forward	TTGCATCTGTTTGTCCACATT
NF1-exon21-Reverse	CACTTTTCTTCCCCGCTTAC

### 2.2.1. Other cell lines

The HT1080 and HEK293T cell lines were originally purchased by our lab from the American Type Culture Collection (ATCC). These cell lines were used for various experiments detailed below.

## **2.3. RNA extraction from frozen cells sections and cell lines**

### **2.3.1. MiRNeasy Mini Kit (Qiagen)**

Total RNA was extracted from fresh frozen tissue and cell lines using the miRNeasy extraction kit (Qiagen Ltd, Crawley, West Sussex, UK), following the manufacturer's instructions. This kit allows the extract of all RNA species including the small RNA fraction containing miRNAs amongst others.

Before starting any RNA extraction, the bench surface and Pipettes were all cleaned with RNaseZAP (Ambion) and all precautions necessary were taken throughout RNA extraction procedure to avoid RNA degradation. RNA extractions were carried out on an RNA dedicated area. In addition, a separate set of pipettes was devoted for RNA extraction, and aerosol barrier pipette tips were used.

For the fresh frozen tissue, between 20 to 30 tissue sections, 20 µm thick were used for RNA extraction. Every 10<sup>th</sup> section was stained with H&E and examined by a pathologist to ensure that all sections used for RNA extraction were comprised of at least 70% tumour cells. The fresh frozen sections were placed in Eppendorf tubes containing 700 µl of Qiazol lysis reagent and the tubes were then vortexed for 15 seconds to disrupt the cells before freezing at -80 °C.

Subconfluent cell cultures were initially washed twice with phosphate buffered saline (PBS) and the PBS was then aspirated off using sterile Pasteur pipette. 700 µl of Qiazol reagent were added to the cells and swirled around the dish several times to lyse the cells. The lysate was then placed in a 1 ml Eppendorf tube and immediately frozen at – 80 °C.

The Qiazol treated tissues and cell cultures were stored at -80 °C for up to a maximum of 2 weeks before continuing with the RNA extraction. The lysate was then thawed, vortexed and left at room temperature for 5 minutes to promote dissociation of nucleoprotein complexes. This was followed by the addition of 140 µl of chloroform to each sample. The tube was shaken vigorously for 15 s and then left to stand at room temperature for another 2-3 minutes before spinning at 13,000 rpm, 15 minutes at 4 °C. Following the centrifugation step the sample becomes separated into three layers; an upper aqueous phase containing RNA, a white interface and a lower organic layer. The upper, aqueous layer was carefully removed and measured using a Gilson pipette before being placed in a 2 ml tube. 1.5 volumes of 100% ethanol were added to each sample and the tube was vortexed briefly to mix. 700 µl of the mix was then transferred to a miRNeasy mini spin column placed inside a collecting tube and the column was centrifuged at 10,000 rpm, 15 s at room temperature. The elute was discarded and the remainder of the sample was placed on the column which was spun again. The column was then washed by adding 350 µl of RWT buffer to the column and spinning at 10,000 rpm, for 15 s in room temperature. On column DNase digestion

was then performed by mixing 10 µl of DNase I with 70 µl of buffer RDD and pipetting the mixture directly onto the column membrane. The columns were then left at room temperature for 15 minutes. The 500 µl of RWT buffer was then pipetted into the column to wash the membrane and the column was then spun for 15 sec at 10,000 rpm, room temperature. The flow through was discarded and 500 µl of RPE buffer were added to the column which was spun again. The flow through was discarded and the column was washed by adding another 500 µl of RPE to the column and spinning for 2 minutes at 10,000 rpm to dry the column membrane. The column was then placed in a 1.5 ml Eppendorf tube and 50 µl of RNase free water was added directly to the middle of the column membrane. The RNA was then eluted from the column by spinning at 10,000 rpm for 1 minute at room temperature. The concentration and purity of the RNA elute was examined using a NanoDrop Ultra-Violet/Visible micro-volume spectrophotometer (Thermoscientific). The A<sub>260</sub>/A<sub>280</sub> and A<sub>260</sub>/A<sub>230</sub> absorption ratios as well as RNA concentration were noted and the rest of the RNA sample was then aliquoted in several smaller tubes and stored at -80 °C.

## **2.4. cDNA synthesis**

Total RNA was reverse transcribed into cDNA using the Superscript III First-Strand Synthesis kit (Invitrogen Ltd/Life Technologies Ltd, Paisley, Scotland, UK). Briefly, 200 ng of total RNA were mixed with 1 µl of 50 ng/µl random hexamers and 1 µl of 10 mM dNTP mix and the volume was made up to 10

$\mu\text{l}$  with RNase free water. The mixture was incubated at 65 °C for 5 minutes then chilled on ice for 1 minute before adding the following: 2  $\mu\text{l}$  of 10 x RT buffer, 4  $\mu\text{l}$  of 25 mM  $\text{MgCl}_2$ , 2  $\mu\text{l}$  of 0.1M DTT, 1  $\mu\text{l}$  of RNaseOUT (40U/ $\mu\text{l}$ ) and 1  $\mu\text{l}$  of SuperScript III RT (200 U/ $\mu\text{l}$ ). The mixture was incubated for 10 minutes at room temperature followed by a 50 minute incubation at 50 °C. The reaction was terminated by incubating the tube at 85 °C for 5 minutes and then chilling on ice. 1  $\mu\text{l}$  (2U) of RNase H was added to the mix and incubated at 37 °C for 20 minutes before storing at – 20 °C.

MicroRNA specific cDNA was prepared using the TaqMan® miRNA Reverse Transcription Kit (Applied Biosystems) following the manufacturers' instructions. The following master mix was prepared in a polypropylene tube by scaling up the volumes to the desired number of RT reactions: 0.15  $\mu\text{l}$  of 100 mM dNTPs, 1  $\mu\text{l}$  MultiScribe™ reverse transcriptase (50 units/ $\mu\text{l}$ ), 1.5  $\mu\text{l}$  10 x reverse transcription buffer, 0.19  $\mu\text{l}$  of RNase Inhibitor (20 units/ $\mu\text{l}$ ), 4.16  $\mu\text{l}$  nuclease-free water. For each RT reaction 7  $\mu\text{l}$  of RT master mix was mixed with 5  $\mu\text{l}$  RNA (1 ng/ $\mu\text{l}$ ) and 3  $\mu\text{l}$  of 5 x RT primer (custom made by Applied biosystems) in a separate tube on ice. The reaction components were mixed thoroughly by inverting then placed on a thermal cycler which was programmed to run for 30 minutes at 16 °C, 30 minutes at 42 °C and 5 minutes at 85 °C followed by an infinite hold at 4 °C. All RT samples were stored at -20 °C until ready for use.

## **2.5. Quantitative Reverse Transcription polymerase chain reaction (qRT-PCR)**

### **2.5.1. Quantitative PCR with double-stranded DNA-binding dyes as reporters (SYBR Green assay) to test gene expression**

qRT-PCRs were carried in Microamp optical 96-well plates (Applied Biosystems, Birchwood, Warrington, UK) using SYBR green PCR Master Mix (Applied Biosystems). The following qRT-PCR master mix was prepared in a polypropylene tube by scaling up the volumes to the desired number of PCR reactions: 12.5 µl of SYBR green PCR Master Mix, 0.75 µl of each forward and reverse oligonucleotide primer (10 µM), 10 µl nuclease-free H<sub>2</sub>O and 1 µl of template cDNA (prepared using Superscript III First-Strand Synthesis kit). Thermal cycling was carried out on a Realplex4 Mastercycler (Eppendorf, Cambridge, UK) using a 520 nm filter and the following thermal cycling profile: 10 minutes at 95 °C followed by 40 cycles of 15 s at 95 °C and 1 minute at 60 °C followed by a final ramping step to generate a melt curve. All reactions were performed in duplicate.

The different primers used for qRT-PCR are shown in Table 2-6. All Primers were designed using the online software Universal Probe Library Assay Design Centre (Roche, Burgess Hill, UK).

The mRNA expression of the gene of interest in human samples was quantified using  $2^{-\Delta\text{Ct}}$  method (Livak & Schmittgen 2001; Schmittgen & Livak 2008). The relative gene expression level in cell lines was determined using the comparative Ct method ( $2^{-\Delta\Delta\text{Ct}}$ ) and normalised to *GAPDH* housekeeping gene.

The forward and reverse primer concentration was optimised for amplification efficiency and primer-dimer formation monitored by a ramping step (melting curve).

**Table 2-6: List of primer sequences used for qRT-PCR**

Primer name	Primer Sequence (5' -> 3')
NF1-Forward	ATTA CTT CAG CAAG GCC ATG TTAG
NF1-Reverse	AAG GAT TTG CTAT GTGCC AGGG AC
COL1A1-Forward	GGG ATT CCCT GGAC CTA AAG
COL1A1-Reverse	GGA ACAC CT CGCT CTCCA
COL5A2-Forward	TGGA ATCCCT GGAC CCAT TT
COL5A2-Reverse	CCT TCTT TACCT GAAG GACCAA
COL21A1-Forward	GCAT GTGAG ATT CCT GGATT TA
COL21A1-Reverse	GTTTT CCCG GAG GACA AATAC
COL4A1-Forward	GTAT TTTT CACAC GTAAG CACATT CG
COL4A1-Reverse	CCCT GCTG AGGT CTGT GAACA
COL4A2-Forward	GTGG CCAAT CACT GGTGT CA
COL4A2-Reverse	CCTCC ATTGC ATT CGAT GAA
ROBO1 Forward	GCGT GCAG TACTA AGGGA ACA
ROBO1 Reverse	GGCT TCTT ACAT GAAC ATAAT GAA
TGFB3-Forward	TCAG CCTCTCTCTGTCCACTT
TGFB3-Reverse	CATCAC CGTTGGCTCAGGG
MMP2-Forward	CCACT GCCTTCGATACAC
MMP2-Reverse	GAGCC ACTCTCTGGAATCTTAAA
MMP-9 Forward	GGGAC GCAGACATCGTCATC
MMP-9 Reverse	TCGTCATCGTCGAAATGGGC
DNMT3A Forward	AGTACGACGACGACGGCTA
DNMT3A Reverse	CACACTCCACGCAAAAGCAC
DNMT3B Forward	CCCATTTGACTTGGTGATTGGC
DNMT3B Reverse	CCGGCCTGTACCCTCATA C
WT1 Forward	CACAGCACAGGGTACGAGAG
WT1 Reverse	CAAGAGTCGGGGCTACTCCA
S100B Forward	TGGCCCTCATCGACGTTTTTC
S100B Reverse	ATGTTCAAAGAACTCGTGGCA
GAPDH Forward	GGAGTCAACGGATTTGGTCGTA
GAPDH Reverse	GGCAACAATATCCACTTTACCAGAGT

## 2.5.2. Fluorescent reporter probe methods

### (Quantitation of microRNA by TaqMan assay)

MicroRNA expression in each sample, and the cell line, was measured using TaqMan microRNA assays technology (Applied Biosystems) on Realplex4 Mastercycler (Eppendorf). This qRT-PCR method specifically detects mature microRNA, but not precursor microRNA. The TaqMan assay was performed using the same amount of total RNA (5 ng) that was transcribed into cDNA (Applied Biosystems), and Ct-values were recorded. An internal control small RNA, RNU66 was used to normalise the microRNA expression data for each sample (Applied Biosystems). The amplification step was performed in a Microamp optical 96-well plate (Applied Biosystems). Each well contained 1.33  $\mu$ l of template DNA and a reaction master mix containing 10  $\mu$ l TaqMan Universal PCR master Mix II (Applied Biosystems), 1  $\mu$ l of the probe and 7.67  $\mu$ l Nuclease free water. The amplification was performed on Realplex4 Mastercycler (Eppendorf), with a first step at 95 °C for 10 minutes and then 40 cycles with 95 °C for 15 s, 60 °C for 1 minute with a fluorescent reading at the end of this step (FAM dye, 520 nM filter and VIC dye, 550 nM). The expression of the miRNA of interest in human samples was quantified using  $2^{-\Delta\text{CT}}$  method (Livak & Schmittgen 2001; Schmittgen & Livak 2008). The relative gene expression level in cell line was determined using the comparative Ct method ( $2^{-\Delta\Delta\text{CT}}$ ) (Livak & Schmittgen 2001; Schmittgen & Livak 2008), relative to the housekeeping RNU66. All qPCR assays were run with appropriate controls including the Non-Template Control (NTC).

## **2.6. Cell culture**

### **2.6.1. Thawing cells from liquid nitrogen**

Cells retrieved from liquid nitrogen were thawed by placing the cryovial in a 37 °C water bath. The thawed cell suspension was then added to a tube containing 10 ml of the appropriate cell culture medium and spun at 1200 rpm for 5 minutes, room temperature, to pellet the cells. The supernatant was then removed and the cell pellet was resuspended in 1 ml of fresh culture medium. The cell suspension was then added to a 75 cm<sup>2</sup> tissue culture flasks containing 10 ml of the appropriate culture medium which had been pre-warmed to 37 °C.

### **2.6.2. Cell maintenance**

sNF96.2 cells were grown in Dulbecco's Modified Eagle Medium (DMEM) (Invitrogen) supplemented with 10% Fetal bovine serum (FBS) (GIBCO), 100 U/ml penicillin G and 100 µg/ml streptomycin (Invitrogen). The cultures were maintained in a 37 °C incubator with 5% CO<sub>2</sub> and high humidity.

HT1080 and HEK293T cell cultures were maintained in RPMI media supplemented with 10% fetal bovine serum (FBS) (GIBCO), 100 U/ml penicillin G and 100 µg/ml streptomycin (Invitrogen). The cultures were maintained in a 37 °C incubator with 5% CO<sub>2</sub> and high humidity.

### **2.6.3. Cell trypsinisation**

Cells cultures were passaged 1 in 4 when they reached 80% - 90% confluence using Tyrpsin-EDTA (GIBCO). 1:3 to 1:10, depending of their growth rate, two to three times a week.

### **2.6.4. Freezing cells in liquid nitrogen**

Cells were stored frozen in FBS supplemented with 10% DMSO at a density of 1 to 3 million per ml. Cells were trypsinised from 75 cm<sup>2</sup> tissue culture flasks and washed in PBS, spun, then placed in cryovials containing 1 ml of FBS with 10% DMSO. Then the vials are placed in an alcohol-graded freezing container(s) and put in a -80 °C freezer. (The isopropanol allows the vial temperature to decrease at 1 °C /min) and left to freeze overnight. For long-term storage (> 1 month), I moved the vials to the vapour phase of liquid nitrogen storage. In the freezing process It is Important to use healthy cells that are growing in log phase and the medium is replaced 24 h before freezing.

### **2.6.5. Trypan blue cell viability assay**

Cell viability was measured in cells treated with Trypan blue (Sigma Aldrich, Dorset, UK) using a Neubauer haemocytometer (Weber Scientific International Ltd., Middlesex, UK). The haemocytometer and coverslip were first thoroughly cleaned by rinsing in distilled water followed by a wash in 70% ethanol. The haemocytometer and coverslip were allowed to dry and

the coverslip was then placed over the counting chamber. A 10 µl suspension of freshly trypsinised cells was mixed with an equal volume of Trypan blue stain (Sigma, UK). 10 µl of the Trypan blue mixed cells were pipetted onto the edge of the cover slip and allowed to run into the counting chamber until it was completely filled with sample. The haemocytometer was then examined under a light microscope using a 20 x objective lens. Dead cells stain blue with Trypan blue but live cells remain colourless. The total number of live cells in each of the 4 large corner squares plus the middle square was counted. Because each square has surface area of 1 mm<sup>2</sup> and a depth of 0.1 mm, giving it a volume of 0.1 mm<sup>3</sup>, so the sum of the cells (total) in the five squares represents cell count per 0.5 mm<sup>3</sup>. To determine cell count per ml the sum of cell number is multiplied by  $2 \times 10^3$ .

### **2.6.6. Live cell imaging using IncuCyte (Growth curve)**

The rate of cellular proliferation was determined during and after transfection using a non-invasive live cell imaging system within the incubator, the Incucyte FLR (Essen BioScience, Welwyn Garden City, Herts, UK) and its companion software version 2010A (Essen BioScience). A kinetic quantification of the growth of the cells was obtained by recording the average well confluency from at least nine points per well. The cells were

placed in the Incucyte and the growth was recorded for up to a week with measurements at least every 2 h.

### **2.6.7. MTS cell viability assay**

MTS is a tetrazolium compound [3-(4, 5-dimethylthiazol-2-yl)-5-(3-carboxymethoxyphenyl)-2-(4-sulfophenyl)-2H-tetrazolium, inner salt; MTS] which is reduced by living cells into a coloured product. sNF96.2 Cells were seeded in triplicate onto 96 well plates at a density of  $2 \times 10^3$  cells in 100  $\mu$ l of culture medium. The number of cells was then estimated at 24, 48, 72 and 96 h using the MTS based CellTiter 96R Aqueous One Solution Cell Proliferation Assay (Promega) as instructed by the manufacturer. Briefly the culture medium was discarded and replaced with 100  $\mu$ l of fresh culture medium. 20  $\mu$ l of MTS solution was added to each well and the plate was then placed in an incubator at 37 °C and 5% CO<sub>2</sub> for 1 h. The reaction was then stopped by adding 25  $\mu$ l of 10% SDS. The plate was then placed in a Varioskan Flash plate-reader and the absorbance readings at 490 nm wavelength were measured by the SkanIt software programme (Thermo Scientific).

## **2.6.8. Cell migration analysis**

### **2.6.8.1. Scratch/wound healing assays for cell migration**

The scratch wound healing assay was performed using the approach previously described by (Liang et al. 2007). sNF96.2 cells ( $3 \times 10^4$ ) were seeded in 24-well plates containing 0.5 ml of culture medium. The cells were left to grow in a 37 °C, 5% CO<sub>2</sub> incubator for 16 – 24 h until confluent. On reaching confluence, a scratch was made through the central axis of the plate using the Essen BioScience Wound-Maker for 24-well plates. The wells were then washed twice with PBS and the appropriate culture medium was added to the cells. The growth of cells in the scratch area was then imaged and recorded for 6 days using the Incucyte Live imaging system (Essen BioScience, Welwyn Garden City, Herts, UK) (section 2.6.6). All experiments were performed in triplicate.

### **2.6.8.2. Transwell assay**

Cell migration was assessed using 24-well transwells with 8 µm pore Membrane type of membrane (Corning distributed by Appleton Woods, Birmingham, UK). 1 ml of complete DMEM with 10% FBS was placed in the bottom of the wells and sNF96.2 Cells were plated at a density of  $2.5 \times 10^3$  cells in 100 µl of DMEM without FBS inside each transwell. After 6 h incubation at 37 °C and 5% CO<sub>2</sub>, the wells were rinsed with PBS and the cells were fixed onto the membrane and stained with GelRed. Migrated cells

on the membrane were counted in four fields where the cells were evenly distributed (regularly spaced apart from one another).

## **2.7. MiRNA microarray expression profiling**

MiRNA profiling of neurofibromas and MPNST samples was performed using the Human miRNA microarray V2 (Agilent). This microarray quantifies 723 human miRNAs by ~15,000 probes. miRNA probe sequences were sourced from miRBase (<http://www.mirbase.org/>). Each miRNA is quantified by 20 randomly distributed probes; 5 sequence variations per miRNA are repeated 4 times at different locations across the chip. Probes were designed to distinguish miRNAs from the same family which differ by no more than one nucleotide.

### **2.7.1. Sample preparation**

Tissue was disrupted and homogenised using the Tissue-Tearor (Biospec Products). RNA was extracted using the miRNeasy mini kit (quiagen) Prior to further processing for microarray analysis, the abundance and quality of the small RNA fraction was assessed using the Agilent small RNA Kit, according to manufacturer's instructions. 1-20 ng of total RNA was loaded in 1 µl onto the small RNA chip; nucleic acid fragments were separated electrophoretically according to size. Samples plus the small RNA ladder were denatured before use by heating to 70 °C for 2 min, and then stored on

---

ice. The electrophoretic gel and sample dye were prepared and loaded onto the chip according to manufacturer's instructions. RNA between 6 and 150 nts was visualised using the Agilent 2100 Bioanalyzer (Agilent). The miRNA fraction was assessed by the size of the peak at 10-40 nt on the electrophoregram, only those samples with a sufficient miRNA content were used for miRNA microarray analysis. 100 ng of total RNA was incubated with 0.7  $\mu$ l Calf Intestine Alkaline phosphatase (25 unit/ $\mu$ l, TaKaRa) at 37 °C for 30 min to dephosphorylate the sample according to manufacturer's instructions. Dephosphorylated RNA was then denatured by treatment with 5  $\mu$ l of 100% DMSO and heating to 100 °C for 7.5 min, samples were then placed on ice. Fluorescent miRNA was generated by labelling the RNA with Cyanine 3-pCp at the 3' end according to manufacturer's instructions. Briefly, ligation master mix was prepared with the following: 2  $\mu$ l 10 x T4 RNA ligase buffer (New England Biolabs), 2  $\mu$ l RNase-Free Water, 3  $\mu$ l pCp-Cy3 (Agilent), 1  $\mu$ l NEB T4 RNA ligase (20 units/ $\mu$ l, New England Biolabs) giving a total volume of 8  $\mu$ l per sample. The ligation mixture was added to the sample and incubated at 16 °C for 2 hrs. Labelled RNA was made up to a total volume of 50  $\mu$ l with ddH<sub>2</sub>O, then purified by passing the sample through Micro Bio-spin 6 columns (BioRad), according to manufacturer's instructions. These columns contain Bio-Gel P, which desalts samples and removes unincorporated dye, smaller RNA fragments are retained while larger molecules are excluded.

### 2.7.2. miRNA microarray hybridization and scanning

Clean, labelled miRNA samples were then prepared for hybridisation following manufacturer's protocol. Briefly, 10 x blocking agent (GE Healthcare) was reconstituted with 125 µl of nuclease-free water. Labelled samples were dried using a speed-vac, spinning at 45 °C for 1 h. RNA was re-suspended in 18 µl of DNase/RNase-free water and 4.5 µl of the 10 X GE Blocking Agent added to each sample. 22.5 µl of 2 x Hi-RPM Hybridization buffer was added and samples incubated for 5 min at 100 °C. Labelled miRNA was then hybridised to miRNA microarrays and scanned following manufacturer's protocol. The hybridisation mixture was added to a clean gasket slide and loaded into the Agilent SureHyb chamber base. Samples were rotated and hybridised at 55 °C for a minimum of 20 hrs. After which, chips were washed with Gene Expression wash buffer (Agilent) containing Triton X-102 according to manufacturer's protocol. Washed chips were scanned using the Agilent microarray scanner and data extracted with the Agilent Feature Extraction Software.

### 2.7.3. miRNA microarray data analysis

A quality control (QC) report was generated and assessed after scanning to confirm that the experimental procedure was successful. Agilent miRNA arrays were analysed by Dr. S. Henderson (CR-UK Viral Oncology group, UCL) using the 'limma' package for the R programming language and additional custom methods. Background subtraction was undertaken for all probes, negative values were given a small positive value. Sets of probes for

each gene were converted to  $\log_2$  and a summary calculated from the median. Differential expression between summary probe set values was then calculated using the 'limma' methodology.

## **2.8. MicroRNA mimics transfection of sNF96.2 cells**

The MPNST cells, sNF96.2 were seeded at a density of  $5 \times 10^4$  per 6-well 16 h prior to transfection. 100 nM of either miR-29c mimics (Dharmacon Inc., Lafayette, CO, USA) or scrambled oligonucleotides (Dharmacon Inc., Lafayette, CO, USA) were transfected in 1 ml of OPTI-MEM (Invitrogen) using Oligofectamine™ (Invitrogen), according to manufacturer's instructions. The medium was then changed 24 h post-transfection. Cells were harvested after 24 h, 48 h, and 72 h following exposure to the mimics, after which total RNA including microRNA were extracted (Qiagen).

## **2.9. DNA methylation detection**

### **2.9.1. Genomic DNA extraction**

#### **2.9.1.1. Genomic DNA extraction from fresh frozen tissue and cell lines**

Genomic DNA was extracted from fresh frozen tissue and cell lines using Qiagen's DNeasy kit (Qiagen, Crawley, West Sussex, UK) following the manufacturer's instructions. For the fresh frozen tissue, twenty frozen sections (20 µm thick) were used for DNA extraction from each tissue sample. These were cut in advance and stored at -80 °C until ready for use. In the case of cell lines, DNA was extracted from cells grown in 75 cm<sup>2</sup> size flasks. The cells were harvested in advance using Trypsin-EDTA as described in section 2.6.3 They were then washed twice with PBS and stored at -80 °C until ready for use.

The tissue sections or cell pellet were digested by the addition of 180 µl of ALT buffer mixed with 20 µl of proteinase K. The samples were mixed thoroughly with the lysis solution making sure the cell pellets were completely disrupted and that all cells and tissue were completely immersed in the lysis solution. The samples were then incubated in a 56 °C water bath, for 10 minutes in the case of cell lines and for 1 to 2 h in the case of tissue samples until the tissue was completely lysed. 200 µl of AL buffer were then added to each sample and mixed thoroughly by vortexing. 200 µl of 100%

ethanol were then added to each sample which was vortexed again. The sample was then pipetted into a DNeasy Mini spin column placed inside a 2 ml collection tube and centrifuged at 8000 rpm for 1 minute. The flow through and collection tube were discarded and the spin column was placed inside a fresh 2 ml collection tube. 500 µl of AW1 buffer were pipetted into the spin column and then centrifuged at 8000 rpm for 1 minute. The flow through and collection tube were discarded and the spin column was placed inside a fresh 2 ml collection tube. 500 µl of AW2 buffer were added to the column and this was centrifuged again for 3 minutes at 14,000 rpm to dry the DNeasy membrane. The flow through and collection tube were discarded and the spin column was placed inside a clean 1.5 ml tube. 100 or 200 µl of Buffer AE (depending on the starting amount of tissue or cells in the sample) was pipetted directly on to the column membrane and this was left to stand at room temperature for 1 minute before spinning for 1 minute at 8000 rpm to elute the DNA. The concentration and purity of the DNA sample was then analysed using a Nanodrop UV spectrophotometer. A note was made of the A260/A280 and A260/A230 ratios as well as the DNA concentration readings. The DNA was samples were then stored at -20 °C.

#### **2.9.1.2. Genomic DNA extraction from formalin fixed paraffin embedded (FFPE) tissue**

Genomic DNA was extracted from formalin fixed paraffin embedded (FFPE) tissue using QIAamp DNA FFPE Tissue kit (Qiagen, Crawley, West Sussex, UK) following the manufacturer's instructions. For the FFPE tissue, twenty

sections (20 µm thick) were used for DNA extraction from each tissue sample. These were cut in advance and stored at 4 °C until ready for use.

First, 1 ml xylene was added to the sections in 1.5 ml microcentrifuge tube and vortexed vigorously for 10 s. Then centrifuged at full speed for 2 min at room temperature. Then the supernatant was removed by pipetting. Then 1 ml ethanol (96–100%) was added to the pellet, and mix by vortexing. The reason for adding ethanol was to extract residual xylene from the sample. Then centrifuged at full speed for 2 min at room temperature. Next, the supernatant was removed by pipetting. Then the tube was opened and incubated at room temperature for 10 min to evaporate all residual ethanol. Then the pellet was resuspend in 180 µl Buffer ATL With 20 µl proteinase K added, and mixed by vortexing. Next, incubate at 56 °C for 1 h (or up to 2 hrs until the sample has been completely lysed). Then Incubated at 90 °C for 1 h to reverse formaldehyde modification of nucleic acids. 200 µl Buffer AL was then added to the sample, and vortexed. Next 200 µl ethanol (96–100%) was add and mixed by vortexing to yield a homogeneous solution. The entire lysate was then transferred to the QIAamp MinElute column (in a 2 ml collection tube) and centrifuged at 8000 rpm for 1 min. Next, 500 µl Buffer AW1 was added and centrifuged at 8000 rpm for 1 min. Then 500 µl of Buffer AW2 was add centrifuged at 8000 rpm for 1 min. Finally, the QIAamp MinElute column was placed in a clean 1.5 ml microcentrifuge tube and 20–100 µl Buffer ATE was applied to the centre of the membrane and incubated

at room temperature (15–25 °C) for 1 min, then centrifuged at full speed for 1 min.

The concentration and purity of the DNA sample was then analysed using a Nanodrop UV spectrophotometer. A note was made of the A260/A280 and A260/A230 ratios as well as the DNA concentration readings. The DNA samples were then stored at – 20 °C.

### **2.9.2. Bisulphite treatment of DNA**

This technique involves treating methylated DNA with bisulfite, which converts unmethylated cytosines into uracil. Methylated cytosines remain unchanged during the treatment.

About 500 ng DNA was treated using EZ DNA Methylation-Gold™ Kit (Zymo Research, Orange, CA, USA) according to the manufacturer's protocol. Briefly, 130 µl of CT Conversion Reagent was added to up to 20 µl of DNA sample and mixed, then heated to 98 °C for 10 minutes and then 64 °C for 2.5 h and kept at 4 °C. M- Binding Buffer was added (600 µl) to a Zymo-Spin IC Column, then the sample was added and the column was centrifuged at full speed (> 10,000 rpm) for 30 s. The flow-through was discarded and 100 µl of M-Wash Buffer was added to the column. The column was centrifuged for 30 s and 200 µl of M-Desulphonation buffer was added to the column and left for 15-20 minutes at room temperature. The column was then centrifuged at 10,000 rpm for 30 s. A wash step was then performed by addition of 200 µl of M-Wash Buffer to the column after which the column was centrifuged for

30 s. This wash step was repeated twice. M-Elution buffer (10 µl) was added directly to the column matrix and the bisulfite-treated DNA was collected in 1.5 ml micro-tubes and stored at -20 °C.

### **2.9.3. PCR and pyrosequencing of bisulphite treated and control samples**

Bisulfite-treated DNA was used for generating PCR-amplified templates for pyrosequencing using target specific primers (described in Table 2-7). The primers were designed using the PyroQ assay design software (Biotage, Uppsala, Sweden). A common tag was placed on either the forward or the reverse primer (depending on the strand to be sequenced), and a universal biotinylated primer was used for all reactions as described previously (Tost & Gut 2007). Two rounds of bisulphite-PCR cycling conditions included denaturation at 95 °C for 4 minutes, followed by 10 cycles of 94 °C for 15 s, touchdown from 60–50 °C (reducing 1 °C per cycle) for 15 s and 72 °C for 20 s followed by a further 30 cycles at a 50 °C annealing temperature. The second PCR used 2 µl of a 1:10 dilution of the first PCR as template and the same cycling conditions. All products were confirmed to be single bands by agarose gel electrophoresis. Touchdown PCR is a method for expanding specificity of PCR reactions. Touchdown PCR utilises a cycling steps where the annealing temperature is continuously decreased (e.g. 1-2 °C/every cycle). The initial annealing temperature ought to be a few degrees over the specified  $T_m$  of the preparations. The annealing temperature is then steadily

diminished until it reaches the calculated annealing temperature of the primers or a few degrees beneath. Amplification is then kept using this annealing temperature.

Ten microlitres of the biotinylated PCR product was sequenced according to the manufacturer's recommendation. Pyrosequencing was carried out on the PSQ HS 96 System using Pyro Gold Reagent kits (PSQ 96MA, Biotage). Sample preparation as follow: 2  $\mu$ l streptavidin beads (GE Healthcare, Buckinghamshire, UK), 38  $\mu$ l PyroMark binding buffer (Qiagen), 10  $\mu$ l PCR product and 30  $\mu$ l ddH<sub>2</sub>O were mixed and incubated for 10 minutes on a shaking table at 1500 rpm. Employing the Biotage Q96 Vacuum Workstation, DNA was separated, denatured and washed then 0.3  $\mu$ M sequencing primer in 12  $\mu$ l of annealing buffer is added. Then the samples are incubated at 80 °C for 2 minutes for primer annealing then left to cool to room temperature. This technique is a sequencing-by-synthesis method where a sequencing primer hybridises to the target DNA template. The deoxyribonucleotide triphosphates (dNTPs) are used by the enzyme polymerase to synthesise a new DNA strand. The dispensation order of dNTPs is according to assay design (PyroQ assay design software). When the complementary dNTP is dispensed, it will be incorporated into the newly synthesised DNA and this causes release of a pyrophosphate (PPi). The enzymes sulfurylase convert the released PPi into adenosine triphosphate (ATP). Then luciferase uses the ATP to convert luciferin to oxyluciferin, and this generates visible light which then captured and presented as a peak in

the program). The degree of methylation of each CpG position in a sequence is determined from the ratio of T (thymine) and C (cytosine). All runs contained standard curves, which comprised a range of control methylated DNA (0%, 20%, 40%, 60%, 80% and 100%) to allow standardised direct comparisons between different primer sets. Methylation was quantified using Pyro Q-CpG Software (Biotage) that calculates the ratio of converted Cs (Ts) to unconverted Cs at each CpG and expresses this as a percentage of DNA methylation.

**Table 2-7: List of primer sequences used for pyrosequencing**

Gene	Primer	Sequence
CDKN2A	F	TTTTATATTTTTTTGGTTTAGTAGTTAGTT
	R	AACCACTAAAACCTCATTATATAACACTC
	S	ACTCCTTTTCTTCTTACAACCCTA
WT1	F	GGGGATATGTTAGTTATATTGGTTTTG
	R	ATTTCCACAACCTACTTTTCTCTA
	S	GTTTAGTAAGAAGGTAGGTAGTA
S100B	F	AGGGTGGAAGGTTATAGATTTT
	R	ACTAACCCCCCTATTCAAAAACCTCCAATC
	S	GAAGGTTATAGATTTTTAGAGT

Key: F= forward; R= reverse; S= sequencing.

## 2.10. 5-aza-2'-deoxycytidine treatment of sNF96.2 MPNST cells

The effects of DNA methylation on expression of various genes in sNF96.2 cells was examined by treating this cell line with 5-aza-2'-deoxycytidine (5-aza-dC). This compound is an epigenetic modifier which inhibits DNA methyltransferase activity resulting in global demethylation of DNA and activation of gene expression by chromatin remodelling (Claus et al., 2005; Hackanson & Daskalakis, 2014).

The optimum dose of 5-aza-dC that could be used to induce global hypomethylation of DNA in sNF96.2 cells with minimal cytotoxic effects was first determined empirically. The sNF96.2 cells ( $2 \times 10^4$ ) were initially seeded per well in 24 well plates (7 plates were used) and grown for 1 day. The medium was then removed from each plate and replaced with fresh medium containing 5-aza-dC (Sigma-Aldrich, St. Louis, MO) at one of the following concentrations: 0.25  $\mu\text{M}$ , 0.5  $\mu\text{M}$ , 1  $\mu\text{M}$ , 2  $\mu\text{M}$ , 3  $\mu\text{M}$ , 5  $\mu\text{M}$ , and 10  $\mu\text{M}$ . The different cell cultures were maintained in the same concentration of 5-aza-dC for a maximum period of 7 days. The viability of cells grown in each different concentration of 5-aza-dC was measured by Trypan Blue assay as described in section 2.6.5. Cells were incubated for 7 days with 5-aza-dC with the culture media being replaced every 24 h with fresh media containing 1  $\mu\text{M}$  5-aza-dC. All experiments were carried out in triplicate.

## 2.11. Protein isolation and Western blot analysis

To test protein expression by Western blotting ten sections (each 20  $\mu\text{m}$ ) were cut from snap-frozen tumours as described above and placed into micro-tubes. A tumour lysate was produced using Radio-Immunoprecipitation Assay (RIPA) lysis buffer (150 mM NaCl, 1% IGEPAL® CA-630, 0.5% sodium deoxycholate, 0.1% sodium dodecyl sulfate, 50 mM Tris [pH 8.0]) containing both phosphatase and protease inhibitor cocktails (Sigma-Aldrich). Lysates were incubated on ice for 15 minutes and then centrifuged at 13,000 rpm and 4 °C for 10 minutes to remove debris. Proteins were quantified with BCA protein assay kit (Fisher Scientific UK Ltd, Loughborough, Leicestershire, UK). Thirty micrograms of protein lysate were resolved by SDS-8% polyacrylamide gel electrophoresis (SDS-8% PAGE) and transferred to a polyvinylidene fluoride (PVDF) Immobilon-P transfer membrane (Millipore Corporation, Bedford, MA, USA) by standard wet electro-transfer methods. The membrane was blocked with PBS, 0.1% Tween 20, 5% BSA for a minimum of 30 minutes and probed with the appropriate primary antibody overnight at 4 °C. Blots were washed three times (15 minutes each) in 1 X PBS with 0.1% Tween 20 (PBS-T) and incubated for 1 h at room temperature with the appropriate secondary horseradish peroxidase (HRP)-conjugated antibody, followed by further washing and enhanced using chemiluminescence (ECL) detection

(GEHealthcare Ltd, Amersham, Buckinghamshire, UK). The primary antibodies used included: mouse monoclonal (CA-4001) matrix metalloproteinase (MMP2), rabbit monoclonal (EP1254) MMP9 (dilution 1:1000; incubation overnight at 4 °C, Abcam, Cambridge, Cambs., UK), MMP3 (dilution 1:50; incubation overnight at 4 °C, Santa Cruz Biotechnology, Inc., Santa Cruz, CA, USA), rabbit monoclonal S100B (dilution 1:1000, incubation overnight at 4 °C, Abcam ab52642) and GAPDH mouse monoclonal antibody (6C5) at dilution 1:5000; incubation 1 h at room temperature (Advanced Immunochemical Inc., Long Beach, CA, USA).

## 2.12. Gelatin Zymography

Two days after siRNA transfection of sNF96.2 cells, the medium was changed to serum-free medium (350 µl Optimem; Invitrogen) for overnight incubation after which the supernatant was collected and spun to remove floating cells. At the same time, the cells were lysed using lysis buffer (0.1% Triton x-100 in 0.05 Trizma base, 0.2 M NaCl, 0.005 CaCl<sub>2</sub>) in non-reduced conditions (no heating or reducing reagents). The supernatants and cell extracts were separated using 10% acrylamide gels containing 0.1% gelatin type A from porcine skin (Sigma-Aldrich, Dorset, UK) with non-reducing conditions. The gels were incubated in a 2.5% Triton X-100 solution at room temperature with gentle agitation for 1 h and then soaked in reaction buffer (50 mM Tris-HCl (pH 7.5), 200 mM NaCl, and 10 mM CaCl<sub>2</sub>) at 37 °C overnight. The gels were stained with 0.5% Coomassie Blue R250 in

30% methanol/10% glacial acetic acid in H<sub>2</sub>O for 1 h and then de-stained (staining solution without Coomassie Blue) for 0.5 h after which they were fixed in 0.2% glacial acetic acid. Zones of gelatinolytic activity were revealed by negative staining.

## 2.13. Sequencing of *NF1* gene

In order to detect the presence or absence of mutation in *NF1* gene in our cell line, fifty nanograms of genomic DNA were amplified by the following touchdown PCR protocol. It is a method for expanding specificity of PCR reactions. Touchdown PCR utilises a cycling steps where the annealing temperature is continuously decreased (e.g., 1-2 °C/every cycle). The initial annealing temperature ought to be a few degrees over the specified T<sub>m</sub> of the preparations. The annealing temperature is then steadily diminished until it reaches the calculated annealing temperature of the primers or a few degrees beneath. Amplification is then kept using this annealing temperature.

Steps involved initial heating at 95 °C for 15 minutes. The annealing temperature being reduced by 1 °C per cycle, from 65 °C to 56 °C, followed by 35 further cycles at 56 °C. The PCR reaction was performed in a total volume of 50 µl containing 5 µl of 10X Hotstart buffer I, 0.2 µM dNTP, 10 pM of each primer, 1 U of Hotstart DNA polymerase (Qiagen). PCR products were purified using Qiagen PCR Purification kit (Qiagen) and sent for DNA direct sequencing at the Scientific Support Services at UCL Cancer

Institute/Wolfson Institute for Biomedical Research (WIBR). Direct sequencing reactions were run using GenomeLab™ DTCS Quick Start chemistry (Beckman Coulter UK Ltd, High Wycombe, Bucks., UK) and were analysed on a CEQ™ 8000 Genetic Analysis System (Beckman Coulter).

## **2.14. Immunohistochemistry (IHC)**

### **2.14.1. Slide staining**

Three µm thick paraffin-embedded sections were de-waxed by successive baths of xylene, ethanol and water, pre-treated and incubated with the primary antibody; Anti-S100 beta antibody (ab52642; Abcam, Cambridge, UK). Pre-treated slides were either stained manually with the Ventana iVIEW DAB kit (Ventana Medical Systems, Strasbourg, France) following the manufacturer's instructions. The slides were counterstained with haematoxylin. A positive and a negative control (e.g., no primary antibody added) were performed on tissue controls. An H&E was performed for each slide to review its histology. The slides were kindly revised to confirm the scoring by Dr. Nischalan Pilly (Pathologist at Department of Pathology, RNOH).

### **2.14.2. Immunohistochemistry scoring**

Both the intensity of the staining and the number of cells stained were scored for each slide. For the number of cells stained per 10 contiguous HPF, a score of 0 was given when no or sparse tumour cells (less than 1%) were

stained, 1 for less than 10%, 2 for between 11 and 60% and 3 for above 60%. For the staining intensity, a score of 0 corresponded to an absence of staining, 1 to a weak staining intensity (less intense than the positive control), 2 to a medium staining intensity (comparable to the positive control) and 3 to a high staining intensity (above the positive control). The score of each of the duplicated scores for the same case were then averaged, to give a final score for the staining intensity and for the extent of the staining. Unequivocally immunoreactive cases, with a score for intensity equal or above 1 and a score for the % of cells stained over 1, were considered as expressing the protein. Cases not immunoreactive, with a score equal or below 1 for the extent of the immunoreactivity, were considered as negative for protein expression.

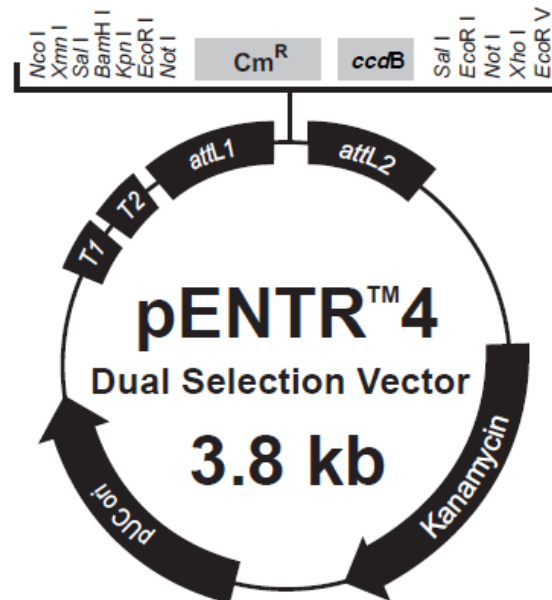
## 2.15. *S100B* expression cloning

### 2.15.1. PCR cloning strategy

The *S100B* cDNA was cloned using a PCR cloning strategy. The first step was to design 5' and 3' PCR primers containing different restriction enzymes. There were two criteria used to select restriction enzymes for cloning. Firstly, there had to be no restriction sites present within the region to be cloned. The cDNA sequence to be cloned was obtained from the NCBI GenBank depository of sequenced DNA: this was then entered into the web site <http://tools.neb.com/NEBcutter2/>. This program identified all user specified restriction enzyme sites present within the sequence; enzymes which did not cut the DNA could then be selected. The second criterion in selecting restriction enzymes was the presence of the restriction site within the multiple cloning site (MCS) of the vector. These were restriction enzyme sites included into a defined region of the vector during vector design to facilitate the cloning process. Primers complimentary to the beginning and end of the sequence to be cloned were designed using Invitrogen OligoPerfect primer designing tool ([www.invitrogen.com](http://www.invitrogen.com)). The DNA sequence to be cloned was entered into the program: variables including primer length, C/G composition, product length and primer melting temperature were then specified. Once complimentary primers had been designed and the appropriate restriction enzymes selected, a random sequence of junk DNA was added to the ends of both primers, this facilitated

restriction enzymes digestion. PCR was performed with 2  $\mu$ l of 10  $\mu$ M forward and reverse primers, 1  $\mu$ l of 10 mM dNTPs (Invitrogen), 5  $\mu$ l PfuTurbo 10 x reaction buffer (Stratagene) or 10  $\mu$ l of HotStart HiFidelity 5X PCR Buffer (Qiagen), 1  $\mu$ l of PfuTurbo DNA polymerase (2.5 units) (Stratagene) or 1  $\mu$ l of HotStart HiFidelity DNA polymerase (2.5 units) (Qiagen) and 100-1000 ng of template DNA made up to a final volume of 50  $\mu$ l with ddH<sub>2</sub>O. PCR conditions were as specified by the manufacturer's instructions, typically the polymerase was activated and DNA denatured by incubating at 95 °C for 2-5 minutes. Followed by 20-40 cycles of 95 °C for 1 minute, 55 °C for 1 minute, 72 °C for 1 minute, during which double-stranded DNA is denatured, primers anneal and polymerase-mediated elongation of PCR produced occurs. The final step was elongation step of 7 minutes at 72 °C; this ensured that any remaining single-stranded DNA was fully extended. Variables in the PCR program were cycle number, extension time and primer annealing temperature. Extension time was dictated by the length of the product, with 1 minute/1 kb of DNA, primer annealing temperature was governed by the base composition and length of primers. The melting temperature of primers was calculated using the formula  $2(A/T) + 4(G/C)$ . However, to determine experimentally the optimum primer annealing temperature, a temperature gradient PCR was performed. In this program the annealing temperature increases in defined increments across the PCR block, the products were then run on a gel and the temperature yielding the maximum PCR product was used for subsequent cloning. Non-template controls, whereby all reactions minus template DNA were run to confirm

reagents were uncontaminated. Amplification of the PCR product of the correct size was confirmed by resolving the product on an agarose gel, the correct sequence was then confirmed by direct sequencing. The PCR clone is inserted in the pENTR 4 dual selection (Invitrogen) (Figure 2-1) using appropriate restriction enzymes (New England Biolabs). Next, I performed the LR recombination reaction between pENTR clones and pLenti PGK PuroDEST (w529-2) destination vectors (Figure 2-2). (LR is a recombination reaction between an attL-containing entry clone and an attR-containing destination vector). LR reactions containing 300 ng destination plasmid DNA, 300 ng pENTR plasmid DNA, 4  $\mu$ l LR clonase reaction buffer and 4  $\mu$ l LR clonase enzyme were made up to 20  $\mu$ l with TE (pH 8.0). LR reactions were incubated at 25 °C for 1 h. Reactions were terminated by the addition of proteinase K (2  $\mu$ g) and incubation at 37 °C for 10 minutes.



**Comments for pENTR™4**  
**3757 nucleotides**

*rrnB* T1 transcription termination sequence: bases 106-149

*rrnB* T2 transcription termination sequence: bases 281-308

*attL1*: bases 358-457 (complementary strand)

Chloramphenicol resistance gene (Cm<sup>R</sup>): bases 611-1269

*ccdB* gene: bases 1611-1916

*attL2*: bases 1986-2085

Kanamycin resistance gene: bases 2208-3017

pUC origin: bases 3081-3754

**Figure 2-1: pENTR 4 dual selection entry vector map**

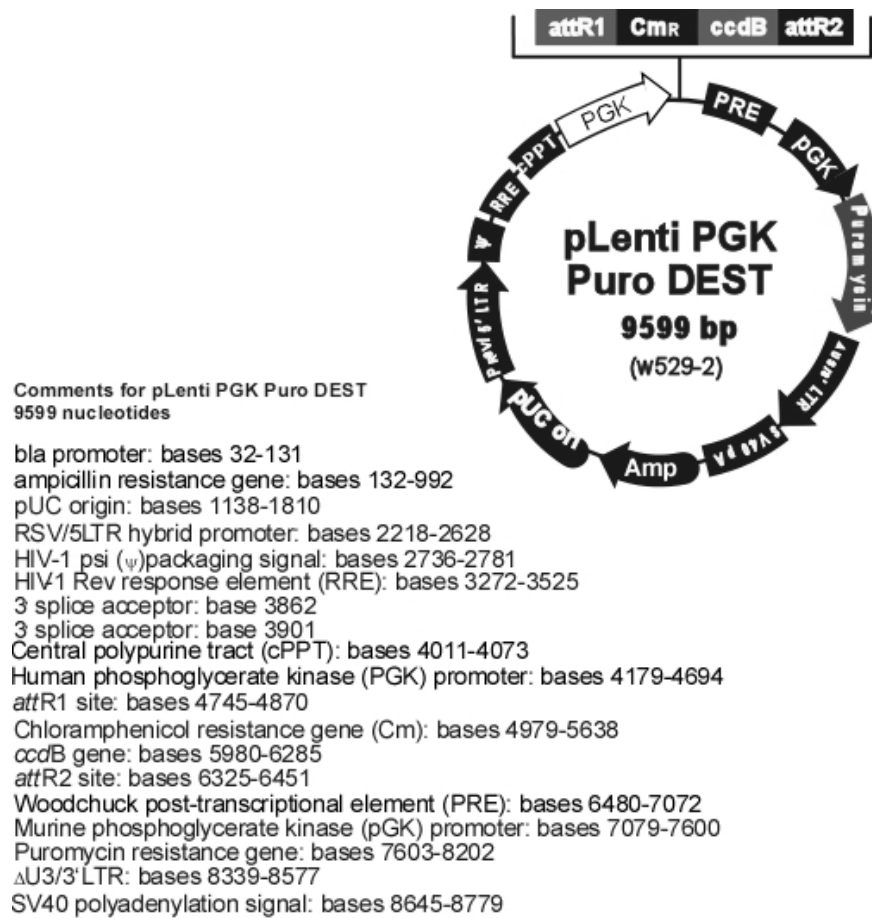


**Figure 2-2: pLenti PGK PuroDEST destination vector map**

## 2.15.2. Restriction enzyme digestion

Restriction enzyme digestion was performed on plasmid DNA to confirm the presence of a cloned insert. All restriction enzyme digests were performed for 1 h at 37 °C with 5-10 units of each enzyme in a total volume of 15-25 µl. Included in the restriction enzyme mix was 10 x restriction enzyme buffer and ~1 µg of DNA. The appropriate buffer was selected by consulting New England Biolabs enzyme buffer compatibility chart (<https://www.neb.com/tools-and-resources/interactive-tools/double-digest-finder>) and determining in which buffer the two enzymes had maximum activity. After restriction enzyme digestion, 6X DNA loading buffer (Fermentas) was added and the product resolved by electrophoresis on an agarose gel, the product was then excised and cleaned up using QIAquick Gel Extraction Kit (Qiagen). Alternatively, digested PCR products were purified directly using the QIAquick Gel Extraction Kit.

### **2.15.3. Plasmid Ligation**

Ligation reactions were performed in a total volume of 20  $\mu$ l using 20 units (1  $\mu$ l) of T4 DNA ligase and 2  $\mu$ l of 10X T4 DNA ligase buffer (New England Biolabs). Varying ratios of insert to plasmid DNA were used in ligation reactions, always keeping the insert at higher concentration to the plasmid DNA to encourage ligation and prevent vector re-ligation. Two different restriction enzymes were used in the cloning process, this aided cloning of the fragment in the correct orientation and minimised vector re-ligation. In addition, prior to ligation 200- 1000 ng of gel purified restriction digested vector was incubated with 2  $\mu$ l (2 units) of shrimp alkaline phosphatase (Promega) as well as 10 x enzyme buffer (Promega). The enzyme-DNA mixture was incubated at 37 °C for 15 minutes after which the alkaline phosphatase was inactivated by heating to 65 °C for 15 minutes. Alkaline phosphatase treatment is another measure designed to minimise vector re-ligation, promoting the uptake of cloned insert. Typically, the highest ratio of insert to vector was used depending on the DNA concentration of the insert. Ligation reactions were carried out at 16 °C overnight.

#### **2.15.4. Bacterial transformation**

Plasmid DNA was amplified through chemical transformation and expansion of bacterial cultures. One vial of 50  $\mu$ l DH5-Alpha chemically competent E.coli (Invitrogen) was transformed with 1-5  $\mu$ l of ligation reaction or plasmid DNA (~100 ng). Bacteria were incubated on ice for a minimum of 5 minutes and then heat shocked at 42 °C for 30 s, after which they were placed on ice. 250  $\mu$ l of room temperature SOC media (Invitrogen) was added to each vial of bacteria and incubated at 37 °C for 1 h with shaking. After shaking, 200  $\mu$ l was streaked on Ampicillin containing LB agar plates. Plates were incubated overnight at 37 °C. Successfully transformed bacteria contained an Ampicillin-resistant cassette, and therefore survived Ampicillin selection growing to form visible colonies, which were then picked for subsequent expansion.

### **2.15.5. Plasmid purification**

Plasmid DNA was extracted from transformed bacterial cultures using Qiagen miniprep or maxiprep kits according to manufacturer's instructions. Minipreps were performed on 5 ml of bacterial cultures typically transformed with ligation reactions during the cloning process in order to test for the presence of a DNA insert. Minipreps yielded approximately 20 µg of plasmid DNA. For minipreps, a single bacterial colony was picked and placed into 5 ml of Lysogeny Broth (LB) containing the antibiotic Ampicillin, which was grown overnight at 37 °C with shaking. Bacteria were pelleted by spinning at 3000 rpm for 15 minutes in a desktop centrifuge. The bacterial pellet was re-suspended, lysed and neutralised through an alkaline lysis method according to manufacturer's instructions (Qiagen). Cellular debris and genomic DNA were pelleted by spinning at 13000 rpm in a desktop centrifuge. The resulting clear solution containing the plasmid DNA was passed through a mini-prep column by spinning at 13000 rpm in a desktop centrifuge for 1 minute. Wash steps were performed according to manufacturer's protocol and clean plasmid DNA solution was eluted in 50 µl of ddH<sub>2</sub>O. Maxipreps were performed on 300 ml of bacterial culture from which bacteria were pelleted through spinning at 3500 rpm for 15 minutes at 4 °C. The pellet was resuspended, lysed and neutralised according to manufacturer's instructions. Genomic DNA was pelleted through centrifuging the solution at 3500 rpm for 30 minutes at 4 °C. Subsequent wash steps and elution were performed according to manufacturer's instructions. The culture was centrifuged at

4,000 rpm for 15 minutes at 4 °C. The pellets were then pooled and resuspended in 5 ml of buffer P1, and lysed with 10 ml of buffer P2. The tubes were inverted for mixing and incubated for 5 minutes at room temperature. Ten ml of pre-chilled buffer P3 were added to neutralise the reaction and the solution was incubated for 20 minutes on ice before centrifugation at 3,500 rpm for 30 minutes at 4 °C. The plasmid in the supernatant obtained was bound to the column, washed twice with 30 ml of QC buffer and eluted in 5 ml of QF buffer. Maxipreps typically yielded ~1 µg/µl of plasmid DNA. Plasmid DNA concentration and purity was quantified by measuring the absorbance at 260 nm/230 nm and the absorbance at 260 nm/280 nm respectively using a NanoDrop UV spectrophotometer. The plasmid with the *S100B* insert clones was sequenced confirming that it had the expected sequence. The primers used were: forward primer 5'GTTGACCGAATCACCGACCT3' and reverse primer 5'AGAGGTTGATTGTCTGAGCGG3'.

### **2.15.6. Agarose gel electrophoresis**

Gel electrophoresis was performed to visualise DNA and or for gel purification. Typically 1% weight/volume (w/v) agarose (Sigma) in TAE buffer (Tris-acetate 0.4 M, ethylenediaminetetraacetic acid (EDTA) 0.01 M) gels were used to resolve DNA fragments > 200 bp. For resolution of DNA < 200 bp 2-4% agarose gels were used. DNA was visualised through the addition of 0.04 mg/ml of GelRed Nucleic acid stain (Biotium). Agarose gels were electrophoresed in TAE buffer at a voltage of 100 V. DNA bands in the gel were visualised using the G:BOX gel documentation system (Syngene). DNA ladders (Fermentas) of the appropriate size range were separated alongside experimental samples to estimate the size of DNA molecules.

### **2.15.7. DNA extraction from agarose gel**

Agarose gel extraction was performed on PCR products or digested plasmids to be used for subsequent ligation or sequencing. Gel extraction was performed using the QIAquick Gel Extraction Kit (Qiagen). Excised DNA-containing gel pieces were weighed and three times the volume of QG buffer added. Gel was dissolved in QG buffer by incubating at 50 °C until all gel was in solution. Then an equivalent volume of isopropanol was added and samples loaded onto the QIAquick spin column and processed according to manufacturer's protocol. DNA was eluted from the column in 30 µl of ddH<sub>2</sub>O. The QIAquick kit was also used to clean up PCR products which had been restriction digested, these products were not run on a gel as digesting the product had little effect on size and therefore electrophoresis was unnecessary. After restriction digest, 300 µl of QG buffer was added to the DNA, followed by 100 µl of isopropanol. The sample was then loaded onto the column and processed according to the manufacturer's instructions. DNA was eluted in 30 µl of ddH<sub>2</sub>O.

### **2.15.8. Lentivirus production**

HEK293T cells were maintained in DMEM media supplemented with 10% FBS and 1% penicillin and streptomycin. They were split 3 times per week at a ratio of 1:4 using 0.05 mM trypsin/EDTA. The day before the transfection, the cells were seeded in a 10 cm dish at a density of 3.5 million cells in 8 ml of complete medium and incubated at 37 °C, 5% CO<sub>2</sub>. On the day of transfection, the following mixture was prepared in 1.5 ml micro-tube; 1 µg p8.91 (gag-pol expressor), 1 µg pMDG.2 (VSV-G expressor), 1.5 µg plasmid DNA containing the *S100B* insert and sterile TE to final volume of 15 µl. In a second microtube, 10 µl Fugene (Roche Diagnostics Ltd., Burgess Hill, West Sussex, UK) was added to 200 µl Optimem (Invitrogen) for each of the transfection mixtures. The DNA mix was added to the Optimem-Fugene mix and left at room temperature for 15 minutes. The medium was changed with fresh complete medium and the Optimem/DNA/Fugene mix was added to the cells and incubated overnight at 37 °C, 5% CO<sub>2</sub>. After 24 h, the medium was changed to fresh complete medium. At 48 h, the lentivirus-containing supernatant was collected in a 10 ml syringe (Fisher) and filtered through a 0.45 µm filter (VWR International Ltd., Lutterworth, Leicestershire, UK) into a 50 ml tube. The supernatant was aliquoted and stored at -80 °C.

### 2.15.9. Lentivirus titration

The day before titration, HEK293T cells were seeded at  $0.5 \times 10^5$  cells per well in 6 well plates in 2 ml of complete medium and incubated overnight at 37 °C, 5% CO<sub>2</sub>. Different concentrations of the virus stock to be titrated were added together with 8 µg/ml polybrene (Sigma-Aldrich) to different wells and incubated for two days. The cells were detached with trypsin/EDTA (Invitrogen) and DNA was extracted.

In order to determine the number of lentiviral copies per infected cell (c/c) qPCR was performed for glyceraldehydes 3-phosphate dehydrogenase (GAPDH) and the lentiviral packaging signal. Genomic DNA was extracted 48 h post lentiviral infection. Primers (Table 2-8) were used at a concentration of 0.7 µM and probes at 0.15 µM. Reactions were performed in a total volume of 50 µl using the Absolute QPCR ROX and dUTP mix (ABgene) and 0.01 units AmpErase (Applied Biosystems). 10 µl of genomic DNA at a concentration of 50 ng/µl was added to the reactions. The q-PCR conditions used were as follows: 50 °C for 2 minutes followed by 95 °C for 15 minutes and 40 cycles of 95 °C for 15 sec and 60 °C for 1 minute. Reactions were run in optical 96-Well Thermal Cycling Plates (Applied Biosystems) on Realplex4 Mastercycler (Eppendorf). The number of c/c was determined by adjusting the number of lentiviral constructs present to the number of cells analysed, using *GAPDH*. For each sample a neat and 1/10 dilution of genomic DNA was run, a negative control of ddH<sub>2</sub>O was performed for all PCRs.

**Table 2-8: List of primers sequences used for Lentiviral titration**

Primer Name	Primer Sequence (5' -> 3')
GAPDH (Forward)	GGAGTCAACGGATTTGGTCGTA
GAPDH (Reverse)	GGCAACAATATCCACTTTACCAGAGT
GAPDH (TaqMan probe)	FAM-GGCAACAATATCCACTTTACCAGAGT-TAMRA
Lentiviral (Forward)	GCACGGCAAGAGGCGA
Lentiviral (Reverse)	CGCACCCATCTCTCTCCTTCTA
Lentiviral (TaqMan probe)	FAM-CGGCGACTCTCTCCTTCTA-TAMARA

### **2.15.10. Infection of sNF96.2 cells with Lentivirus**

Stable infected sNF96.2 cells were selected in 1 µg/ml puromycin (Sigma-Aldrich). A puromycin-kill curve is performed to determine the optimal concentration needed for selection where the minimum antibiotic concentration to use is the lowest concentration that kills 100% of untransduced cells and maximal survival transduced cells in 3-4 days.

## 2.16. Statistical analysis

All experiments were performed in independent replicates. Error bars correspond to the standard deviation from the calculated mean. SPSS (Statistical Package for the Social Sciences; Version 22.0, Chicago, IL) was used for all statistical analyses. Mean value and standard deviation were calculated using descriptive statistics. Comparison of means was performed by one-way analysis of variance. Two-tailed Student's *t*-test (for continuous and normally distributed data), one-way ANOVA (for normal unpaired continuous data comparing more than two groups) were used where appropriate, and differences were considered statistically significant if  $p < 0.05$ . The Spearman rho test was used for regression analysis to correlate two not normally distributed continuous sets of data and the Pearson's correlation test for normally distributed continuous sets of data.

# **3. Role of miR-29c in the progression of neurofibroma to MPNST**

## **3.1. Introduction**

MicroRNAs (miRNAs) are small (~22 nucleotides) non-coding RNAs that can regulate gene expression by hybridising to complementary target mRNAs, resulting in either inhibition of translation or mRNA degradation (Ambros 2001; Bartel 2004). miRNAs can influence a wide variety of biological processes, including cell proliferation, differentiation and cell death (Schickel et al. 2008) . miRNAs are also involved in the development of cancer where they have been shown to act as both tumour suppressor genes, e.g., miR-15, miR-16, miR-29 family and let-7, (Cimmino et al. 2005; S. M. Johnson et al. 2005; Mott et al. 2007) as well as oncogenes, e.g., miR-155 and miR-21 (Kluiver et al. 2005; Chan et al. 2005). The mechanism by which miRNAs mediate their effects in cancer includes the regulation of migration and invasion of tumour cells (Ma et al. 2007; Yu et al. 2007). The star forms (\*) of miRNA represent the opposite complementary strand of the guide strand; these are generally found to be less expressed compared with the non-star forms and are preferentially degraded (Schwarz et al. 2003).

Previous investigations into the role of miRNAs in the pathogenesis of MPNSTs in patients with and without neurofibromatosis type 1 are limited and have resulted in different miRNAs being implicated in the development of MPNSTs from neurofibromas. In one study of patients with and without neurofibromatosis type 1, using miRNA expression microarrays, Subramanian et al. (2010) demonstrated up-regulation of 5 micro-RNAs (miR-214, miR-377, miR409-3p, miR-487b, and miR-99b) and downregulation of 5 others (miR-517, miR-34a, miR-29a, miR-30e-5p and miR-27a) in MPNSTs compared to neurofibromas (Subramanian et al. 2010). In another study of 6 MPNSTs and 6 neurofibromas by Itani et al. 2012, the miRNA expression analysis demonstrated up-regulation of 6 miRNAs (miR-21, miR-135b, miR-152, miR-130b, miR-92, and miR-15b) and down-regulation of 3 others (miR-125b, miR-127, and miR-302d) in MPNSTs compared to neurofibromas. Using qRT-PCR method, they confirmed the miRNA profiling for the miRNAs which shows more than 2 fold difference in expression, namely miR-21, miR-135b, miR-125b, miR-127, and miR-302d in neurofibromas, MPNSTs and normal nerve. The qRT-PCR showed that only miR-21 which shows significantly higher expression in MPNST higher than that in neurofibromas and normal nerves. Accordingly, they studied miR-21 further and showed that transfection of miR-21 inhibitor significantly increased apoptotic activity through increasing caspase activity, suppressed cell growth, and upregulated protein level of PDCD4 tumour suppressor which has been reported previously as a target for miR-21; indicating that

miR-21 inhibitor could induce cell apoptosis of MPNST cells (Itani et al. 2012).

Masliah-Planchon et al. (2013) examined miRNAs expression in 50 neurofibromas and 15 MPNSTs from patients with neurofibromatosis type 1 and reported miR-139-5p, miR-150, miR-338-3p, miR-195, miR-146a, miR-95, let7b, miR-186, miR885-5p and miR-200c as significantly downregulated in MPNST relative to neurofibromas. However, 103 miRNAs were found to be upregulated in MPNST relative to neurofibromas (Masliah-Planchon et al. 2013).

## 3.2. Aims

The aims of this part of the project were threefold:

- Determine which miRNAs may be important in development of MPNSTs by looking for differentially expressed miRNAs in neurofibromas and MPNSTs from patients with neurofibromatosis type 1.
- Select a potential miRNA candidate for further study and examine its *in vitro* effect(s) on cell growth and proliferation following expression of the selected miRNA in an MPNST derived cell line.
- Identify the specific targets of any putative miRNA candidate.

## 3.3. Results

### 3.3.1. miRNA microarrays demonstrate down-regulation of miR-29 family in MPNSTs versus neurofibromas

In order to identify any miRNAs that may play an important role in pathogenesis of MPNSTs, the miRNA microarray expression data from 10 neurofibromas and 10 malignant peripheral nerve sheath tumours (MPNSTs), which had previously been generated in our lab (by Dr Nadège Presneau), were analysed by hierarchical clustering to look for differentially expressed genes. Details of the clinical samples (which are all derived from neurofibromatosis type 1 patients) and miRNA microarrays used are given in chapter 2.

Using this approach (with a cut off value of  $q = 8.48E-03$  for the least significant miRNA) 16 miRNAs were identified as significantly differentially expressed in MPNSTs and neurofibroma (Figure 3-1A). The majority, fourteen, were downregulated in MPNSTs. These included miR-30e\*, miR-29c\*, miR-29c, miR-340\*, miR-30c, miR-139-5p, miR-195, miR-151-5p, miR-342-5p, miR-146a, miR-150, miR-223, let-7a and let-7g. The remaining two however, miR-210 and miR-339-3p, were found to be upregulated in MPNST compared with neurofibromas.

---

Of the 16 differentially expressed genes miR-29c was of particular interest since, as well as showing significant reduction in the level of expression in MPNSTs, this miRNA has also been implicated in a variety of other malignancies (Mraz et al. 2009; Stamatopoulos et al. 2009; Ding et al. 2011; Sengupta et al. 2008; Fabbri et al. 2007; Pass et al. 2010). miR-29c also belongs to a family of miRNAs which includes miR-29a, b, c\*, b-1\*. All the miR-29 family members share a common sequence of the seed region and are therefore predicted to target largely overlapping sets of genes. As an initial step, I decided to examine whether other members of the miR-29 family might also be differentially expressed in MPNSTs relative to neurofibromas. Generation of a supervised heat-map for the miR-29 family including miR-29a, b, c\* and b-1\*, demonstrated that these were also significantly downregulated in MPNST compared with neurofibromas with a  $p < 0.05$  (Figure 3-1B).

I next focussed my attention on miR-29c for further studies. I concentrated on the mature form of miR-29c since the star forms of miRNA are generally found to be less expressed *in vivo* compared with the non-star forms (Schwarz et al. 2003). In addition, the mature form of miRNA is the one that incorporate in the RNA induced silencing complex (RISC) which causes its stabilisation and this process is accompanied by destruction of the (\*) form (Schwarz et al. 2003).

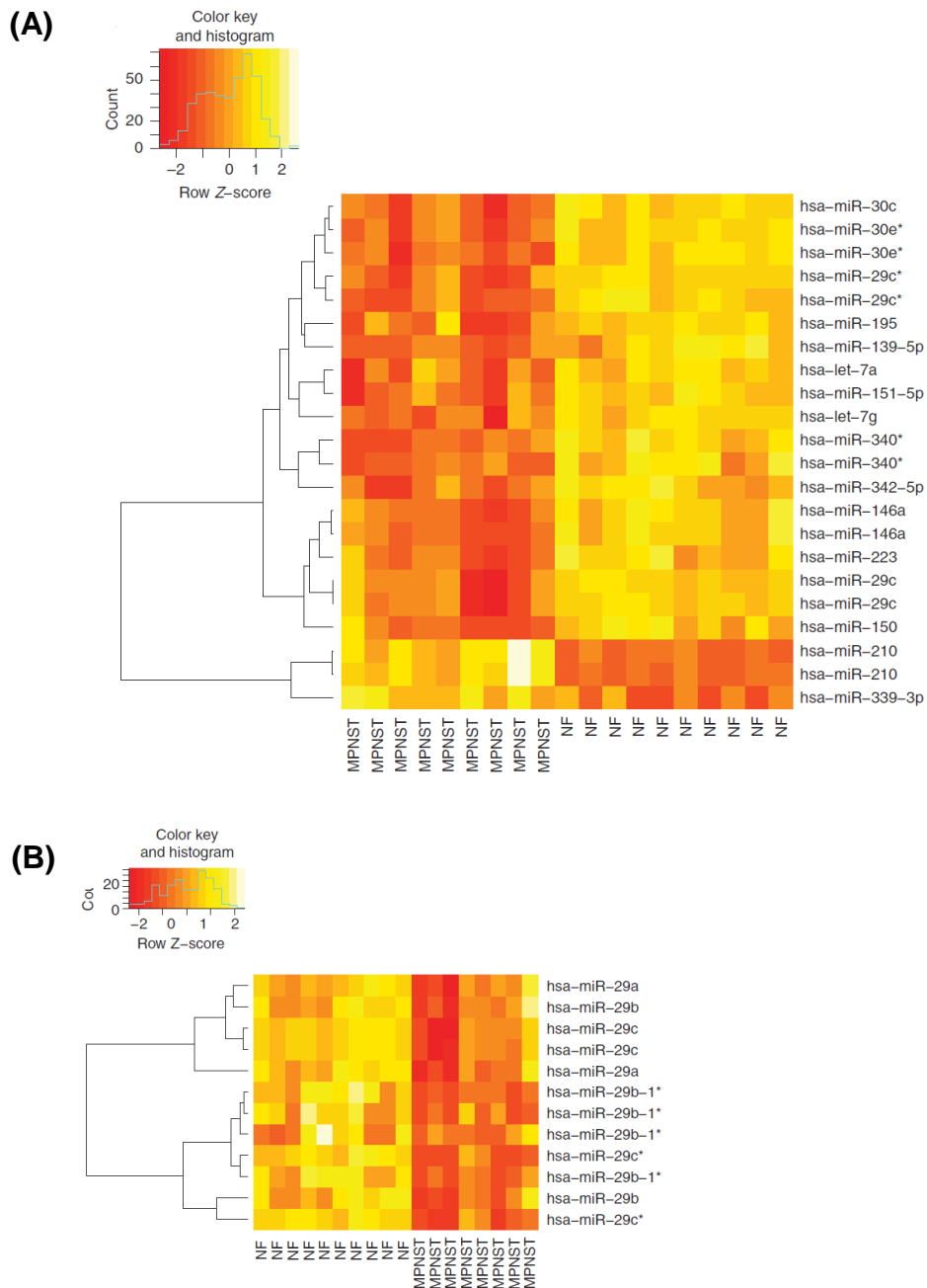


### Figure 3-1: miRNA expression profiling of neurofibromas and MPNSTs by microarray analysis

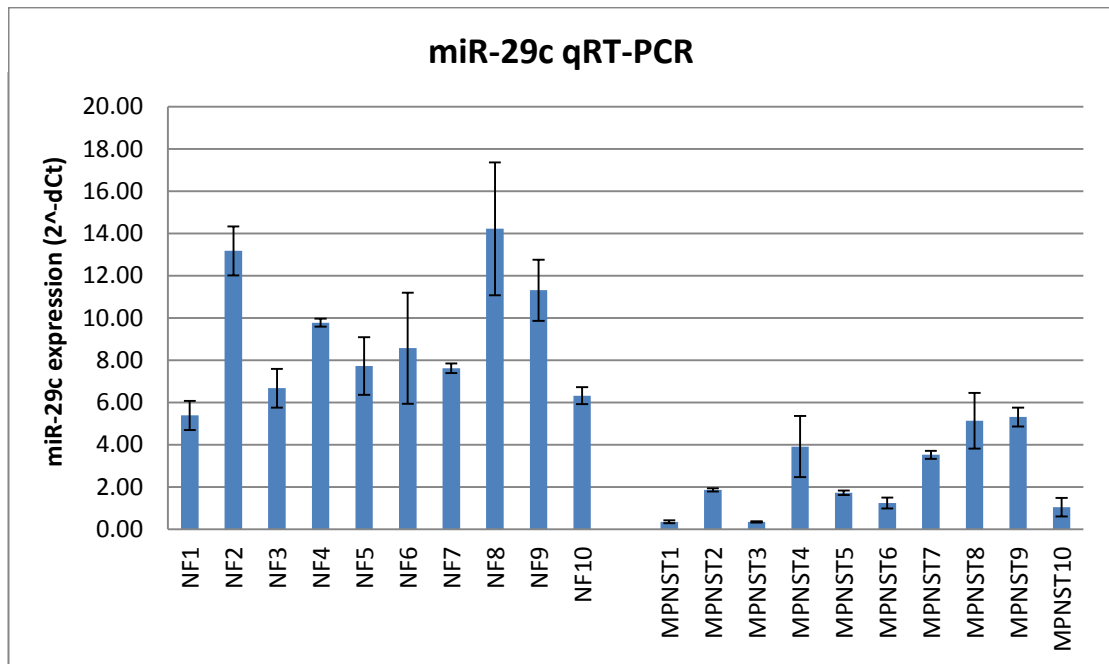
Microarray expression data from 10 neurofibromas and 9 MPNSTs are shown. (A) Unsupervised hierarchical clustering analysis representing the 16 most significant differentially expressed miRNAs (with a cut off of  $q = 8.48E-03$  for the least significant miRNA) demonstrating up-regulation of miR-210 and miR-339-3p and downregulation of the remaining 14 miRNAs in MPNSTs compared to neurofibromas. (B) Supervised heat-map of miR-29 family demonstrating significantly reduced expression of all miR-29 family members in MPNSTs relative to neurofibromas ( $p < 0.05$ ). The columns in each heat map represent individual tumour samples and the rows represent relative expression levels of individual miRNAs in each tumour. The yellow and orange colours indicate relatively high and low expression, respectively.

### **3.3.2. Confirmation of decreased miR-29c expression in MPNSTs versus neurofibromas by qRT-PCR**

In order to validate the results from the miRNA microarray experiments, the expression of the mature form of miR-29c was examined in the 10 neurofibromas and 10 MPNSTs by quantitative reverse transcription polymerase chain reaction (qRT-PCR) using a commercially available TaqMan reporter assay. Details of the assay and quantification methods used are as previously described in chapter 2. The small nucleolar RNA, RNU66, was used as a control for normalization of the qRT-PCR data. RNU66 is an ideal candidate for use as an internal control in Real time quantitative PCR since it exhibits abundant and constant expression across a wide variety of human tissues. All experiments were conducted in duplicate and the data was analysed using the ( $2^{\Delta\Delta Ct}$ ) method.

The results from the miR-29c qRT-PCR experiments can be seen in Figure 3-2. These demonstrated a significant reduction in expression of miR-29c in MPNSTs compared to that in neurofibromas ( $p < 0.001$ ) thus confirming the previous findings from the microarray expression data.

(A)



(B)

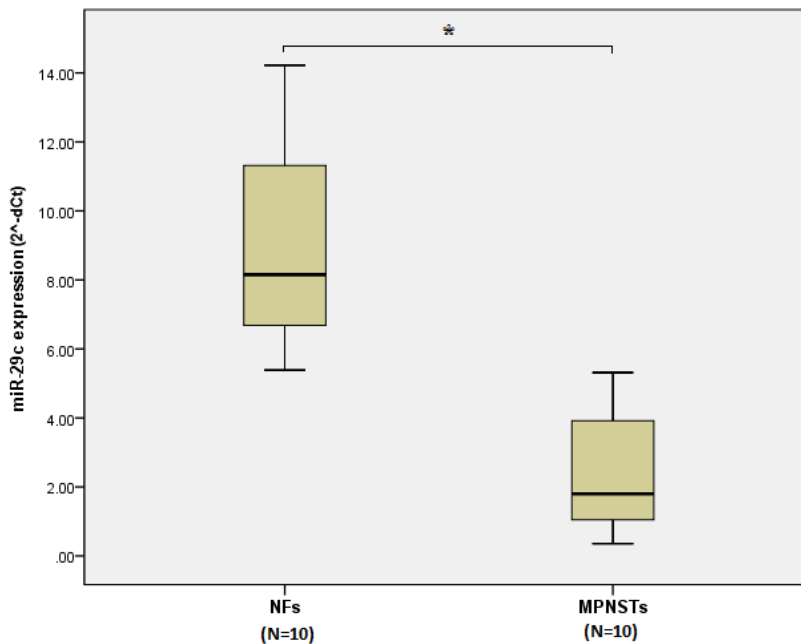


**Figure 3-2: Downregulation of miR-29c expression in MPNSTs compared to neurofibromas demonstrated by qRT-PCR**

(A) Bar graph demonstrating miR-29c expression levels in 10 neurofibromas and 10 MPNSTs. The qRT-PCR data was normalised to expression of RNU66 nucleolar RNA. Each bar represents the average results of two technical replicates from one experiment. Error bars represent standard deviation. (B) Summary of the miR-29c qRT-PCR results. The box plots show the median, interquartile boxes, 95<sup>th</sup> percentile range for miR-29c expression in 10 neurofibromas and 10 MPNSTs (unpaired Student's *t*-test, \**p* < 0.001).

### 3.3.3. *NF1* mRNA expressed at low levels in MPNSTs and neurofibromas

Biallelic inactivation at the *NF1* gene locus is a hallmark of all neurofibromas and MPNSTs (Legius et al. 1993; Colman et al. 1995). In order to confirm the genotype of our 10 neurofibromas and 10 MPNSTs as being null for the *NF1* gene, I examined the levels of *NF1* mRNA expression in these samples using a SYBR green-based qRT-PCR. Details of the *NF1* primers and thermo-cycling conditions used are given in chapter 2. The sNF96.2 cell line, which is derived from an *NF1*-deficient human MPNST cell line, was used as a negative PCR template control for *NF1* mRNA expression and the human embryonic kidney cell line HEK293T, which is wild-type homozygous for the *NF1* gene, was used as a positive PCR template control. The qRT-PCR data was normalised to the *GAPDH* gene and all experiments were performed in duplicate. A summary of the *NF1* qRT-PCR can be seen in Figure 3-3. The expression of *NF1* mRNA in the 10 NFs and 10 MPNSTs was found to be extremely low compared to expression in the wild-type HEK293T cells and resembled more closely the data from the negative control sNF96.2 cell line. This finding along with loss of heterozygosity of the neurofibromin 1 locus, as recently reported by SNP genotyping analysis on the pooled samples from the same 10 neurofibromas and 10 MPNST (Feber et al. 2011), is consistent with functionally biallelic inactivation of neurofibromin 1 gene these tumour samples (Legius et al. 1993; Colman et al. 1995).

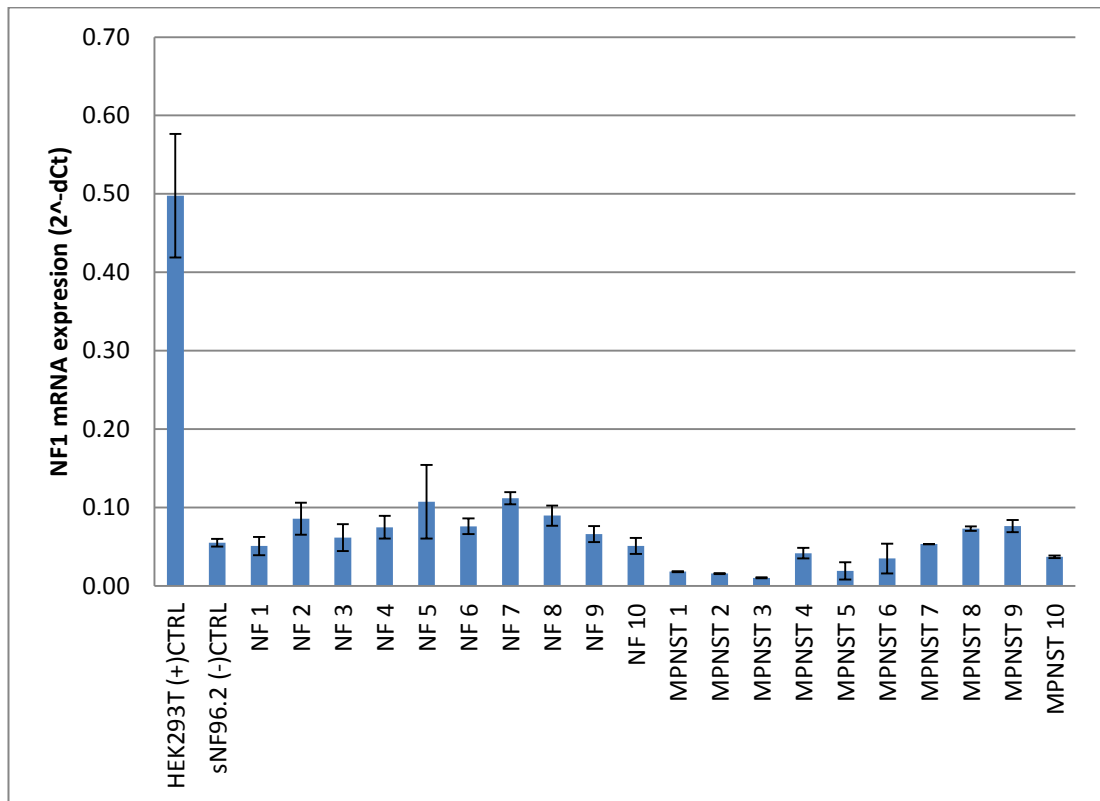


**Figure 3-3: Low levels of *NF1* mRNA expression in neurofibromas and MPNSTs**

qRT-PCR of *NF1* mRNA expression in 10 neurofibromas and 10 MPNSTs. The HEK293T cell line, which is homozygous wild-type for the *NF1* gene, was used as a positive PCR control and the sNF96.2 MPNST-derived cell line, which is null for the *NF1* gene, was used as a negative template control. The qRT-PCR data was normalised to *GAPDH* gene. The results shown represent the average of two technical replicates from one experiment. Error bars represent standard deviation. The data is consistent with biallelic inactivation of *NF1* in all 10 neurofibromas and 10 MPNSTs.

### **3.3.4. miR-29c expression in different types of sarcomas and low-grade tumours**

Having determined that miR-29c is expressed at low levels in MPNSTs relative to neurofibromas I decided to look at the expression of this miRNA in other sarcomas and low-grade tumours. I selected 35 fresh frozen tumours for examination including 4 Neurofibromas, 3 MPNSTs, 4 Liposarcomas, 4 Osteosarcomas, 4 Synovial Sarcomas, 4 Rhabdomyosarcomas, 3 Solitary fibrous tumours, 3 Fibromatosis desmoid type, 2 Chondromas and 2 Chondroblastomas. Total RNA was isolated from frozen sections prepared from each tumour, and the miR-29c qRT-PCR was carried out as previously described for the MPNSTs and neurofibromas using a TaqMan reporter assay (Chapter 2). The results from these qRT-PCR demonstrated relatively low levels of miR-29c expression in most of these different tumour types compared with expression in neurofibromas. Chondroblastomas exhibited relatively high levels of miR-29c compared to all the other tumours types followed by the solitary fibrous tumours although the error bars were fairly large in the latter case. These findings suggest that miR-29c could play a role in the pathogenesis of a wide variety of sarcomas and low-grade tumours in addition to MPNSTs.

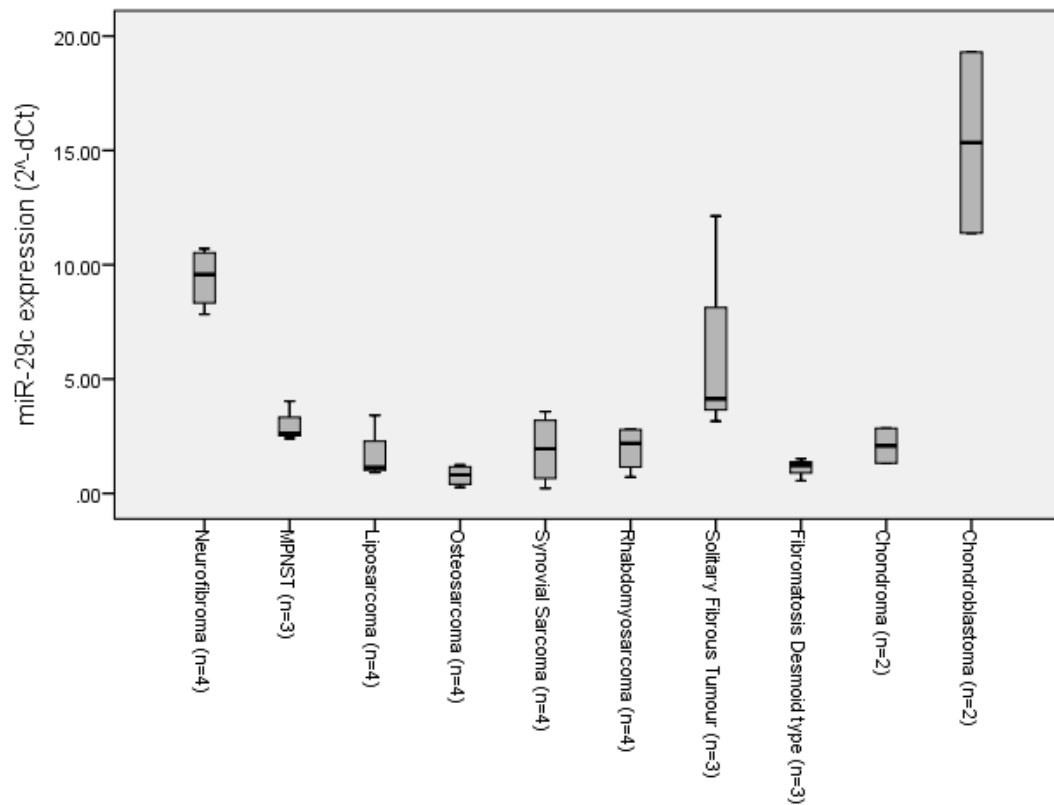


**Figure 3-4: miR-29c expression in neurofibromas and MPNSTs compared with other sarcomas and low-grade tumours**

qRT-PCR results demonstrating relatively low levels of miR-29c expression in nearly all the different sarcomas and low-grade tumours compared to expression in neurofibromas. Chondroblastomas demonstrate relatively high levels of miR-29c expression. Box plots show the median, interquartile boxes and 95<sup>th</sup> percentile range for miR-29c expression. The number of each tumour type analysed is given in brackets. The qRT-PCR data was normalised to expression of RNU66 nucleolar RNA. The results shown represent the average of two technical replicates from one experiment.

### **3.3.5. *In vitro* studies on the MPNST- derived sNF96.2 cell line**

#### **3.3.5.1. Confirmation of *NF1* gene mutation in sNF96.2 cell line**

In order to determine what role miR-29c might play in the in pathogenesis of MPNSTs, functional studies were carried out *in vitro* using the MPNST-derived cell line sNF96.2. This cell line was chosen because it had previously been shown in our lab to express very low levels of mature miR-29c (Dr Nadege Presneau personal communication). As a preliminary step, the sNF96.2 cell line was first genotyped to confirm the presence of a germline mutation in exon 21 (3683delC) of the neurofibromin (*NF1*) gene and loss of the remaining wild-type (WT) *NF1* allele as has previously been documented in this cell line (Perrin et al. 2007). DNA was extracted from cultured sNF96.2 cells and the region around exon 21 of the *NF1* gene, which encompasses the single nucleotide deletion, was amplified by PCR and sequenced (details of the PCR and sequencing methods are given in chapters 2). DNA from the HT1080 fibrosarcoma cell line which is known to be homozygous wild-type for the *NF1* gene was also amplified and sequenced for use as a control. The results of the sequencing analysis, which confirmed presence of the *NF1* gene mutation in the sNF96.2 cell line, are shown in Figure 3-5.

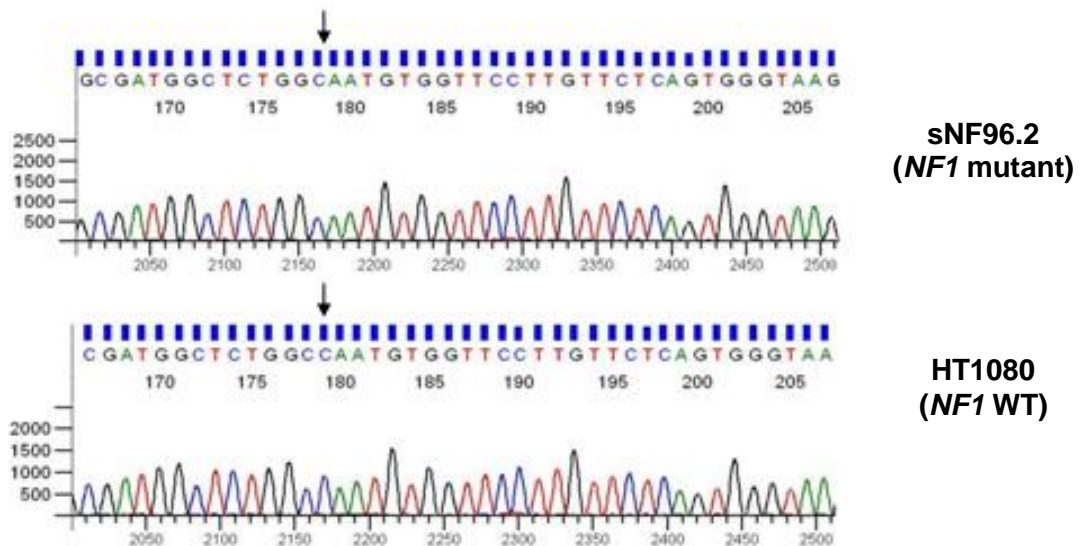


**Figure 3-5: Single nucleotide deletion in the *NF1* gene of sNF96.2**  
Sequencing of *neurofibromin 1* (*NF1*) exon 21 confirms the homozygous deletion (3683delC) in exon 21 of sNF96.2 cells. The normal *NF1* sequence is demonstrated in HEK293T cells which are wild-type for *NF1*.

### **3.3.5.2. Transfection of miR-29c into MPNST-derived cell line sNF96.2**

Having confirmed that the sNF96.2 cell line has a mutation in the *NF1* gene, the effects of expressing miR-29c in this cell line were examined *in vitro* by transfecting synthetic miR-29c mimics into the cell line using oligofectamine as described in chapter 2. Control experiments in which sNF96.2 cells were transfected with scrambled oligonucleotides were also carried out at the same time. The efficiency of transfection was examined at two time points following the start of transfection; RNA was extracted from transfected cells at 24 and 48 h and the levels of miR-29c expression was then determined by qRT-PCR as previously described (chapter 2). The results demonstrated an increase of miR-29c expression in the cells transfected with synthetic miR-29c mimics at 24 h compared to control cells transfected with scrambled nucleotides and the was even more marked at 48 h post-transfection (Figure 3-6). These findings demonstrated that the miR-29c mimics had successfully been transfected and were being expressed in the MPNST-derived sNF96.2 cell line.

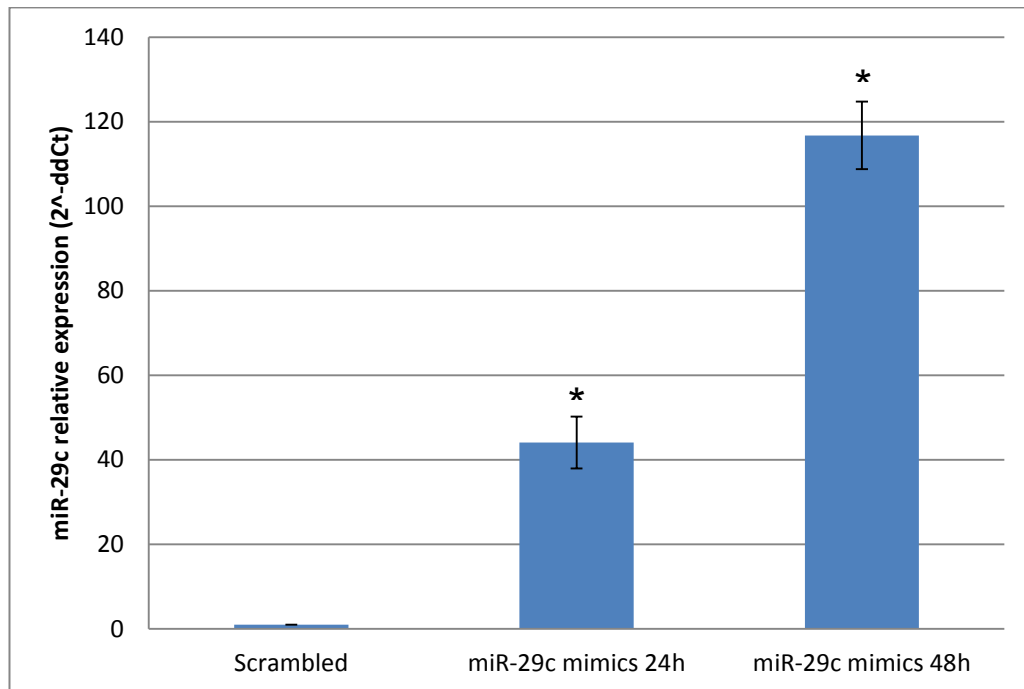


**Figure 3-6: Increased miR-29c expression following transfection of SNF96.2 cells**

qRT-PCR results demonstrating increased miR-29c expression in cells transfected with miR-29c mimics compared to control cells transfected with scrambled oligonucleotides at 24 and in 48 h post-transfection (paired Student's *t*-test, \**p* < 0.001 at 24 and 48 h). The qRT-PCR data was normalised to expression of RNU66 nucleolar RNA. Bars represent the average results obtained from three independent experiments (three biological replicates). Error bars represent standard deviation.

### **3.3.5.3. Functional effects of miR-29c transfection on proliferation and migration of sNF96.2 cells**

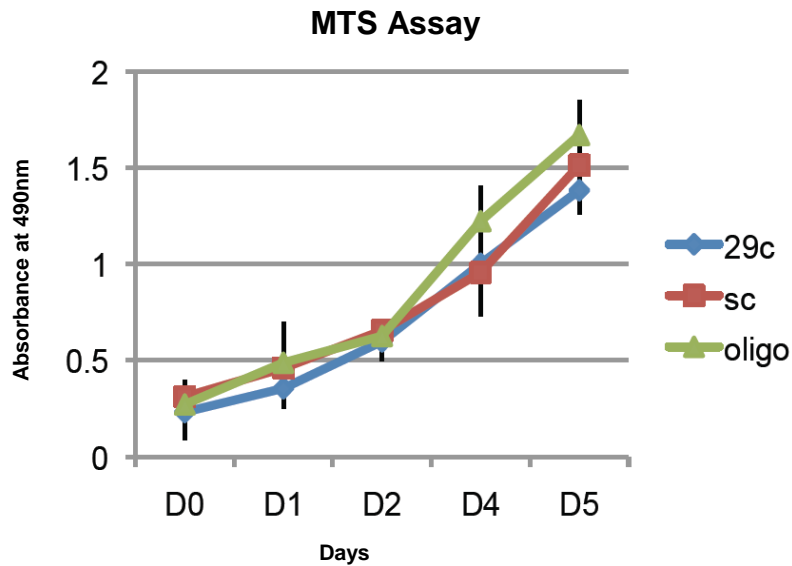
#### **3.3.5.3.1. Cell proliferation**

Next, I wanted to examine miR-29c *in vitro* effects on cell proliferation. Following successful transfection of miR-29c into sNF96.2 cells, functional studies examining the effects of miR-29c expression on cell proliferation and migration were carried out on the transfected cells.

Cell proliferation was assessed over a 5 day period using two different methods; (i) MTS assay which detects cell viability via a colorimetric assay and (ii) Kinetic Live Cell Imaging by the IncuCyte™ System that gives updates on cell confluence in real-time. Details of both assays can be found in chapter 2.

The results from the MTS assay, which are summarised in Figure 3-7A, showed no significant difference in cell proliferation following transfection of sNF96.2 cells with either miR-29c mimics or scrambled oligonucleotides. The live cell imaging data was found to be in agreement with that obtained by MTS assay i.e. there was no significant difference in cell proliferation following transfection of sNF96.2 cells with either miR-29c mimics or scrambled oligonucleotides (control) over a 5 day period (Figure 3-7B). These findings suggest miR-29c does not significantly alter cell proliferation when expressed in MPSNT-derived cells.

(A)



(B)

**Incucyte Imaging Growth Rates**

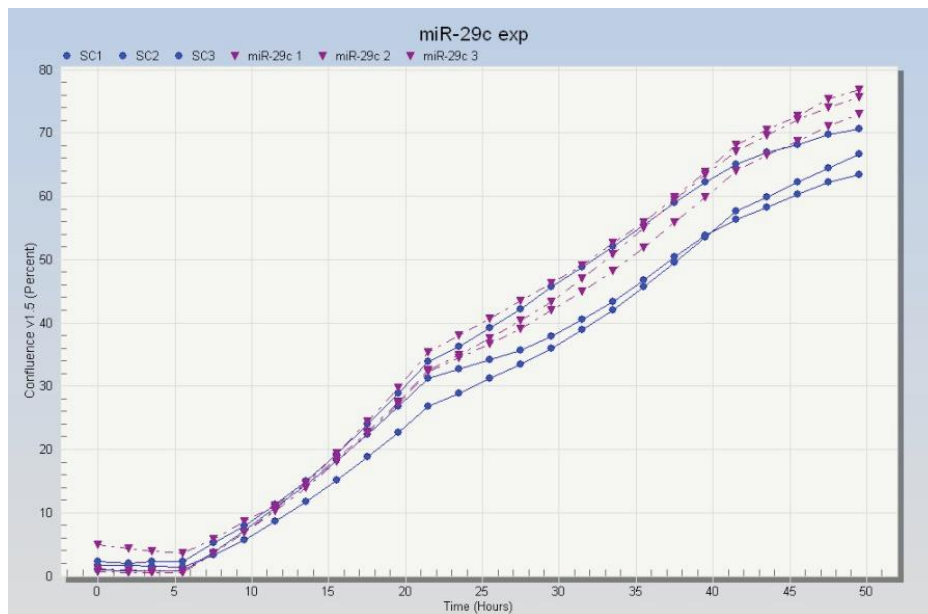


**Figure 3-7: sNF96.2 cell proliferation following miR-29c transfection**

(A) MTS assay showing no significant difference in proliferation between sNF96.2 cells transfected with miR-29c mimics (test cells) or scrambled oligonucleotides (controls). Cells were plated on Day 0 and transfected 24 h later (Day 1). Cell viability was measured at five separate time points (Days 0 to 5). The results are expressed as units of absorbance at 490 nm wavelength vs days after transfection. The results shown represent the average results from three independent experiments (three biological replicates). Error bars represent standard deviation (B) Incucyte quantification of cell confluence over 50 hs showing no significant difference in proliferation rates between control and test cells. The data is expressed as percentage confluence vs number of hours. The graph show the results obtained from three replicate transfections from one experiment.

### **3.3.5.3.2. Cell migration**

Following the cell proliferation analyses I wanted to test the effect of miR-29c expression on cell migration. Cell migration was analysed in sNF96.2 cells using transwell plates and the scratch/wound healing assays. These assays are described in more detail in chapter 2.

Figure 3-8 A and B demonstrates the results from the cell migration assay which revealed significantly fewer numbers of miR-29c-transfected sNF96.2 cells had invaded the transwell membranes compared to control cells transfected with scrambled oligonucleotides.

The scratch-wound healing assay was carried on sNF96.2 cells transfected with either miR-29c mimics or scrambled oligonucleotides. On reaching confluence, a scratch was made through the central axis of each well in cell culture plate, and the growth of cells in the scratch area was monitored using time-lapse photography. At 60 h post-transfection I found a significant reduction in the number of miR-29c transfected cells which had migrated into the wound area compared to control cells transfected with scrambled oligonucleotides (Figure 3-8C).

The findings suggest that miR-29c expression may play an important role in suppressing the migratory behaviour of MPSNT- derived cells.

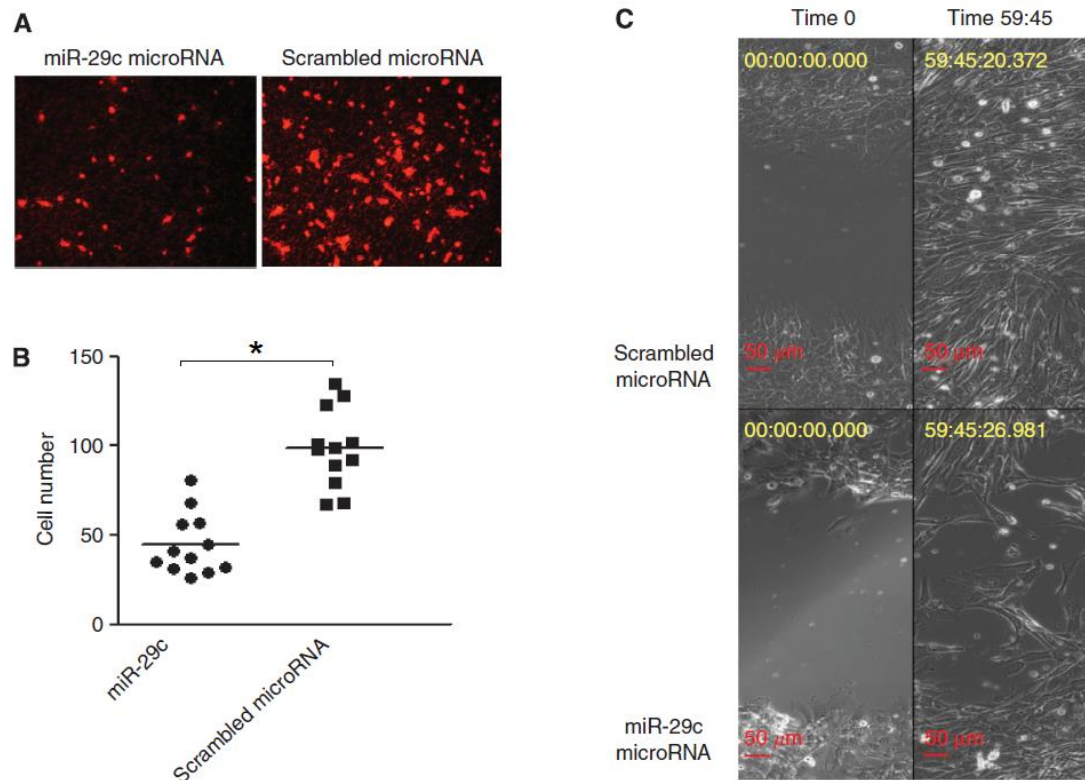


### Figure 3-8: miR-29c transfection inhibits sNF96.2 cell migration

(A) Cell migration assay showing MPSNT-derived sNF96.2 cells attached to transwell membranes. Around 25000 cells were transferred to individual wells 2 days post-transfection and after 6 h incubation the cells were fixed and stained with GelRed. Markedly fewer numbers of miR-29c-transfected cells are visible on the bottom of the transwell membrane compared to controls. The migrated cells on the membrane were counted in four fields where the cells were evenly distributed and the graph (B) shows the average number of cells in each field from three independent experiments (three biological replicates). Horizontal bars depict mean number of cells (unpaired Student's *t*-test, \* $p < 0.05$ ). (C) *In vitro* scratch wound healing assay demonstrating fewer numbers of miR-29c transfected sNF96.2 cells migrating into the wound area compared to control cells 60 h post-transfection.

### 3.3.6. *In silico* prediction of miR-29c targets implicated in migration

Following the demonstration that miR-29c expression can inhibit the migration of MPNST-derived cells, I next set out to identify specific mRNAs that may be targeted by miR-29c. Predicted targets of miR-29c were sought *in silico* using TargetScan (<http://www.targetscan.org/>), PicTar (<http://pictar.mdc-berlin.de/>) and MiRanda (<http://www.microrna.org/microrna/home.do>) software algorithms which are specifically designed for the identification of microRNA targets (Bartel 2009). Different prediction algorithms usually have a high degree of overlap, however, they are not 100% identical, and there is often a need to crosscheck multiple algorithms to get an additional layer of confidence for the true positive targets. Using these three algorithms, I identified a list of 223 predicted gene targets for miR-29c.

Next, I performed a functional classification of the 223 predicted targets using the DAVID program (<http://david.abcc.ncifcrf.gov/>). Based on the functional classification, the top category identified was extracellular matrix genes (Table 3-1). Table 3-2 describes the predicted miR-29c target genes relevant to migration in three different *in silico* databases (TargetScan, PicTar, and MiRanda); where 0 i.e. not present in database 1 i.e. present in database. SUM i.e. the sum of the three *in silico* databases. I conclude from this that collagen genes are predicted targets for miR-29c in all the three *in silico* databases, which make them interesting for further studies.

**Table 3-1: Gene ontology analysis for miR-29c predicted target genes identified extracellular matrix genes as the top category.**

No. of Genes	p-value	Annotations
13	4.10E-09	GO:0030198 :extracellular matrix organization (BP)
49	4.96E-06	GO:0010556 :regulation of macromolecule biosynthetic process (BP)
48	4.86E-06	GO:2000112 :regulation of cellular macromolecule biosynthetic process (BP)
50	5.24E-06	GO:0031326 :regulation of cellular biosynthetic process (BP)
25	1.03E-05	GO:0022008 :neurogenesis (BP)
48	1.21E-05	GO:0010468 :regulation of gene expression (BP)
24	1.04E-05	GO:0048699 :generation of neurons (BP)
49	1.02E-05	GO:0019219 :regulation of nucleobase, nucleoside, nucleotide and nucleic acid metabolic process (BP)
6	1.90E-05	GO:0071230 :cellular response to amino acid stimulus (BP)
6	3.24E-05	GO:0071418 :cellular response to amine stimulus (BP)
18	5.10E-05	GO:0031175 :neuron projection development (BP)
41	0.000266939	GO:0051252 :regulation of RNA metabolic process (BP)
17	0.000255123	GO:0072358 :cardiovascular system development (BP)
18	0.000263187	GO:0048666 :neuron development (BP)
41	0.000332515	GO:0006351 :transcription, DNA-dependent (BP)
13	0.000778813	GO:0001944 :vasculature development (BP)
5	0.00091948	GO:0043588 :skin development (BP)

**Table 3-2: Description of selected predicted target genes relevant to migration and invasion in three different *in silico* databases (TargetScan, PicTar, and MiRanda)**

Gene	Target	PicTar	MiRanda	SUM
<b>Collagens</b>				
COL1A1	1	1	1	3
COL1A2	1	1	1	3
COL4A4	1	1	1	3
COL4A5	1	1	1	3
COL4A1	1	1	1	3
COL4A3	1	1	1	3
COL4A2	1	1	1	3
COL5A3	1	1	1	3
COL5A2	1	1	1	3
COL6A3	1	1	1	3
COL7A1	1	1	1	3
COL11A1	1	1	1	3
COL22A1	1	1	1	3
<b>Matrix metalloproteinases</b>				
MMP2	0	1	0	1
MMP24	0	0	0	0
<b>Transforming growth factor beta</b>				
TGB3	0	1		1
<b>Desintegrin and metalloproteases</b>				
ADAMTS6	1	1	0	2
ADAMTS7	1	1	0	2
ADAMTS9	1	1	0	2
ADAMTS10	0	0	1	1
ADAMTS17	1	0	1	2
ADAMTS18	1	1	1	3
ADAM19	0	1	0	1
<b>Integrins</b>				
ITGB1	0	0	1	1
ITGA6	0	1	0	1
ITGA11	0	1	0	1

Key: 0= not present in database; 1= present in database; SUM= sum of three *in silico* databases

Further analysis of the data from our previous gene expression microarray performed on neurofibroma and MPNST (Henderson et al. 2005) showed that extracellular matrix genes which are predicted targets for miR-29c are more highly expressed in MPNST as compared to neurofibroma (Figure 3-9).

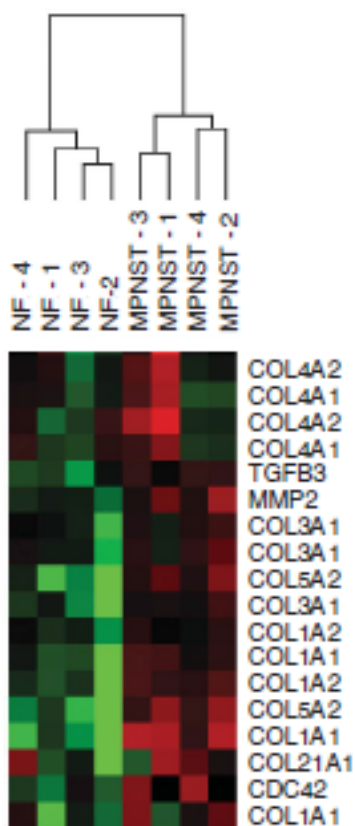


**Figure 3-9: Extracellular matrix genes are highly expressed in MPNSTs compared to neurofibromas**

Heat-map demonstrating high expression of ECM genes in MPNSTs using gene expression microarrays. Red boxes depict genes that are highly expressed. Genes with low levels of expression are depicted by green boxes.

### 3.3.7. miR-29c targets collagen matrix genes

My *in silico* target prediction analyses identified the extracellular matrix (ECM) genes *COL1A1*, *COL1A2*, *COL4A1*, *COL4A2*, *COL5A2* and *COL21A1* as possible targets for miR-29c. These ECM genes have previously been identified in our lab by gene expression microarray analysis as being overexpressed in MPSNTs compared to expression in neurofibromas (Henderson et al. 2005). I therefore decided to examine whether ectopic expression of miR-29c *in vitro* could have an influence on the expression of these ECM genes. This was done by analysing the expression of these genes by qRT-PCR in miR-29c transfected sNF96.2 cells and control cells transfected with scrambled oligonucleotides.

Details of the qRT-PCR experiments including primers used are given in chapter 2. The results of these qRT-PCR experiments are summarised in Figure 3-10. A significant reduction in expression (between 65% - 85%) of all six ECM target genes was found in miR-29c-transfected sNF96.2 cells compared to controls (Figure 3-10). These findings suggest miR-29c may play a role in development of MPSNTs by down-regulating expression of ECM genes and in particular *COL1A1*, *COL1A2*, *COL4A1*, *COL4A2*, *COL5A2*, and *COL21A1*.

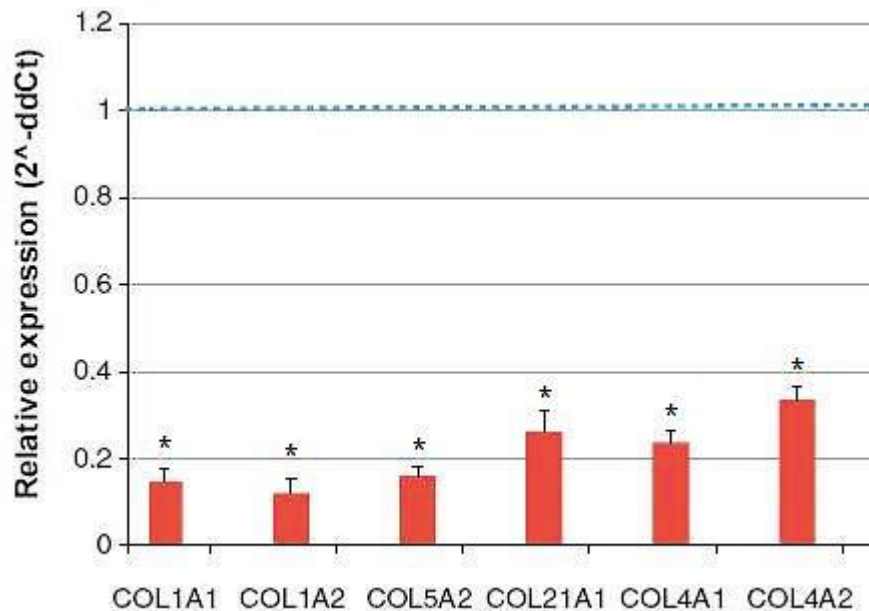


**Figure 3-10: Down-regulation of collagen gene expression in miR-29c transfected sNF96.2 cells**

qRT-PCR results demonstrating reduced expression of 6 collagen genes in miR-29c-transfected sNF96.2 cells relative to expression in control cells transfected with scrambled oligonucleotides (which are all given the value 1), (paired Student's *t*-test, \**p* < 0.001). The qRT-PCR data was normalised to *GAPDH* gene. Bars represent the average results from three independent experiments (three biological replicates). Error bars represent standard deviation.

### **3.3.8. miR-29c directly influenced MMP2 but indirectly inhibits MMP9 activity**

The reduced migration of sNF96.2 cells following transfection with miR-29c mimics led me to speculate as to whether this could be a result of decreased proteolytic activity in these cells. Previous analyses in our lab using zymography have shown that sNF96.2 cells transfected with miR-29c mimics have reduced proteolytic activity. Specifically, the bands corresponding to Matrix metalloproteinases 2 and 9 (MMP2 and MMP9) were shown to be absent in zymographs of supernatants taken from miR-29c-transfected sNF96.2 cells (Figure 3-11A). In order to throw more light on these findings I decided to examine the expression of *MMP2* and *MMP9* in miR-29c-transfected sNF96.2 cells at both the mRNA and protein level by qRT-PCR and Western blot analysis. Details of the qRT-PCR and Western blot techniques used are described in Chapter 2.

Western blots were prepared using extracts from sNF96.2 cells transfected with miR-29c mimics or scrambled nucleotides and probed using antibodies for MMP2 and MMP9 antibodies. The results from the Western blot analysis demonstrated clear expression of the 92 KDa MMP9 protein in miR-29c-transfected sNF96.2 cells as well as in the control cells (Figure 3-11B). Expression of *MMP9* mRNA transcripts was also confirmed by qRT-PCR in both test and control sNF96.2 transfected cells. MMP2 protein (72 KDa) however was not detectable in miR-29c-transfected sNF96.2 cells, although it was expressed in control sNF96.2 cells. In addition, a significant reduction

of *MMP2* mRNA expression was demonstrated by qRT-PCR in miR-29c transfected sNF96.2 cells compared to control cells.

These findings demonstrate that the inhibition of MMP9 proteolytic activity in miR-29c-transfected sNF96.2 cells is not due to direct abrogation of *MMP9* mRNA or protein expression but may be brought about indirectly through an as yet unknown mechanism (I will investigate this in the next section). MMP2 activity on the other hand appears to be directly influenced by expression of miR-29c in sNF96.2 cells; expression of miR-29c leads to reduced expression of *MMP2* mRNA, which in turn leads to diminished MMP2 protein expression thus reducing MMP2 enzyme activity in these cells.

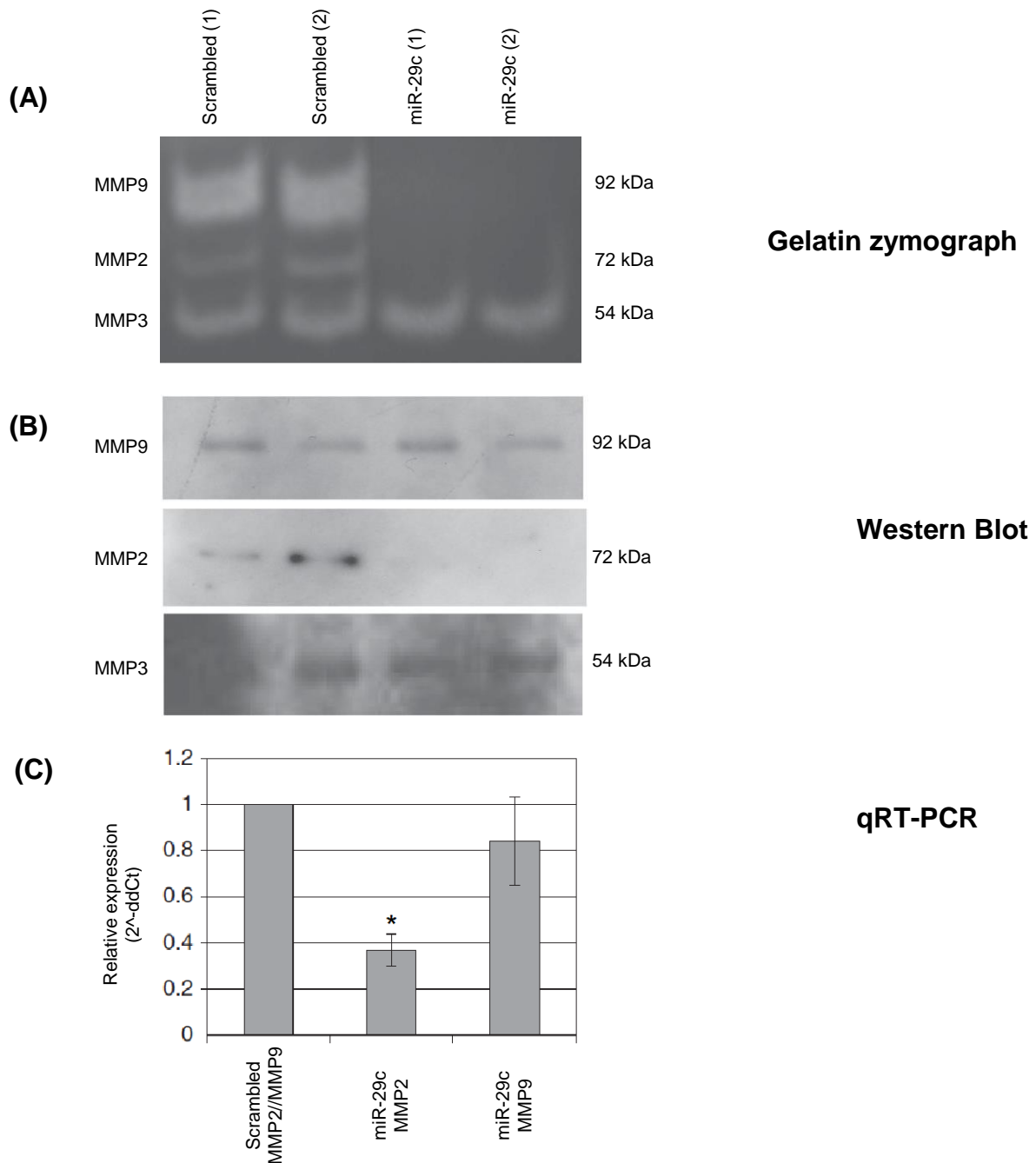


**Figure 3-11: MMP2 and MMP9 activity & expression in miR-29c transfected sNF96.2 cells**

(A) Zymograph of supernatants from sNF96.2 cells transfected with miR-29c mimics (test) or scrambled oligonucleotides (control). Zones of gelatinolytic activity are visualised as transparent bands against a dark background. The MMP2 and MMP9 bands are visible in control cells but absent in the test cells. MMP3 expression is visible in all samples. (B) Western blots demonstrating expression of MMP9 and MMP3 protein in all cultures. MMP2 protein is clearly visible in control cells but is absent in miR-29c transfected cells. (C) qRT-PCR data demonstrating significantly reduced *MMP2* mRNA (paired Student's *t*-test, \**p* < 0.01) but no significant alteration of *MMP9* mRNA expression in miR-29c-transfected sNF96.2 cells compared to that in control cells. The qRT-PCR data was normalised to *GAPDH* gene. The bars represent the average results from three independent experiments (three biological replicates). Error bars represent standard deviation. Zymograph image courtesy of Dr. Malihe Eskandarpour.

### **3.3.9. miR-29c partially inhibits MMP9 activity through influencing *TGFB3***

Another predicted target of miR-29c predicted by my *in silico* analysis is Transforming Growth Factor Beta3 (*TGFB3*). This gene is particularly interesting as a link between MMPs and the *TGFB* gene family has previously been demonstrated in breast cancer (Wiercinska et al. 2010). I therefore decided to investigate whether *TGFB3* is a target of miR-29c in MPSNT-derived cells by examining the expression of this gene in miR-29c-transfected cells by qRT-PCR. Details of the *TGFB3* primers and qRT-PCR protocol used are described in more detail in chapter 2. The results from these experiments demonstrated a significant reduction in *TGFB3* mRNA expression at 24 h following transfection of sNF96.2 cells with miR-29c-mimics compared to expression in control cells transfected with scrambled oligonucleotides, and by 48 h, the expression of *TGFB3* mRNA was reduced by almost 50% in the miR-29c-transfected cells (Figure 3-12). These findings suggest miR-29c expression may have an important influence on the expression of *TGFB3* as well as affecting the expression of *MMP2* in MPNSTs.

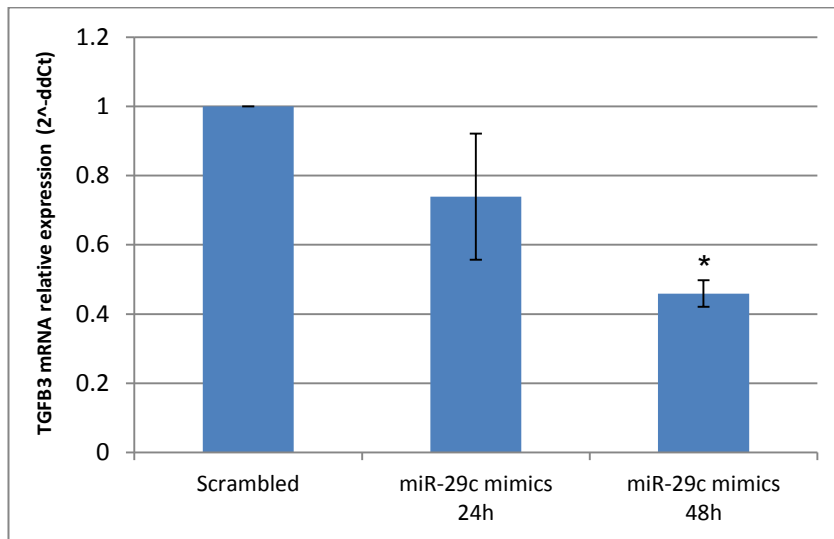


**Figure 3-12: Downregulation of *TGFB3* mRNA is induced by miR-29c**

qRT-PCR data demonstrating down-regulation of *TGFB3* mRNA expression in sNF96.2 cells transfected with miR-29c mimics at 24 and 48 h following transfection with miR-29c mimics compared to expression in control cells transfected with scrambled oligonucleotides (paired Student's *t*-test, \**p* < 0.01 after 48 h). The qRT-PCR data was normalised to *GAPDH* gene. Bars represent the average results from three independent experiments (three biological replicates). Error bars represent standard deviation.

I next investigated a possible link between *TGFB3* and *MMP2* or *MMP9* by reducing the expression of *TGFB3* in sNF96.2 cells and examining the effect(s) this might have on the expression of *MMP2* and *MMP9*. *TGFB3* mRNA expression was inhibited by transfecting anti-*TGFB3* siRNA into wild-type sNF96.2 as described in chapter 2. The cells were harvested 24 and 48 h following transfection and the mRNA expression of *TGFB3* in the siRNA transfected cells was measured by qRT-PCR and compared to expression of *TGFB3* in control sNF96.2 cells, which had been transfected with scrambled oligonucleotides. The results of the *TGFB3* qRT-PCRs are shown in Figure 3-13A. At 24 h post-transfection, there was a 30% reduction in the expression in *TGFB3* mRNA expression in the anti-*TGFB3* siRNA transfected cells compared to expression in control cells. By 48 h, the

*TGFB3* mRNA expression was reduced by more than 50% in the anti-*TGFB3* siRNA transfected cells. Having demonstrated successful inhibition of *TGFB3* mRNA expression by siRNA the *MMP2* and *MMP9* mRNA and protein expression were examined in the anti-*TGFB3* siRNA treated cells, as well as control cells, by qRT-PCR and western blot analysis as previously described (Chapter 2). The results from these experiments demonstrated no significant alteration in the expression of *MMP2* or *MMP9* at either the mRNA transcript or protein level following inhibition of *TGFB3* mRNA expression in sNF96.2 cells (Figure 3-13 B & C respectively).

The *MMP9* and *MMP2* enzyme activity in the supernatant of anti-*TGFB3* siRNA-treated cultures and control sNF96.2 cells was then examined by gelatine zymography as described in chapter 2. The results of these experiments are shown in Figure 3-13D. Inhibition of *MMP9* and *MMP2* activity was clearly demonstrated in the supernatants of anti-*TGFB3* siRNA treated cells compared to that in supernatants of control cells, as demonstrated by reduced intensity of the *MMP2* and *MMP9* transparent bands on the zymography gel.

My findings suggest that *TGFB3* does not have a direct influence on the expression of *MMP9* and *MMP2* mRNA or protein but may indirectly bring about partial inhibition of *MMP9* and *MMP2* activity by an as yet unknown mechanism. Since *TGFB3* expression was also shown to be under the influence of miR-29c, my findings suggest that miR-29c may influence the activity of *MMP2* and *MMP9* through targeting *TGFB3*.

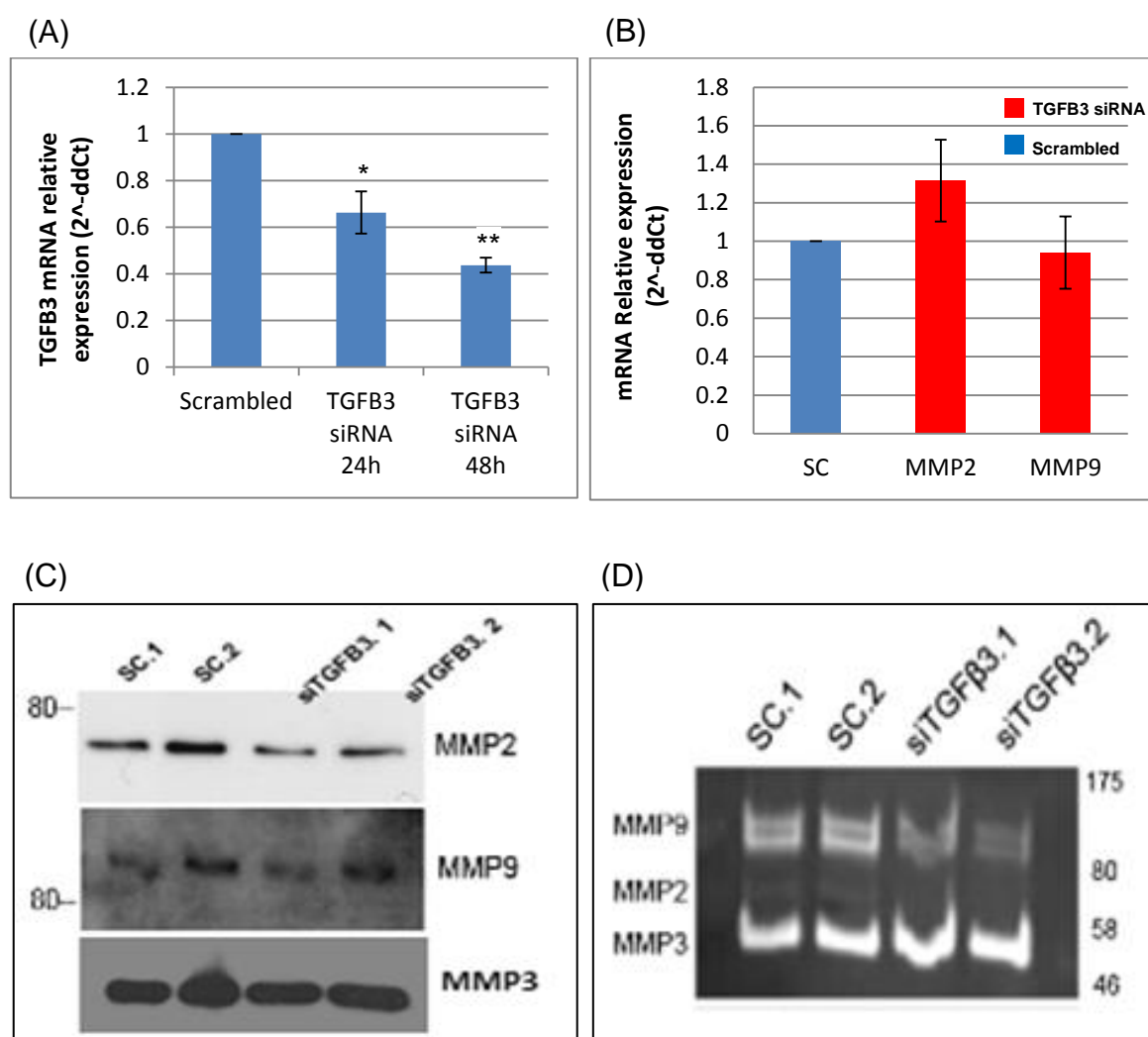


**Figure 3-13: Down-regulation of *TGFβ3* mRNA expression partially inhibits MMP9 and MMP2 activity**

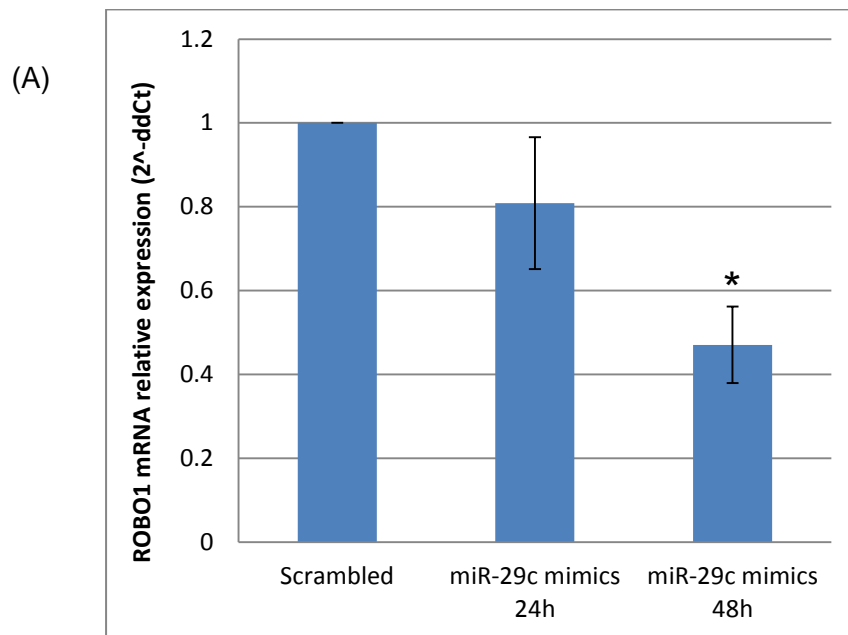
(A) qRT-PCR demonstrating down-regulation of *TGFβ3* mRNA expression in sNF96.2 cells 48 h after transfection with anti-*TGFβ3* siRNA compared to expression in control cells transfected with scrambled oligonucleotides (SC), (paired Student's *t*-test, \**p* < 0.05 and \*\**p* < 0.01 at 24 and 48 h, respectively). (B) qRT-PCR demonstrating no alteration in *MMP2* or *MMP9* mRNA levels in anti-*TGFβ3* siRNA treated sNF96.2 cells compared to expression in control cells. The qRT-PCR data in (A) and (B) was normalised to *GAPDH* gene. Bars represent the average results from three independent experiments (three biological replicates). Error bars represent standard deviation. (C) Western blot demonstrating no significant change in *MMP2* or *MMP9* protein expression in sNF96.2 cells transfected with anti-*TGFβ3* siRNA compared to expression in control cells. (D) Gelatin zymography of supernatants from sNF96.2 cells showing decreased activity of *MMP2* and *MMP9*, but not *MMP3*, in cells treated with anti-*TGFβ3* siRNA compared to control cells transfected with scrambled oligonucleotide as demonstrated by reduced intensity of the transparent bands on the gel.

### 3.3.10. Suppression of *ROBO1* expression by miR-29c

Another interesting gene which I identified *in-silico* as a potential target of miR-29c is *ROBO1*. This gene has been reported to be involved in cancer cell migration and invasion in gliomas as well pancreatic cancer and breast cancer (Dontula et al., 2013; Hang et al., 2014; Yang et al., 2012). Closer inspection of previous microarray data from our laboratory (Henderson et al. 2005) also revealed *ROBO1* to be significantly highly expressed in MPNSTs compared to neurofibromas ( $p < 0.01$ ).

In order to determine whether *ROBO1* is a target for miR-29c, I examined the expression of *ROBO1* by qRT-PCR in sNF96.2 cells, which had previously been transfected with miR-29c mimics or scrambled oligonucleotides. Details of the cell transfection and *ROBO1* qRT-PCR protocols are given in chapter 2. The qRT-PCR results demonstrated a significant reduction in *ROBO1* mRNA levels at 24 h following transfection of miR-29c into sNF96.2 cells compared to expression in control cells transfected with scrambled oligonucleotides. At 48 h post-transfection, the expression of *ROBO1* mRNA was further reduced to approximately 50% of that in the control cells ( $p < 0.05$ ) (Figure 3-14A). The findings demonstrate that miR-29c can influence and down-regulate the expression of *ROBO1* transcript in MPNST-derived cells.

In order to confirm these findings at the protein level, the expression ROBO1 protein was examined in the transfected cultures by Western blot analysis. The HEK293T cell line was used as a positive control for ROBO1 protein expression and GAPDH was used as a control for protein loading onto the western blot gels. The results of the Western blot analysis can be seen in Figure 3-14B. A strong 180 KDa ROBO1 protein signal was clearly visible in control HEK293T cells. However only a very weak ROBO1 protein signal was seen in control cells transfected with scrambled oligonucleotides and there was no evidence of ROBO1 protein expression in the cells transfected with miR-29c. These findings suggest that despite *ROBO1* mRNA being expressed in sNF96.2 cells, the transcript is not translated into ROBO1 protein at any detectable level.



(B)

#### ROBO1 Western Blot

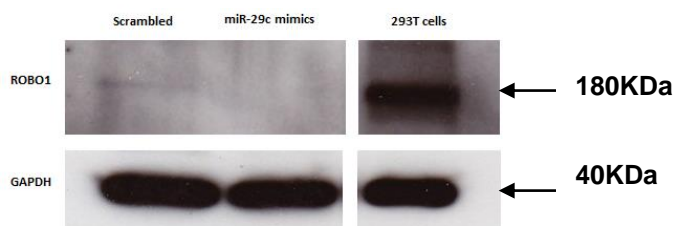


#### Figure 3-14: Downregulation of *ROBO1* expression following transfection of sNF96.2 cells with miR-29c

(A) qRT-PCR data demonstrating significant reduction in *ROBO1* mRNA expression in sNF96.2 cells at 24 and 48 h following transfection with miR-29c mimics compared to expression in control cells transfected with scrambled nucleotides (paired Student's *t*-test, \* $p < 0.05$ ). The qRT-PCR data was normalised to *GAPDH* gene. Bars represent the average results from three independent experiments (three biological replicates). Error bars represent standard deviation.

(B) Western blot demonstrating very weak expression of the 180 KDa *ROBO1* protein at 48 h following transfection of sNF96.2 cells with scrambled nucleotides and no visible *ROBO1* protein in cells transfected with miR-29c mimics. Strong expression of *ROBO1* can be seen in the HEK293T positive control cells. *GAPDH* was used as a protein loading control.

### 3.4. Summary of results

Using microRNA microarray analysis of 10 MPNSTs and 10 neurofibromas 16 differentially expressed genes were identified. Of these, miR-29c was of particular interest since, as well as showing a significant reduction in levels of expression in MPNSTs; this miRNA has also been implicated in a variety of other malignancies. Other members of the miR-29 family were examined using the same microarrays and showed that expression of miR-29a, b, c\* and b-1\*, as well as miR-29c, were also significantly downregulated in MPNSTs relative to neurofibromas. I then focussed my attention on miR-29c for further studies. Using qRT-PCR, I confirmed decreased expression of miR-29c in MPNSTs and also demonstrated relatively low levels of miR-29c expression in a variety of other sarcomas and low-grade tumours compared to expression neurofibromas.

In order to determine what role miR-29c might play in the pathogenesis of MPNSTs, *in vitro* functional studies were carried out using the MPNST-derived cell line sNF96.2, which had previously been shown to express very low levels of mature miR-29c. The sNF96.2 cell line was first sequenced to confirm presence of a germline mutation in exon 21 (3683delC) of the neurofibromin (*NF1*) gene as well as loss of the remaining wild-type *NF1* allele. The effects of miR-29c expression on cell proliferation and migration were then examined by transfecting the sNF96.2 cell line with miR-29c mimics. Using the MTS assay and Incucyte kinetic live cell imaging, I found miR-29c expression does not significantly alter the proliferation of sNF96.2

cells. However, using transwell plates and the scratch/wound healing assays I showed that miR-29c expression could inhibit the migration of sNF96.2 cells.

Predicted targets of miR-29c were sought *in silico* using TargetScan, PicTar and MiRanda databases. I identified a list of 223 predicted gene targets for miR-29c. Functional classification of these 223 predicted targets using the DAVID programme, identified the top category was extracellular matrix genes.

The collagen genes *COL1A1*, *COL1A2*, *COL4A1*, *COL4A2*, *COL5A2*, and *COL21A1* were identified as possible targets for miR-29c in all three data databases. These ECM genes had also previously been identified in our lab by gene expression microarrays as being overexpressed in MPSNTs compared neurofibromas. Using qRT-PCR, I showed that the expression of all six collagen genes was significantly reduced in the miR-29c expressing sNF96.2 cells.

Previous analyses have demonstrated reduced MMP2 and MMP9 proteolytic activity miR-29c-transfected sNF96.2 cells. I examined expression of *MMP2* and *MMP9* at both the mRNA and protein level in these cells by qRT-PCR and Western blot analysis. I showed that expression of *MMP2* mRNA and protein is significantly inhibited in miR-29c-transfected sNF96.2 cells. However, *MMP9* mRNA and protein remained largely unaltered.

Transforming Growth Factor Beta3 (*TGFB3*) is another target of miR-29c predicted by my *in silico* analysis. I showed *TGFB3* mRNA expression is

significantly downregulated in miR-29c- transfected sNF96.2 cells. However, I found no significant alteration in expression of *MMP2* or *MMP9* at either mRNA transcript or protein level following anti-*TGFb3* siRNA treatment of wild-type sNF96.2 cells, although inhibition of MMP9 and MMP2 activity was observed in the supernatants of these cells by gelatine zymography.

Another potential target of miR-29c identified *in-silico* is *ROBO1*. Closer inspection of previous microarray data from our laboratory revealed *ROBO1* to be significantly highly expressed in MPNSTs compared to neurofibromas. Western blot analysis demonstrated no visible *ROBO1* protein in cells transfected with miR-29c mimics. However, only very weak *ROBO1* protein expression was detected in control cells transfected with scrambled nucleotides.

## 4. Relationship between miR-29c and DNMT3A and 3B

### 4.1. Introduction

The relationship between microRNAs and DNA methyltransferases (DNMTs) has been studied in several types of cancer including lung, breast and hepatocellular (Fabbri et al. 2007; Kogure et al. 2014). DNMT3A and -3B have the ability to introduce methyl groups onto CpG sites that were previously unmethylated on the parental template strands of DNA, hence called “*de novo*” methyltransferases (Okano et al. 1999). On the other hand, DNMT1 is responsible for maintenance of methylation; hence, it is called the “maintenance methyltransferase”. It prefers to target the hemimethylated DNA (with methylation of only one DNA strand) 10 fold more than the unmethylated strand. The function of DNMT1 in the cell is to keep the DNA methylation status stable throughout cell division (Jones & Liang 2009).

The expression of the miR-29 family of microRNAs has been shown to be inversely correlated with the expression of DNMT3A and -3B in lung cancer, and the miR-29s have been shown to directly target both these genes (Fabbri et al. 2007). Another study showed that miR-29a regulates TGF $\beta$  induced epithelial-mesenchymal transition (EMT) by altering its DNA methylation state via the suppression of DNMT3B (Kogure et al. 2013).

Sandhu (2012) examined the expression of microRNAs which are predicted to regulate DNMT3B (miR-29a, miR-29b, miR-29c, miR-148a, miR-148b, miR-26a, miR-26b, miR-203, miR-222) among 10 hypermethylator (express DNMT3B at high levels) and 6 non-hypermethylator (express DNMT3B at low levels) breast cancer cell lines. Results showed that hypermethylator cell lines express lower levels of miR-29c, miR-148a, miR-148b, miR-26a, miR-26b, and miR-203 compared to non-hypermethylator cell lines (Sandhu et al. 2012). The microRNA expression pattern was also shown to correlate inversely with methylation-sensitive gene expression (CEACAM6, CDH1, CST6, ESR1, GNA11, MUC1, MYB, TFF3 and SCNN1A) (Roll et al. 2008) and correlates directly with the methylation status of these genes (Sandhu et al. 2012).

The methylome profile of neurofibroma and MPNST from patients with Neurofibromatosis type 1 have been published and it has been shown that there are hundreds of genes that are differentially methylated between neurofibroma and MPNST (Feber et al. 2011). The samples used in this methylome study were the same tumours analysed in the microRNA array analysis (Chapter 3). As described in chapter 3, the expression of miR-29c is significantly lower in MPNSTs compared to neurofibromas, and because DNMT3A and DNMT3B are known targets for miR-29c (Fabbri et al. 2007) in lung cancer, I hypothesised that a relationship between them might exist in nerve sheath tumours.

## 4.2. Aims

The main objectives of this part of the thesis were twofold:

- To determine the relationship between the expression of miR-29c and expression of DNA methyltransferases *DNMT3A* and *DNMT3B* in MPNSTs and neurofibromas.
- To identify any differentially methylated genes in neurofibromas and MPNSTs that may play an important role in the progression of these tumours.

## 4.3. Results

### 4.3.1. *DNMT3B* mRNA expression is higher in MPNSTs compared to neurofibromas and inversely correlates with miR-29c expression

I previously demonstrated in chapter 3 that expression of miR-29c is significantly lower in MPNSTs compared to neurofibromas. In order to determine if any relationship exists between the expression of miR-29c and the DNA methyltransferases DNMT3A and DNMT3B, I decided to examine the same set of neurofibromas and MPNSTs used in chapter 3 for expression of these two DNA methyltransferases. Of the 20 tumour samples previously examined, sufficient RNA was available from nine MPNSTs and nine neurofibromas for analysis of *DNMT3A* and *DNMT3B* mRNA expression by qRT-PCR. Details of the primers and PCR conditions as well as clinical samples used for the *DNMT3A* and *DNMT3B* qRT-PCR analysis are given in chapter 2.

The results from the *DNMT3A* and *DNMT3B* mRNA qRT-PCR expression data are presented in Figure 4-1. These demonstrated no significant difference in the *DNMT3A* mRNA expression levels between neurofibromas and MPNSTs (unpaired Student's *t*-test,  $p = 0.748$ ). However, *DNMT3B* mRNA expression was found to be significantly higher in the MPNSTs

compared to that in neurofibromas (unpaired Student's t-test,  $p < 0.05$ ; Figure 4-2).

I then compared the *DNMT3A* and *DNMT3B* mRNA expression with the miR-29c expression level in each of the individual tumour samples. The results demonstrated no correlation between the expression of *DNMT3A* and miR-29c (Pearson's correlation test,  $p = 0.748$  and correlation coefficient of  $-0.081$ ; Figure 4-3). However, I found an inverse correlation between the expression of *DNMT3B* mRNA and miR-29c expression in the MPNSTs and neurofibromas (Pearson's correlation test,  $p < 0.05$  and correlation coefficient of  $-0.469$ ; Figure 4-4). These findings suggest that miR-29c expression may have an important influence on the gene methylation pattern in MPNSTs and NFs through regulation of DNMT3B expression.

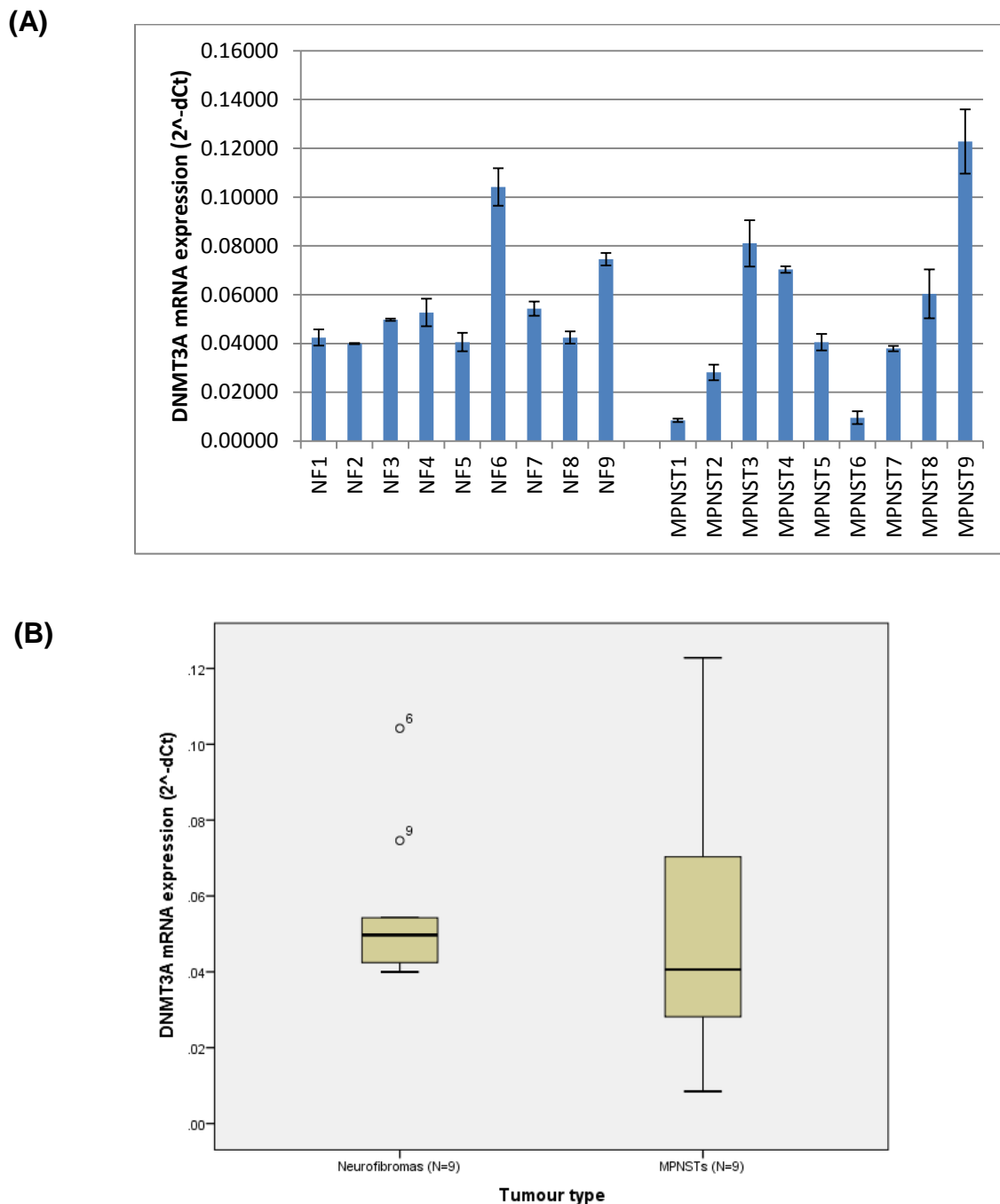
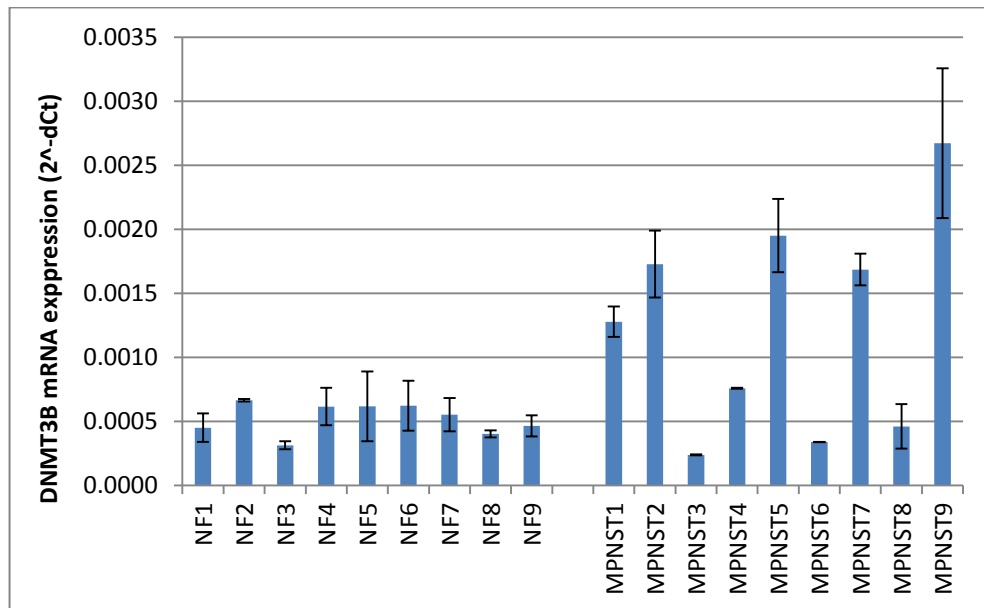


**Figure 4-1: No significant difference in *DNMT3A* mRNA expression between MPNSTs and neurofibromas**

qRT-PCR analysis of *DNMT3A* mRNA expression in 9 neurofibromas and 9 MPNST samples demonstrating no significant differences in *DNMT3A* mRNA expression levels between MPNSTs and NFs. The bar graph (A) shows the *DNMT3B* mRNA expression level in each individual tumour. The qRT-PCR data was normalised to *GAPDH* gene. Bars represent the average results of two technical replicates from one experiment. Error bars represent standard deviation. The box plot (B) shows a summary of the *DNMT3B* qRT-PCR expression data in the 9 neurofibromas and 9 MPNSTs (unpaired Student's *t*-test,  $p = 0.748$ ).

(A)



(B)

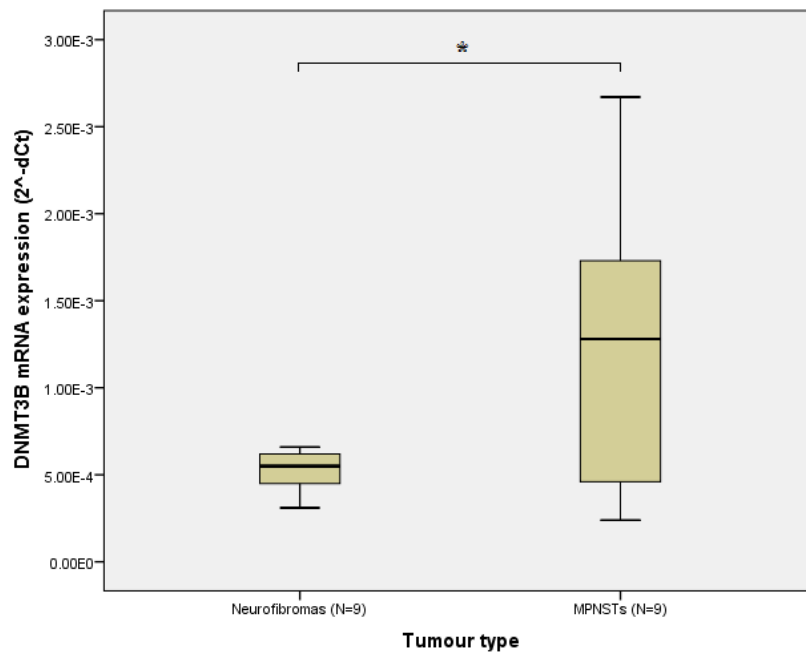


### Figure 4-2: *DNMT3B* mRNA expression is significantly higher in the MPNSTs compared neurofibromas

qRT-PCR analysis of *DNMT3B* mRNA expression in 9 neurofibroma and 9 MPNST samples demonstrating significantly higher levels of *DNMT3B* mRNA expression in the MPNSTs compared neurofibromas. The bar graph (A) shows the *DNMT3B* mRNA expression level in each individual tumour. The qRT-PCR data was normalised to *GAPDH* gene. Bars represent the average results of two technical replicates from one experiment. Error bars represent standard deviation. The box plot (B) gives a summary the *DNMT3B* qRT-PCR expression data in the 9 neurofibromas and 9 MPNSTs (unpaired Student's *t*-test, \**p* < 0.05).

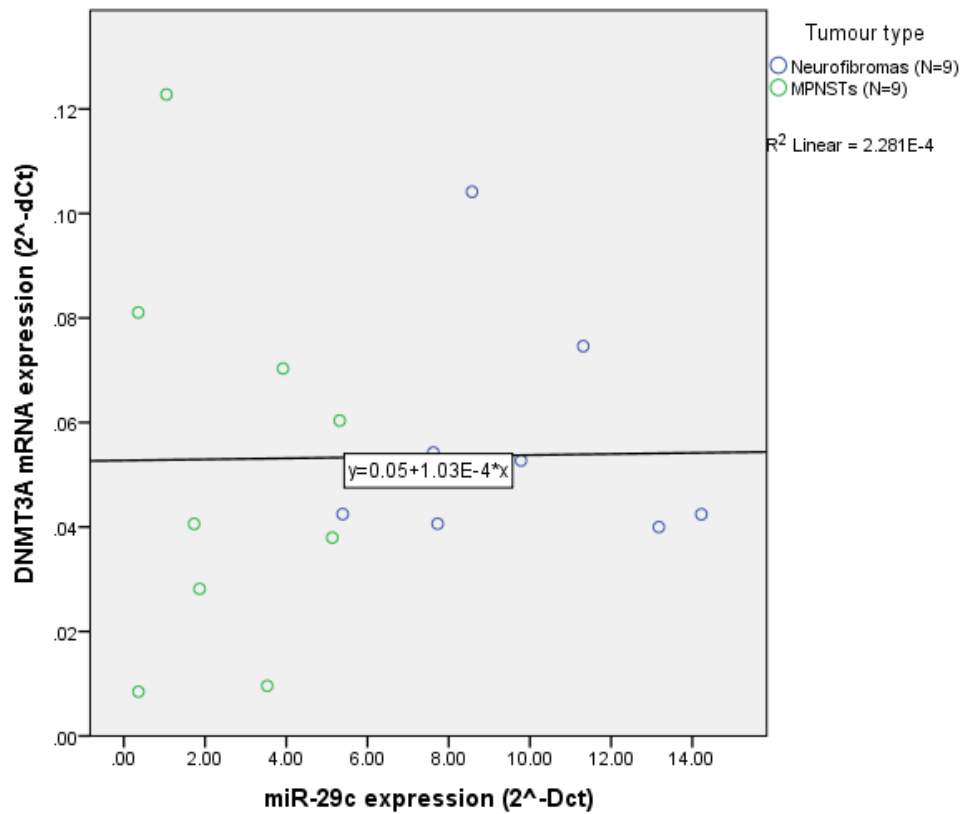


**Figure 4-3: No correlation between miR-29c and *DNMT3A* mRNA expression in MPNSTs and neurofibromas**

The graph shows the qRT-PCR data from 9 neurofibromas and 9 MPNSTs. The *DNMT3A* mRNA expression is plotted against the miR-29c expression level in each individual tumour. The expression of *DNMT3A* mRNA is not correlated with miR-29c expression in MPNSTs and NFs (Pearson's correlation test:  $p = 0.748$  and correlation coefficient of  $-0.081$ ).

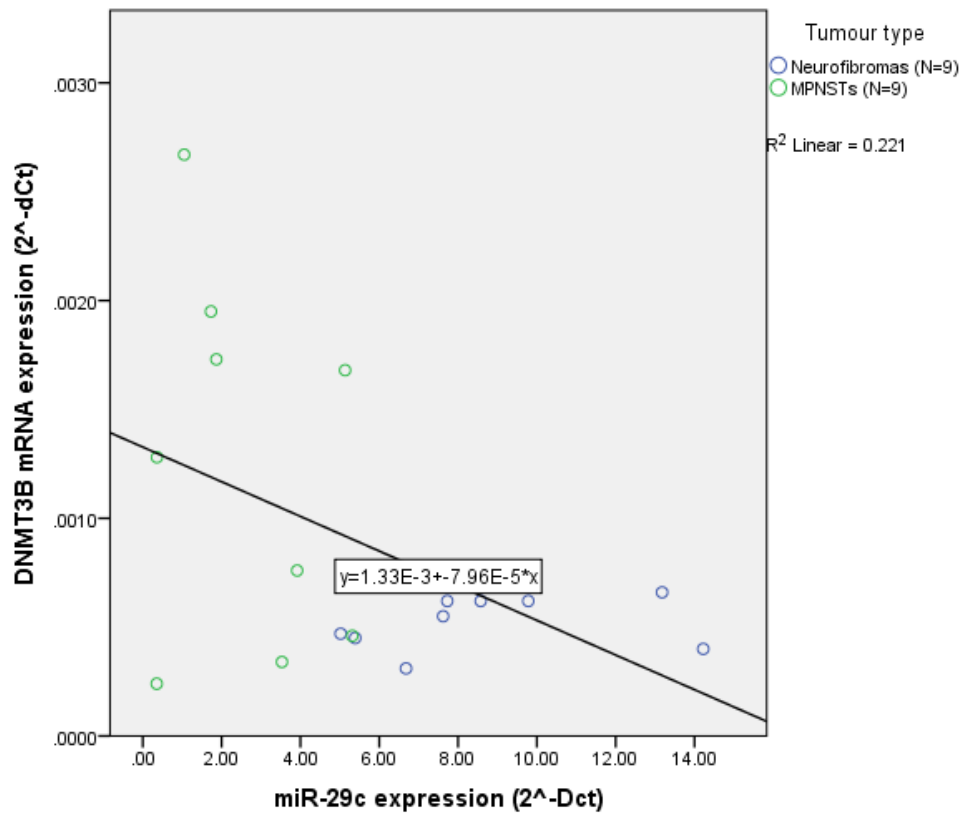


**Figure 4-4: Inverse correlation between miR-29c and *DNMT3B* expression in MPNSTs and neurofibromas**

The graph shows the qRT-PCR data from 9 neurofibromas and 9 MPNSTs. The *DNMT3B* mRNA expression is plotted against the miR-29c expression level in each individual tumour. The expression of *DNMT3B* mRNA is negatively correlated with miR-29c expression in MPNSTs and NFs (Pearson's correlation test:  $p < 0.05$  and correlation coefficient of -0.469).

### 4.3.2. miR-29c inhibits *DNMT3A* and *DNMT3B* expression in sNF96.2 cells

Having demonstrated an inverse correlation between the expression of miR-29c and *DNMT3B* in our tumour samples, I next examined the *in vitro* effects that miR-29c might have on the expression of *DNMT3A* and *DNMT3B*. For this purpose, I employed the use of the MPNST-derived cell line sNF96.2 which was previously had been shown to express very low levels of miR-29c mRNA (Dr Nadège Presneau personal communication). To this end, I transfected the sNF96.2 cell line with miR-29c mimics (test samples) or scrambled oligonucleotides (control cells) as previously described in chapter 2. The *DNMT3A* and *DNMT3B* mRNA expression levels were then determined in sNF96.2 test and control cells by qRT-PCR. See chapter 2 for details of the primers and PCR conditions used.

The results from the *DNMT3A* and *DNMT3B* qRT-PCR experiments are shown in Figure 4-5. These demonstrated a significant reduction in the *DNMT3A* and *DNMT3B* mRNA expression levels following transfection of miR-29c into sNF96.2 cells compared to their expression in control cells. The level of *DNMT3A* mRNA expression at 24 and 48 h following transfection with miR-29c was reduced by approximately 40% (paired Student's *t*-test;  $p < 0.05$ ) and 50% (paired Student's *t*-test;  $p < 0.01$ ) respectively. The level of *DNMT3B* mRNA expression at the same time points was reduced by

approximately 30% (paired Student's *t*-test;  $p < 0.05$ ) and 45% (paired Student's *t*-test;  $p < 0.01$ ) respectively. These findings demonstrate that *DNMT3A* and *DNMT3B* are both targets of miR-29c in MPNST derived cells and lend further support to the idea that miR-29c may have an important influence on gene methylation in MPNSTs by regulating *DNMT3A* and *DNMT3B* expression in these tumours.

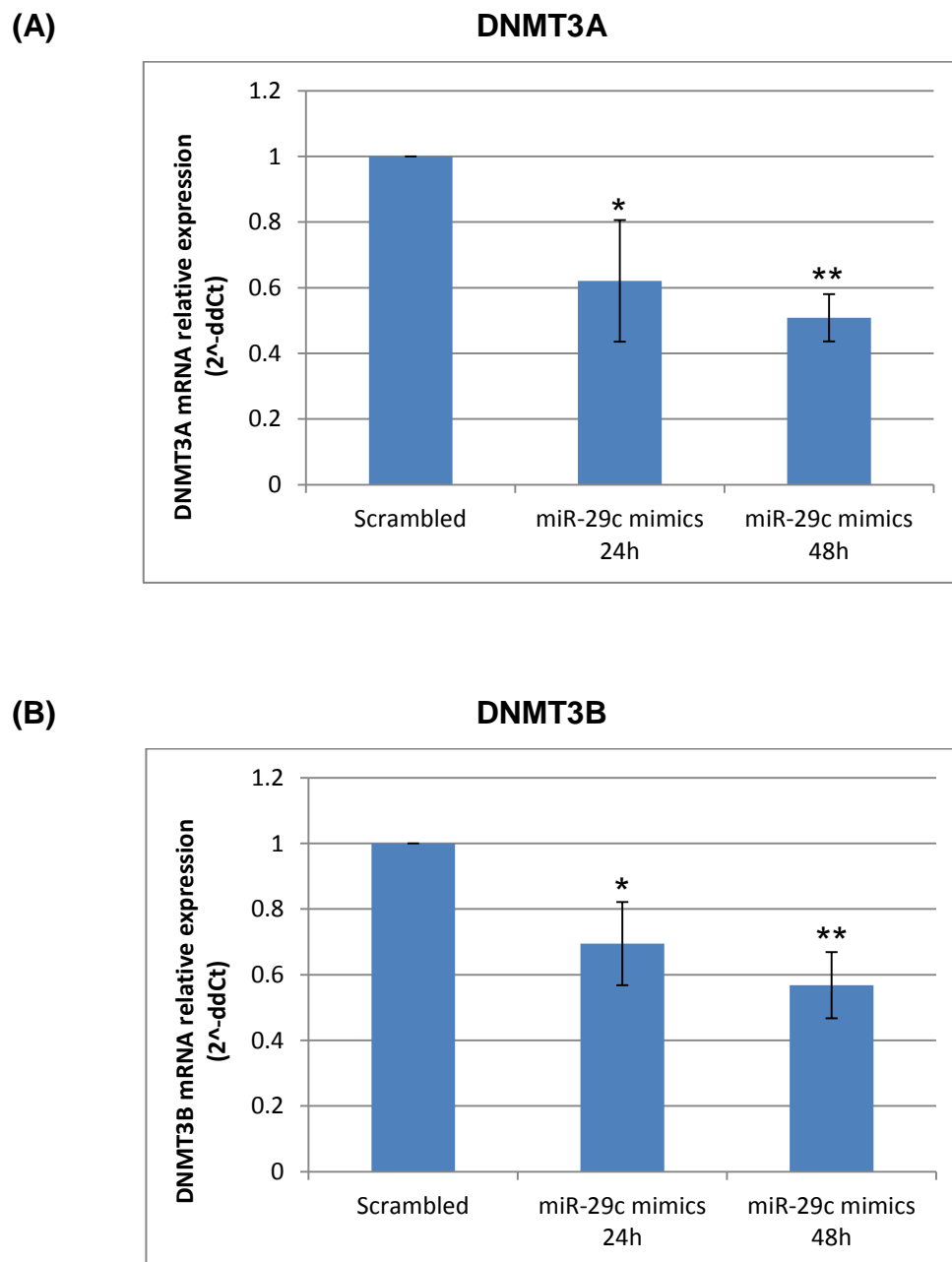


**Figure 4-5: Down-regulation of *DNMT3A* and *DNMT3B* mRNA expression in miR-29c-transfected sNF96.2 cells**

qRT-PCR expression data for *DNMT3A* (A) and *DNMT3B* (B) at 24 and 48 h following transfection of sNF96.2 cells with miR-29c (test samples) or scrambled oligonucleotides (controls). The data is presented as fold difference in *DNMT3A* or *DNMT3B* mRNA levels in test samples compared to that in controls (the control was given the value 1 at both 24 and 48 h). The graphs demonstrate a significant reduction in expression of *DNMT3A* and *DNMT3B* at 24 and 48 h (paired Student's *t*-test; \**p* < 0.05 and \*\**p* < 0.01 for *DNMT3A* at 24 and 48 h, respectively; \**p* < 0.05 and \*\**p* < 0.01 for *DNMT3B* at 24 and 48 h, respectively). The qRT-PCR data was normalised to *GAPDH* gene. Bars represent the average results from three independent experiments (three biological replicates). Error bars represent standard deviation.

### **4.3.3. Identification of candidate genes that may be targets for DNMTs in MPNSTs and Neurofibromas**

Following my demonstration that DNMT3A and DNMT3B are downregulated by miR-29c *in vitro*, I next decided to look for candidate genes that may be differentially methylated between neurofibromas and MPNSTs. I first derived a list of possible candidates from the results of the methylome analysis by Feber et al. 2011 and identified a long list of 607 genes. In order to narrow down this list further, I compared it with the list of 1551 genes previously reported by the gene expression microarray studies of Subramanian et al. 2010 as differentially expressed between neurofibromas and MPNSTs. I found 41 genes in common between the two studies of Feber et al (2011) and Subramanian et al. (2010) (Table 4-1). I then examined the literature in order to determine where any of these genes had been proven to be differentially expressed between neurofibromas and MPNSTs. I finally decided to focus my studies on 3 genes *S100B*, *CDKN2A*, and *WT1*, which I thought were strong candidates as possible targets of DNMTs in MPNSTs. As well as being differentially methylated these genes had previously been verified as being differentially expressed between MPNSTs and neurofibromas (Feber et al. 2011; Subramanian et al. 2010; Karamchandani et al., 2012; Parenti et al. 2014). In addition they have been reported to play a role in other types of cancer (Fang et al. 2009; Fraizer et al. 2004; van Dieck et al. 2010).

**Table 4-1: Genes which are differentially methylated and differentially expressed in MPNSTs compared to neurofibromas**

Serial	Gene symbol	Gene description
1	ADAM23	ADAM metallopeptidase domain 23
2	AIF1	Allograft inflammatory factor 1
3	AIG1	Androgen-induced 1
4	AKAP6	A kinase (PRKA) anchor protein 6
5	ALDH3A2	Aldehyde dehydrogenase 3 family, member A2
6	ANK2	Ankyrin 2, neuronal
7	APOD	Apolipoprotein D
8	ARHGEF10	Rho guanine nucleotide exchange factor (GEF) 10
9	AZGP1	Alpha-2-glycoprotein 1, zinc
10	C13orf18	Chromosome 13 open reading frame 18
11	C13orf23	Chromosome 13 open reading frame 23
12	C2	Complement component 2
13	CAMSAP1L1	Calmodulin regulated spectrin-associated protein 1-like 1
14	CHML	Choroideremia-like (Rab escort protein 2)
15	EP300	E1A binding protein p300
16	FAM63B	Family with sequence similarity 63, member B
17	FXYD3	FXYD domain containing ion transport regulator 3
18	GFM1	G elongation factor, mitochondrial 1
19	ID4	Inhibitor of DNA binding 4
20	KLF4	Kruppel-like factor 4 (gut)
21	LETMD1	LETM1 domain containing 1
22	LY96	Lymphocyte antigen 96
23	MAP3K2	Mitogen-activated protein kinase kinase kinase 2
24	OCLN	Occludin
25	PCMTD2	Protein-L-isoaspartate O-methyltransferase domain containing 2
26	PLXDC2	Plexin domain containing 2
27	PTK2	PTK2 protein tyrosine kinase 2
28	RDH13	Retinol dehydrogenase 13 (all-trans/9-cis)
29	S100B	S100 calcium binding protein, beta (neural)
30	SERBP1	SERPINE1 mRNA binding protein 1
31	SOAT1	Sterol O-acyltransferase 1
32	SORBS1	Sorbin and SH3 domain containing 1
33	SOX10	SRY (sex determining region Y)-box 10
34	TARDBP	TAR DNA binding protein
35	TMEM18	Transmembrane protein 18
36	TXNIP	Thioredoxin interacting protein
37	VANGL1	Vang-like 1 (van gogh, Drosophila)
38	VKORC1L1	Vitamin K epoxide reductase complex, subunit 1-like 1
39	ZNF33A	Zinc finger protein 33A
40	ZNF516	Zinc finger protein 516
41	ZNRF2	Zinc and ring finger 2

#### **4.3.4. Hypermethylation of *CDKN2A*, *WT1* and *S100B* is frequent in MPNSTs compared to neurofibromas in human samples**

The methylation status of *CDKN2A*, *WT1* and *S100B* was examined in our 10 neurofibromas and 10 MPNSTs by bisulfite pyrosequencing analysis covering 5 to 7 CpG sites within each gene (Figure 4-6 to Figure 4-8). The CpG sites chosen for study were selected from previously available methylome data (Feber et al. 2011) based on the fact they were clustered within regulatory regions of the genes and exhibited differential methylation between neurofibromas and MPNSTs. Details of protocol used for pyrosequencing can be found in chapter 2.

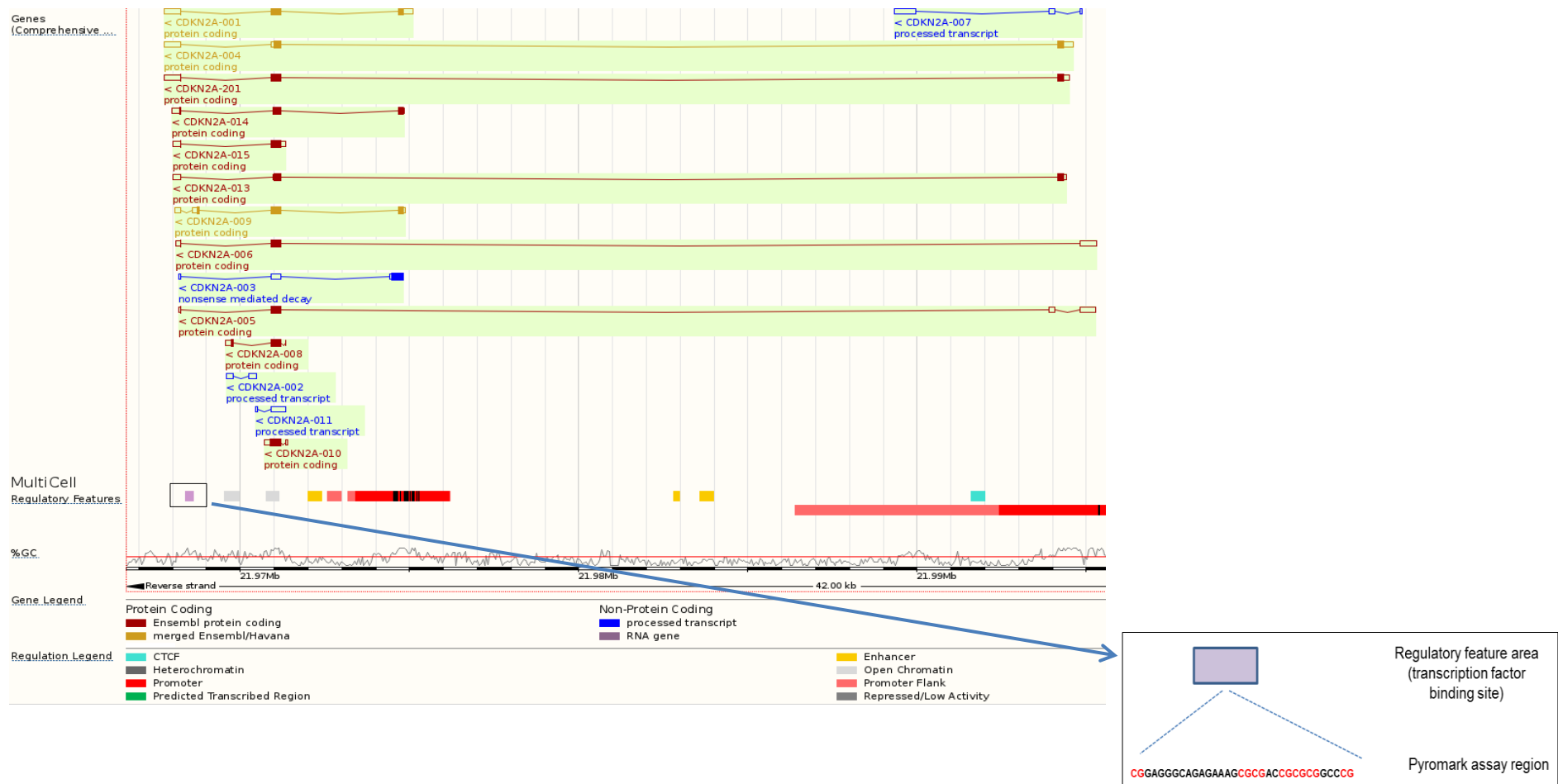
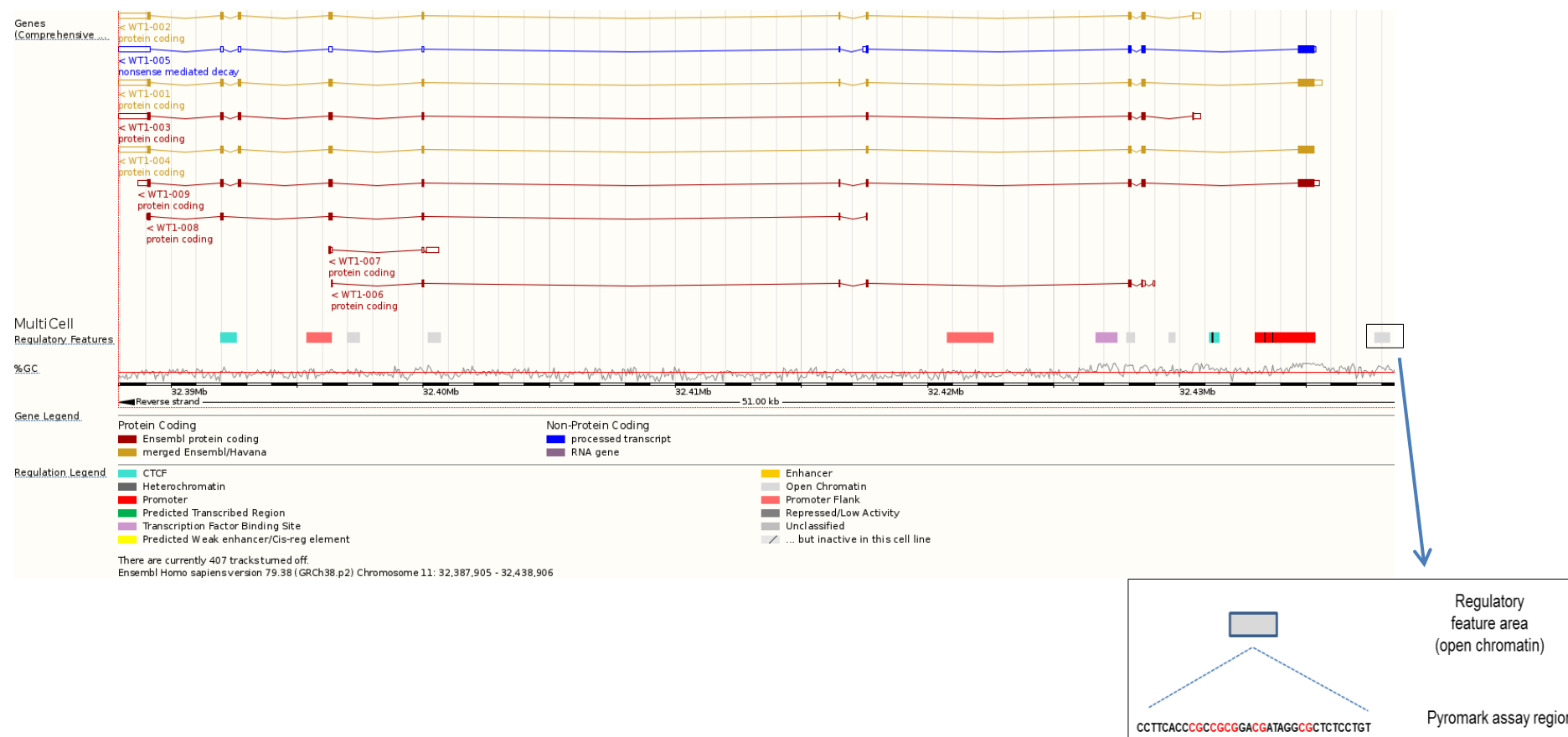


Figure 4-6: *CDKN2A* gene as depicted by ensemble showing location of the regulatory feature area (transcription factor binding site), which was examined by pyrosequencing. The zoom box shows the DNA sequence within this area and location of the 7 CpG sites which are highlighted in red.



**Figure 4-7: *WT1* gene as depicted by ensemble showing location of the regulatory feature area (open chromatin), which was examined by pyrosequencing. The zoom box shows the DNA sequence within this area and location of the 5 CpG sites which are highlighted in red.**

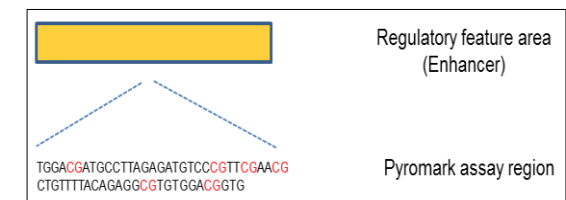
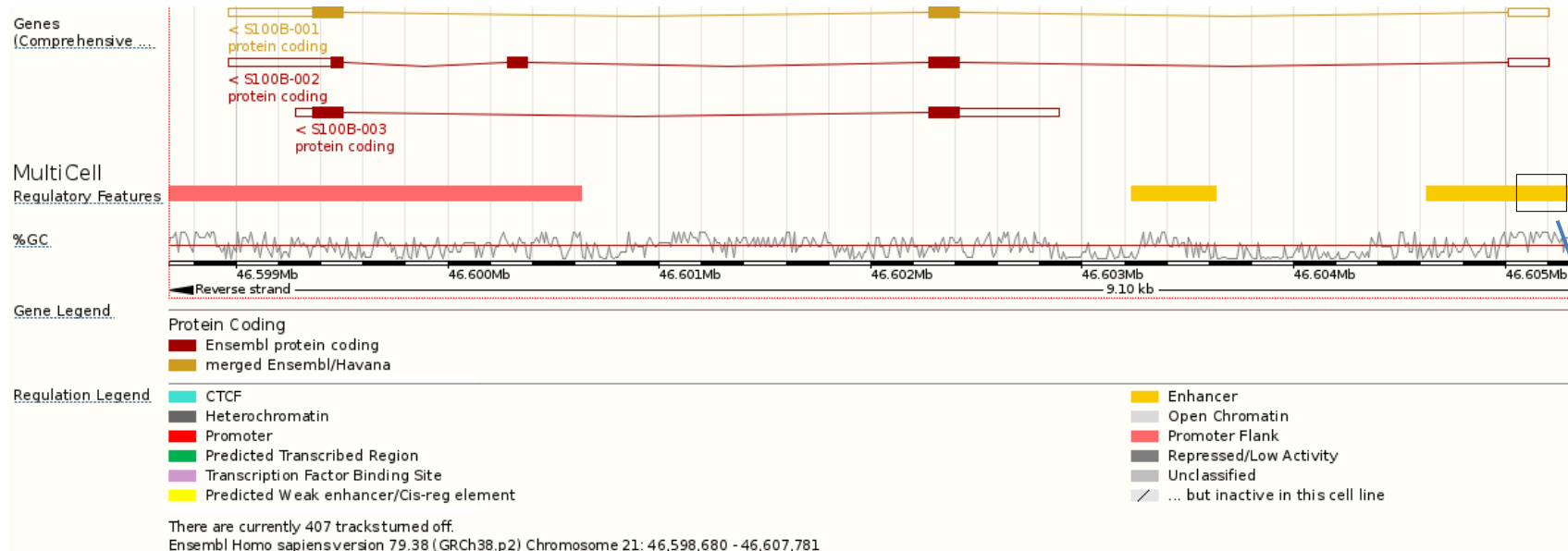
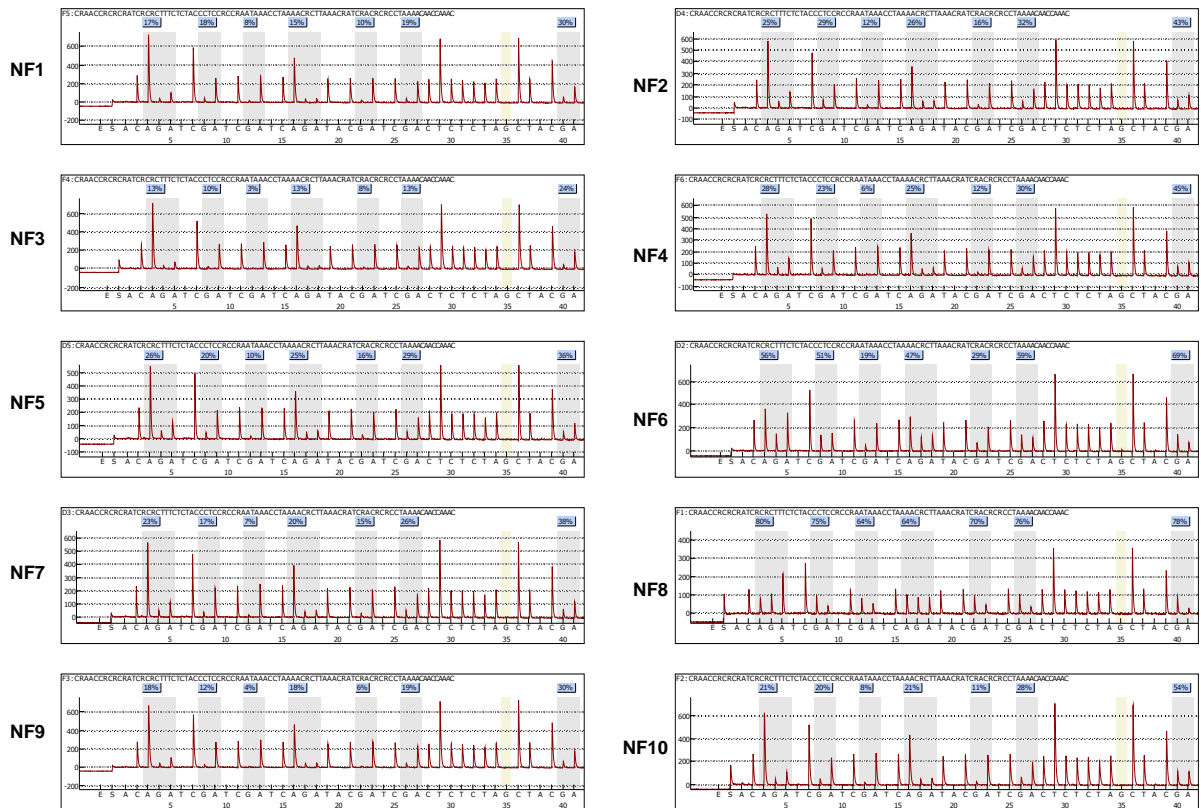
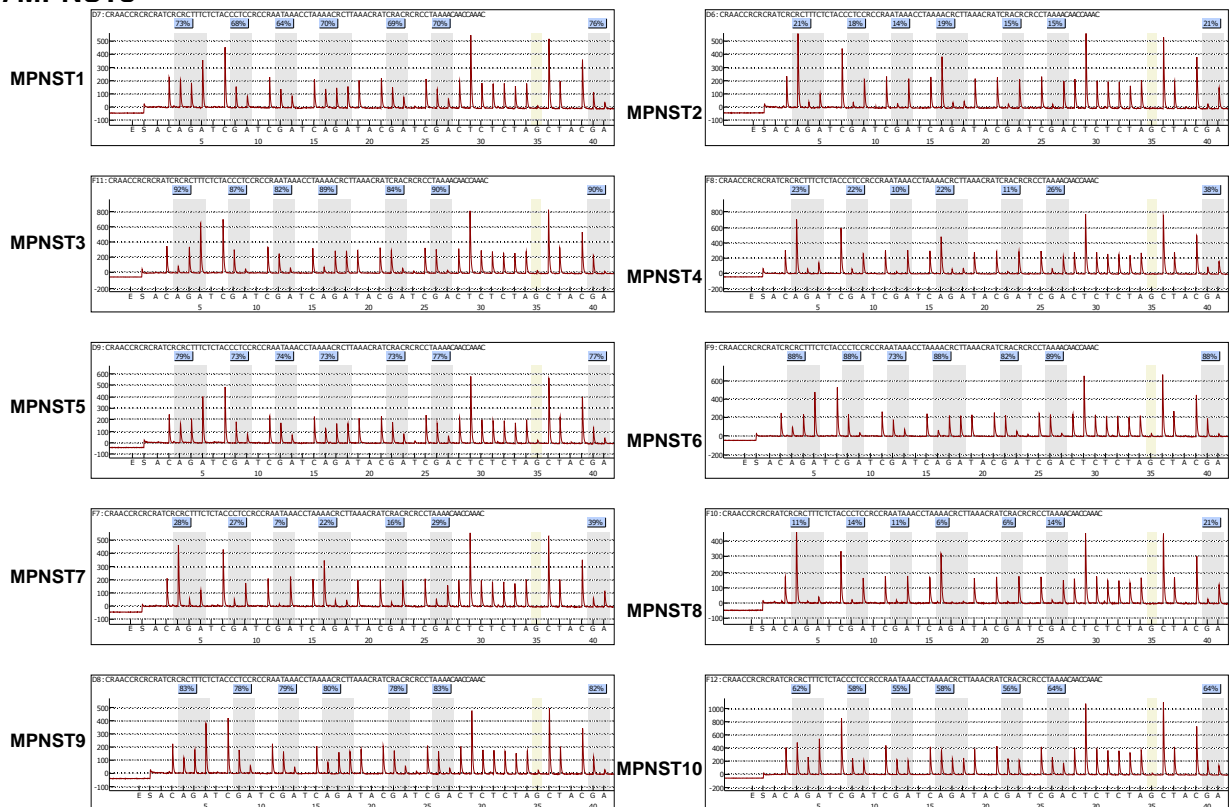


Figure 4-8: *S100B* gene as depicted by ensemble showing location of the regulatory feature area (enhancer), which was examined by pyrosequencing. The zoom box shows the DNA sequence within this area and location of the 6 CpG sites which are highlighted in red.

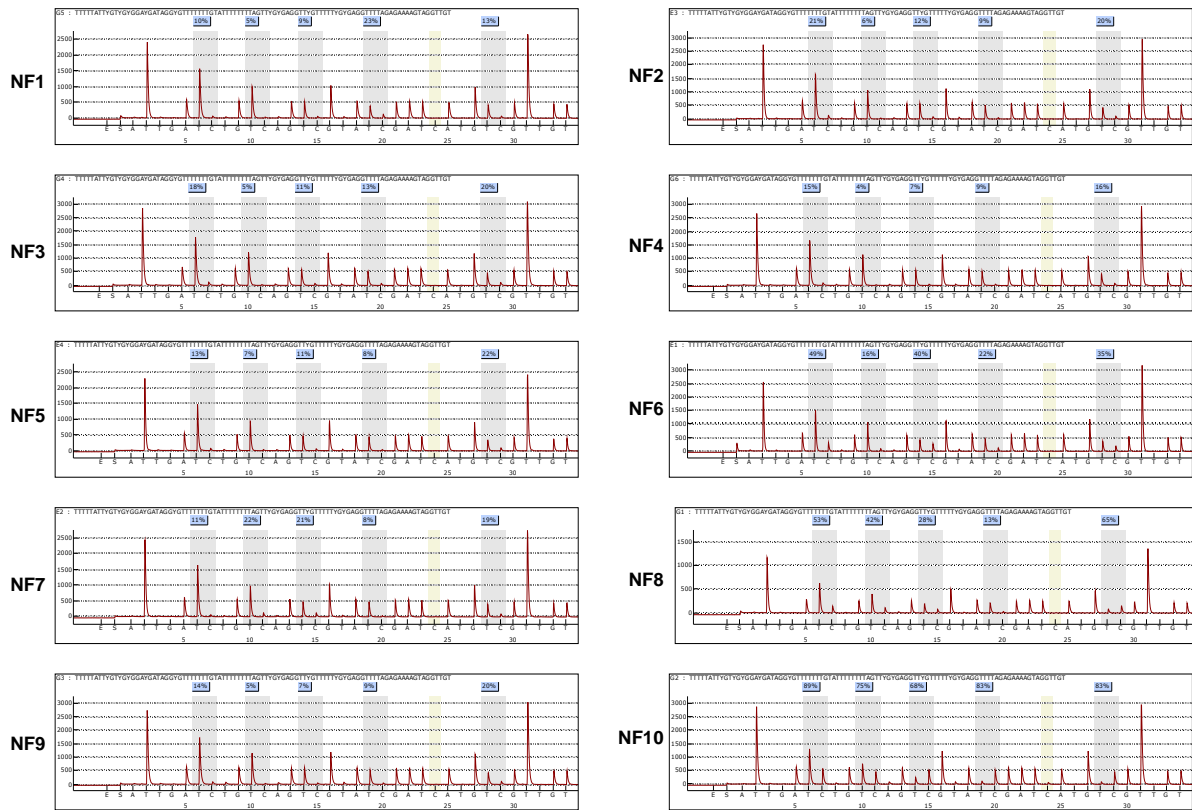
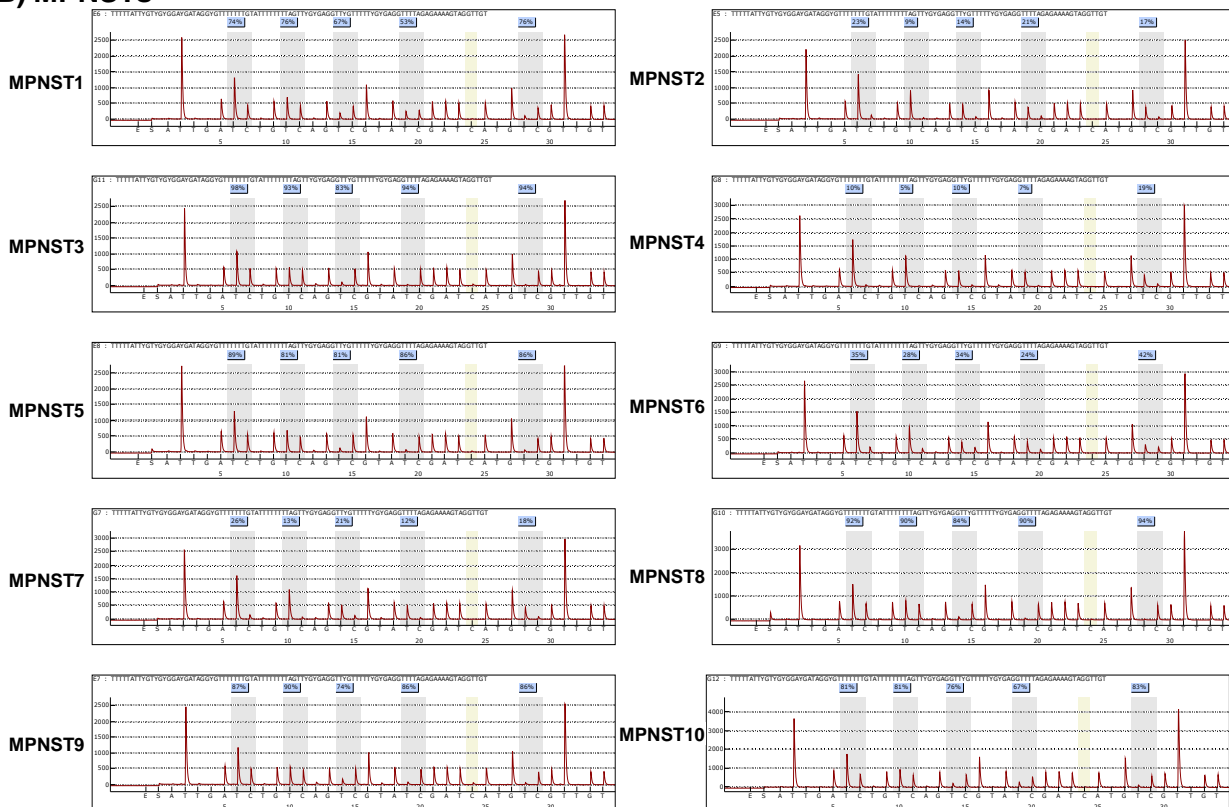
The *CDKN2A*, *WT1*, and *S100B* pyrosequencing data obtained from all 10 NFs and 10 MPNSTs analysed are shown in Figure 4-9, Figure 4-10 and Figure 4-11 respectively. Each box in the figures represents an individual pyrogram from a single tumour sample. The shaded bars indicate the positions of the CpGs analysed and the level of methylation at each CpG site is expressed as a percentage in the blue boxes on top of the bars.

The results from each pyrogram are summarised in Table 4-2. The average level of gene methylation in each sample was calculated by adding the % methylation at each CpG site and dividing this by the total number of CpG sites within each pyrogram. Any gene with an average methylation value of greater than 50% was considered to be hypermethylated.

The results demonstrated hypermethylation of *CDKN2A* and *WT1* in 6 MPNSTs compared to only 1 neurofibroma (unpaired Student's *t*-test,  $p < 0.05$  and  $< 0.01$  respectively) and *S100B* was hypermethylated in 7 MPNSTs compared to only 2 neurofibromas (unpaired Student's *t*-test,  $p < 0.01$ ). The overall data suggests that methylation of *CDKN2A*, *WT1* and *S100B* is more frequent in MPNSTs compared to neurofibromas and may play a role in the pathogenesis of MPNSTs from neurofibromas.

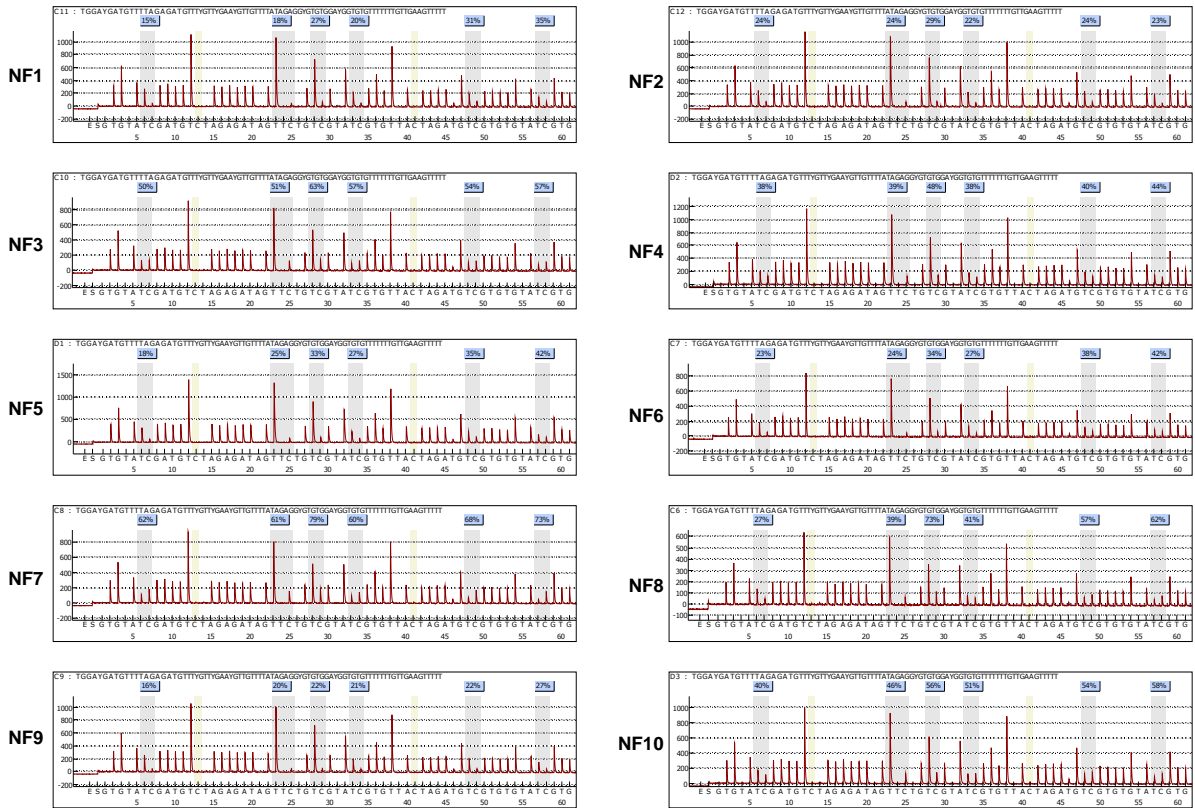
**(A) Neurofibromas****(B) MPNSTs****Figure 4-9: Methylation analysis of *CDKN2A* in Neurofibromas and MPNSTs**

Each box is the pyrogram from a single neurofibroma (A) or MPNST (B). Each shaded column indicates a CpG dinucleotide examined and the percentage methylation at that CpG dinucleotide is indicated above. The yellow shaded boxes are internal bisulfite modification control assessments. The results demonstrate that *CDKN2A* is hypermethylated in MPNSTs compared to neurofibromas.

**(A) Neurofibromas****(B) MPNSTs****Figure 4-10: Methylation analysis of *WT1* in Neurofibromas and MPNSTs**

Each box represents the pyrogram from a single neurofibroma (A) or MPNST (B). Each shaded column indicates a CpG dinucleotide examined and the percentage of methylation at that CpG dinucleotide is indicated above. The yellow shaded boxes are internal bisulfite modification control assessments. The results demonstrate that *WT1* is hypermethylated in MPNSTs compared to neurofibromas.

**(A) Neurofibromas**



**(B) MPNSTs**

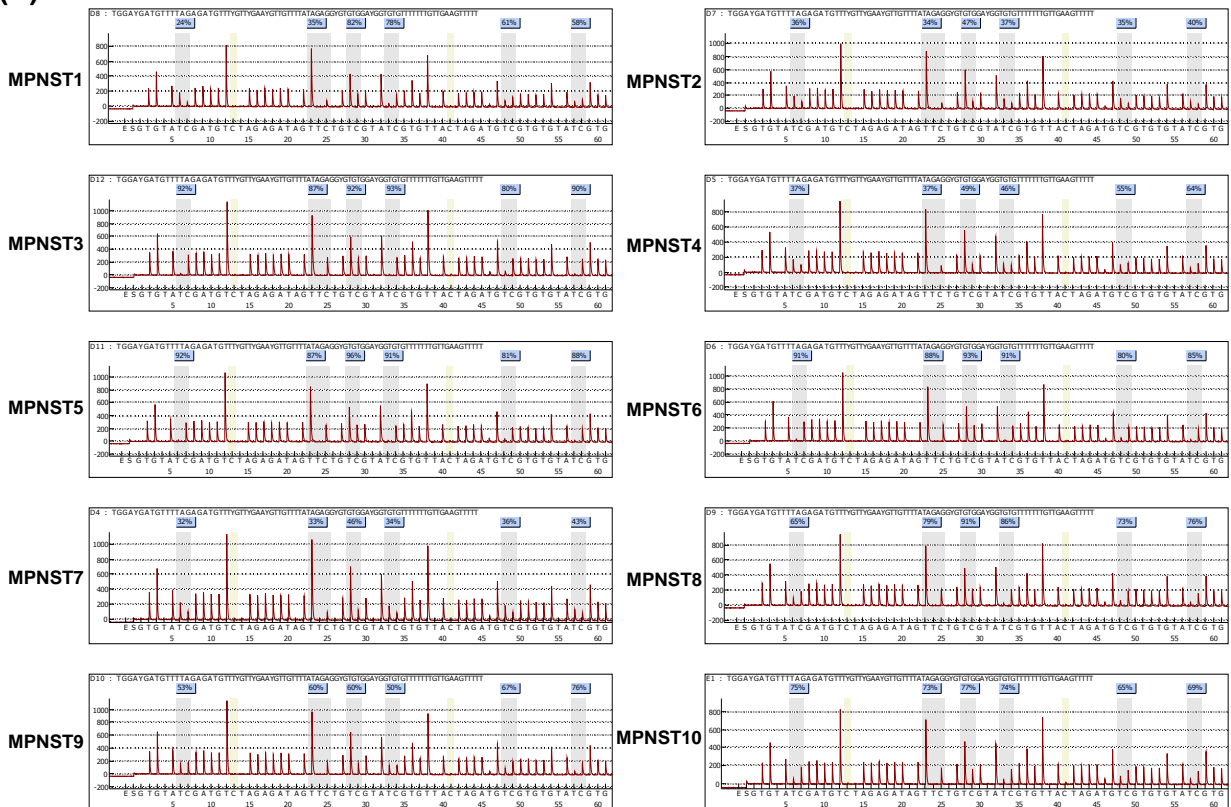


**Figure 4-11: Methylation analysis of *S100B* in Neurofibromas and MPNSTs**

Each box represents the pyrogram from a single neurofibroma (A) or MPNST (B). Each shaded column indicates a CpG dinucleotide examined and the percentage of methylation at that CpG dinucleotide is indicated above. The yellow shaded boxes are internal bisulfite modification control assessments. The results demonstrate that *S100B* is significantly hypermethylated in MPNSTs compared to neurofibromas.

Tumour	CpG methylation levels %		
	<i>CDKN2A</i>	<i>WT1</i>	<i>S100B</i>
NF1	17	12	24
NF2	26	13	24
NF3	12	13	55
NF4	24	10	41
NF5	23	12	30
NF6	47	32	31
NF7	21	16	67
NF8	72	40	50
NF9	15	11	21
NF10	23	80	50
MPNST1	70	69	56
MPNST2	17	17	38
MPNST3	88	92	89
MPNST4	22	10	48
MPNST5	75	85	89
MPNST6	85	33	88
MPNST7	24	18	37
MPNST8	12	90	78
MPNST9	80	85	61
MPNST10	60	78	72

**Colour code:**

Methylation %
0-25%
26-50%
51-75%
76-100%

**Table 4-2: Hypermethylation of *CDKN2A*, *WT1*, and *S100B* in MPNSTs vs Neurofibromas**

Each box represents the average level of CpG methylation in each gene individual pyrogram. The results demonstrate a significantly higher level of *CDKN2A*, *WT1*, and *S100B* gene methylation in MPNSTs compared to neurofibromas (unpaired Student's *t*-test,  $p < 0.05$  for *CDKN2A*;  $p < 0.01$  for *WT1*;  $p < 0.01$  for *S100B*).

### **4.3.5. Increased expression of *WT1* and *S100B* in 5-aza-dC-treated sNF96.2 cells**

Having shown that *CDKN2A*, *WT1*, and *S100B* are hypermethylated in MPNSTs compared to neurofibromas, I next wanted to determine whether this methylation within the regulatory regions of these genes has any bearing on their expression. In order to test this, I decided to examine the expression of *CDKN2A*, *WT1*, and *S100B* mRNA in the sNF96.2 cell line following treatment with 5-Aza-2'-deoxycytidine (5-aza-dC). This drug is an epigenetic modifier which inhibits DNA methyltransferase activity and leads to progressive global demethylation of DNA during replication in proliferating cells (Claus et al., 2005; Hackanson & Daskalakis, 2014) thus resulting in activated gene expression. Before I could begin these experiments, however, it was necessary to determine the optimum dose of 5-aza-dC that could be used to treat the sNF96.2 cells and allow a reasonable level ( $\geq 50\%$ ) of cell viability over a 7 day period. In order to do this, an optimisation step was performed whereby sNF96.2 cells were grown in culture medium treated with various concentrations of 5-aza-dC (0.25  $\mu\text{M}$ , 0.5  $\mu\text{M}$ , 1  $\mu\text{M}$ , 2  $\mu\text{M}$ , 3  $\mu\text{M}$ , 5  $\mu\text{M}$  and 10  $\mu\text{M}$ ) and allowed to grow for a period of a week after which cell viability was measured using the Trypan Blue assay as described in chapter 2.

The results from these experiments demonstrated the optimum dose of 5-aza-dC that sNF96.2 cells could tolerate over 7 days of treatment was 1  $\mu\text{M}$ .

Following this, a fresh batch of cell cultures then was grown for a period 4 and 7 days in culture medium containing 1  $\mu$ M 5-aza-dC, replacing the culture medium every 24 h with fresh media containing 1  $\mu$ M 5-aza-dC. The cells were harvested on days 4 and 7. DNA and RNA were then extracted from each of these as well as from a batch of control sNF96.2 cells, which had been grown without 5-aza-dC treatment. All experiments were carried out in triplicate.

The treated and untreated control sNF96.2 cells were analysed for methylation of *S100B* by pyrosequencing as described in the previous section. The results of these experiments which are summarised in Figure 4-12 demonstrated a significant reduction of *S100B* gene methylation (by approximately 15% at each of the 6 CpG sites examined) in the 5-aza-dC-treated cells compared to that in control cells (paired Student's *t*-test,  $p < 0.01$ ). I did not examine the methylation status of *CDKN2A* and *WT1* in the 5-aza-dC treated and untreated cells but since 5-aza-dC is a global inhibitor of DNA methylation, the *S100B* pyrosequencing data were considered a good indicator that the whole sNF96.2 genome had been successfully demethylated following treatment with 5-aza-dC.

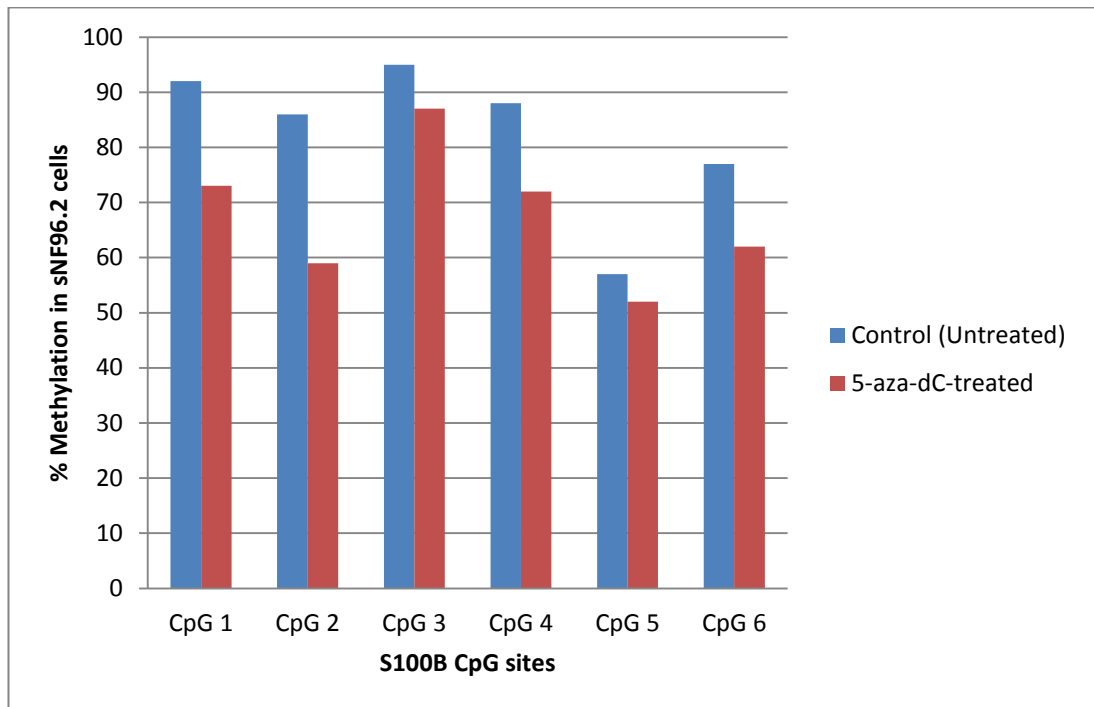


**Figure 4-12: Decreased *S100B* gene methylation in 5-aza-dC-treated sNF96.2 cells**

Pyrosequencing data demonstrating percentage methylation at 6 CpG islands in the *S100B* gene of sNF96.2 cells which had been grown in culture medium containing 1  $\mu$ M 5-aza-dC and in control cells grown without 5-aza-dC for 1 week. The graph demonstrates a reduction of *S100B* gene methylation by approximately 15% at each of the 6 CpG sites examined (paired Student's *t*-test,  $p < 0.01$ ).

I next examined the effects that hypomethylation might have on the expression of *S100B* and *WT1* in the sNF96.2 cell line. This was done by qRT-PCR analysis of the gene transcripts at days 4 and 7 following the start of 5-aza-dC treatment in sNF96.2 cells. Details of these experiments including qRT-PCR primers and protocols used are as described in chapter 2. The results of these qRT-PCR experiments demonstrated a significant increase in expression of both *S100B* and *WT1* mRNA at both time points in 5-aza-dC treated cells compared to untreated control cells (Figure 4-13A). The expression *WT1* mRNA increased by approximately 50% in sNF96.2 cells after 4 days of 5-aza-dC treatment (paired Student's *t*-test,  $p < 0.05$  and at 7 days the *WT1* mRNA expression in 5-aza-dC treated cells was more than double the level of expression in the control untreated cells ( $p < 0.01$ ). *S100B* mRNA transcript was not detectable in control untreated sNF96.2 cells but 5-aza-dC treatment resulted in detectable levels of *S100B* mRNA expression on day 4 and ( $p < 0.05$ ) on 7 day the level of *S100B* mRNA expression was increased by another 70% approximately ( $p < 0.05$ ) (Figure 4-13B). The *WT1* mRNA expression is presented in Figure 4-13A as relative expression ( $2^{-\Delta\Delta Ct}$ ), however, the *S100B* mRNA expression is presented in Figure 4-13B as ( $2^{-\Delta Ct}$ ) because there was no detectable mRNA in the untreated cells so I was not able to calculate the relative expression.

I was unable to obtain any data from the *CDKN2A* gene or transcript in the sNF96.2 cell line as both the bisulfite converted DNA and the cDNA from this

cell line failed to give any amplifiable PCR product. It is possible that the *CDKN2A* gene has been deleted in this cell line.

My findings indicate that hypermethylation of CpG sites of *S100B* and *WT1* can lead to inhibition of gene transcription and suggest that DNA methylation may provide an important epigenetic mechanism for controlling the expression of *WT1* and *S100B* within MPNST-derived cells.

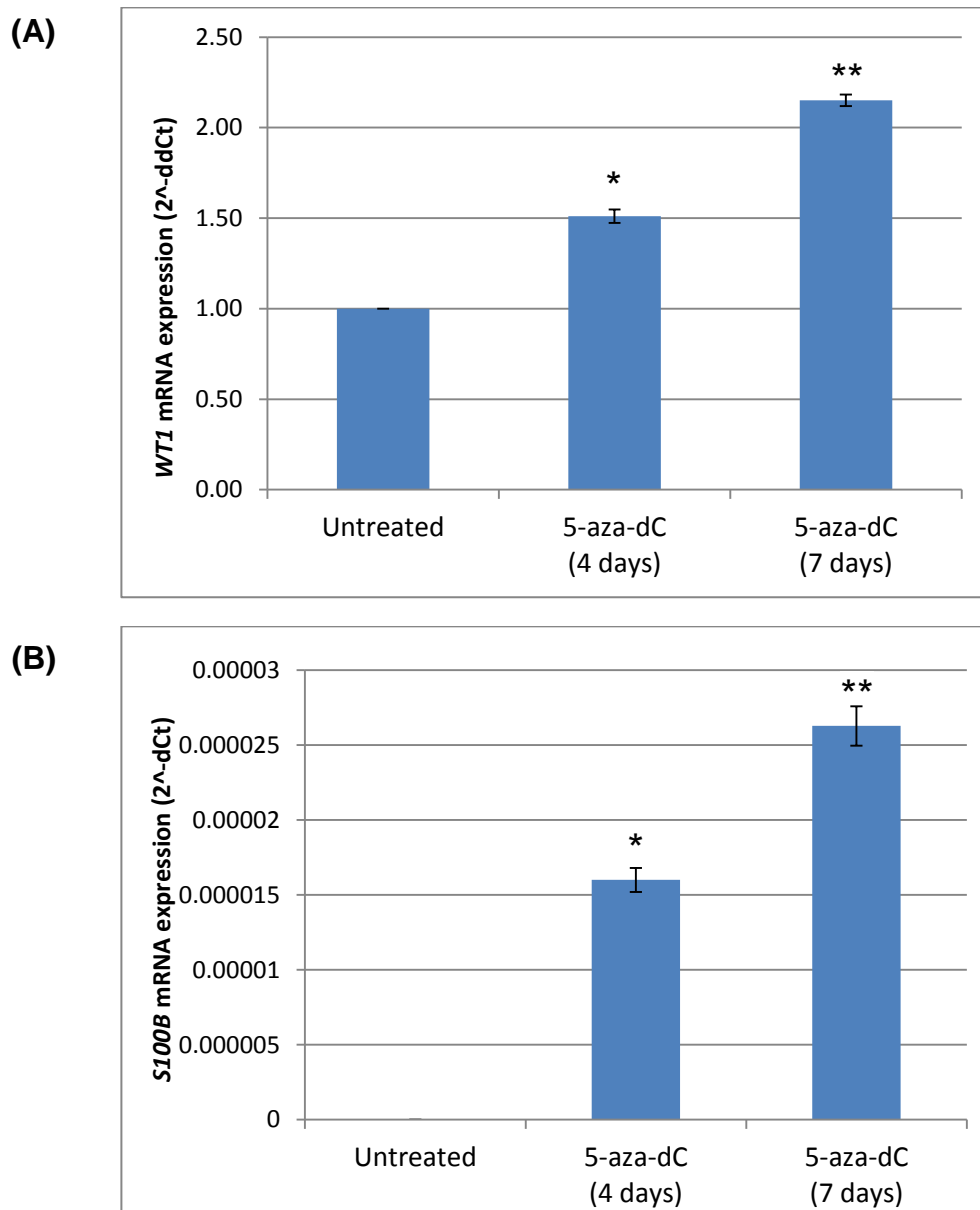


**Figure 4-13: Increased expression of *WT1* and *S100B* mRNA in 5-aza-dC treated sNF96.2 cells**

qRT-PCR results demonstrating (A) 1.5 fold and > 2 fold increase in *WT1* mRNA expression at 4 days and 7 days, respectively, following treatment of sNF96.2 cells with 5-aza-dC (1  $\mu$ M) compared to that in untreated control cells (paired Student's *t*-test, \* $p < 0.05$  and \*\* $p < 0.01$  at 4 and 7 days, respectively). Expression of *WT1* in control cells remained constant at both time points and was given the value 1. (B) *S100B* mRNA was not detectable in control untreated sNF96.2 cells but its' expression was significantly increased at day 4 (paired Student's *t*-test, \* $p < 0.05$  and \*\* $p < 0.01$  at 4 and 7 days, respectively). Expression of *S100B* mRNA on day 7 was approximately 70% higher than on day 4. The *WT1* expression is presented as relative expression ( $2^{-ddCt}$ ) but the *S100B* mRNA expression is presented as  $2^{-dCt}$  because there was no detectable mRNA in the untreated cells. The qRT-PCR data was normalised to *GAPDH* gene. Bars represent the average results obtained from three independent experiments (three biological replicates). Error bars represent standard deviation.

#### **4.3.6. *S100B* and *WT1* DNA methylation is frequent in high grade MPNST as compared with low grade MPNST and Neurofibromas**

Having demonstrated that demethylation of sNF96.2 MPNST cells results in re-expression of *S100B* mRNA and increased the expression of *WT1* mRNA, I wanted to test whether there any relationship between methylation of these genes and tumour grade. I first tested the level of *S100B* and *WT1* gene methylation in a cohort of 80 MPNSTs and 80 neurofibromas using bisulfite pyrosequencing. The MPNST samples include high grade (grade 3; n = 56), intermediate (grade 2; n = 20) and low grade (grade 1; n= 4) tumours. I examined the DNA methylation state of 6 and 5 CpGs within the regulatory regions of *S100B* and *WT1* respectively and the average DNA methylation level across the CpGs within these areas was measured.

My results demonstrated that methylation of *S100B* is significantly higher in MPNSTs compared to neurofibromas (Table 4-3). The average percentage of *S100B* methylation is 75% in MPNST compared to 34% in neurofibroma (Figure 4-14; unpaired Student's *t*-test,  $p < 0.001$ ). In addition, analysis of different grades of MPNST showed that *S100B* is significantly hypermethylated in grade 3 compared to grade 1 (unpaired Student's *t*-test,  $p < 0.001$ ) and grade 2 tumours ( $p < 0.05$ ). Hypermethylation of *S100B* was also significantly higher in grade 2 compared grade 1 tumours ( $p < 0.001$ ; one-way ANOVA test between all groups,  $p < 0.001$ ; Table 4-5). The average

*S100B* percentage methylation was 75% in grade 3, 62% in grade 2 and 22% in grade 1 tumours (Figure 4-16).

*WT1* DNA methylation was also found to be significantly higher in MPNSTs compared to neurofibromas (Table 4-4). The *WT1* average percentage methylation was 49% in MPNST compared to 11% in neurofibromas (unpaired Student's *t*-test,  $p < 0.001$ ; Figure 4-15). In addition, *WT1* was significantly hypermethylated in grade 3 compared to grade 1 tumours ( $p < 0.05$ ) and *WT1* in grade 2 tumours was significantly hypermethylated compared to grade 1 tumours ( $p < 0.05$ ). However there was no significant difference in methylation levels between grade 2 and grade 3 MPNSTs ( $p = 0.835$ ; One-way ANOVA test between all groups,  $p = 0.111$ ; Table 4-6). The *WT1* average percentage methylation was 49% in grade 3, 48% in grade 2 and 23% in grade 1 (Figure 4-17).

## NFs

8	66	7	25
30	57	30	1
24	40	60	33
58	45	46	23
33	45	49	48
55	29	44	37
43	31	33	6
54	51	35	26
50	45	63	59
37	56	68	22
67	37	21	39
17	18	66	20
33	43	9	49
15	16	51	22
49	21	51	25
11	23	11	21
19	20	47	14
9	29	18	20
33	32	6	22
42	21	34	36

## MPNSTs

79	18	87	98
28	88	88	23
90	29	79	67
37	60	90	79
84	34	83	91
69	72	48	30
45	93	80	39
79	70	48	81
77	85	78	97
44	86	33	89
17	66	85	69
63	85	30	76
72	77	81	91
80	12	88	86
87	49	90	71
48	34	76	77
80	71	80	92
77	69	86	84
83	84	43	87
76	60	100	88

Colour code:

Methylation %
0-25%
26-50%
51-75%
76-100%

**Table 4-3: *S100B* DNA methylation is significantly higher in MPNSTs compared to neurofibromas**

Methylation of the *S100B* gene was examined by pyrosequencing in 80 neurofibromas (A) and 80 MPNSTs (B). Each box represents the average methylation level (expressed as percentage) of 6 CpG dinucleotides within the gene regulatory area in a single tumour. The results demonstrate a significantly higher level of *S100B* gene methylation in MPNSTs (average= 75%) compared to neurofibromas (34% average) (unpaired Student's *t*-test,  $p < 0.001$ ).

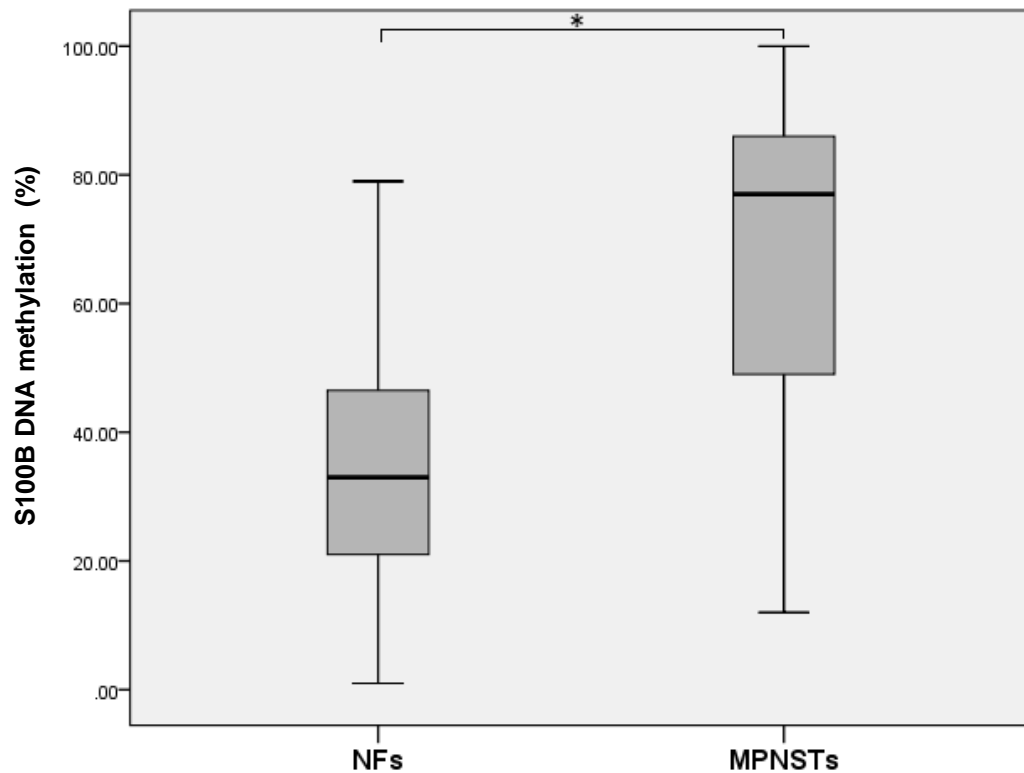


**Figure 4-14: Hypermethylation of *S100B* in MPNSTs vs Neurofibromas**

Box plot shows the mean methylation level of 6 CpG sites within the regulatory area of *S100B* gene in 80 neurofibromas and 80 MPNSTs. The average level of *S100B* gene methylation is significantly higher in MPNSTs (75%) compared to that in neurofibromas (34%) (unpaired Student's *t*-test, \* $p < 0.001$ ). Error bars represent standard deviation.

NFs (N=80)				MPNSTs (N=80)			
10	14	26	14	52	51	17	16
12	9	20	5	45	58	91	89
11	26	14	5	58	39	88	66
2	11	3	4	8	57	51	74
14	21	4	17	5	97	20	37
8	2	11	9	85	61	27	76
12	11	11	15	62	68	21	70
3	4	10	22	24	18	26	62
2	21	10	6	2	74	54	31
6	14	15	11	12	32	90	79
59	8	10	2	85	85	59	16
7	13	5	6	90	73	43	57
1	8	4	9	23	78	88	30
2	9	8	3	40	63	75	87
16	1	4	9	76	17	74	63
28	9	1	18	5	10	38	82
8	37	10	12	66	46	8	95
17	7	12	11	62	24	15	25
7	15	11	12	59	38	71	17
9	12	15	23	52	20	18	34

**Colour code:**

Methylation %
0-25%
26-50%
51-75%
76-100%

**Table 4-4: *WT1* gene methylation level is significantly higher in MPNSTs compared to neurofibromas**

Methylation of *WT1* gene regulatory area was analysed by pyrosequencing in 80 Neurofibromas (A) and 80 MPNSTs (B). Each box represents the average methylation level of 5 CpG dinucleotides within a single tumour. The results demonstrate a significantly higher level of *WT1* gene methylation in MPNSTs (average = 49 %) compared to neurofibromas (11 % average) (unpaired Student's *t*-test,  $p < 0.001$ ).

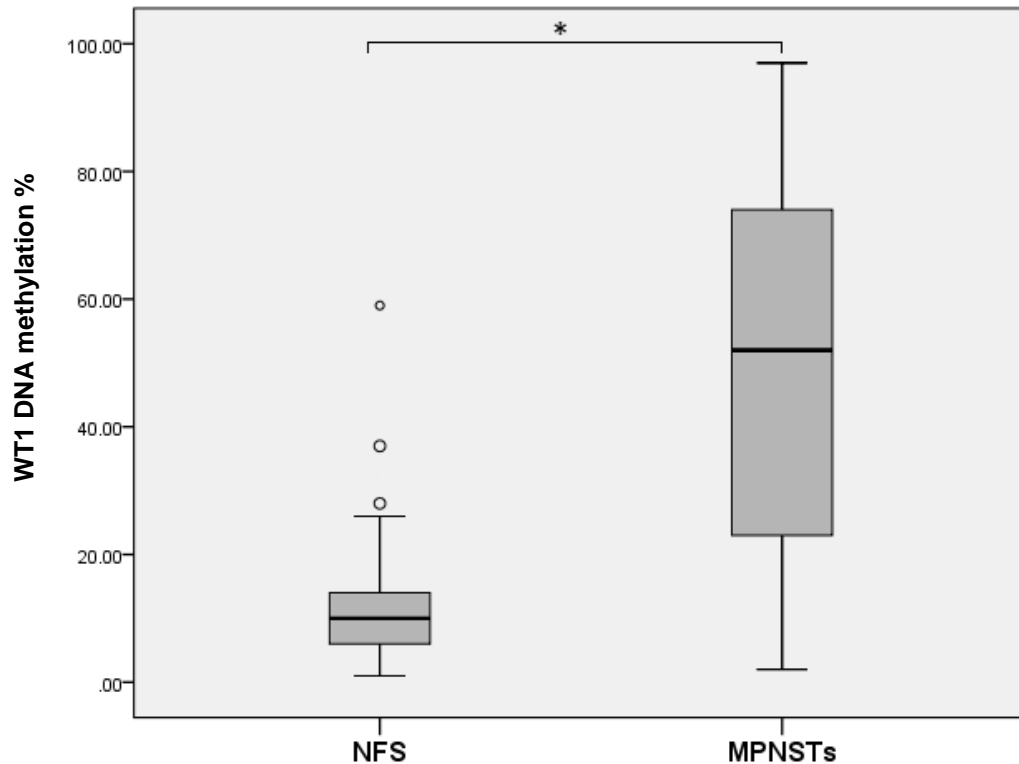


**Figure 4-15: Hypermethylation of *WT1* in MPNSTs vs Neurofibromas**

Box plot shows the mean methylation level of 5 CpG sites within the *WT1* gene regulatory area of 80 neurofibromas and 80 MPNSTs. The average level of *WT1* gene methylation is significantly higher in MPNSTs (49%) compared to that in neurofibromas (11%) (unpaired Student's *t*-test, \* $p < 0.001$ ). Error bars represent standard deviation.

Grade 1 (N=4)	Grade 2 (N=20)	Grade 3 (N=56)
28	90 45	80 85 48 76 91 71
18	37 79	77 86 80 80 30 77
29	49 77	83 66 48 86 39 92
12	34 44	76 85 78 43 81 84
	71 17	88 77 33 100 97 87
	69 63	60 87 85 60 89 88
	84 72	34 88 30 98 69
	79 80	72 79 81 23 76
	84 87	93 90 88 67 91
	69 48	70 83 90 79 86

Colour code:

Methylation %
0-25%
26-50%
51-75%
76-100%

**Table 4-5: *S100B* is significantly hypermethylated in high grade MPNSTs compared to lower grades**

Methylation of the *S100B* gene regulatory region was analysed by pyrosequencing in 80 MPNSTs. Each box represents the average methylation level of 6 CpG dinucleotides within a single tumour. The average *S100B* gene methylation level in grade 1 MPNSTs = 22% (4 cases); grade 2 = 65% (20 cases); and grade 3 = 81% (56 cases). Unpaired Student's *t*-test, grade 1 vs. grade 2,  $p < 0.001$ ; Grade 1 vs. grade 3,  $p < 0.001$ ; grade 2 vs. grade 3,  $p < 0.05$ . One-way ANOVA test between all groups,  $p < 0.001$ .

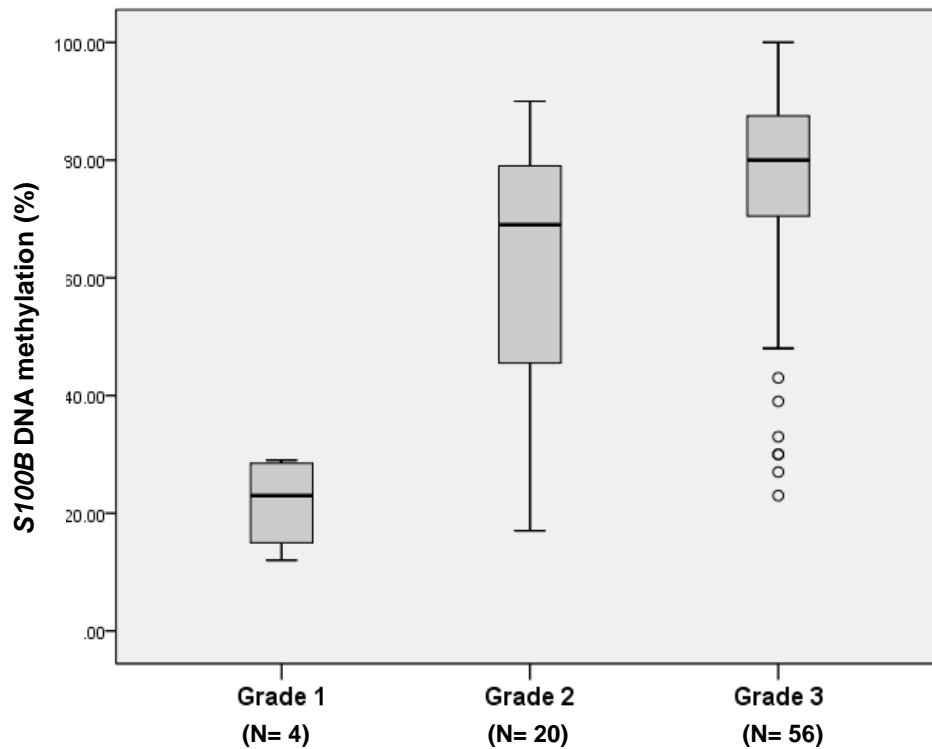


**Figure 4-16: Hypermethylation of *S100B* with increasing grade of MPNST**

Box plot demonstrating the mean methylation level of 6 CpG sites within the *S100B* gene regulatory area from 80 MPNSTs of different grades (4 grade 1, 20 grade 2, and 56 grade 3 tumours). The results demonstrate significantly higher levels of *S100B* gene methylation with increasing grade of MPNST. Unpaired Student's *t*-test, grade 1 vs. grade 2,  $p < 0.001$ ; Grade 1 vs. grade 3,  $p < 0.001$ ; grade 2 vs. grade 3,  $p < 0.05$ . One-way ANOVA test between all groups,  $p < 0.001$ .

Grade 1 (N= 4)	Grade 2 (N= 20)	Grade 3 (N= 56)
24	5 76	51 75 74 87 51 85
38	85 5	20 17 37 63 58 73
20	62 66	27 38 76 82 39 78
8	24 62	21 8 70 95 57 63
	2 59	26 15 62 25 97 34
	12 52	54 71 31 74 61 10
	85 17	90 18 79 52 68
	90 91	59 16 16 45 18
	23 88	43 89 57 58 74
	40 51	88 66 30 17 32

Colour code:

Methylation %
0-25%
26-50%
51-75%
76-100%

**Table 4-6: *WT1* is significantly hypermethylated in high grade MPNSTs compared to lower grades**

Methylation of the *WT1* gene regulatory area was analysed by pyrosequencing in 80 MPNSTs. Each box represents the average methylation level of 5 CpG dinucleotides within a single tumour. The average level of *WT1* methylation in grade 1 MPNSTs = 23% (4 tumours); grade 2 = 48% (20); and grade 3 = 49% (56). Grade 1 vs. grade 2, unpaired Student's *t*-test ( $p < 0.05$ ). Grade 1 vs. grade 3 ( $p < 0.05$ ). Grade 2 vs. grade 3 ( $p = 0.835$ ). One-way ANOVA test between all groups  $p = 0.111$ .

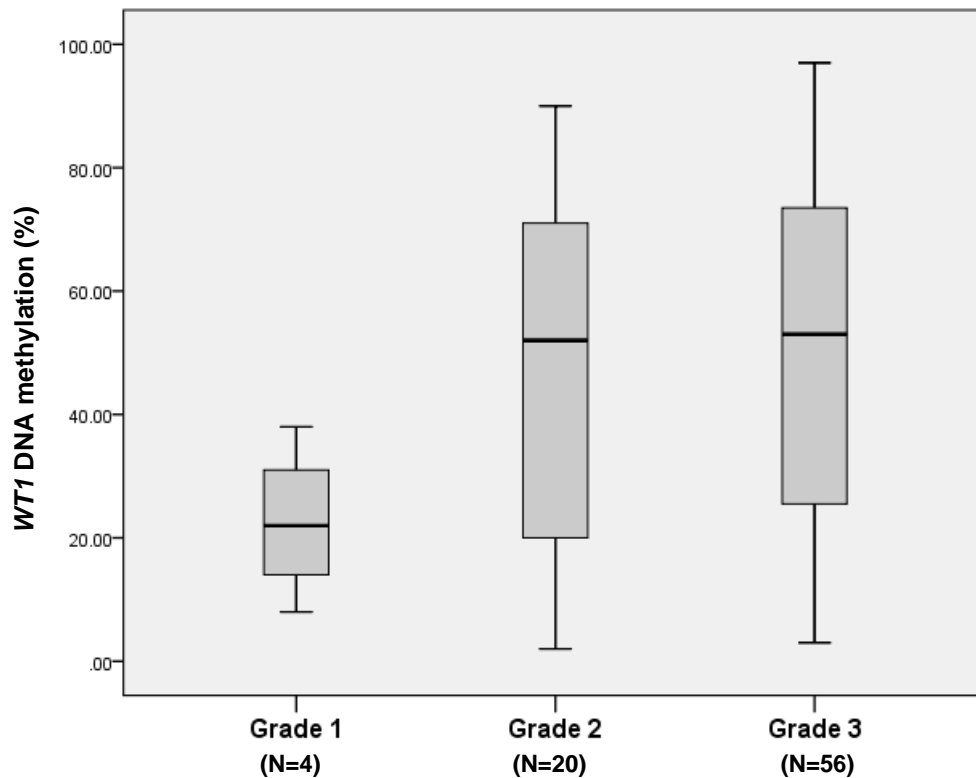


**Figure 4-17: Hypermethylation of *WT1* with increasing grade of MPNST**

Box plot shows the mean methylation level of 5 CpG sites within the *WT1* gene regulatory area from 80 MPNSTs of different grades (4 grade 1; 20 grade 2; and 56 grade 3). The results demonstrate significantly higher levels of *WT1* gene methylation in grade 2 and grade 3 MPNSTs compared to that in grade 1 tumours (unpaired Student's *t*-test,  $p < 0.05$ ). However there is no significant difference in levels of *WT1* methylation between grade 2 and grade 3 MPNSTs (unpaired Student's *t*-test,  $p = 0.835$ ). Comparison between all groups showed no significant difference (one-way ANOVA test,  $p = 0.111$ ).

## 4.4. Summary of Results

In this chapter, I examined fresh frozen tissue from 9 MPNSTs and 9 neurofibromas by q-RT-PCR and demonstrated a significantly higher level of DNMT3B mRNA expression in MPNSTs compared to that in neurofibromas. However, I found no significant difference in DNMT3A mRNA expression between the benign and malignant nerve sheath tumours.

I showed that miR-29c expression inversely correlates with DNMT3B mRNA expression in MPNSTs and neurofibromas. However, no correlation was found between miR-29c and DNMT3A mRNA expression in MPNSTs and neurofibromas.

My *in vitro* analyses demonstrated a significant reduction in DNMT3A and DNMT3B mRNA levels following transfection of miR-29c into sNF96.2 cells.

From my examination of the *in silico* data and published literature I identified *S100B*, *CDKN2A* and *WT1* as differentially methylated and differentially expressed between MPNSTs and neurofibromas. I therefore considered these as potential targets of DNMTs in MPNSTs.

Pyrosequencing analysis of *CDKN2A*, *WT1*, and *S100B* in a larger cohort of 80 MPNSTs and 80 neurofibromas FFPE tissue samples revealed hypermethylation of these three genes is more frequent in MPNSTs compared to neurofibromas. In addition, *S100B* and *WT1* DNA methylation

was found to be higher in high grade MPNST as compared with low grade MPNST.

I next looked at the expression of *WT1* and *S100B* by qRT-PCR following global demethylation of sNF96.2 cells by treatment with 5-Aza-2'-deoxycytidine (5-aza-dC) and showed that this leads to a significant increase in levels of *WT1* and *S100B* mRNA expression in this cell line.

My findings suggest miR-29c may have an important influence on gene methylation in MPNSTs and neurofibromas by regulating the expression of *DNMT3B*. In addition, the inhibition of *S100B* and *WT1* expression by hypermethylation may play an important role in the pathogenesis of MPNSTs from neurofibromas and in the progression of MPNSTs from low grade to high-grade tumours.

# **5. Analysis of S100B and WT1 candidates as potential tumour regulators in nerve sheath tumours**

## **5.1. Introduction**

S100 protein immunoreactivity in formalin-fixed paraffin-embedded material was first suggested as a diagnostic tool for diagnosis in a range of tumours (Nakajima et al. 1982). Nakajima et al. showed that S100 was expressed in the cells of eosinophilic granuloma, Hand-Schüller-Christian disease and Letterer-Siwe disease as well as in epidermal Langerhans cells and interdigitating reticulum cells in the lymph node, spleen and thymus (Nakajima et al. 1982). Subsequently, additional studies identified the expression of S100 in further tumour types including rhabdomyosarcoma, Ewing sarcoma, and synovial sarcoma (Coindre et al. 1988; Shimada et al. 1988; Fisher & Schofield 1991).

The known human S100 protein family consists of twenty-one members. They are small proteins of molecular weight between 9 kDa and 14 kDa (Marenholz et al. 2004; Donato 2003; Zimmer et al. 2013). They have been

shown to regulate different cellular functions using a calcium-dependent mechanism and they have also been shown to have a potential role in tumour formation and metastasis (Böni et al. 1997; Petersson et al. 2009; Keijser et al. 2006; Maelandsmo et al. 1997).

S100B protein is most abundant in neural tissue and it is commonly used by pathologists as a marker to indicate glial cell and Schwann cell differentiation (Hachem et al. 2005). S100B protein functions through intracellular and extracellular mechanisms and depending on its concentration, secreted S100B protein exerts either cytotropic or cytotoxic effects (Astrand et al. 2013). Lévy et al. showed that *S100B* mRNA is significantly downregulated in MPNST as compared to neurofibromas (Lévy et al. 2004).

WT1 was first discovered as a tumour suppressor in the paediatric kidney malignancy, nephroblastoma, or Wilms' tumour (WT) (Gessler et al. 1990; Call et al. 1990; Little & Wells 1997). WT1 can function as an oncogene in addition to its tumour suppressor function. It has been shown in a mouse model that WT1 can suppress growth and tumour formation (Smith et al. 2000; Fraizer et al. 2004; Luo et al. 1995). A study on acute myeloid leukaemia showed that 10-15% of cases studied had *WT1* mutation (King-Underwood et al. 1996). In contrast, an oncogenic role for WT1 in acute myeloid leukaemia has been suggested (McMaster et al. 1995; Barragán et al. 2004) where increased level of WT1 was associated with a poor response to therapy. In another study on acute myeloid leukaemia, a group of patients with poor prognosis showed high expression of WT1 and Bcl-2 (Karakas et

al. 2002). The methylation of *WT1* CpG islands has been detected in squamous cell carcinomas of the uterine cervix, suggesting it can be used for cervical cancer screening (Lai et al. 2008). *WT1* expression has been identified in various neural crest tumours including peripheral nerve sheath tumours e.g. neurofibromas and schwannomas (Schittenhelm et al. 2010; Singh et al. 2012). *WT1* overexpression has been detected also in MPNST using real-time RT-PCR (Ueda et al. 2003). A recent study has shown that silencing of *WT1* in sNF96.2 MPNST cell line Inhibits cell proliferation (Parenti et al. 2014).

In chapter 4, I have shown that *S100B* and *WT1* are frequently hypermethylated in MPNST compared to neurofibromas and the methylation is higher with the higher grade of tumour. I have also shown that demethylation of sNF96.2 MPNST cells cause re-expression of *S100B* mRNA and increased the expression of *WT1* mRNA (Chapter 4). Here, I focus on *S100B* and *WT1* as they have shown response to demethylation in sNF96.2 MPNST cells.

Although there are some studies in the literature that have discussed the expression of *WT1* (Schittenhelm et al., 2010; Parenti et al., 2014) or *S100B* protein in MPNST (Lévy et al. 2004; Nonaka et al. 2008), my work is the first to shed light on the possible regulatory mechanism of those genes through DNA methylation in MPNST.

## 5.2. Aims

The aims of this chapter were threefold:

- Examine the *S100B* and *WT1* mRNA expression pattern in MPNSTs and neurofibromas and determine whether there is any correlation between expression of these genes and their DNA methylation status.
- Test the protein expression using any of these two genes that might demonstrate a significant correlation between gene expression and methylation.
- Carry out functional studies in an MPNST-derived cell line of the selected potential regulator(s).

## 5.3. Results

### 5.3.1. *S100B* mRNA expression is low in MPNST compared to neurofibromas and inversely correlated with DNA methylation.

In chapter 4, I have shown that the *S100B* and *WT1* genes are frequently hypermethylated in MPNST compared to neurofibromas and also demonstrated that the level of their DNA methylation is elevated in higher grade tumours. I have also shown that global DNA demethylation of sNF96.2 MPNST-derived cells results in re-expression of *S100B* mRNA and increases expression of *WT1* mRNA (Chapter 4). In order to determine whether any relationship exists between the expression of *S100B* and *WT1* mRNA transcripts and their DNA methylation status, I decided to examine our fresh frozen human MPNSTs and neurofibromas by pyrosequencing and qRT-PCR as described in the previous chapter. However only 9 samples from each of the 10 MPNSTs and 10 neurofibromas was available for analysis this time.

The results of the *WT1* qRT-PCR data from the two different groups of tumour are summarised in Figure 5-1. These demonstrated no significant difference in *WT1* mRNA expression between MPNSTs and Neurofibromas (unpaired Student's *t*-test,  $p = 0.694$ ; Figure 5-1). However, expression of

*S100B* mRNA was found to be significantly lower in MPNSTs compared to neurofibromas (unpaired Student's *t*-test,  $p < 0.01$ ) as shown in (Figure 5-3)

I next compared the *WT1* and *S100B* mRNA expression levels with the *S100B* and *WT1* gene methylation levels in these tumour samples. The CpG methylation for the same samples has been analysed previously in section 4.3.4.

I observed a significant inverse correlation between the level of *S100B* mRNA expression and the level of *S100B* gene methylation in these tumours as demonstrated in Figure 5-4 (Pearson's correlation coefficient of -0.590,  $p < 0.01$ ). However, I found no correlation between the level of *WT1* mRNA expression and the level of *WT1* gene methylation (Pearson's correlation coefficient of -0.051,  $p = 0.841$ ), see Figure 5-2.

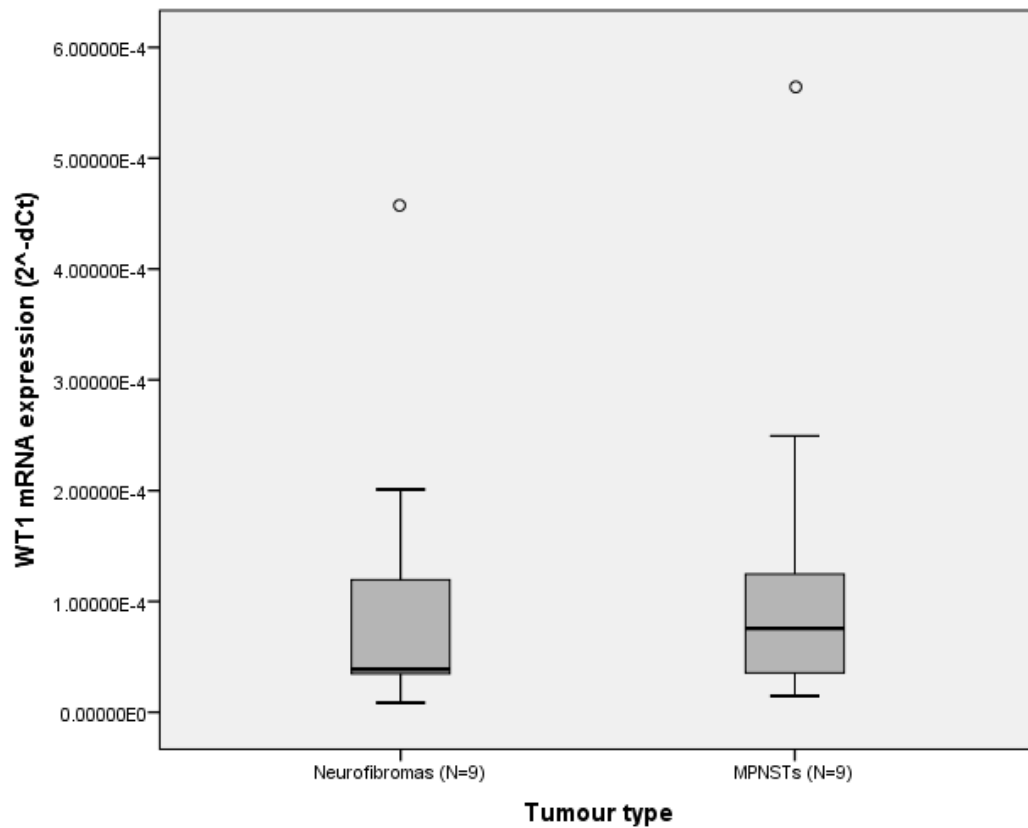


**Figure 5-1: *WT1* mRNA expression shows no significant difference between MPNSTs and neurofibromas**

Box plot shows qRT-PCR results of *WT1* mRNA expression levels in 9 neurofibromas and 9 MPNSTs. The *WT1* mRNA levels were normalised to expression of *GAPDH* gene. The results shown are representing the average of 2 technical replicates from one experiment. Error bars correspond to standard deviation. Neurofibromas vs. MPNSTs, unpaired Student's *t*-test,  $p = 0.694$ .

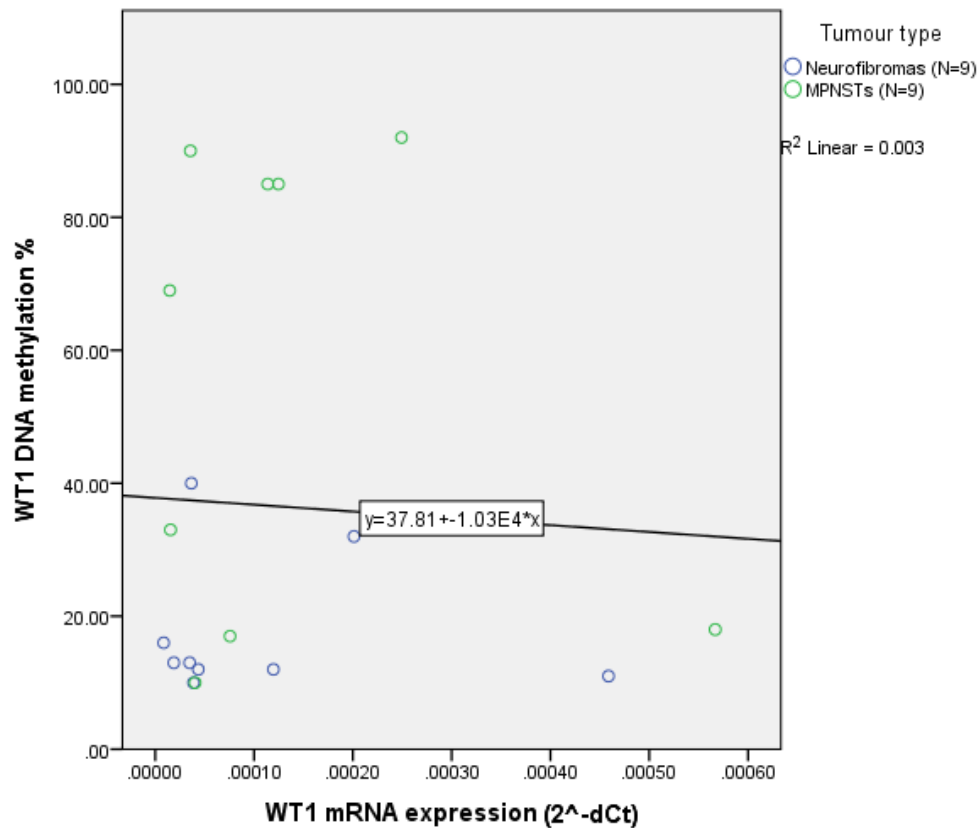


**Figure 5-2: *WT1* mRNA expression does not correlate with the level of *WT1* gene methylation**

qRT-PCR and pyrosequencing analysis demonstrates no correlation between *WT1* mRNA expression and methylation of the corresponding *WT1* DNA in MPNSTs and neurofibromas (Pearson's correlation test,  $p = 0.841$ , correlation coefficient of  $-0.051$ ).

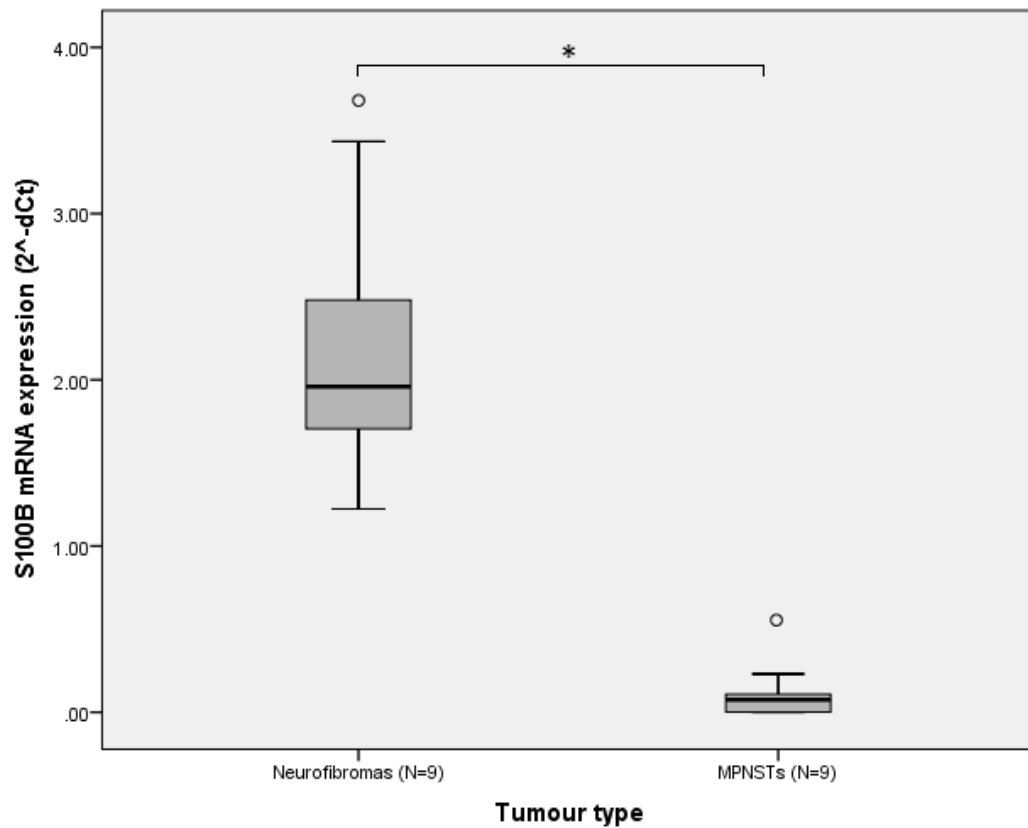


**Figure 5-3: *S100B* mRNA expression is significantly lower in MPNSTs compared to neurofibromas**

Box plot shows qRT-PCR analysis of *S100B* mRNA expression level in 9 neurofibromas and 9 MPNSTs. The *S100B* mRNA levels were normalised to expression of the *GAPDH* gene. The results shown are representing the average of 2 technical replicates from one experiment. Error bars correspond to standard deviation. Neurofibromas vs. MPNSTs, unpaired Student's *t*-test, \**p* < 0.01.

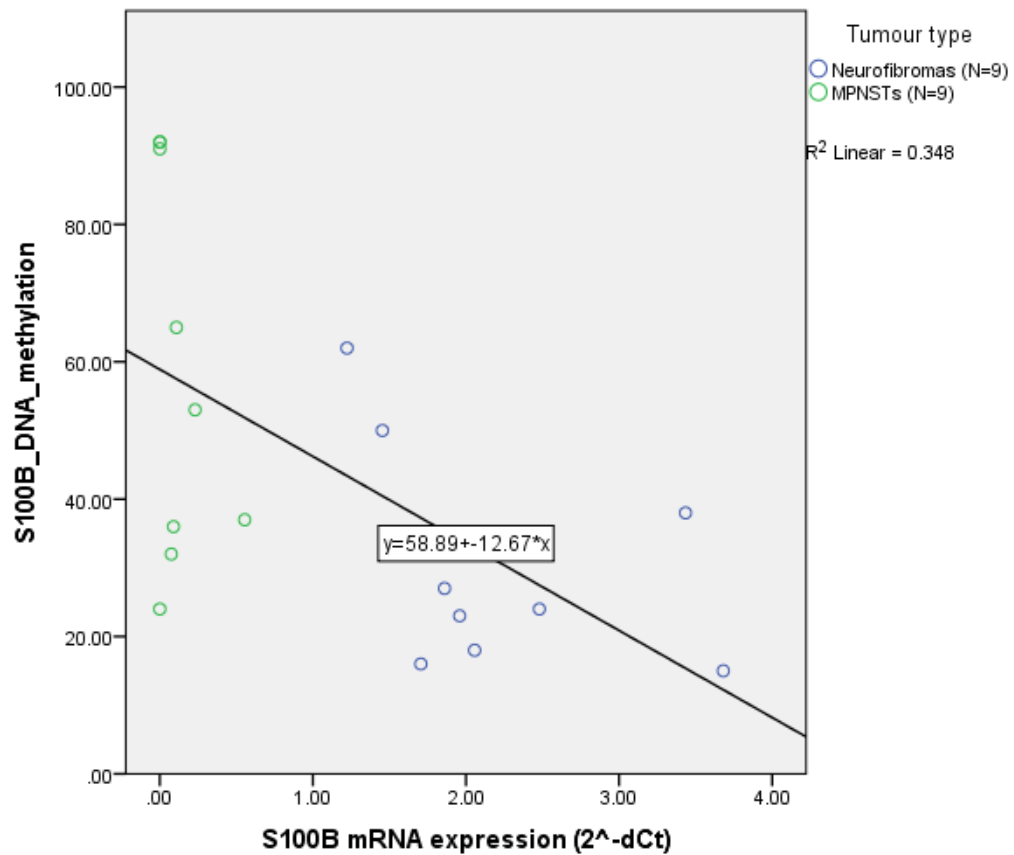


**Figure 5-4: *S100B* mRNA expression inversely correlates with level of *S100B* gene methylation**

qRT-PCR and pyrosequencing data demonstrates a significant inverse correlation between *S100B* mRNA expression and DNA methylation status of the corresponding *S100B* gene in MPNSTs and neurofibromas (Pearson's correlation test,  $p < 0.01$ , correlation coefficient of -0.590).

### **5.3.2. S100 IHC staining inversely correlates with CpG methylation**

Having demonstrated that *S100B* mRNA expression is significantly lower in MPNSTs compared to Neurofibromas and significantly correlates with methylation of CpG sites within the *S100B* gene regulatory region (Figure 5-4); I next examined the expression of S100B protein in human MPNSTs and neurofibromas. IHC staining of S100B protein was performed on FFPE tissue samples from a selected cohort of 15 MPNSTs and 15 neurofibromas. 10 of the 15 MPNSTs chosen were highly hypermethylated at the *S100B* regulatory region (> 75% methylation), 10 of the neurofibromas were hypomethylated (< 25% methylation), and 5 each of the MPNSTs and neurofibromas chosen were intermediate-methylated (25 - 75% methylated). Details of the IHC staining protocol are described in chapter 2.

Table 5-1 gives a summary of the S100B IHC results obtained from the 15 MPNSTs and 15 neurofibromas. The IHC staining intensity was scored as 0 for no staining; 1 for weak staining; 2 for moderate staining; and 3 for strong staining of S100B protein. The percentage of tumour cells stained positive within each tumour sample was also scored as 0 for < 1% of tumour stained; 1 for 1 – 10% of tumour stained; 2 for 11 – 60% of tumour stained; and 3 for > 60% of tumour stained. A combined score was then calculated for each tumour sample by adding together the score for intensity of staining and score for percent of tumour cells stained.

The results of the IHC analysis demonstrated negative or focal weak staining of S100B protein in 7 out of the 10 hypermethylated MPNST samples. Focal strong staining of S100B was also seen in 3 of the hypermethylated MPNSTs. In the neurofibromas, diffuse strong staining of S100B protein was seen in 9 out of 10 hypomethylated cases. Diffuse moderate staining of S100B protein was seen in only one of these cases. In the 10 intermediate-methylated tumour samples different patterns of S100B protein staining was observed; 1 sample was S100B negative, 2 cases showed focal weak staining, 2 showed diffuse moderate staining and 5 cases demonstrated diffuse strong staining for S100B.

I next compared the S100B protein staining pattern with the corresponding *S100B* DNA methylation level in each of the 15 MPNSTs and 15 neurofibromas. The results of this analysis, which are summarised in Figure 5-5 showed that tumours which are negatively stained or show focal weak or focal strong staining of S100B protein are largely hypermethylated (MPNSTs). The hypomethylated tumours (neurofibromas) mainly exhibited diffuse moderate or diffuse strong IHC staining for S100B (Figure 5-5). In other words there is a significant inverse correlation between the expression of S100B protein and methylation of CpG sites within the regulatory region of the corresponding *S100B* gene in MPNSTs and neurofibromas (Pearson's correlation test, correlation coefficient of -0.716,  $p < 0.001$ ; Figure 5-6). Examples of the of different types of S100B IHC staining patterns obtained can be seen in Figure 5-7.

**Table 5-1: *S100B* gene methylation level and protein staining score in Neurofibromas and MPNSTs**

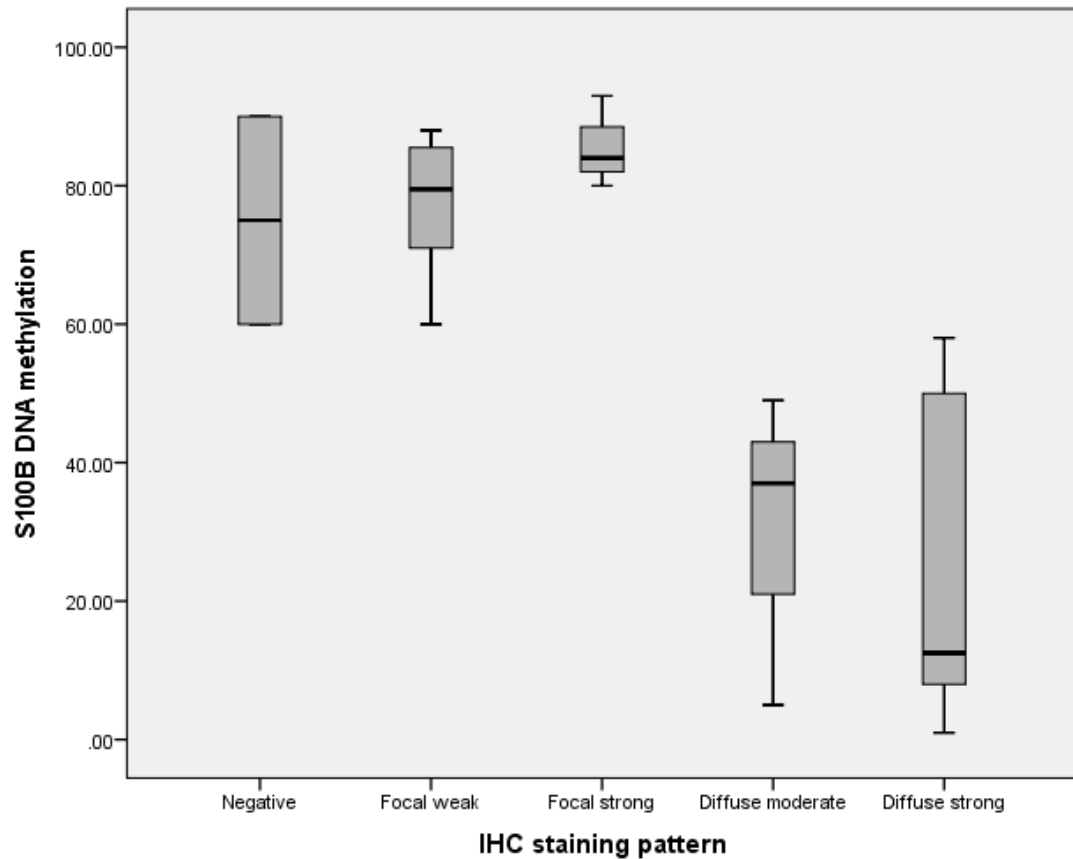
Tumour Diagnosis	<i>S100B</i> % methylation	Staining pattern	Extent of Staining	Staining intensity	Combined Staining score
MPNST 1	79	F	1	1	2
MPNST 2	79	F	1	1	2
MPNST 3	80	F	1	1	2
MPNST 4	84	F	1	1	2
MPNST 5	87	F	1	1	2
MPNST 6	90	-	0	0	0
MPNST 7	84	F	1	3	4
MPNST 8	80	F	2	3	5
MPNST 9	88	F	1	1	2
MPNST 10	93	F	1	3	4
MPNST 11	63	F	1	1	2
MPNST 12	60	-	0	0	0
MPNST 13	60	F	1	1	2
MPNST 14	37	D	2	2	4
MPNST 15	49	D	3	2	5
NF 1	58	D	3	3	6
NF 2	55	D	3	3	6
NF 3	54	D	2	3	5
NF 4	50	D	3	3	6
NF 5	49	D	3	3	6
NF 6	8	D	3	3	6
NF 7	11	D	3	3	6
NF 8	9	D	3	3	6
NF 9	16	D	3	3	6
NF 10	5	D	3	2	5
NF 11	9	D	3	3	6
NF 12	6	D	3	3	6
NF 13	1	D	3	3	6
NF 14	6	D	3	3	6
NF15	14	D	3	3	6

Key: F= focal; D= diffuse.

Extent of staining refers to percentage of tumour cells which are positive: 0= < 1%; 1= 1-10%; 2= 10-60% and 3= > 60%.

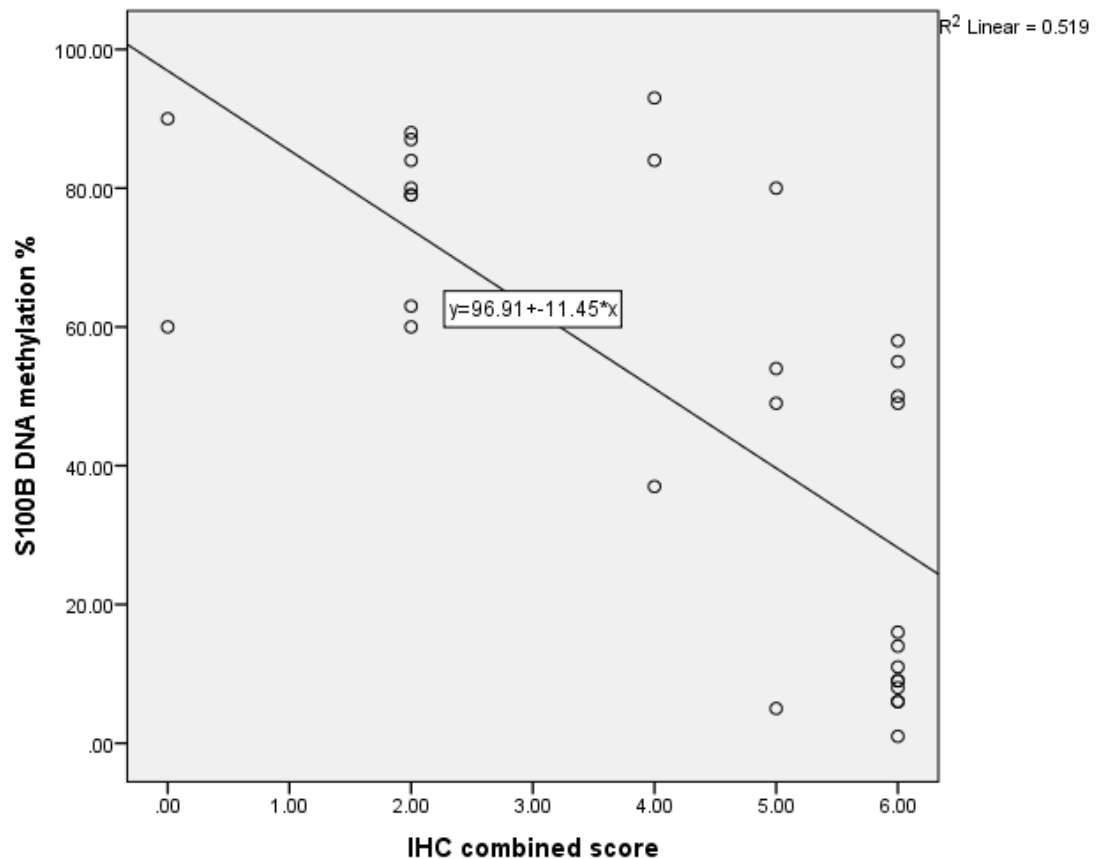
Staining intensity is scored as 0= none; 1= weak; 2= moderate; and 3= strong.

The combined staining score represents the sum of the scores for extent and intensity of staining in each individual tumour.



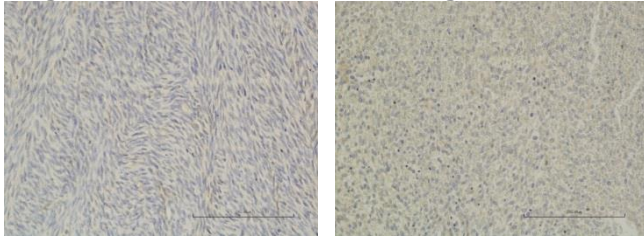
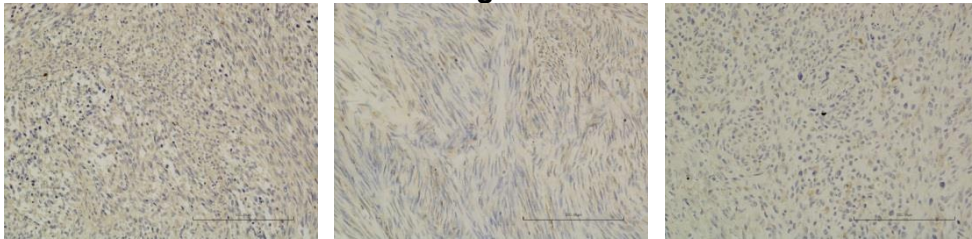
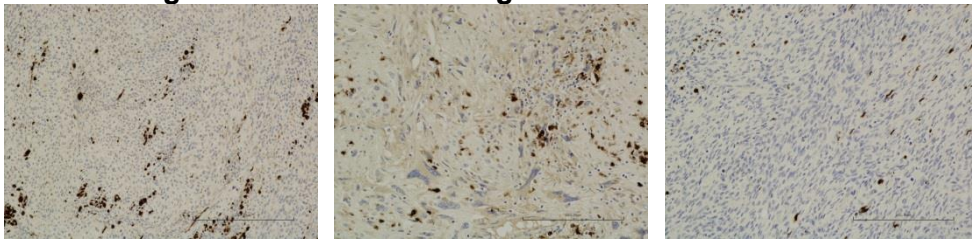
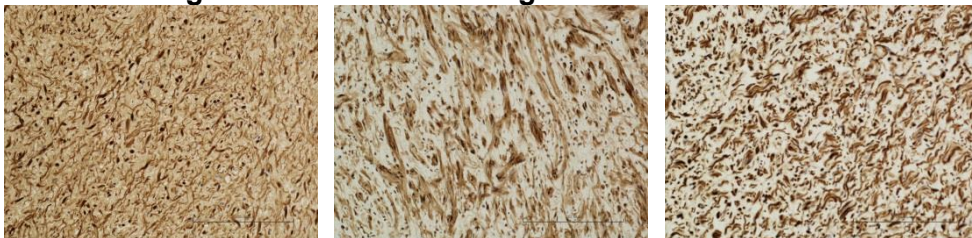
**Figure 5-5: *S100B* gene methylation level versus protein expression pattern in NFs and MPNSTs**

Box plot shows the average *S100B* DNA methylation percentage in tumours with different patterns of *S100B* protein expression. The samples exhibiting no expression or focal (weak, moderate or strong) expression of *S100B* protein were all MPNSTs (13 cases) with hypermethylated *S100B* gene. A significant correlation between hypomethylation of *S100B* gene and diffuse (moderate or strong) expression of *S100B* protein was also demonstrated in the tumour samples. All cases exhibiting diffuse, strong *S100B* protein expression were neurofibromas (n=14); the cases demonstrating diffuse, moderate protein expression comprised two MPNSTs and one neurofibroma.



**Figure 5-6: S100B protein expression inversely correlates with level of S100B gene methylation**

Graph shows the methylation level (expressed as a percentage) of 6 CpG islands within the *S100B* gene regulatory region plotted against the combined immunostaining score of S100B protein in 30 individual tumours (15 MPNSTs and 15 NFs). The results demonstrate a significant inverse correlation between the level of *S100B* gene methylation and S100B protein expression (Pearson's correlation test,  $p < 0.001$ , correlation coefficient of  $-0.716$ ).

**Negative S100B immunostaining in 2 MPNSTs:****Focal weak S100B immunostaining in 2 MPNSTs:****Focal strong S100B immunostaining in 3 MPNSTs:****Diffuse moderate S100B immunostaining in 2 MPNSTs and 1 neurofibroma:****Diffuse strong S100B immunostaining in 3 neurofibromas:****Figure 5-7: S100B protein expression in MPNSTs and neurofibromas**

Representative examples of different S100B immunostaining patterns. S100B protein, which appears as brown staining, is expressed in both cytoplasm and nuclei of cells. The highest intensity and extent of staining is seen in the 3 neurofibromas (bottom panel).

### **5.3.3. Cloning of *S100B* into lentivirus expression vector**

Having demonstrated that *S100B* protein expression is decreased in MPNSTs compared to neurofibromas, I next examined the role that *S100B* might play in the pathogenesis of MPNSTs. This was done by carrying out functional studies using the sNF96.2 cell line that is known not to express endogenous *S100B* protein or mRNA transcript. I aimed to re-express *S100B* in this cell line by transducing it with an *S100B* lentivirus expression vector (pLenti PGK PuroDEST) and examine any observable effects that *S100B* expression might have on cell proliferation and migration.

I used a standard cloning technique to insert *S100B* cDNA into an expression vector (pLenti PGK PuroDEST) using a PCR cloning strategy as described in chapter 2. Briefly, *S100B* cDNA was first amplified by RT-PCR and the resulting amplicon was then checked by agarose gel electrophoresis and direct sequencing to confirm the correct product had been amplified. The *S100B* RT-PCR product was then inserted into the pENTR 4 dual selection vector using appropriate restriction enzymes and then recombined into a PGK PuroDEST (w529-2) destination vector as described in chapter 2. The destination vector containing *S100B* cDNA was then transfected into lentivirus which was then used to infect the sNF96.2 cells. Lentivirus containing empty vector was also prepared and used to transfect a separate

culture of sNF96.2 cells for use as a control. Stably transduced cells were then selected by growing them in the presence of Puromycin (see chapter 2 for details).

The expression of *S100B* in the transduced sNF96.2 cells was then examined at both the mRNA and protein level by qRT-PCR and Western blot analysis. The results of the qRT-PCR demonstrated no detectable *S100B* mRNA transcript in sNF96.2 cells transduced with empty viral vector but a significant level of *S100B* mRNA expression was detected in the sNF96.2 cells transduced with *S100B* expressing vector (unpaired Student's *t*-test,  $p < 0.001$ ; Figure 5-8A).

The Western blot analysis also demonstrated clear expression of *S100B* protein in sNF96.2 cells transduced with *S100B* expressing viral vector. However in the sNF96.2 cells transduced with empty vector there was no evidence of any *S100B* protein expression on the Western blot (Figure 5-8B).

The data from the qRT-PCR and Western blot analysis indicated that I had managed to successfully transduce *S100B* cDNA into the sNF96.2 cells and that *S100B* was successfully being transcribed into mRNA and translated into protein at significant levels in this cell line.

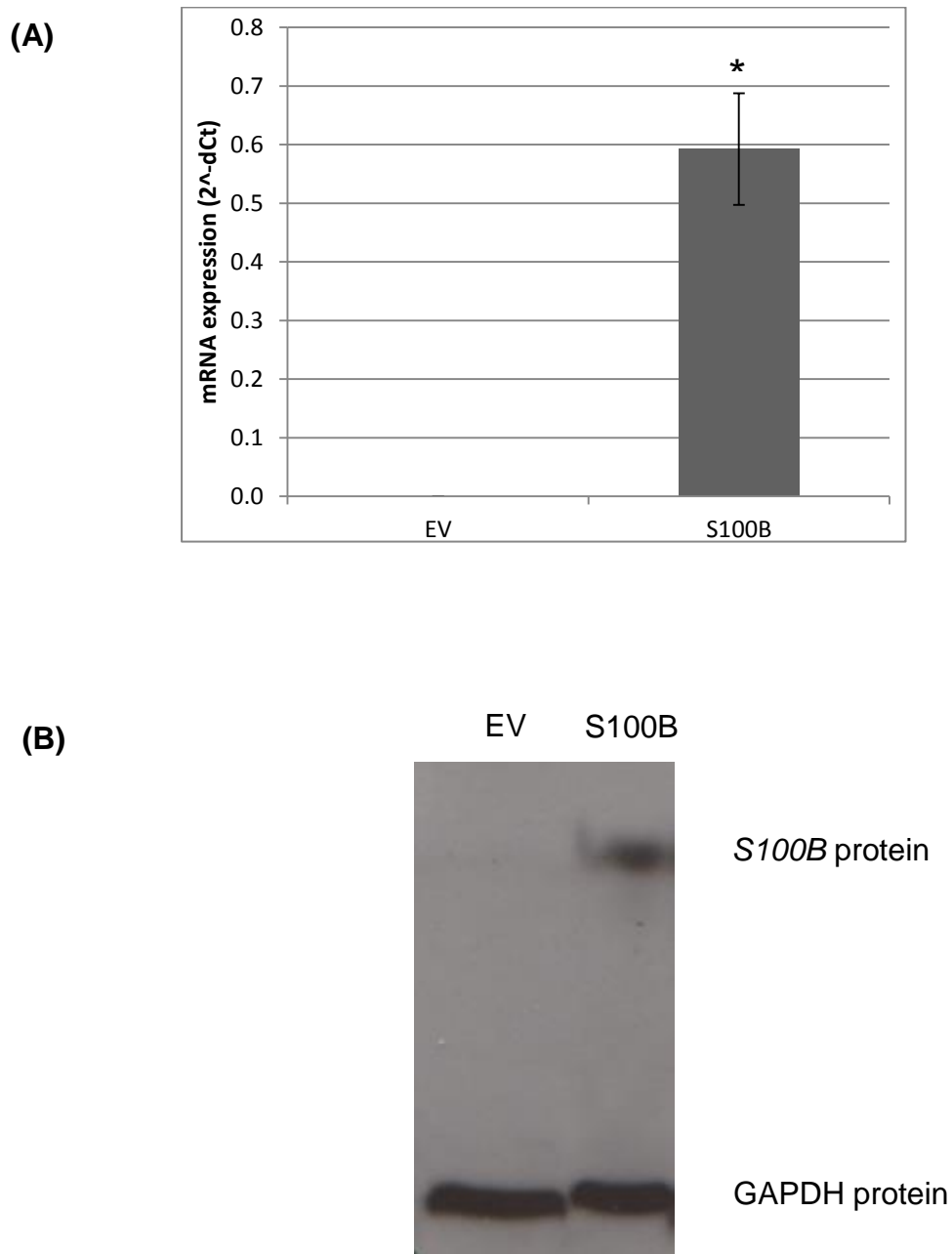


**Figure 5-8: *S100B* mRNA & protein expression following transduction of sNF96.2 cells with *S100B* expression vector**

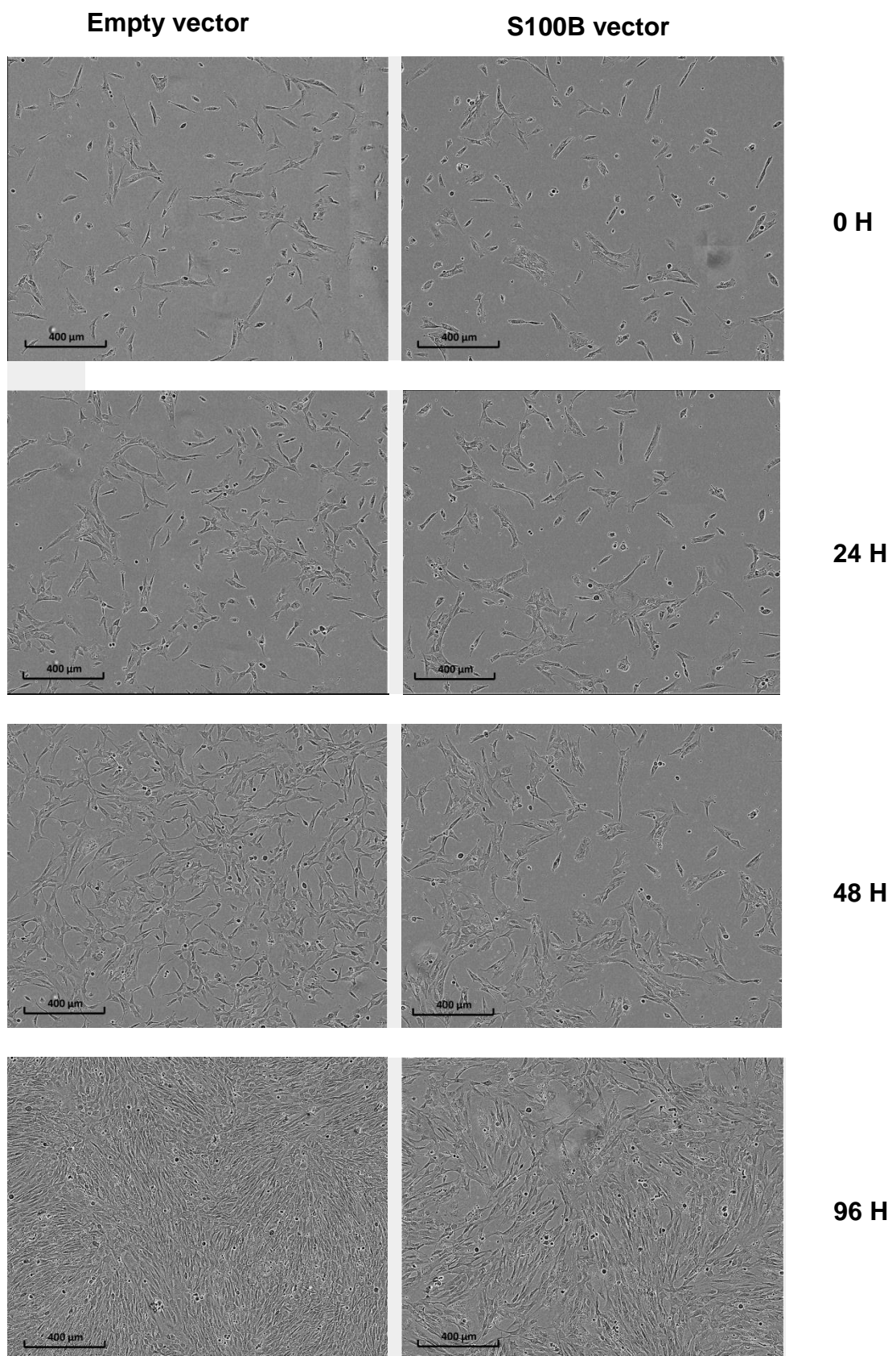
(A) qRT-PCR demonstrating *S100B* mRNA expression in sNF96.2 cells transduced with *S100B* expressing lentiviral vector but not in control cells transduced with lentivirus containing empty vector (unpaired Student's *t*-test, \**p* < 0.001). The qRT-PCR data was normalised to *GAPDH* gene. Bars represent the average results obtained from three independent experiments (three biological replicates). Error bars represent standard deviation. (B) Western blot demonstrating expression of *S100B* protein in sNF96.2 cells transduced with *S100B* expressing viral vector but not in control cells transduced with virus containing empty vector. *GAPDH* was used as a protein loading control.

### **5.3.1. Re-expression of *S100B* in sNF96.2**

#### **MPNST cells causes reduced cell proliferation**

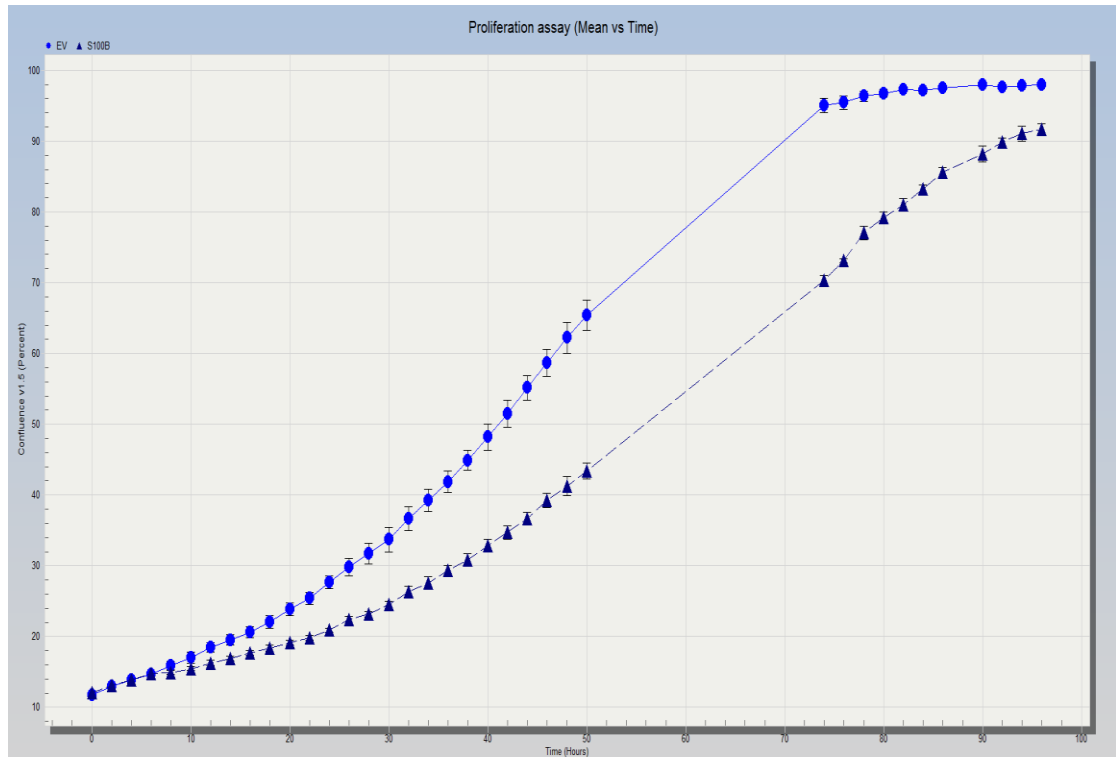
Following successful transduction of *S100B* cDNA into sNF96.2 cells, functional studies were carried out in order to determine the effects(s) if any, that *S100B* expression might have on the proliferation and migration of these MPNST-derived cells. Cell proliferation was assessed using the MTS assay and Incucyte Kinetic Live Cell imaging™ System (details of which can be found in chapter 2). Results from the Incucyte live imaging system can be seen in Figure 5-9. Cells were imaged every 2 h for a total period of 96 h and the IncuCyte Analyser software was used to obtain real-time updates on cell confluence changes over the experimental time.

Figure 5-10 shows the proliferation curves obtained over the four day growth period. The results demonstrated a significant decrease in proliferation of sNF96.2 cells transduced with *S100B* expressing viral vector compared to that in control cells transduced with empty viral vector. The differences in proliferation between test and control cells became evident very early on, at around 10 h into the experiment, and by 50 h, there was a greater than 20 % difference in confluence levels between test and control sNF96.2 cells. The difference in growth is highly significant at 72 h ( $p < 0.001$ ).



**Figure 5-9: Incucyte imaging of lentivirus transduced sNF96.2 cells**

Differences in confluency between S100B expressing sNF96.2 cells (test cases) and cells transduced with empty viral vector (controls). The images demonstrate a significant decrease in proliferation of test cells compared with control cells.



**Figure 5-10: Decreased proliferation of S100B expressing sNF96.2 cells**  
Incucyte live imaging proliferation assay showing percentage confluence of sNF96.2 cells transduced with S100B expressing lentiviral vector and control cells transduced with virus containing empty vector over a 96-h period. The data points represent the averages of three technical replicates from one representative experiment. Error bars represent standard deviation. There is a significant reduction in proliferation of sNF96.2 cells expressing S100B compared to control cells,  $p < 0.001$  at 72 h).

The results from the MTS proliferation assay are shown in Figure 5-11. This assay was conducted over a total period of 4 days and absorbance measurements were taken at 0, 2, and 4 days following the start of the experiment. There was no significant difference in absorbance measurements between the test and control cells at the start of the experiment (day 0) but at day 2 there was a significant (> 50%) reduction in absorbance readings from S100B expressing cells compared to that in control cells. By day 2, the absorbance readings from the MTS assay began to plateau for both the test and control cell lines (paired Student's *t*-test,  $p < 0.01$  at day 2).

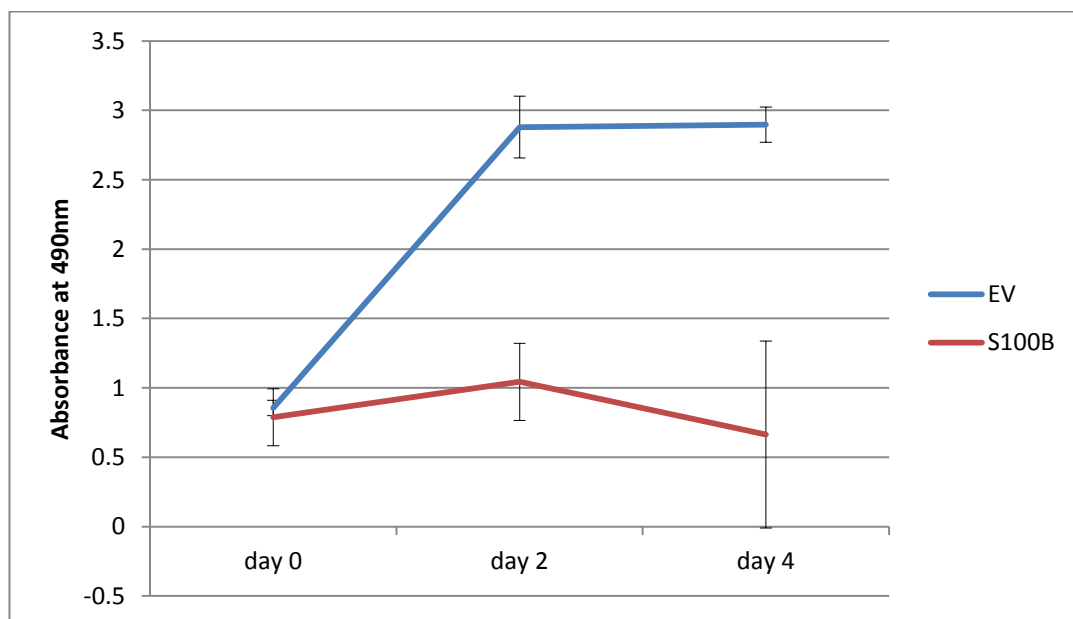


**Figure 5-11: Decreased viability of S100B expressing sNF96.2 cells**

Cell viability was measured by MTS assay in sNF96.2 cells transduced with S100B expressing vector (test cells) or with empty viral vector (controls) at 0, 2 and 4 days following seeding of  $2 \times 10^3$  cells in 100  $\mu$ l of culture medium into each well of 96 well plates. Data points represent the mean absorbance measurements from three independent experiments (three biological replicates). Error bars represent standard deviation. By day 2 there was a significant reduction in viability of test cells compared to controls (paired Student's *t*-test,  $p < 0.01$  at day 2).

The result from the Incucyte live cell imaging and MTS assay demonstrate that S100B expression in sNF96.2 cells has an inhibitory effect on cell proliferation and suggests a tumour suppressor role for S100B in MPNSTs.

Following the cell proliferation and viability assays the effect of S100B expression on migration of sNF96.2 cells was assessed using the scratch-wound healing assay, details of which can be found in chapter 2. Briefly, the test and control sNF96.2 cells were seeded in triplicate into 24-well plates and left to grow until confluency was reached overnight. A scratch was then made through the central axis of the plate using the Essen BioScience Wound-Maker and images of the scratch area were recorded every 2 h for a total of 30 h using the IncuCyte™ live cell imaging system. The results demonstrated no significant differences in migration rates between S100B expressing sNF96.2 cells or control cells transduced with empty vector (Figure 5-12).

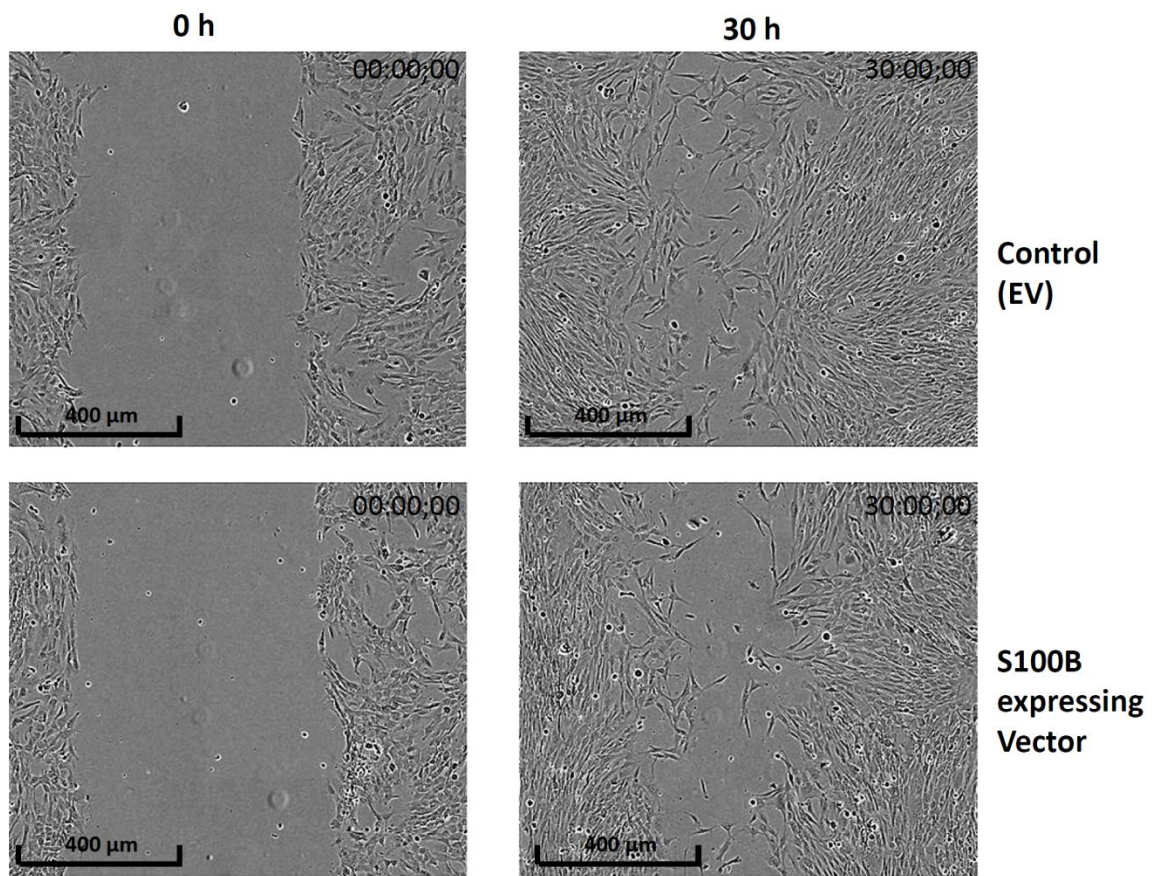


**Figure 5-12: Cell motility rate unaltered in S100B expressing sNF96.2 cells**

Scratch wound-healing motility assay showing sNF96.2 cells transduced with S100B expression vector (test cells) and control cells transduced with empty vector. Images were taken using the Incucyte live cell imaging system immediately after a scratch was made through the central axis of each plate at 0 h, and 30 h later. The number of cells, which had migrated into the scratch area, was found to be comparable in both test and control cells.

### 5.3.2. *S100B* gene methylation unaltered by miR-29c expression in sNF96.2 cells

Having demonstrated that *S100B* expression can affect the proliferation of MPNST-derived sNF96.2 cells I next set out to determine whether *S100B* gene methylation might be influenced by the expression of miR-29c in this line. I therefore examined the methylation status of the *S100B* gene regulatory region in sNF96.2 cells transfected with miR-29c mimics (test cells) and in control cells transfected with scrambled oligonucleotides. DNA was extracted from test and control cells 48 h following transfection and examined by bisulfite pyrosequencing as previously described. The results from these experiments demonstrated no significant differences in the level of methylation at 6 CpG sites within the *S100B* gene regulatory region between the test and control sNF96.2 cells (unpaired Student's *t*-test,  $p = 0.375$ ) (Figure 5-13). Although these results show that ectopic expression of miR-29c has no influence on the methylation status of *S100B* in this cell line, the findings do not rule out the possibility that *S100B* gene methylation could still be influenced by miR-29c during the early stages of MPNST development via its effects on expression of the *de novo* methylators DNMT3A and DNMT3B.

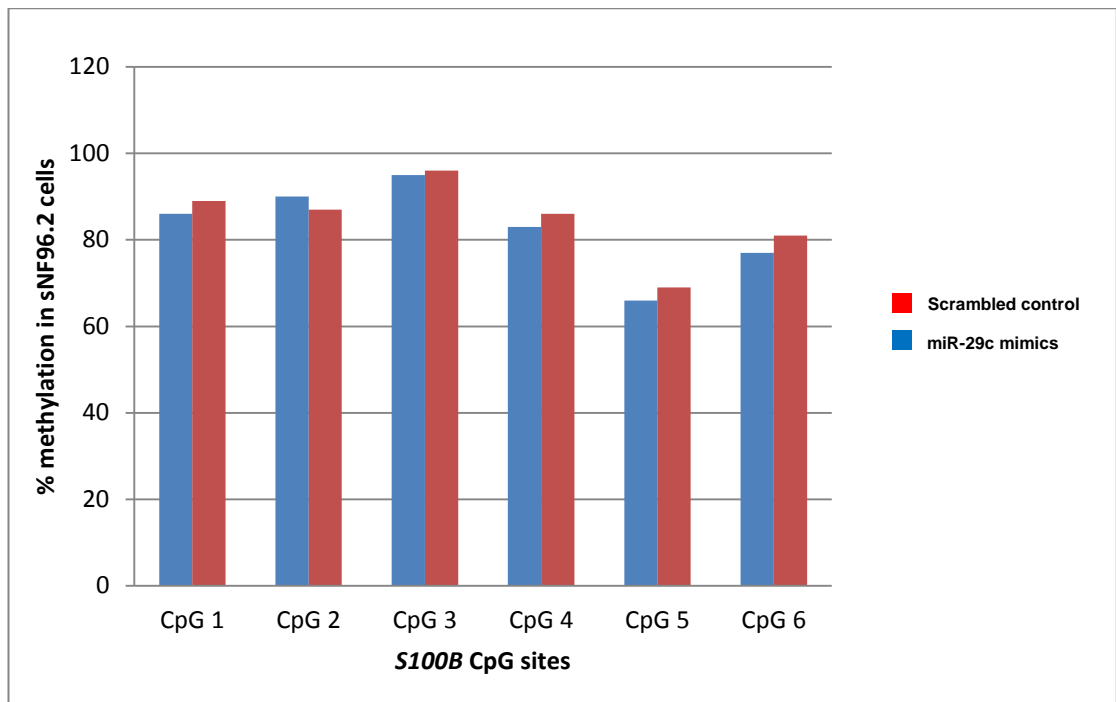


**Figure 5-13: *S100B* gene methylation unaltered by miR-29c expression in sNF96.2 cells**

Bisulfite pyrosequencing of the *S100B* gene regulatory region in sNF96.2 cells transfected with miR-29c mimics (test cells) or with scrambled oligonucleotides (controls) demonstrates no significant differences in the level of methylation at 6 CpG sites between test and control cells (paired Student's *t*-test,  $p = 0.375$ ).

## 5.4. Summary of results

In this chapter, I have shown that *S100B* mRNA expression is significantly lower in MPNST compared with neurofibromas and inversely correlates with the level of methylation at CpG sites within the *S100B* gene regulatory region.

However, I observed no significant difference in the level of *WT1* mRNA expression between MPNSTs and neurofibromas and no correlation was found between the level of *WT1* mRNA expression and methylation status of the *WT1* gene.

I then compared the *S100B* IHC staining pattern with the corresponding *S100B* DNA methylation pattern in each of 15 MPNSTs and 15 neurofibromas and demonstrated a significant inverse correlation between *S100B* protein expression and the level of methylation at *S100B* gene regulatory region.

In order to examine the role that *S100B* might play in the pathogenesis of MPNSTs functional studies were carried out using sNF96.2 cells that had been transduced with a *S100B* expressing lentiviral vector. I found that *S100B* expression in sNF96.2 cells had an inhibitory effect on cell proliferation and viability but had no effect on the migratory behaviour of these cells.

I next set out to determine whether *S100B* gene methylation might be influenced by the expression of miR-29c in this line. However, an examination of the methylation status of the *S100B* gene regulatory region in sNF96.2 cells that had been transfected with miR-29c mimics demonstrated no significant alteration in the level of methylation at the *S100B* gene regulatory region in response to miR-29c expression.

My findings suggest that *S100B* functions as a tumour suppressor and its expression is epigenetically controlled by methylation in MPNSTs.

## 6. Discussion

### 6.1. Role of miR-29c in the progression of neurofibroma to MPNST

The underlying mechanisms by which neurofibromas transform to MPNST remain largely unknown but increased understanding of these processes could potentially provide novel opportunities for early diagnosis and/or therapy in patients. Much evidence has accumulated in recent years highlighting the important influence of microRNAs on various physiological and pathological processes, including tumour biology where they mediate their effect as either tumour suppressor genes or oncogenes (Calin & Croce 2006; Di Leva & Croce 2010; Esquela-Kerscher & Slack 2006; Garzon et al. 2006; Pasquinelli et al. 2005).

Previous investigations into the role of miRNAs in the pathogenesis of MPNSTs in patients with and without neurofibromatosis type 1 are limited and have resulted in different miRNAs being implicated in the development of MPNSTs from neurofibromas. In the earliest of these studies Subramanian et al. (2010) carried out miRNA expression profiling for 482 known and predicted human miRNAs on 23 peripheral nerve sheath tumours (6 MPNSTs, 11 neurofibromas and 6 schwannomas) and reported distinct miRNA expression profiles for MPNSTs and benign tumours. In comparison

with benign tumours, five miRNAs (miR-214, miR-377, miR409-3p, miR-487b and miR-99b) were relatively upregulated and five (miR-517, miR-34a, miR-29a, miR-30e-5p and miR-27a) were downregulated in MPNSTs. All the MPNSTs, which were reported as demonstrating a significant downregulation of miR-34a by Subramanian et al. (2010), were also described as exhibiting a *TP53* inactivation gene expression signature. They demonstrated that exogenous expression of p53 in MPNST cells induces miR-34a and other miRNAs, a finding that is consistent with published data showing that miR-34a expression is regulated by p53 (Chang et al. 2007; He et al. 2007).

miR-34a was not found to be significantly differentially expressed in our MPNSTs compared to neurofibromas although we did show that 6 out of the 9 MPNST showed lower expression of miR-34a, whereas lower expression was detected in only three neurofibromas. It is noteworthy that the *TP53* gene expression signature of our 10 MPNSTs was unknown. In this context it is of interest that all of our patients had neurofibromatosis type 1, whereas it is not known if this were the case for the six patients in Subramanian's study. This is relevant as *TP53* mutations are reported to occur in ~25% of MPNSTs, and that the minority of these (36%) are found in tumours from patients with neurofibromatosis type 1 (Verdijk et al. 2010). Hence, it is interesting to speculate that the different genetic background on which MPNSTs arise provide an explanation for the discrepant miR-34a results. An alternative explanation for the discrepancy between the two studies is that different miRNA microarray platform were used, and the small numbers of

cases included in the studies could have compounded this. Nonetheless, it is reassuring that we reproduced the finding published by Subramanian *et al* (2010) that miR-29a was significantly downregulated in MPNST. None of the other miRNAs mentioned in Subramanian's study however, were found to be amongst our list of differentially expressed genes in MPNSTs and neurofibromas.

In a more recent study, Masliah-Planchon *et al.* (2012) examined 9 dermal neurofibromas, 41 plexiform neurofibromas, and 15 MPNSTs from neurofibromatosis type 1 patients using the TaqMan Low Density Array, which included 377 highly characterised human miRNAs. They reported 113 miRNAs as differentially expressed between plexiform neurofibromas and MPNSTs. Of these 103 were significantly upregulated in MPNSTs and 10 were downregulated. This finding is in sharp contrast to the findings in our study where the majority of miRNAs (14/16) were downregulated in MPNST relative to neurofibromas. It is of interest that miR-210 and miR-339-3p, which we found to be upregulated in our study, are also upregulated in Masliah-Planchon *et al.* study. The downregulated genes reported by Masliah-Planchon *et al.* (2012) included miRNAs (miR-139-5p, miR-150, miR-195 and miR-146a) that were also among our list of significantly downregulated miRNAs thus suggesting they may play an important role in the pathogenesis of MPNSTs and should perhaps be singled out for further study in these tumours. It is also interesting that a member of the lethal 7 (let7) family (let7b) was amongst the list of relatively downregulated miRNAs

in MPNSTs by Masliah-Planchon et al. (2012) as two members of this family, let-7a and let-7g were also amongst our list of downregulated genes in MPNSTs. let-7 miRNAs regulate key differentiation processes during development. In addition, the expression of let-7 members has previously been reported to be significantly low in human cancers where it is thought they may play an important role as tumour suppressors by targeting RAS. (Grosshans et al. 2005; Takamizawa et al. 2004; Peter 2009).

Itani et al. (2012) tested 6 neurofibromas and 6 MPNSTs and reported that miR-21, miR-135b, miR-152, miR-130b, miR-92, and miR-15b were upregulated in MPNST compared to neurofibromas, whereas the expression levels of miR-125b, miR-127, and miR-302d were downregulated in MPNST compared to neurofibromas. In our cohort, we did not observe these particular differences to statistical significance. An explanation for the discrepancy between our study and the other studies is that different microRNA microarray platforms were used, and the small numbers of cases included in the studies could have compounded this. In addition using samples from different genetic background or possible different ethnic group might contribute to this discrepancy between results.

We have also demonstrated that all members of the miR-29 family, that is miR-29a, b, c, c\* and b-1\* are significantly downregulated in MPNSTs compared to neurofibromas. The involvement of these miRNAs in MPNSTs is perhaps not surprising since these miRNAs have previously been reported to be aberrantly expressed in a wide variety of cancers (Castilla et al. 2011;

Nguyen et al. 2014; Fabbri et al. 2007; Iorio et al. 2005; Li et al. 2011; Sengupta et al. 2008; Xiong et al. 2010; Zhao et al. 2010; Calin et al. 2005). The miR-29 family of miRNAs have extensive sequence homology at the 5' seed region, which is important for RNA target recognition and specificity (Bartel, 2004). This, coupled with the fact that an mRNA can be simultaneously repressed by more than one miRNA species (Doench & Sharp 2004), makes it conceivable that the miR-29 family members might be acting on the same target, or may be regulating multiple genes within the same or related pathways in neurofibromas and MPNSTs. I found the miR-29 family interesting to be studied further because all the members of the family are differentially expressed between neurofibromas and MPNSTs.

I next focussed my attention on miR-29c specifically for further analysis. This particular miR-29 was chosen for a number of important reasons. Firstly this miRNA was more significantly differentially expressed compared to the other miR-29 family members in neurofibromas and MPNSTs. Secondly it has been implicated in a variety of other cancers including chronic lymphocytic leukaemia (Mraz et al. 2009; Stamatopoulos et al. 2009), oesophageal squamous cell carcinoma (Ding et al. 2011), nasopharyngeal carcinoma (Sengupta et al. 2008), lung cancer (Fabbri et al. 2007) which made it an attractive molecule to study. I concentrated on the mature form of miR-29c since the star forms (\*) of miRNA are generally found to be less expressed *in vivo* compared with the non-star forms (Schwarz et al. 2003). In addition the mature form of miRNA is the one that incorporate in the RNA-induced

silencing complex (RISC) which causes its stabilisation and this process is accompanied by destruction of the (\*) form (Schwarz et al. 2003). In addition I conveniently had available to me an MPNST-derived cell line, sNF96.2, which had previously been shown to be *NF1* mutant (Perrin et al. 2007) and I verified this *NF1* mutation using direct sequencing. We also found previously in our lab sNF96.2 cells to express very low levels of miR-29c, therefore suitable for functional studies involving transfection of miR-29c.

I have shown that the ectopic expression of miR-29c (using synthetic miR-29c mimics) leads to reduced migration of MPNST-derived cells but does not significantly affect their proliferation. These findings are consistent with previous reports that proliferation and migration are often mutually exclusive cellular phenomena (Zheng et al., 2009). The inhibitory actions of miR-29c expression on cell migration has previously been demonstrated in other cancers such as nasopharyngeal carcinoma, gastric cancer, bladder cancer and pancreatic cancer (Cui et al. 2015; Jiang et al. 2015; Fan et al. 2014; Sengupta et al. 2008). However, in glioma and gastric cancer miR-29c was found to have an inhibitory effect on both proliferation and migration (Fan et al. 2013; Y. Wang et al. 2013; Han et al. 2015) On the other hand, it has been demonstrated that miR-29c suppresses cell proliferation and induced apoptosis in oesophageal carcinoma, bladder cancer and hepatocellular carcinoma (Wang et al. 2011; Fan et al. 2014; Ding et al. 2011). Its possible miR-29c expression could have different effects on cell proliferation and migration depending on the cell context.

The migratory behaviour of mammalian cells is known to be influenced by a variety of factors including the extracellular matrix. The extracellular matrix is composed of a complex set of molecules which are secreted by cells and plays an important role in maintaining tissue integrity by providing structural as well as well as biochemical support to surrounding cells. It can also act as a reservoir for a variety of growth factors/cytokines e.g., adhesion molecules and receptor tyrosine kinases. The function of the ECM is brought about by a finely tuned remodelling process achieved through breakdown and replacement of tissue and involves MMPs, which degrade various collagens and non-collagenous ECM glycoproteins (Patterson et al., 2001). Alterations of the constituent elements of ECM can have been shown to have profound effects on the proliferation, survival, and migration of surrounding cells often seen in various disease states (Russo et al. 2005; Newby 2006; Daley et al. 2008).

In order to throw more light on the mechanism(s) by which miR-29c exerts its effects in MPNST cells I examined several ECM genes whose expression is known to be affected by this molecule. I demonstrated reduced expression of the collagen genes *COL1A1*, *COL1A2*, *COL4A1*, *COL4A2*, *COL5A2* and *COL21A1* as well as the matrix metalloproteinase *MMP2* in response to miR-29c expression. High levels of extracellular collagens have previously been associated with increased invasiveness of many types of tumour cells *in vitro* and with increased metastasis in animal models (Menke et al. 2001; Koenig et al. 2006; Shintani et al. 2006; Chintala et al. 1996; Kaufman et al. 2005) as

well as an increased likelihood of metastasis in several types of human solid tumours (Ramaswamy et al. 2003). Overexpression of *MMP2* has also been shown to be involved in cell migration and is associated with the metastatic potential of malignant tumours (Xu et al. 2005).

It is of interest that the collagens types that are targeted by miR-29c are those that are also degraded by MMP2, and that both sets of genes are upregulated in MPNST as shown in our previously published GEM study (Henderson et al. 2005).

My findings of increased expression of some collagens and *MMP2*, together with reduced migration of MPNST cells after introducing of miR-29c, argue that miR-29c acts as a tumour suppressor gene in MPNST and mediates its effect through modifying tumour migration by mediating its effect through both collagens and MMP2. As *MMP2* is a confirmed target of the miR-29 family (Steele et al. 2010), the MMP2 inactivation in the miR-29c-transfected sNF96.2 cells can be explained as a post transcriptional regulatory event. Alternatively, MMP9 inactivation by miR-29c could be through an indirect pathway.

Amongst the numerous molecules known to be targeted by microRNAs is Transforming growth factor beta (TGFB). This protein exists as three isoforms, TGFB 1-3, which share more than 97% sequence identity in mammalian tissue. The 3 isoforms are secreted cytokines involved in regulation of many processes including embryogenesis, differentiation,

proliferation, motility, ECM production and homeostasis in nearly all types of cells and tissues (Watabe & Miyazono 2009; Huang & Huang 2005; Li et al. 2010; Sugiyama et al. 2013; Wu & Hill 2009). The TGFB pathway has also been shown to play an important role in tumorigenesis exerting differential effects on cancer cells depending on the stage of disease; TGFB has been shown to act as tumour suppressor in normal cells and early stage cancers whereas in the later stages of many cancers TGFB can behave as a tumour promoter by virtue of its ability to induce epithelial to mesenchymal transition (EMT), promote angiogenesis and degradation of the ECM all of which assist tumour invasion and metastasis (Tang et al. 2003; Wakefield & Roberts 2002; Siegel et al. 2003). Although most members of the TGFB family are targeted by one or more miRNAs the relationship between these two classes of molecules is a complex one since miRNAs production can also be influenced either directly or indirectly by TGFB. An association between various miR-29 family members and TGFB has previously been demonstrated in animal models of renal lung and cardiac fibrosis (Ramdas et al. 2013; Qin et al. 2011; Y. Zhang et al. 2014; Winbanks et al. 2011). Within the context of cancer Jiang et al. (2014) recently showed that TGFB/Smad3 regulated miR-29c expression negatively by binding to the *MIR29C* promoter, leading to the loss of miR-29c in PANC cells (Jiang et al. 2014). Downregulation of miR-29b has also been shown to enhance TGFB signaling in breast cancer cells (Chou et al. 2013).

I have identified *TGFB3* as a potential target for miR-29c in MPNST derived cells and also showed that *TGFB3*, in addition to *MMP2*, is downregulated in response to ectopic expression of miR-29c in MPNST-derived cells. However, I failed to identify any direct links between *TGFB3* expression and the expression of *MMP2* or *MMP9* since silencing of *TGFB3* had no significant effects on expression of *MMP2* or *MMP9* at either the mRNA or protein level in MPNST derived cells. However, using zymography I observed a reduction in *MMP2* and *MMP9* proteolytic activity in the supernatants of miR-29c transfected MPNST-derived cells which would suggest that *MMP2* and *MMP9* may be indirect targets of *TGFB3*. As far as I am aware there are no reported studies looking at *TGFB3* expression in MPNSTs. However, Watanabe et al. (2001) examined 8 cases of MPNST arising within a neurofibroma associated with neurofibromatosis type 1 and demonstrated higher expression of transforming growth factor  $\beta$ 1 (*TGFB1*) in the areas of MPNST than in the neurofibromatous areas (Watanabe et al. 2001). Although one cannot directly extrapolate the findings with *TGFB1* to the other *TGFB* isoforms, the possibility that all 3 isoforms may be under the influence of miR-29c or indeed other microRNAs in MPNSTs is something that will need to be determined empirically in future studies. However, my findings so far would seem to support the hypothesis that *TGFB3* expression is negatively influenced by miR-29c expression in MPNST-and that the loss of miR-29c in MPNSTs may lead to overexpression of *TGFB3* with possibly a concomitant increase in tumour promoting signals.

Roundabout 1 (ROBO1) belongs to a family of highly conserved transmembrane cell surface receptors that in humans also includes ROBO2, ROBO3 and ROBO4. ROBO proteins were first identified in the 1990s as axon guidance molecules in the fruit fly *Drosophila* (Murray & Whittington 1999). ROBO proteins act as receptors for the Slit family of secreted proteins and together the Slit/ROBO1 axis has been shown to be important development of a various vital organs such as kidneys, lungs breasts and liver (Macias et al. 2011; Piper et al. 2000; Liu et al. 2003). In addition to organogenesis, Slit/ROBO1 signalling has been implicated in a variety of cellular processes including cell proliferation, cell motility, cell adhesion and angiogenesis (Prasad et al. 2004; Huang et al. 2015; Yeh et al. 2014; Chen et al. 2010). Aberrant expression of Slits and ROBOs has over the last decade also been shown to play an important role in a variety of human diseases including cancer (Legg et al. 2008; London & Li 2011; London et al. 2010; Wu et al. 2001). ROBOs have been shown to be both up-regulated or downregulated in a variety of human cancers {reviewed by (Ballard & Hinck 2012)} which suggests that they can act as both tumour suppressors, providing negative growth signals to cancers or as oncogenes, promoting cancer progression. I have identified *ROBO1* as a potential target of miR-29c in MPNSTs by *in silico* prediction analysis and demonstrated using microarray expression data that *ROBO1* is significantly highly expressed in MPNSTs compared to neurofibromas. Furthermore, I provided *in vitro* evidence that *ROBO1* mRNA expression is significantly downregulated in response to ectopic expression of miR-29c in MPNST-derived sNF96.2 cells.

These findings suggest *ROBO1* over-expression in MPNSTs is acting as an oncogene and that miR-29c acts as tumour suppressor by targeting *ROBO1* expression in neurofibromas. However, the lack of any detectable *ROBO1* protein in sNF96.2 cells despite the expression of *ROBO1* mRNA would seem to contradict the view that *ROBO1* is acting as an oncogene in this cell line. My findings suggest that despite *ROBO1* mRNA being expressed in sNF96.2 cells, the transcript is not being translated into *ROBO1* protein at any significant level which would be more in line with *ROBO1* acting as a tumour suppressor in this cell line. However, one must bear in mind the possibility that this cell line may not be representative of the situation in the fresh tumour samples. At this stage, it is not possible to reach any conclusions about the role of *ROBO1* in MPNSTs pathogenesis other than to say that its transcription appears to be under the control of miR-29c. Another miRNA that is known to target *ROBO1* is miR-218. miR-218 has been shown to behave as a tumour suppressor, inhibiting the invasion and migration of glioma, pancreatic, nasopharyngeal and gastric cancer cells through the *ROBO1* signalling pathway (Tie et al. 2010; Alajez et al. 2011; Gu et al. 2015; Rheinheimer et al. 2013). In order to throw more light on the role of *ROBO1* in MPNST pathogenesis the expression of *ROBO1* mRNA and protein will need to be examined in the fresh frozen neurofibromas and MPNSTs by qRT-PCR and western blot analysis, respectively, in addition to carrying out functional studies which target *ROBO1* expression directly using siRNA.

In conclusion, I provide data suggesting that miR-29c is a tumour suppressor the loss of which plays a pivotal role in the progression of nerve sheath tumours by increasing their invasive/migratory properties.

## 6.2. Relationship between miR-29c and DNA methyltransferases 3A and 3B

DNA methylation at the 5-position of cytosine plays an important role in maintaining chromatin structure and regulating gene transcription and is essential for mammalian development (Jin et al. 2011). The pattern of DNA methylation in mammalian cells is generated *de novo* by DNA methyltransferases DNMT3A and DNMT3B, which are highly expressed during embryogenesis but are downregulated in differentiated adult somatic cells (Okano et al. 1999). DNMT1 is the most abundant DNA methyltransferase in adult cells and is responsible for the maintenance of DNA methylation (Robertson et al. 1999). Disruptions in the pattern of DNA methylation have been implicated in the pathogenesis of a variety of human diseases including cancer (Jones & Baylin 2007; Berdasco & Esteller 2010). Human cancers generally exhibit global hypomethylation of their DNA which is also accompanied by region-specific DNA hypermethylation (Wild & Flanagan 2010). Silencing of tumour suppressor genes by hypermethylation of their promoters regions is a common feature in many human malignancies and cancer cell lines and is thought to arise in part from the increased levels of DNMTs expression in these tumours (Baylin 2005) e.g., overexpression of *DNMT1*, *DNMT3A* and *DNMT3B* has been reported in liver cancer (Saito et al. 2001). There is also much evidence to suggest that repression of gene transcription by DNA methylation has a causal role in cancer pathogenesis

rather than just being a bystander effect e.g., alterations of DNA methylation have been shown in early precancerous conditions and in some cases histologically normal appearing tissue in association with chronic inflammation or infection with pathogens (Kanai & Hirohashi 2007). Increasing levels of DNMT1, DNMT3A, and DNMT3b expression, along with increasing numbers of methylated genes, have also been demonstrated in the advancement of normal tissue to malignancy such as the case with progression from normal liver to chronic hepatitis/cirrhosis to hepatocellular carcinomas (Sceusi et al. 2011). In addition, a significant association between aberrant DNA methylation or elevated DNMT3A/DNMT3B expression and poorer tumor differentiation, increased tumor aggressiveness and poor prognosis has also been demonstrated in some cancers e.g., increased DNA methylation in renal cell carcinomas has been shown to significantly correlate with higher histological grade, an infiltrating growth pattern and vascular involvement (Arai et al. 2006) and overexpression of DNMT3B has been shown to correlate with poor prognosis in breast cancer and cutaneous melanoma (Roll et al. 2008; Nguyen et al. 2014). Patients with low levels of DNMT1 expression have also been reported to demonstrate a better response to chemotherapy and overall survival than those with higher levels of DNMT1 expression in their tumours (Mutze et al. 2011). Furthermore, the inhibition of DNA methyltransferase expression has been to be associated with an increase in tumour suppressor gene expression and reduction in tumorigenicity (Brueckner et al. 2005).

There have are few reported studies on DNA methylation in MPNSTs and the number of clinical samples examined in each has also been very small (Bradtmöller et al. 2012; Danielsen et al. 2015; Lee et al. 2014) Feber et al. (2011) carried out a whole-genome comparative methylome analysis of MPNSTs and benign neurofibromas and reported a complex pattern of epigenetic changes during disease progression. In contrast to other tumour types, significant global hypomethylation was not observed in MPNSTs. However, the predominant targets of aberrant methylation in the MPNST genome were found to be the satellite regions, promoters and CpG islands (Feber et al. 2011).

The role of DNMTs in human neurofibromas and MPNSTs has not previously been investigated. I examined the expression of *DNMT3A* and *DNMT3B* expression in these tumours and showed that *DNMT3B* mRNA expression is significantly higher in MPNSTs compared to neurofibromas. However, I found no significant difference in *DNMT3A* mRNA expression between the benign and malignant nerve sheath tumours. Although our tumour numbers were small (only 9 MPNSTs and 9 neurofibromas), these findings are not unusual since *DNMT3B* is found to be frequently expressed in cancer tissues compared to *DNMT3A* and *DNMT1* which are expressed at lower frequencies (Robertson et al. 1999) e.g., overexpression of *DNMT3B* but not *DNMT3A* has been reported in breast cancer (Sandhu et al. 2012) and Burkitt lymphoma (Robaina et al. 2015) among others e.g., primary leukaemia (Ostler et al. 2007). However since both enzymes can methylate

most genomic targets, it is possible that increased expression of just one of these DNMTs will be sufficient to bring about DNA hypermethylation in cancers. Conversely, the absence of either can lead to decreased methylation that would not be the case if they were functionally redundant.

The lack of any observable increase in *DNMT3A* expression in our tumour samples does not rule out the possibility that this DNMT is involved in MPNST pathogenesis. It is still possible DNMT3A could exert some effect via its interaction with DNMT3B. DNMT3A and DNMT3B are known to form a complex in mammalian cells and have been shown to mutually stimulate one another as a result of this direct interaction (Li et al. 2007). The majority of DNMT3B transcripts in cancer encode catalytically active protein but over 20 splice variants of DNMT3B have been identified in cancer cell lines and primary leukaemias, many of which are catalytically inactive (Ostler et al. 2007). Some of these inactive DNMT3B isoforms have been shown to modulate the activity of DNMT3A–DNMT3L complexes so it's possible the genomic methylation pattern could be altered as a result of this interaction (Van Emburgh & Robertson 2011; Jurkowska et al. 2011; Li et al. 2013; Shah et al. 2010) One also cannot rule out the possibility that mutations in DNMT3A, as well as DNMT3B could also play a role in MPNST pathogenesis since carcinogen-related mutations have been shown to occur in the catalytic and non-catalytic domains of these DNMTs (Wang et al. 2006; Ley et al. 2010).

The regulation of DNMTs is thought to be one of the mechanisms by which microRNAs exert their tumour suppressor activities in cells. The miR-29 family members possess complementary sequences to the 3'-UTRs of DNMT3A and DNMT3B and the regulation of these DNMTs by miR-29s, as well as by other miRNA family members, is well documented in the literature. For example, the expression of *DNMT3A* and *DNMT3B* in lung cancer has been shown to be directly targeted by, and inversely correlates with, expression of miR-29 family members (Fabbri et al. 2007). *In addition, re-expression of miR-29s has been shown to reduce DNMT3B mRNA levels in hypermethylator breast cancer cell lines and to restore normal patterns of DNA methylation in lung cancer cell lines by targeting DNMT3A and DNMT3B* (Sandhu et al. 2014; Fabbri et al. 2007). These findings give support to the hypothesis that expression of miR-29s can contribute to the epigenetic DNA modifications in cancer.

*DNMT3A* and *DNMT3B* were identified by my *in silico* data as potential targets of miR-29c. Having shown that miR-29c expression is altered in MPNSTs compared to neurofibromas I wished to establish whether any relationship exists between the expression of miR-29c and the DNA methylation status of these tumours. My findings showed that *DNMT3B* mRNA expression is higher in MPNSTs compared to neurofibromas and inversely correlates with miR-29c expression. However, I found no significant difference in *DNMT3A* mRNA expression between the benign and malignant nerve sheath tumours and there was no correlation between *DNMT3A* and

miR-29c expression in our tumour samples. This finding suggested that miR-29c expression may contribute to epigenetic DNA modification in MPNSTs by targeting *DNMT3B*. I decided to test hypothesis by examining the effect of exogenous miR-29c expression in the MPNST-derived sNF96.2 cell line and found that this induced down-regulation of endogenous *DNMT3A* and *DNMT3B* expression in these cells. These findings are consistent with previous reports on the negative influence of miR-29c on the expression of *DNMT3A* and *DNMT3B* in other malignancies including lung cancer, malignant melanoma, Burkitt lymphoma, breast cancer and gastric cancer (Fabbri et al. 2007; Nguyen et al. 2014; Robaina et al. 2015; Sandhu et al. 2014; Cui et al. 2015; Sandhu et al. 2012).

Although I managed to demonstrate *in vitro* that *DNMT3A* mRNA is downregulated in response to ectopic expression of miR-29c, I found no correlation between miR-29c and *DNMT3A* expression in our tumour samples. However, this doesn't rule out the possibility that *DNMT3A* could still be targeted by miR-29c and play a role in MPNST pathogenesis since DNMTs are known to be regulated by a variety of factors e.g., at the post-transcriptional level by other miRNAs (such as miR-148a, miR-148b, miR-26a, miR-26b, miR-203 and miR-222) (Duursma et al. 2008; Sandhu et al. 2014) or at the level of gene transcription by modification of the primary DNA sequence through gene amplification or activating gene mutations or via the influence of transcription factors (Shen et al. 2002; Singal et al. 2005; Montgomery et al. 2004; Cebrian et al. 2006; Im et al. 2014). Also since

DNMT3B is known to directly associate with DNMT3A (Li et al. 2007), it is possible that that miR-29 could indirectly affect DNMT3A activity via its influence on the expression of DNMT3B.

Carcinogenesis related mutations in the catalytic and non-catalytic domains of DNMT3A and DNMT3B have previously been described in a variety of diseases and cancers including colorectal cancer, MDS, AML, T-cell lymphoma, ICF syndrome (Immunodeficiency, Centromere instability, Facial abnormalities) , breast and lung (Couronné et al. 2012; Ley et al. 2010; Walter et al. 2011; Weemaes et al. 2013; Xu et al. 1999). The possibility that mutations in *DNMT3A* and *DNMT3B* could somehow contribute to MPNST pathogenesis, therefore, cannot be ruled out. However, the mechanism by which *DNMT3B* is over-expressed in cancer is not thought to result from mutation, amplification or increased *trans*-activation but rather through post-transcriptional regulation by microRNAs (Veeck & Esteller 2010; Sandhu et al. 2012).

The results from our microRNA microarray expression data revealed that expression of miR-29a, b, c\* and b-1\* as well as miR-29c, are also significantly downregulated in MPNSTs relative to neurofibromas. The possibility that *DNMT3A* and *DNMT3B* might also be regulated by other miR-29 family members or even other microRNAs in MPNSTs also cannot be ruled out at this stage since.

Although I have not examined the relationship between miR-29c and *DNMT1*, the involvement of this DNMT in MPNST pathogenesis cannot be ruled out since miR-29 family members have been shown to influence the expression of DNA methyltransferases *DNMT1*, *DNMT3A*, and *DNMT3B* at both RNA and protein levels in acute myeloid leukaemia cells (Garzon et al. 2009).

As well as inhibiting DNMTs, miR-29 family members have also been reported to repress the activities of two major factors involved in DNA demethylation, namely thymine DNA glycosylase (TDG) and the ten-eleven translocation protein 1 (TET1). It is therefore conceivable that the methylation status of a cells' genome may be influenced by miR-29s not only through their effects on DNMTs but also via their actions on DNA demethylases (Morita et al. 2013).

Following my *in vitro* demonstration that *DNMT3A* and *DNMT3B* are downregulated by miR-29c, my next goal was to identify any candidate genes that could be targets of DNMTs in MPNSTs. I compared the methylome data of Feber et al (2011) with the gene expression microarray data of Subramanian et al (2010) and searched the literature for reports of any genes proven to be differentially expressed in neurofibromas and MPNSTs. I finally settled on 3 genes for further study, *S100B*, *CDKN2A* and *WT1*, which had previously been verified as differentially methylated (Feber et al. 2011) and differentially expressed between MPNSTs and neurofibromas; (Subramanian et al. 2010; Karamchandani et al. 2012;

Parenti et al. 2014) In addition, these genes had also been shown to play a role in other types of human cancers (Fang et al. 2009; Fraizer et al. 2004; van Dieck et al. 2010).

Pyrosequencing analysis of *CDKN2A*, *WT1*, and *S100B* in 10 MPNSTs and 10 neurofibromas fresh frozen tissue samples revealed hypermethylation of these three genes is more frequent in MPNSTs compared to neurofibromas which suggested these genes were potential targets of gene silencing by methylation during pathogenesis of MPNSTs from neurofibromas.

*CDKN2A* is an important tumour suppressor gene, which is frequently inactivated by mutations, deletions, or methylation in a wide variety of human malignancies. The gene codes for three distinct proteins known which are generated by alternative splicing of an overlapping set of exons in the gene (Quelle et al. 1995). The most well studied of these are the p16 (INK4a) and the p14 (ARF) proteins. These play an important role in regulating the G1 to S phase transition of the cell cycle; p16 functions by inactivating the cyclin-dependent kinases, CDK4 and CDK6, which phosphorylate the retinoblastoma protein and p14 stabilises the p53 tumour suppressor protein by sequestering and inhibiting MDM2 which is responsible for the degradation of p53 (Stott et al. 1998; Stein et al. 1999).

Loss of function of the *CDKN2A* gene has been reported to occur in around half to nearly all cases MPNSTs (Nielsen et al. 1999; Perrone et al. 2003; Endo et al. 2011; Lee et al. 2014; Kourea et al. 1999; Menon et al. 1990) The

majority of these inactivations have been reported to occur as a result of homozygous deletions of the *CDKN2A* gene (Lee et al. 2014; Endo et al. 2011; Carter et al. 2001) Inactivation of the *CDKN2A* gene via gene mutations and epigenetic silencing by methylation of the 5' CpG island of the p16 promoter region are known to occur in variety of human malignancies (Kawaguchi et al. 2003; O'Riain et al. 2009; Merlo et al. 1995; Baur et al. 1999), but they have rarely been described in MPNSTs (Nielsen et al. 1999; Endo et al. 2011). Endo et al. (2011) and Nielsen et al. (1999) examined MPNSTs that were without homozygous deletion of *CDKN2A* but were unable to detect any mutation in the exons of *CDKN2A* gene and no methylation was found in either the *p14<sup>ARF</sup>* or *p16<sup>INK4a</sup>* promoter (Nielsen et al. 1999; Endo et al. 2011). However, Nielsen et al (1999) did not rule out the possibility that methylation outside of the assayed region of the promoter or alterations in noncoding regions of the *CDKN2A* gene could potentially affect protein expression (Nielsen et al. 1999).

I carefully examined the whole methylome data generated from the study by Feber et al. (2011) and also found no evidence of alteration in the methylation status of the *CDKN2A* gene promoter in MPNSTs compared with neurofibromas. However, I did find a differentially methylated region (DMR) of CpGs near the 3' end of *CDKN2A* gene. CpG islands are often located at the 5' region of gene promoters but several CpG islands have been shown to be located at the 3' end of known genes. The latter have received less attention than CpG islands of gene promoters but in recent years they have

been shown to perform important functions and have also been implicated in cancer development (Shiraishi et al. 2002; Medvedeva et al. 2010).

I examined the differentially methylated region (DMR) near the 3' end of *CDKN2A* by pyrosequencing in our cohort of 10 MPNSTs and 10 neurofibromas and found that hypermethylation of this region was more frequent and more extensive in MPNSTs compared to the neurofibromas. One can speculate that if methylation of this region leads to silencing of the *CDKN2A* gene this could offer a possible explanation for the loss of *CDKN2A* expression in MPNSTs that do not harbour homozygous deletions or mutations of the *CDKN2A* gene. I tried to examine the possibility that expression of *CDKN2A* is controlled by methylation in the 5-aza-dC- treated and untreated sNF96.2 cell line but I was unable to amplify the *CDKN2A* gene for pyrosequencing and were also unable to get *CDKN2A* mRNA transcript by RT-PCR. The most likely explanation for this was that the *CDKN2A* gene may be deleted in this cell line. Since I was unable to demonstrate that *CDKN2A* is regulated by methylation, I therefore decided not to pursue this gene for any further in my study.

The *WT1* gene resides on 11p13 and codes for a zinc-finger transcription factor, which plays an important role in cellular growth and development. This gene was originally identified as a tumour suppressor in a paediatric cancer of the kidney known as Wilms tumour (Gessler et al. 1990; Call et al. 1990; Little & Wells 1997). However over-expression of the *WT1* gene has been demonstrated in a variety of solid cancers including those of the brain

(Schittenhelm et al. 2010) lung (Oji et al. 2002), breast (Domfeh et al. 2008), colon (Koesters et al. 2004), pancreas (Oji et al. 2004) and melanoma (Wagner et al. 2008) in addition to haematologic malignancies such as leukaemia (Kerst et al. 2008) which is more compatible with its function as an oncogene rather than a tumour suppressor. Moreover, silencing of the *WT1* using RNAi has been shown to inhibit cell proliferation, induce apoptosis and decrease resistance to chemotherapeutic agents in a variety of malignant cell cultures (X. Wang et al. 2013; Chen 2001; Clark et al. 2010; Zamora-Avila et al. 2007; Zapata-Benavides et al. 2002; Navakanit et al. 2007). The role of the *WT1* gene therefore is very much context driven its dual functionality is thought in part to be due to the existence of at least 36 *WT1* transcript isoforms (Lee & Haber 2001; Ellisen 2002; Hohenstein & Hastie 2006). Both the sense (*WT1*) and antisense transcripts (*WT1-AS*) of *WT* gene have been shown to be transcribed and CpG hypermethylation has been shown to be an important mechanism of *WT1* and *WT-AS* gene inactivation in cancer e.g., decreased methylation in the enhancer region of the *WT1* gene has been described in two-thirds of tumours from *WT1* patients (Mares et al. 2001) and hypermethylation at a CTCF binding site downstream of the *WT1* gene is associated with elevated *WT1* transcriptional activity (Zitzmann et al. 2014). Methylation of CpG islands in the 5' region of *WT1* gene is also significantly increased in NSCLC (Bruno et al. 2012) and hypermethylation of the *WT1* promoter was demonstrated in human breast cancer to be associated with lack of expression of *WT1* (Laux et al. 1999). In ovarian clear cell adenocarcinoma, both the *WT1* and *WT1-*

AS genes have been reported to be inactivated by promoter methylation (Kaneuchi et al. 2005).

The *WT1* gene has been reported to be expressed in neurofibromas and schwannomas but not in normal glial cells (Schittenhelm et al. 2010; Singh et al. 2012). In MPNSTs the *WT1* gene transcript has been demonstrated to be over expressed in MPNSTs (Ueda et al. 2003) which suggests it functions as an oncogene in this type of malignancy. This is supported by a recent study in which silencing of *WT1* by siRNA in MPNST-derived sNF96.2 cells resulted in inhibition of cell proliferation (Parenti et al. 2014). This was shown to be associated with a decrease in the levels of PI3K, pAKT and Cyclin D1 proteins which play an important role in regulating the cell cycle, cell survival and proliferation (Parenti et al. 2014).

I confirmed that expression of the *WT1* gene is influenced by methylation in MPNST-derived cells by showing *WT1* mRNA transcript is elevated in response to treatment of sNF96.2 cells with the demethylating agent 5-aza-dC. In addition, my pyrosequencing data demonstrated not only a significant difference in the level of methylation between neurofibromas and MPNSTs in the DNA region examined but DNA methylation of this region was also found to be higher in high grade MPNST as compared with low-grade tumours. However, I found no correlation between expression of the *WT1* gene and the methylation status of this region. This suggests that expression of the *WT1* gene is not influenced by methylation of this DNA region. Furthermore, I found no significant differences in the level of *WT1* mRNA expression

between our neurofibromas and MPNSTs, which suggests that expression of the *WT1* gene does not play a significant role in the pathogenesis of MPNSTs from neurofibromas. My findings are consistent with those of Inagak et al. (2011) who examined WT1 protein and mRNA transcript in normal nerve root, neurofibromas, schwannomas and MPNST and reported WT1 expression is not higher in peripheral nerve tumours than in normal peripheral nerves (Inagaki et al. 2011). Similarly Schittenhelm et al. (2010) examined WT1 expression by immunohistochemistry in both neurofibromas and MPNSTs and reported the expression of the WT1 protein was independent of tumour malignancy or grade of malignancy (Schittenhelm et al. 2010).

*S100B* expression was found in my study to be influenced by DNA methylation as demonstrated by the increased expression of its mRNA transcript in 5-aza-dC-treated sNF96.2 cells. The increased methylation of the *S100B* DNA region examined in our MPNSTs compared with that in our neurofibromas and the fact that levels of DNA methylation were found to increase with increasing grade of MPNST suggested *S100B* was a strong candidate for epigenetic regulation during development of MPNSTs. My findings with *S100B* are discussed in more detail in the following section.

### **6.3. S100B as a potential tumour regulator in nerve sheath tumours**

S100B belongs to a family of homologous calcium binding proteins known as S100 proteins of which there are twenty-one members known in humans (Zimmer et al. 2013). The genes coding for the majority of *S100* reside in a cluster on human chromosome 1q21. They are normally expressed in cells derived from the neural crest (Schwann cells, and melanocytes), chondrocytes, adipocytes, myoepithelial cells, macrophages, Langerhans cells, dendritic cells, and keratinocytes and some breast epithelial cells (Marenholz et al. 2004; Wilson et al. 1991; Coppola et al. 1998; Heizmann et al. 2002).

Despite the structural similarities (Elder & Zhao 2002; Pedrocchi et al. 1994; Cross et al. 2005; Donato et al. 2013; Heizmann et al. 2002; Marenholz et al. 2004; Roth et al. 2003) proteins are involved in a variety of intracellular and extracellular functions that regulate many processes such as cell growth, differentiation, proliferation, migration, survival, cell cycle regulation and (Donato 2001; Donato 2007; Heizmann et al. 2002; Marenholz et al. 2004; Roth et al. 2003; Leukert et al. 2006) expression of S100 proteins has been found in a variety of human diseases including chronic inflammation, neurodegeneration, cardiomyopathies, atherosclerosis as well as a wide variety of human malignancies (Pietzsch 2010; Salama et al. 2008).

Unlike the majority of *S100* genes, the *S100B* gene is located on chromosomes 21q22.3. *S100B* is normally expressed at high levels in astrocytes, oligodendrocytes and Schwann cells and its expression has been reported to be elevated in anaplastic astrocytomas and glioblastomas (Camby et al. 1999) as well as melanomas (Salama et al. 2008). Because of its high levels of expression in neural tissue, *S100B* is commonly used in pathology as a marker for glial cell and Schwann cell differentiation (Hachem et al. 2005). In MPNSTs *S100B* has been reported to be downregulated by a number of investigators e.g., in a study of 14 neurofibromas and 9 MPNSTs Lévy et al. (2004) demonstrated *S100B* mRNA expression was significantly downregulated in malignant tumours compared to expression in benign tumours (Lévy et al. 2004). Nonaka et al. (2008) examined *S100B* expression in 86 neurofibromas and 77 MPNSTs by immunohistochemistry and demonstrated diffuse staining of *S100B* in all neurofibromas examined but less than one-third of MPNSTs showed focal staining of *S100B* (Nonaka et al. 2008). A similar finding was reported by Karamchandani et al. (2012) whereby *S100B* protein staining was seen in 52 of 55 neurofibroma but only 15 of 78 MPNSTs (Karamchandani et al. 2012). Despite the very striking differences in *S100B* protein and transcript expression between MPNSTs and neurofibromas, I have found no reports investigating *S100B* regulation and function in PNSTs.

In this thesis, I have shown that *S100B* expression in MPNST-derived cells is influenced by DNA methylation as demonstrated by the increased expression

of its mRNA transcript in 5-aza-dC-treated sNF96.2 cells. Furthermore, I have shown that the level of methylation in the *S100B* regulatory region examined (an enhancer area) is higher in MPNSTS than in neurofibromas. In addition, the level of methylation in the *S100B* regulatory region (enhancer) was shown to increase with increasing grade of MPNST. These findings suggest that *S100B* expression is epigenetically regulated by methylation during MPNST pathogenesis. My demonstration of an inverse correlation between methylation of the *S100B* regulatory region and expression of its mRNA transcript and protein adds support to this hypothesis. In addition, epigenetic regulation of *S100B* has previously been demonstrated in animal studies e.g., methylation of the *S100B* promoter was reported to play a role in expression of the *S100B* gene during embryonic development of the mouse brain (Namihira et al. 2004; Shimosaki et al. 2005). In the study by Namihira et al. (2004), the expression of *S100B* was shown to be associated with the demethylation of one of four methylated cytosine residues in the *S100B* promoter. The loss of methylation at this one CpG site was accompanied by a decrease in binding of MECP2 (methyl CpG binding protein 2) to the *S100B* gene promoter which suggested that it was the binding of MeCp2 to the methylated CpG site that inactivated the *S100B* gene (Namihira et al. 2004). Another study by Malup et al. (2007) revealed a tissue specific pattern of *S100B* gene methylation in BALB/cLac mice. Hypomethylation of the *S100B* gene was demonstrated in the brain of these mice in comparison that in tissues from other organs (Malup et al. 2007). These findings are consistent with the known effects of methylation on gene

expression and with the pattern of *S100B* gene expression in different organs. In addition, demethylation of *S100B* has been shown to be influenced by binding of nuclear factor I to the *S100B* gene promoter, which occurs in response to activation of the Notch I signalling pathway. This is thought to bring about activation of *S100B* and other astrocyte specific genes during development of astrocytes from mammalian neural precursors (Namihira et al. 2009).

Epigenetic regulation by methylation has also reported in other S100 family members in connection with various human malignancies e.g., re-expression of *S100A4* was demonstrated in lymphoma cells after treatment with the DNA methyltransferase inhibitor, 5-aza-cytidine (Tulchinsky et al. 1995). Similarly, re-expression of *S100A2* was reported after 5-aza-cytidine treatment of mammary carcinoma epithelial cells (Lee et al. 1992) and *S100A6* was re-expressed following the 5-aza-cytidine treatment of hepatoma cells (Leśniak et al. 2000). Furthermore, *S100A10*, *S100A3*, *S100A11*, and *S100P* were shown to re-expressed in different medulloblastoma cell lines following 5-aza-cytidine treatment (Lindsey et al. 2007). In other studies, expression of *S100P* was found to depend on hypomethylation of the *S100P* gene in prostate carcinoma (Wang et al. 2007), pancreatic cancer (Sato et al. 2004) and cervical carcinoma cells (Jakubícková et al. 2005). *S100A2* is downregulated in many cancers, and its repression has been shown to mediated by site-specific hypermethylation in breast cancer (Wicki et al. 1997). Chen et al. (2009) reported an apparent

association between S100A4 protein expression and integrin signalling in cancer cells. They showed that 5 of 7 CpGs in the intronic area examined were mostly unmethylated in MDA-MB-435 cells that stably expressed integrin (Chen et al. 2009).

Although I have shown a significant association between methylation of the *S100B* regulatory region and expression of this gene in PNSTs, the *S100B* gene promoter was not found to be methylated when I examined the previous methylome data of Feber et al. (2011). The position of the *S100B* regulatory area, as determined by the Ensembl database, suggests that it may function as a gene enhancer. Although DNA methylation of enhancer sites have not been studied as much as those of promoters, the relationship between enhancer methylation and gene expression in cancer has, interestingly, been shown to be significantly greater than the relationship between promoter methylation and changes in gene expression (Aran et al. 2013). Also in a review of genome-wide studies of DNA methylation in hematopoietic cells, it was concluded that enhancers, CGI shores, and canyon edges were the most active sites of *de novo* methylation and demethylation in the genome and were more common than in CGIs with high CpG density (Jeong & Goodell 2014).

In order to determine the role that S100B might play in the pathogenesis of MPNSTs I carried out functional studies using sNF96.2 cells that had been transduced with an S100B expressing lentiviral vector. I found that S100B expression in sNF96.2 cells had an inhibitory effect on cell proliferation and

viability. Although there was no effect on the migratory behaviour of sNF96.2 cells, these findings suggested a tumour suppressor role for the S100B in MPNST cells. This is consistent with my finding that *S100B* is hypermethylated in malignant peripheral nerve sheath tumours compared to neurofibromas as it is well established that most tumour suppressors are hypermethylated in many types of cancer (Luczak & Jagodziński 2006). A tumour suppressor role for S100B has previously been suggested by Van Dieck et al. (2010) who showed that S100B might promote p53 tumour suppressor activities through interacting with MDM2 and MDM4. More support for S100B as a tumour suppressor comes from a study on the PC12 cell line that is derived from a pheochromocytoma of the rat adrenal medulla and has an embryonic origin from the neural crest. Arcuri et al 2005 showed that overexpression of S100B in this cell line increased cell proliferation, reduced apoptosis, enhanced cell survival and decreased responsiveness to the differentiating effect of Nerve growth factor (NGF) (Arcuri et al. 2005). However, other reports suggest S100B functions as an oncogene e.g., S100B has been shown to interact with and inhibit p53 phosphorylation and activity (Baudier et al. 1992; Rustandi et al. 1998; Lin et al. 2001) and in malignant melanoma cells p53 levels were found to be restored after inhibiting S100B expression (Lin et al. 2004). In addition it was demonstrated that when p53 levels increase, this up-regulates the transcription of S100B as part of a negative feedback mechanism that contributes to p53 degradation thus leading to unchecked cell proliferation (Lin et al. 2004). Furthermore S100B protein in serum has been shown to correlate with

clinical stage of malignant melanoma and is an independent prognostic marker in stages II and III (Mårtenson et al. 2001; Andrés et al. 2004; Smit et al.; Tarhini et al. 2009).

The question as to whether S100B works as tumour suppressor or an oncogene is still unresolved (van Dieck et al. 2010; Baudier et al. 1992; Rustandi et al. 1998; Lin et al. 2001) but It's possible that S100B may act as both a tumour suppressor or oncogene depending on the cell context as is found to be the case with the *WT1* gene. This would not be unusual since another S100 protein, S100A7, has been shown to function as both an oncogene and tumour suppressor gene; Deol et al. (2011) demonstrated that S100A7 over-expression acts as a tumour suppressor in estrogen receptor-positive {ER $\alpha$ (+)} breast cancer cells through down-modulation of the  $\beta$ -catenin/TCF4 pathway both *in vitro* and *in vivo*. However expression of S100A7 in ER $\alpha$ (-) cells enhances tumorigenicity and is associated with a worse prognosis in patients. The increased expression of different S100B proteins in a wide variety of human malignancies would suggest that they have an oncogenic role. A number of these proteins, e.g., S100A2, S100A4 and S100A6 have been shown to interact with p53 but in some cases they have a stimulatory effect on p53 whilst in others they have been shown to have an inhibitory effect (Lin et al. 2001; Mueller et al. 2005; Grigorian et al. 2001; Scotto et al. 1999; Fernandez-Fernandez et al. 2008; Fernandez-Fernandez et al. 2005; van Dieck et al. 2009). These studies demonstrate that the function of S100 proteins as tumour suppressors or oncogenes

cannot be directly inferred from their up-regulated or downregulated status in malignancies and, therefore, must be determined empirically for each individual protein.

In my final experiment, I set out to determine whether methylation of the *S100B* gene regulatory region might be influenced by expression of miR-29c in MPNST-derived cells. However, an examination of sNF96.2 cells that had been transfected with miR-29c mimics demonstrated no significant alteration in the methylation status of the *S100B* gene regulatory region. It's highly likely methylation of *S100B* is being maintained by DNMT1 in this line which means any influence miR-29c expression might have on the *de novo* methylators, DNMT3A and DNMT3B, will not affect *S100B* methylation. However, my findings do not rule out the possibility that *S100B* gene methylation could still be influenced by miR-29c during the early stages of MPNST development via its effects on DNMT3A and DNMT3B. Although DNMT1, in addition to DNMT3A and DNMT3B, has previously been reported to be influenced by expression of miR-29 members, (Garzon et al. 2009) my results do not support the idea that DNMT1 is being influenced by miR-29c expression in sNF96.2 cells.

In conclusion, I have demonstrated that miR-29c may play an important role in the progression of nerve sheath tumours by influencing the expression of DNMT3A and DNMT3B. I also suggest a tumour suppressor role for *S100B* in MPNST cells and open the gate for further studies on the mechanism by which *S100B* perform its effect on MPNSTs.

## 7. Future work

The data presented here provides a basis for several new projects. One area that needs more investigation is the relationship between epigenetic and genetic changes. I showed here that *CDKN2A* is hypermethylated in our MPNSTs compared to neurofibromas. It has been reported previously that the tumour suppressor *CDKN2A* shows lower expression in most of MPNST samples compared to neurofibromas but this loss of expression cannot be explained by genetic changes in all the cases (Nielsen et al. 1999; Endo et al. 2011). A study investigating *CDKN2A* genetic modification and DNA methylation can highlight the interplay between genetics and epigenetics in nerve sheath tumours.

Other epigenetic changes like histone modifications might also have a role of progression of neurofibroma to MPNST. Recently a study showed a role of Polycomb repressive complex 2 (PRC2) components (EED or SUZ12) in progression of neurofibroma to MPNST through loss of trimethylation at lysine 27 of histone 3 (H3K27me3) (Lee et al. 2014). This raises the interest to study further the role of PRC2 and histone methylation in the context of the methylome and pyrosequencing data that I highlighted in this study. We started in our lab to test EED and SUZ12 expression in neurofibromas and MPNSTs and compare its expression with the differentially methylated genes.

Another appealing research worth pursuing is to investigate the link between S100B and p53. My findings suggest a tumour suppressor role for S100B in MPNST cells and open the gate for further studies on the mechanism by which S100B performs its' effect in MPNSTs. A possible mechanism for S100B function has been suggested by Van Dieck et al (2010) who proved experimentally that S100B may promote p53 tumour suppressor activity through interacting with MDM2 and MDM4 (van Dieck et al. 2010). It is worth testing the link between S100B and p53 in nerve sheath tumours.

## 8. Reference list

- Abramowicz, A. & Gos, M., 2014. Neurofibromin in neurofibromatosis type 1 - mutations in NF1 gene as a cause of disease. *Developmental period medicine*, 18(3), pp.297–306.
- Adams, E.G. et al., 2011. Multiple, unilateral lisch nodules in the absence of other manifestations of neurofibromatosis type 1. *Case reports in ophthalmological medicine*, 2011, p.854784.
- Akbarnia, B.A. et al., 1992. Prevalence of scoliosis in neurofibromatosis. *Spine*, 17(8 Suppl), pp.S244–8.
- Alajez, N.M. et al., 2011. MiR-218 suppresses nasopharyngeal cancer progression through downregulation of survivin and the SLIT2-ROBO1 pathway. *Cancer research*, 71(6), pp.2381–91.
- Alizadeh, S. et al., 2014. Mir-55 inhibition can reduce cell proliferation and induce apoptosis in Jurkat (Acute T cell Leukemia) cell line. *Iranian journal of pediatric hematology and oncology*, 4(4), pp.141–50.
- Allison, K.H. et al., 2005. Superficial malignant peripheral nerve sheath tumor: a rare and challenging diagnosis. *American journal of clinical pathology*, 124(5), pp.685–92.
- Alwan, S. et al., 2007. Associations of osseous abnormalities in Neurofibromatosis 1. *American journal of medical genetics. Part A*, 143A(12), pp.1326–33.
- Ambros, V., 2001. microRNAs: tiny regulators with great potential. *Cell*, 107(7), pp.823–6.

- Andrés, R. et al., 2004. Prognostic value of serum S-100B in malignant melanoma. *Tumori*, 90(6), pp.607–10.
- Angelov, L. et al., 1998. Neurogenic sarcoma: experience at the University of Toronto. *Neurosurgery*, 43(1), pp.56–64.
- Aoki, Y. et al., 2005. Germline mutations in HRAS proto-oncogene cause Costello syndrome. *Nature genetics*, 37(10), pp.1038–40.
- Arai, E. et al., 2006. Regional DNA hypermethylation and DNA methyltransferase (DNMT) 1 protein overexpression in both renal tumors and corresponding nontumorous renal tissues. *International journal of cancer. Journal international du cancer*, 119(2), pp.288–96.
- Aran, D., Sabato, S. & Hellman, A., 2013. DNA methylation of distal regulatory sites characterizes dysregulation of cancer genes. *Genome biology*, 14(3), p.R21.
- Arcuri, C. et al., 2005. S100B increases proliferation in PC12 neuronal cells and reduces their responsiveness to nerve growth factor via Akt activation. *Journal of Biological Chemistry*, 280(6), pp.4402–14.
- Ars, E. et al., 2000. Mutations affecting mRNA splicing are the most common molecular defects in patients with neurofibromatosis type 1. *Human molecular genetics*, 9(2), pp.237–47.
- Astrand, R., Undén, J. & Romner, B., 2013. Clinical use of the calcium-binding S100B protein. *Methods in molecular biology (Clifton, N.J.)*, 963, pp.373–84.
- Babovic-Vuksanovic, D. et al., 2012. Multiple orbital neurofibromas, painful peripheral nerve tumors, distinctive face and marfanoid habitus: a new syndrome. *European journal of human genetics : EJHG*, 20(6), pp.618–25.

- 
- Ball, M.P. et al., 2009. Targeted and genome-scale strategies reveal gene-body methylation signatures in human cells. *Nature biotechnology*, 27(4), pp.361–368.
- Ballard, M.S. & Hinck, L., 2012. A roundabout way to cancer. *Advances in cancer research*, 114, pp.187–235.
- Barault, L. et al., 2008. Hypermethylator phenotype in sporadic colon cancer: study on a population-based series of 582 cases. *Cancer research*, 68(20), pp.8541–6.
- Barragán, E. et al., 2004. Prognostic implications of Wilms' tumor gene (WT1) expression in patients with de novo acute myeloid leukemia. *Haematologica*, 89(8), pp.926–33.
- Bartel, D.P., 2009. MicroRNAs: target recognition and regulatory functions. *Cell*, 136(2), pp.215–233.
- Bartel, D.P.D.P., 2004. MicroRNAs: Genomics, Biogenesis, Mechanism, and Function. *Cell*, 116(2), pp.281–297.
- Baudier, J. et al., 1992. Characterization of the tumor suppressor protein p53 as a protein kinase C substrate and a S100b-binding protein. *Proceedings of the National Academy of Sciences of the United States of America*, 89(23), pp.11627–31.
- Baur, B.A.S. et al., 1999. Frequent Methylation Silencing of p15.
- Baylin, S.B., 2005. DNA methylation and gene silencing in cancer. *Nature clinical practice. Oncology*, 2 Suppl 1(December), pp.S4–11.
- Baylin, S.B. & Ohm, J.E., 2006. Epigenetic gene silencing in cancer - a mechanism for early oncogenic pathway addiction? *Nature reviews. Cancer*, 6(2), pp.107–16.

- Berdasco, M. & Esteller, M., 2010. Aberrant epigenetic landscape in cancer: how cellular identity goes awry. *Developmental cell*, 19(5), pp.698–711.
- Berger, A.H., Knudson, A.G. & Pandolfi, P.P., 2011. A continuum model for tumour suppression. *Nature*, 476(7359), pp.163–169.
- Bird, A., 2007. Perceptions of epigenetics. *Nature*, 447(7143), pp.396–8.
- Birindelli, S. et al., 2001. Rb and TP53 pathway alterations in sporadic and NF1-related malignant peripheral nerve sheath tumors. *Laboratory investigation; a journal of technical methods and pathology*, 81(6), pp.833–44.
- Böni, R. et al., 1997. Ca(2+)-binding proteins S100A6 and S100B in primary cutaneous melanoma. *Journal of cutaneous pathology*, 24(2), pp.76–80.
- Bottillo, I. et al., 2010. Germline mosaicism in neurofibromatosis type 1 due to a paternally derived multi-exon deletion. *American journal of medical genetics. Part A*, 152A(6), pp.1467–73.
- Bradtmöller, M. et al., 2012. Impaired Pten expression in human malignant peripheral nerve sheath tumours. *PloS one*, 7(11), p.e47595.
- Brems, H. et al., 2007. Germline loss-of-function mutations in SPRED1 cause a neurofibromatosis 1-like phenotype. *Nature genetics*, 39(9), pp.1120–6.
- Brems, H. et al., 2009. Glomus tumors in neurofibromatosis type 1: genetic, functional, and clinical evidence of a novel association. *Cancer research*, 69(18), pp.7393–7401.
- Brooks, J., 1999. Disorders of soft tissue. In S. Sternberg, ed. *Diagnostic Surgical Pathology*. Philadelphia: Lipincott Williams and Wilkins, pp. 131–221.
- Brosius, S., 2010. A history of von Recklinghausen's NF1. *Journal of the history of the neurosciences*, 19(4), pp.333–48.

- Brown, R.W., Tornos, C. & Evans, H.L., 1992. Angiosarcoma arising from malignant schwannoma in a patient with neurofibromatosis. *Cancer*, 70(5), pp.1141–4.
- Brueckner, B. et al., 2005. Epigenetic reactivation of tumor suppressor genes by a novel small-molecule inhibitor of human DNA methyltransferases. *Cancer research*, 65(14), pp.6305–11.
- Bruno, P. et al., 2012. WT1 CpG islands methylation in human lung cancer: a pilot study. *Biochemical and biophysical research communications*, 426(3), pp.306–9.
- Calin, G.A. et al., 2005. A MicroRNA Signature Associated with Prognosis and Progression in Chronic Lymphocytic Leukemia — NEJM. *The New England journal of medicine*, 353(17), pp.1793–801.
- Calin, G.A. et al., 2002. Frequent deletions and down-regulation of micro- RNA genes miR15 and miR16 at 13q14 in chronic lymphocytic leukemia. *Proceedings of the National Academy of Sciences of the United States of America*, 99(24), pp.15524–9.
- Calin, G.A. & Croce, C.M., 2006. MicroRNA signatures in human cancers. *Nature reviews. Cancer*, 6(11), pp.857–66.
- Call, K.M. et al., 1990. Isolation and characterization of a zinc finger polypeptide gene at the human chromosome 11 Wilms' tumor locus. *Cell*, 60(3), pp.509–20.
- Camby, I. et al., 1999. Supratentorial pilocytic astrocytomas, astrocytomas, anaplastic astrocytomas and glioblastomas are characterized by a differential expression of S100 proteins. *Brain pathology (Zurich, Switzerland)*, 9(1), pp.1–19.
- Carroll, S.L., 2012. Molecular mechanisms promoting the pathogenesis of Schwann cell neoplasms. *Acta neuropathologica*, 123(3), pp.321–48.

- 
- Carter, J.M. et al., 2012. Epithelioid malignant peripheral nerve sheath tumor arising in a schwannoma, in a patient with “neuroblastoma-like” schwannomatosis and a novel germline SMARCB1 mutation. *The American journal of surgical pathology*, 36(1), pp.154–60.
- Carter, T.L., Reaman, G.H. & Kees, U.R., 2001. INK4A/ARF deletions are acquired at relapse in childhood acute lymphoblastic leukaemia: a paired study on 25 patients using real-time polymerase chain reaction. *British journal of haematology*, 113(2), pp.323–8.
- Castilla, M.Á. et al., 2011. Micro-RNA signature of the epithelial-mesenchymal transition in endometrial carcinosarcoma. *The Journal of pathology*, 223(1), pp.72–80.
- Cawthon, R.M. et al., 1990. A major segment of the neurofibromatosis type 1 gene: cDNA sequence, genomic structure, and point mutations. *Cell*, 62(1), pp.193–201.
- Cebrian, A. et al., 2006. Genetic variants in epigenetic genes and breast cancer risk. *Carcinogenesis*, 27(8), pp.1661–9.
- Chai, G. et al., 2010. MicroRNA-10b regulates tumorigenesis in neurofibromatosis type 1. *Cancer Science*, 101(9), pp.1997–2004.
- Chan, J.A., Krichevsky, A.M. & Kosik, K.S., 2005. MicroRNA-21 Is an Antiapoptotic Factor in Human Glioblastoma Cells. *Cancer research*, 65(14), pp.6029–6033.
- Chang, T.-C. et al., 2007. Transactivation of miR-34a by p53 broadly influences gene expression and promotes apoptosis. *Molecular cell*, 26(5), pp.745–52.
- Chaubal, A. et al., 1994. CD34 immunoreactivity in nervous system tumors. *Acta neuropathologica*, 88(5), pp.454–8.

- Chen, H. et al., 2010. Slit-Robo signaling in ocular angiogenesis. *Advances in experimental medicine and biology*, 664, pp.457–63.
- Chen, M. et al., 2009. Integrin alpha6beta4 controls the expression of genes associated with cell motility, invasion, and metastasis, including S100A4/metastasin. *The Journal of biological chemistry*, 284(3), pp.1484–94.
- Chen, Z., 2001. The possible role and application of WT1 in human leukemia. *International journal of hematology*, 73(1), pp.39–46.
- Chintala, S.K. et al., 1996. Role of extracellular matrix proteins in regulation of human glioma cell invasion in vitro. *Clinical & experimental metastasis*, 14(4), pp.358–66.
- Chou, J. et al., 2013. GATA3 suppresses metastasis and modulates the tumour microenvironment by regulating microRNA-29b expression. *Nature cell biology*, 15(2), pp.201–13.
- Cichowski, K. et al., 1999. Mouse models of tumor development in neurofibromatosis type 1. *Science (New York, N.Y.)*, 286(5447), pp.2172–6.
- Cichowski, K. & Jacks, T., 2001. NF1 tumor suppressor gene function: narrowing the GAP. *Cell*, 104(4), pp.593–604.
- Cimmino, A. et al., 2005. miR-15 and miR-16 induce apoptosis by targeting BCL2. *Proceedings of the National Academy of Sciences of the United States of America*, 102(39), pp.13944–13949.
- Cirstea, I.C. et al., 2010. A restricted spectrum of NRAS mutations causes Noonan syndrome. *Nature genetics*, 42(1), pp.27–9.
- Clark, A.J. et al., 2010. Effect of WT1 gene silencing on the tumorigenicity of human glioblastoma multiforme cells. *Journal of neurosurgery*, 112(1), pp.18–25.

- 
- Clark, S.J. et al., 2006. DNA methylation: bisulphite modification and analysis. *Nature protocols*, 1(5), pp.2353–64.
- Clark, S.J. et al., 1994. High sensitivity mapping of methylated cytosines. *Nucleic acids research*, 22(15), pp.2990–7.
- Claus, R., Almstedt, M. & Lübbert, M., 2005. Epigenetic treatment of hematopoietic malignancies: in vivo targets of demethylating agents. *Seminars in oncology*, 32(5), pp.511–520.
- Coindre, J.M. et al., 1988. Immunohistochemical study of rhabdomyosarcoma. Unexpected staining with S100 protein and cytokeratin. *The Journal of pathology*, 155(2), pp.127–32.
- Coindre, J.-M., 2006. Grading of soft tissue sarcomas: review and update. *Archives of pathology & laboratory medicine*, 130(10), pp.1448–53.
- Colman, S.D., Williams, C.A. & Wallace, M.R., 1995. Benign neurofibromas in type 1 neurofibromatosis (NF1) show somatic deletions of the NF1 gene. *Nature Genetics*, 11(1), pp.90–92.
- Coppola, D. et al., 1998. Prognostic significance of p53, bcl-2, vimentin, and S100 protein-positive Langerhans cells in endometrial carcinoma. *Human pathology*, 29(5), pp.455–62.
- Couronné, L., Bastard, C. & Bernard, O.A., 2012. TET2 and DNMT3A Mutations in Human T-Cell Lymphoma. *The New England journal of medicine*, 366(1), pp.95–6.
- Cox, A.D., 2001. Farnesyltransferase inhibitors: potential role in the treatment of cancer. *Drugs*, 61(6), pp.723–32.
- Créange, A. et al., 1999. *Neurological complications of neurofibromatosis type 1 in adulthood.*

- Cross, S.S. et al., 2005. Expression of S100 proteins in normal human tissues and common cancers using tissue microarrays: S100A6, S100A8, S100A9 and S100A11 are all overexpressed in common cancers. *Histopathology*, 46(3), pp.256–69.
- Crowe FW, Schull WJ, N.J., 1956. *A Clinical, Pathological and Genetic Study of Multiple Neurofibromatosis* I. C. C. T. Springfield, ed.,
- Cui, H. et al., 2015. Deregulation between miR-29b/c and DNMT3A Is Associated with Epigenetic Silencing of the CDH1 Gene, Affecting Cell Migration and Invasion in Gastric Cancer R. Samant, ed. *PLOS ONE*, 10(4), p.e0123926.
- Daley, W.P., Peters, S.B. & Larsen, M., 2008. Extracellular matrix dynamics in development and regenerative medicine. *Journal of cell science*, 121(Pt 3), pp.255–64.
- Danielsen, S.A. et al., 2015. Methylated RASSF1A in malignant peripheral nerve sheath tumors identifies neurofibromatosis type 1 patients with inferior prognosis. *Neuro-oncology*, 17(1), pp.63–9.
- Dasgupta, B., 2003. Neurofibromatosis 1: closing the GAP between mice and men. *Current Opinion in Genetics & Development*, 13(1), pp.20–27.
- DeBella, K., Szudek, J. & Friedman, J.M., 2000. Use of the national institutes of health criteria for diagnosis of neurofibromatosis 1 in children. *Pediatrics*, 105(3 Pt 1), pp.608–14.
- DeClue, J.E. et al., 1992. Abnormal regulation of mammalian p21ras contributes to malignant tumor growth in von Recklinghausen (type 1) neurofibromatosis. *Cell*, 69(2), pp.265–73.
- DiCarlo, E.F. et al., 1986. The purely epithelioid malignant peripheral nerve sheath tumor. *The American journal of surgical pathology*, 10(7), pp.478–90.

- 
- Van Dieck, J. et al., 2009. Modulation of the oligomerization state of p53 by differential binding of proteins of the S100 family to p53 monomers and tetramers. *The Journal of biological chemistry*, 284(20), pp.13804–11.
- Van Dieck, J. et al., 2010. S100 proteins interact with the N-terminal domain of MDM2. *FEBS letters*, 584(15), pp.3269–74.
- Digilio, M.C. et al., 2002. Grouping of multiple-lentiginos/LEOPARD and Noonan syndromes on the PTPN11 gene. *American journal of human genetics*, 71(2), pp.389–94.
- Ding, D.-P. et al., 2011. miR-29c induces cell cycle arrest in esophageal squamous cell carcinoma by modulating cyclin E expression. *Carcinogenesis*, 32(7), pp.1025–32.
- Doench, J.G. & Sharp, P.A., 2004. Specificity of microRNA target selection in translational repression. *Genes & development*, 18(5), pp.504–11.
- Domfeh, A.B. et al., 2008. WT1 immunoreactivity in breast carcinoma: selective expression in pure and mixed mucinous subtypes. *Modern pathology: an official journal of the United States and Canadian Academy of Pathology, Inc*, 21(10), pp.1217–23.
- Donato, R. et al., 2013. Functions of S100 proteins. *Current molecular medicine*, 13(1), pp.24–57.
- Donato, R., 2003. Intracellular and extracellular roles of S100 proteins. *Microscopy research and technique*, 60(6), pp.540–51.
- Donato, R., 2007. RAGE: a single receptor for several ligands and different cellular responses: the case of certain S100 proteins. *Current molecular medicine*, 7(8), pp.711–24.

- Donato, R., 2001. S100: a multigenic family of calcium-modulated proteins of the EF-hand type with intracellular and extracellular functional roles. *The international journal of biochemistry & cell biology*, 33(7), pp.637–68.
- Ducatman, B.S. & Scheithauer, B.W., 1984. Malignant peripheral nerve sheath tumors with divergent differentiation. *Cancer*, 54(6), pp.1049–57.
- Dulai, S. et al., 2007. Decreased bone mineral density in neurofibromatosis type 1: results from a pediatric cohort. *Journal of pediatric orthopedics*, 27(4), pp.472–5.
- Duursma, A.M. et al., 2008. miR-148 targets human DNMT3b protein coding region. *RNA*, 14(5), pp.872–877.
- Ehrlich, M., 2002. DNA methylation in cancer: too much, but also too little. *Oncogene*, 21(35), pp.5400–13.
- Elder, J.T. & Zhao, X., 2002. Evidence for local control of gene expression in the epidermal differentiation complex. *Experimental dermatology*, 11(5), pp.406–12.
- Ellisen, L.W., 2002. Regulation of gene expression by WT1 in development and tumorigenesis. *International journal of hematology*, 76(2), pp.110–6.
- Van Emburgh, B.O. & Robertson, K.D., 2011. Modulation of Dnmt3b function in vitro by interactions with Dnmt3L, Dnmt3a and Dnmt3b splice variants. *Nucleic acids research*, 39(12), pp.4984–5002.
- Endo, M. et al., 2011. Prognostic significance of p14ARF, p15INK4b, and p16INK4a inactivation in malignant peripheral nerve sheath tumors. *Clinical cancer research : an official journal of the American Association for Cancer Research*, 17(11), pp.3771–82.

- 
- Esquela-Kerscher, A. & Slack, F.J., 2006. Oncomirs - microRNAs with a role in cancer. *Nature reviews. Cancer*, 6(4), pp.259–69.
- Evans, D.G. et al., 2010. Birth incidence and prevalence of tumor-prone syndromes: estimates from a UK family genetic register service. *American journal of medical genetics. Part A*, 152A(2), pp.327–32.
- Evans, D.G.R. et al., 2002. Malignant peripheral nerve sheath tumours in neurofibromatosis 1. *Journal of Medical Genetics*, 39(5), pp.311–314.
- Fabbri, M. et al., 2007. MicroRNA-29 family reverts aberrant methylation in lung cancer by targeting DNA methyltransferases 3A and 3B. *Proceedings of the National Academy of Sciences of the United States of America*, 104(40), pp.15805–10.
- Fan, Y. et al., 2014. Down-regulation of miR-29c in human bladder cancer and the inhibition of proliferation in T24 cell via PI3K-AKT pathway. *Medical oncology (Northwood, London, England)*, 31(7), p.65.
- Fan, Y. et al., 2013. MiR-29c inhibits glioma cell proliferation, migration, invasion and angiogenesis. *Journal of neuro-oncology*, 115(2), pp.179–88.
- Fang, J.-H. et al., 2011. MicroRNA-29b suppresses tumor angiogenesis, invasion, and metastasis by regulating matrix metalloproteinase 2 expression. *Hepatology (Baltimore, Md.)*, 54(5), pp.1729–40.
- Fang, Y. et al., 2012. MicroRNA-7 inhibits tumor growth and metastasis by targeting the phosphoinositide 3-kinase/Akt pathway in hepatocellular carcinoma. *Hepatology (Baltimore, Md.)*, 55(6), pp.1852–62.
- Fang, Y. et al., 2015. MiR-301a Promotes Colorectal Cancer Cell Growth and Invasion by Directly Targeting SOCS6. *Cellular physiology and biochemistry : international journal of experimental cellular physiology, biochemistry, and pharmacology*, 35(1), pp.227–36.

- Fang, Y. et al., 2009. Molecular characterization of permanent cell lines from primary, metastatic and recurrent malignant peripheral nerve sheath tumors (MPNST) with underlying neurofibromatosis-1. *Anticancer Research*, 29(4), pp.1255–1262.
- Feber, A. et al., 2011. Comparative methylome analysis of benign and malignant peripheral nerve sheath tumours. *Genome Research*, 21(4), pp.515–24.
- Fernandez-Fernandez, M.R., Rutherford, T.J. & Fersht, A.R., 2008. Members of the S100 family bind p53 in two distinct ways. *Protein science: a publication of the Protein Society*, 17(10), pp.1663–70.
- Fernandez-Fernandez, M.R., Veprintsev, D.B. & Fersht, A.R., 2005. Proteins of the S100 family regulate the oligomerization of p53 tumor suppressor. *Proceedings of the National Academy of Sciences*, 102(13), pp.4735–4740.
- Ferner, R.E. et al., 2000. Evaluation of (18)fluorodeoxyglucose positron emission tomography ((18)FDG PET) in the detection of malignant peripheral nerve sheath tumours arising from within plexiform neurofibromas in neurofibromatosis 1. *Journal of neurology, neurosurgery, and psychiatry*, 68(3), pp.353–357.
- Ferner, R.E. & Gutmann, D.H., 2002. International consensus statement on malignant peripheral nerve sheath tumors in neurofibromatosis. *Cancer research*, 62(5), pp.1573–7.
- Ferner, R.E., Hughes, R.A. & Weinman, J., 1996. Intellectual impairment in neurofibromatosis 1. *Journal of the neurological sciences*, 138(1-2), pp.125–33.
- Ferner, R.E.H., 2007. Guidelines for the diagnosis and management of individuals with neurofibromatosis. *Journal of Medical Genetics*, 44(2), pp.81–88.

- Fine, S.W., McClain, S.A. & Li, M., 2004. Immunohistochemical staining for calretinin is useful for differentiating schwannomas from neurofibromas. *American journal of clinical pathology*, 122(4), pp.552–9.
- Fisher, C. & Schofield, J.B., 1991. S-100 protein positive synovial sarcoma. *Histopathology*, 19(4), pp.375–7.
- Fletcher, C.D.M. & Unni, K.K., 2002. World Health Organization Classification of Tumours Pathology and Genetics of Tumours of Soft Tissue and Bone. C. D. M. Fletcher, K. K. Unni, & F. Mertens, eds. *Cancer*, 177(3), pp.1365–76.
- Fraizer, G. et al., 2004. Suppression of prostate tumor cell growth in vivo by WT1, the Wilms' tumor suppressor gene. *International journal of oncology*, 24(3), pp.461–71.
- Friedman, J.M. et al., 2002. Cardiovascular disease in neurofibromatosis 1: report of the NF1 Cardiovascular Task Force. *Genetics in medicine : official journal of the American College of Medical Genetics*, 4(3), pp.105–11.
- Friedman, J.M., 1999. Epidemiology of neurofibromatosis type 1. *American Journal of Medical Genetics*, 89(1), pp.1–6.
- Friedman, J.M., 2002. Neurofibromatosis 1: clinical manifestations and diagnostic criteria. *Journal of child neurology*, 17(8), pp.548–54; discussion 571–2, 646–51.
- Frommer, M. et al., 1992. A genomic sequencing protocol that yields a positive display of 5-methylcytosine residues in individual DNA strands. *Proceedings of the National Academy of Sciences of the United States of America*, 89(5), pp.1827–31.
- Gao, P. et al., 2013. The molecular mechanism of microRNA-145 to suppress invasion-metastasis cascade in gastric cancer. *Oncogene*, 32(4), pp.491–501.

- 
- Garzon, R. et al., 2006. MicroRNA expression and function in cancer. *Trends in molecular medicine*, 12(12), pp.580–7.
- Garzon, R. et al., 2009. MicroRNA-29b induces global DNA hypomethylation and tumor suppressor gene reexpression in acute myeloid leukemia by targeting directly DNMT3A and 3B and indirectly DNMT1. *Blood*, 113(25), pp.6411–8.
- Gessler, M. et al., 1990. Homozygous deletion in Wilms tumours of a zinc-finger gene identified by chromosome jumping. *Nature*, 343(6260), pp.774–8.
- Glass, J.L. et al., 2007. CG dinucleotide clustering is a species-specific property of the genome. *Nucleic acids research*, 35(20), pp.6798–807.
- Gong, M. et al., 2012. MicroRNA-204 critically regulates carcinogenesis in malignant peripheral nerve sheath tumors. *Neuro-oncology*, 14(8), pp.1007–17.
- Gray, M.H. et al., 1990. Immunohistochemical demonstration of factor XIIIa expression in neurofibromas. A practical means of differentiating these tumors from neurotized melanocytic nevi and schwannomas. *Archives of dermatology*, 126(4), pp.472–6.
- Gregorian, C. et al., 2009. PTEN dosage is essential for neurofibroma development and malignant transformation. *Proceedings of the National Academy of Sciences of the United States of America*, 106(46), pp.19479–84.
- Griffiths, S. et al., 2007. Molecular diagnosis of neurofibromatosis type 1: 2 years experience. *Familial cancer*, 6(1), pp.21–34.
- Grigorian, M. et al., 2001. Tumor suppressor p53 protein is a new target for the metastasis-associated Mts1/S100A4 protein: functional consequences of their interaction. *The Journal of biological chemistry*, 276(25), pp.22699–708.

- Grosshans, H. et al., 2005. The temporal patterning microRNA let-7 regulates several transcription factors at the larval to adult transition in *C. elegans*. *Developmental cell*, 8(3), pp.321–30.
- Gu, J.-J., Gao, G.-Z. & Zhang, S.-M., 2015. miR-218 inhibits the migration and invasion of glioma U87 cells through the Slit2-Robo1 pathway. *Oncology letters*, 9(4), pp.1561–1566.
- Guillou, L. et al., 1997. Comparative study of the National Cancer Institute and French Federation of Cancer Centers Sarcoma Group grading systems in a population of 410 adult patients with soft tissue sarcoma. *Journal of clinical oncology : official journal of the American Society of Clinical Oncology*, 15(1), pp.350–62.
- Guo, H. et al., 2010. Mammalian microRNAs predominantly act to decrease target mRNA levels. *Nature*, 466(7308), pp.835–40.
- Hachem, S. et al., 2005. Spatial and temporal expression of S100B in cells of oligodendrocyte lineage. *Glia*, 51(2), pp.81–97.
- Hackanson, B. & Daskalakis, M., 2014. Decitabine. *Recent results in cancer research. Fortschritte der Krebsforschung. Progrès dans les recherches sur le cancer*, 201, pp.269–97.
- Han, T.-S. et al., 2015. MicroRNA-29c mediates initiation of gastric carcinogenesis by directly targeting ITGB1. *Gut*, 64(2), pp.203–14.
- He, L. et al., 2007. A microRNA component of the p53 tumour suppressor network. *Nature*, 447(7148), pp.1130–4.
- Heizmann, C.W., Fritz, G. & Schäfer, B.W., 2002. S100 proteins: structure, functions and pathology. *Frontiers in bioscience : a journal and virtual library*, 7, pp.d1356–68.

- 
- Henderson, S.R. et al., 2005. A molecular map of mesenchymal tumors. *Genome biology*, 6(9), p.R76.
- Herman, J.G. et al., 1996. Methylation-specific PCR: a novel PCR assay for methylation status of CpG islands. *Proceedings of the National Academy of Sciences of the United States of America*, 93(18), pp.9821–6.
- Hirbe, A.C. & Gutmann, D.H., 2014. Neurofibromatosis type 1: a multidisciplinary approach to care. *The Lancet. Neurology*, 13(8), pp.834–43.
- Hirose, T. et al., 2003. Immunohistochemical demonstration of EMA/Glut1-positive perineurial cells and CD34-positive fibroblastic cells in peripheral nerve sheath tumors. *Modern pathology: an official journal of the United States and Canadian Academy of Pathology, Inc*, 16(4), pp.293–8.
- Hochberg, F.H. et al., 1974. Gastrointestinal involvement in von Recklinghausen's neurofibromatosis. *Neurology*, 24(12), pp.1144–51.
- Hohenstein, P. & Hastie, N.D., 2006. The many facets of the Wilms' tumour gene, WT1. *Human molecular genetics*, 15 Spec No, pp.R196–201.
- Hollmann, T.J. & Hornick, J.L., 2011. INI1-deficient tumors: diagnostic features and molecular genetics. *The American journal of surgical pathology*, 35(10), pp.e47–63.
- Holtkamp, N. et al., 2007. MMP-13 and p53 in the progression of malignant peripheral nerve sheath tumors. *Neoplasia (New York, N.Y.)*, 9(8), pp.671–7.
- Huang, S.S. & Huang, J.S., 2005. TGF-beta control of cell proliferation. *Journal of cellular biochemistry*, 96(3), pp.447–62.
- Huang, Z. et al., 2015. USP33 mediates Slit-Robo signaling in inhibiting colorectal cancer cell migration. *International journal of cancer. Journal international du cancer*, 136(8), pp.1792–802.

- 
- Huson, S.M., Harper, P.S. & Compston, D. a, 1988. Von Recklinghausen neurofibromatosis. A clinical and population study in south-east Wales. *Brain : a journal of neurology*, 111 ( Pt 6, pp.1355–81.
- Illingworth, R.S. & Bird, A.P., 2009. CpG islands--'a rough guide'. *FEBS letters*, 583(11), pp.1713–20.
- Im, A.P. et al., 2014. DNMT3A and IDH mutations in acute myeloid leukemia and other myeloid malignancies: associations with prognosis and potential treatment strategies. *Leukemia*, 28(9), pp.1774–1783.
- Inagaki, T. et al., 2011. No Oncogenic Role for WT1 in Peripheral Nerve Sheath Tumors. , pp.95–102.
- Iorio, M. V et al., 2005. MicroRNA gene expression deregulation in human breast cancer. *Cancer research*, 65(16), pp.7065–70.
- Issa, J., 2004. CpG island methylator phenotype in cancer. *Nature reviews. Cancer*, 4(December), pp.988–993.
- Itani, S. et al., 2012. MicroRNA-21 correlates with tumorigenesis in malignant peripheral nerve sheath tumor (MPNST) via programmed cell death protein 4 (PDCD4). *Journal of cancer research and clinical oncology*, 138(9), pp.1501–9.
- Jakubícková, L. et al., 2005. Expression of S100P gene in cervical carcinoma cells is independent of E7 human papillomavirus oncogene. *Acta virologica*, 49(2), pp.133–7.
- Jeong, M. & Goodell, M.A., 2014. New answers to old questions from genome-wide maps of DNA methylation in hematopoietic cells. *Experimental hematology*, 42(8), pp.609–17.

- 
- Jett, K. & Friedman, J.M., 2010. Clinical and genetic aspects of neurofibromatosis 1. *Medicine*, 12(1), pp.1–11.
- Jiang, J. et al., 2014. Reduction of miR-29c enhances pancreatic cancer cell migration and stem cell – like phenotype. , 6(5).
- Jiang, J. et al., 2015. Reduction of miR-29c enhances pancreatic cancer cell migration and stem cell-like phenotype. *Oncotarget*, 6(5), pp.2767–78.
- Jin, B., Li, Y. & Robertson, K.D., 2011. DNA methylation: superior or subordinate in the epigenetic hierarchy? *Genes & cancer*, 2(6), pp.607–17.
- Johnson, H. et al., 2005. Psychological disturbance and sleep disorders in children with neurofibromatosis type 1. *Developmental medicine and child neurology*, 47(4), pp.237–42.
- Johnson, S.M. et al., 2005. RAS is regulated by the let-7 microRNA family. *Cell*, 120(5), pp.635–647.
- Jones, P.A., 2012. Functions of DNA methylation: islands, start sites, gene bodies and beyond. *Nature reviews. Genetics*, 13(7), pp.484–92.
- Jones, P.A. & Baylin, S.B., 2007. The epigenomics of cancer. *Cell*, 128(4), pp.683–92.
- Jones, P.A. & Liang, G., 2009. Rethinking how DNA methylation patterns are maintained. *Nature reviews. Genetics*, 10(11), pp.805–11.
- Jouhilahti, E.-M. et al., 2011. The pathoetiology of neurofibromatosis 1. *The American journal of pathology*, 178(5), pp.1932–9.
- Jurkowska, R.Z., Jurkowski, T.P. & Jeltsch, A., 2011. Structure and function of mammalian DNA methyltransferases. *Chembiochem : a European journal of chemical biology*, 12(2), pp.206–22.

- Kanai, Y. & Hirohashi, S., 2007. Alterations of DNA methylation associated with abnormalities of DNA methyltransferases in human cancers during transition from a precancerous to a malignant state. *Carcinogenesis*, 28(12), pp.2434–2442.
- Kaneuchi, M. et al., 2005. WT1 and WT1-AS genes are inactivated by promoter methylation in ovarian clear cell adenocarcinoma. *Cancer*, 104(9), pp.1924–30.
- Karakas, T. et al., 2002. The coexpression of the apoptosis-related genes bcl-2 and wt1 in predicting survival in adult acute myeloid leukemia. *Leukemia*, 16(5), pp.846–54.
- Karamchandani, J.R. et al., 2012. Sox10 and S100 in the diagnosis of soft-tissue neoplasms. *Applied immunohistochemistry & molecular morphology: AIMM / official publication of the Society for Applied Immunohistochemistry*, 20(5), pp.445–50.
- Kass, S.U., Pruss, D. & Wolffe, A.P., 1997. How does DNA methylation repress transcription? *Trends in genetics : TIG*, 13(11), pp.444–9.
- Kaufman, L.J. et al., 2005. Glioma expansion in collagen I matrices: analyzing collagen concentration-dependent growth and motility patterns. *Biophysical journal*, 89(1), pp.635–50.
- Kawaguchi, K. et al., 2003. Mechanisms of inactivation of the p16INK4a gene in leiomyosarcoma of soft tissue: decreased p16 expression correlates with promoter methylation and poor prognosis. *The Journal of pathology*, 201(3), pp.487–95.
- Kehrer-Sawatzki, H. & Cooper, D.N., 2008. Mosaicism in sporadic neurofibromatosis type 1: variations on a theme common to other hereditary cancer syndromes? *Journal of medical genetics*, 45(10), pp.622–31.

- Keijser, S. et al., 2006. Immunophenotypic markers to differentiate between benign and malignant melanocytic lesions. *The British journal of ophthalmology*, 90(2), pp.213–7.
- Keng, V.W. et al., 2012. PTEN and NF1 inactivation in Schwann cells produces a severe phenotype in the peripheral nervous system that promotes the development and malignant progression of peripheral nerve sheath tumors. *Cancer research*, 72(13), pp.3405–13.
- Kerst, G. et al., 2008. WT1 protein expression in childhood acute leukemia. *American journal of hematology*, 83(5), pp.382–6.
- Khosrotehrani, K. et al., 2005. Subcutaneous neurofibromas are associated with mortality in neurofibromatosis 1: a cohort study of 703 patients. *American journal of medical genetics. Part A*, 132A(1), pp.49–53.
- King-Underwood, L., Renshaw, J. & Pritchard-Jones, K., 1996. Mutations in the Wilms' tumor gene WT1 in leukemias. *Blood*, 87(6), pp.2171–9.
- Kleihues, P. et al., 2002. The WHO classification of tumors of the nervous system. *Journal of neuropathology and experimental neurology*, 61(3), pp.215–25; discussion 226–9.
- Klose, R.J. & Bird, A.P., 2006. Genomic DNA methylation: the mark and its mediators. *Trends in biochemical sciences*, 31(2), pp.89–97.
- Kluiver, J. et al., 2005. BIC and miR-155 are highly expressed in Hodgkin, primary mediastinal and diffuse large B cell lymphomas. *The Journal of pathology*, 207(2), pp.243–9.
- Koenig, A. et al., 2006. Collagen type I induces disruption of E-cadherin-mediated cell-cell contacts and promotes proliferation of pancreatic carcinoma cells. *Cancer research*, 66(9), pp.4662–71.

- Koesters, R. et al., 2004. WT1 is a tumor-associated antigen in colon cancer that can be recognized by in vitro stimulated cytotoxic T cells. *International journal of cancer. Journal international du cancer*, 109(3), pp.385–92.
- Kogure, T. et al., 2013. Involvement of microRNA-29a in epigenetic regulation of transforming growth factor- $\beta$ -induced epithelial-mesenchymal transition in hepatocellular carcinoma. *Hepatology research : the official journal of the Japan Society of Hepatology*.
- Kogure, T. et al., 2014. Involvement of miRNA-29a in epigenetic regulation of transforming growth factor- $\beta$ -induced epithelial-mesenchymal transition in hepatocellular carcinoma. *Hepatology research : the official journal of the Japan Society of Hepatology*, 44(8), pp.907–19.
- Korf, B.R., 1992. Diagnostic outcome in children with multiple café au lait spots. *Pediatrics*, 90(6), pp.924–927.
- Korf, B.R., 1999. Plexiform neurofibromas. *American journal of medical genetics*, 89(1), pp.31–37.
- Kourea, H.P. et al., 1999. Deletions of the INK4A gene occur in malignant peripheral nerve sheath tumors but not in neurofibromas. *The American journal of pathology*, 155(6), pp.1855–60.
- Lagos-Quintana, M. et al., 2003. New microRNAs from mouse and human. *RNA (New York, N.Y.)*, 9(2), pp.175–179.
- Lai, H.-C. et al., 2008. Identification of novel DNA methylation markers in cervical cancer. *International journal of cancer. Journal international du cancer*, 123(1), pp.161–7.
- Laskin, W.B., Weiss, S.W. & Bratthauer, G.L., 1991. Epithelioid variant of malignant peripheral nerve sheath tumor (malignant epithelioid schwannoma). *The American journal of surgical pathology*, 15(12), pp.1136–45.

- 
- Laux, D.E. et al., 1999. Hypermethylation of the Wilms' tumor suppressor gene CpG island in human breast carcinomas. *Breast cancer research and treatment*, 56(1), pp.35–43.
- Lázaro, C. et al., 1994. Neurofibromatosis type 1 due to germ-line mosaicism in a clinically normal father. *The New England journal of medicine*, 331(21), pp.1403–7.
- Le, L.Q. & Parada, L.F., 2007. Tumor microenvironment and neurofibromatosis type I: connecting the GAPs. *Oncogene*, 26(32), pp.4609–16.
- Lee, M.-J. et al., 2012. The systems biology of neurofibromatosis type 1--critical roles for microRNA. *Experimental neurology*, 235(2), pp.464–8.
- Lee, R.C., Feinbaum, R.L. & Ambros, V., 1993. The *C. elegans* heterochronic gene *lin-4* encodes small RNAs with antisense complementarity to *lin-14*. *Cell*, 75(5), pp.843–854.
- Lee, S.B. & Haber, D.A., 2001. Wilms tumor and the WT1 gene. *Experimental cell research*, 264(1), pp.74–99.
- Lee, S.W. et al., 1992. Down-regulation of a member of the S100 gene family in mammary carcinoma cells and reexpression by azadeoxycytidine treatment. *Proceedings of the National Academy of Sciences of the United States of America*, 89(6), pp.2504–8.
- Lee, W. et al., 2014. PRC2 is recurrently inactivated through EED or SUZ12 loss in malignant peripheral nerve sheath tumors. *Nature Genetics*, 46(11), pp.1227–32.
- Legg, J. a et al., 2008. Slits and Roundabouts in cancer, tumour angiogenesis and endothelial cell migration. *Angiogenesis*, 11(1), pp.13–21.

- 
- Legius, E. et al., 2002. PTPN11 mutations in LEOPARD syndrome. *Journal of medical genetics*, 39(8), pp.571–4.
- Legius, E. et al., 1993. Somatic deletion of the neurofibromatosis type 1 gene in a neurofibrosarcoma supports a tumour suppressor gene hypothesis. *Nature Genetics*, 3(2), pp.122–126.
- Legius, E. et al., 1994. TP53 mutations are frequent in malignant NF1 tumors. *Genes, chromosomes & cancer*, 10(4), pp.250–5.
- Leondaritis, G., Petrikkos, L. & Mangoura, D., 2009. Regulation of the Ras-GTPase activating protein neurofibromin by C-tail phosphorylation: implications for protein kinase C/Ras/extracellular signal-regulated kinase 1/2 pathway signaling and neuronal differentiation. *Journal of neurochemistry*, 109(2), pp.573–83.
- Leśniak, W. et al., 2000. Regulation of cell specific expression of calcyclin (S100A6) in nerve cells and other tissues. *Acta neurobiologiae experimentalis*, 60(4), pp.569–75.
- Leukert, N. et al., 2006. Calcium-dependent tetramer formation of S100A8 and S100A9 is essential for biological activity. *Journal of molecular biology*, 359(4), pp.961–72.
- Di Leva, G. & Croce, C.M., 2010. Roles of small RNAs in tumor formation. *Trends in Molecular Medicine*, 16(6), pp.257–267.
- Lévy, P. et al., 2004. Molecular profiling of malignant peripheral nerve sheath tumors associated with neurofibromatosis type 1, based on large-scale real-time RT-PCR. *Molecular cancer*, 3, p.20.
- Ley, T.J. et al., 2010. DNMT3A mutations in acute myeloid leukemia. *The New England journal of medicine*, 363(25), pp.2424–33.

- Li, J.-Y. et al., 2007. Synergistic function of DNA methyltransferases Dnmt3a and Dnmt3b in the methylation of Oct4 and Nanog. *Molecular and cellular biology*, 27(24), pp.8748–59.
- Li, K.K. et al., 2013. DNA methyltransferases in hematologic malignancies. *Seminars in hematology*, 50(1), pp.48–60.
- Li, Y. et al., 2010. Inhibition of TGF- $\beta$  receptor i by siRNA suppresses the motility and invasiveness of T24 bladder cancer cells via modulation of integrins and matrix metalloproteinase. *International Urology and Nephrology*, 42(2), pp.315–323.
- Li, Y. et al., 2011. Progressive miRNA expression profiles in cervical carcinogenesis and identification of HPV-related target genes for miR-29. *The Journal of pathology*, 224(4), pp.484–95.
- Liang, C.-C., Park, A.Y. & Guan, J.-L., 2007. In vitro scratch assay: a convenient and inexpensive method for analysis of cell migration in vitro. *Nature protocols*, 2(2), pp.329–333.
- Lin, J. et al., 2004. Inhibiting S100B restores p53 levels in primary malignant melanoma cancer cells. *The Journal of biological chemistry*, 279(32), pp.34071–7.
- Lin, J. et al., 2001. Inhibition of p53 transcriptional activity by the S100B calcium-binding protein. *The Journal of biological chemistry*, 276(37), pp.35037–41.
- Lindsey, J.C. et al., 2007. Epigenetic deregulation of multiple S100 gene family members by differential hypomethylation and hypermethylation events in medulloblastoma. *British journal of cancer*, 97(2), pp.267–74.
- Lister, R. et al., 2009. Human DNA methylomes at base resolution show widespread epigenomic differences. *Nature*, 462(7271), pp.315–22.

- Listernick, R. et al., 2004. Late-onset optic pathway tumors in children with neurofibromatosis 1. *Neurology*, 63(10), pp.1944–6.
- Listernick, R. et al., 1997. Optic pathway gliomas in children with neurofibromatosis 1: consensus statement from the NF1 Optic Pathway Glioma Task Force. *Annals of neurology*, 41(2), pp.143–9.
- Little, M. & Wells, C., 1997. A clinical overview of WT1 gene mutations. *Human mutation*, 9(3), pp.209–25.
- Liu, J. et al., 2003. Congenital diaphragmatic hernia, kidney agenesis and cardiac defects associated with Slit3-deficiency in mice. *Mechanisms of development*, 120(9), pp.1059–70.
- Livak, K.J. & Schmittgen, T.D., 2001. Analysis of relative gene expression data using real-time quantitative PCR and the 2<sup>-</sup>(Delta Delta C(T)) Method. *Methods (San Diego, Calif.)*, 25(4), pp.402–408.
- Lodding, P., Kindblom, L.G. & Angervall, L., 1986. Epithelioid malignant schwannoma. A study of 14 cases. *Virchows Archiv. A, Pathological anatomy and histopathology*, 409(4), pp.433–51.
- London, N.R. et al., 2010. Targeting Robo4-dependent Slit signaling to survive the cytokine storm in sepsis and influenza. *Science translational medicine*, 2(23), p.23ra19.
- London, N.R. & Li, D.Y., 2011. Robo4-dependent Slit signaling stabilizes the vasculature during pathologic angiogenesis and cytokine storm. *Current opinion in hematology*, 18(3), pp.186–90.
- Lothe, R.A. et al., 2001. Biallelic inactivation of TP53 rarely contributes to the development of malignant peripheral nerve sheath tumors. *Genes, Chromosomes and Cancer*, 30(2), pp.202–206.

- Luczak, M.W. & Jagodziński, P.P., 2006. The role of DNA methylation in cancer development. *Folia histochemica et cytobiologica / Polish Academy of Sciences, Polish Histochemical and Cytochemical Society*, 44(3), pp.143–54.
- Luo, X.N. et al., 1995. The tumor suppressor gene WT1 inhibits ras-mediated transformation. *Oncogene*, 11(4), pp.743–50.
- Ma, L., Teruya-Feldstein, J. & Weinberg, R. a, 2007. Tumour invasion and metastasis initiated by microRNA-10b in breast cancer. *Nature*, 449(7163), pp.682–8.
- Macias, H. et al., 2011. SLIT/ROBO1 signaling suppresses mammary branching morphogenesis by limiting basal cell number. *Developmental cell*, 20(6), pp.827–40.
- Maelandsmo, G.M. et al., 1997. Differential expression patterns of S100A2, S100A4 and S100A6 during progression of human malignant melanoma. *International journal of cancer. Journal international du cancer*, 74(4), pp.464–9.
- Malup, T.K. et al., 2007. Methylation of CpG dinucleotides in the promoter region of the gene encoding the S100b protein in BALB/cLac mice. *Doklady Biochemistry and Biophysics*, 412(1), pp.1–3.
- Marenholz, I., Heizmann, C.W. & Fritz, G., 2004. S100 proteins in mouse and man: from evolution to function and pathology (including an update of the nomenclature). *Biochemical and biophysical research communications*, 322(4), pp.1111–22.
- Mares, J. et al., 2001. Methylation changes in promoter and enhancer regions of the WT1 gene in Wilms' tumours. *Cancer letters*, 166(2), pp.165–71.
- Mårtenson, E.D. et al., 2001. Serum S-100b protein as a prognostic marker in malignant cutaneous melanoma. *Journal of clinical oncology: official journal of the American Society of Clinical Oncology*, 19(3), pp.824–31.

- Martinelli, S. et al., 2010. Heterozygous germline mutations in the CBL tumor-suppressor gene cause a Noonan syndrome-like phenotype. *American journal of human genetics*, 87(2), pp.250–7.
- Masliah-Planchon, J. et al., 2013. MicroRNAome profiling in benign and malignant neurofibromatosis type 1-associated nerve sheath tumors: evidences of PTEN pathway alterations in early NF1 tumorigenesis. *BMC genomics*, 14, p.473.
- Mautner, V.-F. et al., 2008. Assessment of benign tumor burden by whole-body MRI in patients with neurofibromatosis 1. *Neuro-oncology*, 10(4), pp.593–8.
- McCarron, K.F. & Goldblum, J.R., 1998. Plexiform neurofibroma with and without associated malignant peripheral nerve sheath tumor: a clinicopathologic and immunohistochemical analysis of 54 cases. *Modern pathology: an official journal of the United States and Canadian Academy of Pathology, Inc.*, 11(7), pp.612–7.
- McMaster, M.L. et al., 1995. WT1 expression alters tumorigenicity of the G401 kidney-derived cell line. *Cell growth & differentiation: the molecular biology journal of the American Association for Cancer Research*, 6(12), pp.1609–17.
- McMenamin, M.E. & Fletcher, C.D., 2001. Expanding the spectrum of malignant change in schwannomas: epithelioid malignant change, epithelioid malignant peripheral nerve sheath tumor, and epithelioid angiosarcoma: a study of 17 cases. *The American journal of surgical pathology*, 25(1), pp.13–25.
- Medina, P.P., Nolde, M. & Slack, F.J., 2010. OncomiR addiction in an in vivo model of microRNA-21-induced pre-B-cell lymphoma. *Nature*, 467(7311), pp.86–90.
- Medvedeva, Y.A. et al., 2010. Intergenic, gene terminal, and intragenic CpG islands in the human genome. *BMC genomics*, 11, p.48.
- Mendez, H.M. & Opitz, J.M., 1985. Noonan syndrome: a review. *American journal of medical genetics*, 21(3), pp.493–506.

- 
- Menke, a et al., 2001. Down-regulation of E-cadherin gene expression by collagen type I and type III in pancreatic cancer cell lines. *Cancer research*, 61(8), pp.3508–17.
- Menon, A.G. et al., 1990. Chromosome 17p deletions and p53 gene mutations associated with the formation of malignant neurofibrosarcomas in von Recklinghausen neurofibromatosis. *Proceedings of the National Academy of Sciences of the United States of America*, 87(14), pp.5435–9.
- Merlo, a et al., 1995. 5' CpG island methylation is associated with transcriptional silencing of the tumour suppressor p16/CDKN2/MTS1 in human cancers. *Nature medicine*, 1(7), pp.686–692.
- Messiaen, L.M. et al., 2000. Exhaustive mutation analysis of the NF1 gene allows identification of 95% of mutations and reveals a high frequency of unusual splicing defects. *Human mutation*, 15(6), pp.541–55.
- Miller, S.J. et al., 2006. Large-scale molecular comparison of human schwann cells to malignant peripheral nerve sheath tumor cell lines and tissues. *Cancer research*, 66(5), pp.2584–91.
- Mo, W. et al., 2013. CXCR4/CXCL12 mediate autocrine cell- cycle progression in NF1-associated malignant peripheral nerve sheath tumors. *Cell*, 152(5), pp.1077–90.
- Montgomery, K.G. et al., 2004. The DNMT3B C-->T promoter polymorphism and risk of breast cancer in a British population: a case-control study. *Breast cancer research : BCR*, 6(4), pp.R390–4.
- Morita, S. et al., 2013. miR-29 represses the activities of DNA methyltransferases and DNA demethylases. *International journal of molecular sciences*, 14(7), pp.14647–58.

- 
- Mott, J.L. et al., 2007. mir-29 regulates Mcl-1 protein expression and apoptosis. *Oncogene*, 26(42), pp.6133–6140.
- Mraz, M. et al., 2009. miR-34a, miR-29c and miR-17-5p are downregulated in CLL patients with TP53 abnormalities. *Leukemia*, 23(6), pp.1159–63.
- Mueller, A. et al., 2005. The calcium-binding protein S100A2 interacts with p53 and modulates its transcriptional activity. *The Journal of biological chemistry*, 280(32), pp.29186–93.
- Murray, M.J. & Whittington, P.M., 1999. Effects of roundabout on growth cone dynamics, filopodial length, and growth cone morphology at the midline and throughout the neuropile. *The Journal of neuroscience: the official journal of the Society for Neuroscience*, 19(18), pp.7901–12.
- Mutze, K. et al., 2011. DNA methyltransferase 1 as a predictive biomarker and potential therapeutic target for chemotherapy in gastric cancer. *European journal of cancer (Oxford, England : 1990)*, 47(12), pp.1817–25.
- Nakajima, T. et al., 1982. S-100 protein in Langerhans cells, interdigitating reticulum cells and histiocytosis X cells. *Gann = Gan*, 73(3), pp.429–32.
- Namihira, M. et al., 2009. Committed neuronal precursors confer astrocytic potential on residual neural precursor cells. *Developmental cell*, 16(2), pp.245–55.
- Namihira, M., Nakashima, K. & Taga, T., 2004. Developmental stage dependent regulation of DNA methylation and chromatin modification in a immature astrocyte specific gene promoter. *FEBS letters*, 572(1-3), pp.184–8.
- Navakanit, R. et al., 2007. Growth inhibition of breast cancer cell line MCF-7 by siRNA silencing of Wilms tumor 1 gene. *Journal of the Medical Association of Thailand = Chotmaihet thangphaet*, 90(11), pp.2416–21.

- Newby, A.C., 2006. Matrix metalloproteinases regulate migration, proliferation, and death of vascular smooth muscle cells by degrading matrix and non-matrix substrates. *Cardiovascular research*, 69(3), pp.614–24.
- Nguyen, T. et al., 2014. Downregulation of microRNA-29c is associated with hypermethylation of tumor-related genes and disease outcome in cutaneous melanoma. *Epigenetics : official journal of the DNA Methylation Society*, 6(3), pp.388–394.
- Nielsen, G.P. et al., 1999. Malignant transformation of neurofibromas in neurofibromatosis 1 is associated with CDKN2A/p16 inactivation. *American Journal of Pathology*, 155(6), pp.1879–84.
- Nonaka, D. et al., 2008. Differential expression of S100 protein subtypes in malignant melanoma, and benign and malignant peripheral nerve sheath tumors. *Journal of cutaneous pathology*, 35(11), pp.1014–9.
- North, K.N. et al., 1997. Cognitive function and academic performance in neurofibromatosis. 1: consensus statement from the NF1 Cognitive Disorders Task Force. *Neurology*, 48(4), pp.1121–7.
- Nussbaum, R.L., McInnes, R.R. & Willard, H.F., 2007. *Genetics in medicine* 7th ed., Elsevier.
- O’Riain, C. et al., 2009. Array-based DNA methylation profiling in follicular lymphoma. *Leukemia*, 23(10), pp.1858–66.
- Oji, Y. et al., 2002. Overexpression of the Wilms’ tumor gene WT1 in de novo lung cancers. *International journal of cancer. Journal international du cancer*, 100(3), pp.297–303.
- Oji, Y. et al., 2004. Overexpression of the Wilms’ tumor gene WT1 in pancreatic ductal adenocarcinoma. *Cancer science*, 95(7), pp.583–7.

- 
- Okano, M. et al., 1999. DNA Methyltransferases Dnmt3a and Dnmt3b Are Essential for De Novo Methylation and Mammalian Development. *Cell*, 99(3), pp.247–257.
- Ordway, J.M. et al., 2007. Identification of novel high-frequency DNA methylation changes in breast cancer. *PloS one*, 2(12), p.e1314.
- Ostler, K.R. et al., 2007. Cancer cells express aberrant DNMT3B transcripts encoding truncated proteins. *Oncogene*, 26(38), pp.5553–63.
- Ozonoff, S., 1999. Cognitive impairment in neurofibromatosis type 1. *American journal of medical genetics*, 89(1), pp.45–52.
- Pandit, B. et al., 2007. Gain-of-function RAF1 mutations cause Noonan and LEOPARD syndromes with hypertrophic cardiomyopathy. *Nature genetics*, 39(8), pp.1007–12.
- Parenti, R. et al., 2014. Wilms' tumor gene 1 (WT1) silencing inhibits proliferation of malignant peripheral nerve sheath tumor sNF96.2 cell line. *PloS one*, 9(12), p.e114333.
- Pasquinelli, A.E., Hunter, S. & Bracht, J., 2005. MicroRNAs: a developing story. *Current opinion in genetics & development*, 15(2), pp.200–5.
- Pass, H.I. et al., 2010. hsa-miR-29c\* is linked to the prognosis of malignant pleural mesothelioma. *Cancer Research*, 70(5), pp.1916–24.
- Patterson, M.L. et al., 2001. Specific collagenolysis by gelatinase A, MMP-2, is determined by the hemopexin domain and not the fibronectin-like domain. *FEBS letters*, 503(2-3), pp.158–62.
- Pedrocchi, M. et al., 1994. Expression of Ca(2+)-binding proteins of the S100 family in malignant human breast-cancer cell lines and biopsy samples. *International journal of cancer. Journal international du cancer*, 57(5), pp.684–90.

- 
- Perrin, G.Q. et al., 2007. An orthotopic xenograft model of intraneural NF1 MPNST suggests a potential association between steroid hormones and tumor cell proliferation. *Laboratory investigation; a journal of technical methods and pathology*, 87(11), pp.1092–1102.
- Perrone, F. et al., 2003. Neurofibromatosis Type 1-related Malignant Peripheral Nerve Sheath Tumors 1. *Clinical Cancer Research*, 9, pp.4132– 4138.
- Perry, A. et al., 2002. Differential NF1, p16, and EGFR patterns by interphase cytogenetics (FISH) in malignant peripheral nerve sheath tumor (MPNST) and morphologically similar spindle cell neoplasms. *Journal of neuropathology and experimental neurology*, 61(8), pp.702–9.
- Perry, A. et al., 2001. NF1 deletions in S-100 protein-positive and negative cells of sporadic and neurofibromatosis 1 (NF1)-associated plexiform neurofibromas and malignant peripheral nerve sheath tumors. *The American journal of pathology*, 159(1), pp.57–61.
- Peter, M.E., 2009. Let-7 and miR-200 microRNAs: guardians against pluripotency and cancer progression. *Cell cycle (Georgetown, Tex.)*, 8(6), pp.843–52.
- Petersson, S. et al., 2009. Expression patterns of S100 proteins in melanocytes and melanocytic lesions. *Melanoma research*, 19(4), pp.215–25.
- Pietzsch, J., 2010. S100 proteins in health and disease. *Amino acids*.
- Pinney, S.E., 2014. Mammalian Non-CpG Methylation: Stem Cells and Beyond. *Biology*, 3(4), pp.739–51.
- Piper, M. et al., 2000. Expression of the vertebrate Slit gene family and their putative receptors, the Robo genes, in the developing murine kidney. *Mechanisms of development*, 94(1-2), pp.213–7.

- Plass, C. et al., 2013. Mutations in regulators of the epigenome and their connections to global chromatin patterns in cancer. *Nature reviews. Genetics*, 14(11), pp.765–80.
- Prasad, A. et al., 2004. Slit protein-mediated inhibition of CXCR4-induced chemotactic and chemoinvasive signaling pathways in breast cancer cells. *The Journal of biological chemistry*, 279(10), pp.9115–24.
- Purkait, R. et al., 2011. Neurocutaneous syndrome: a prospective study. *Indian journal of dermatology*, 56(4), pp.375–9.
- Qin, W. et al., 2011. TGF- $\beta$ /Smad3 signaling promotes renal fibrosis by inhibiting miR-29. *Journal of the American Society of Nephrology: JASN*, 22(8), pp.1462–74.
- Qu, Y., Dang, S. & Hou, P., 2013. Gene methylation in gastric cancer. *Clinica chimica acta; international journal of clinical chemistry*, 424, pp.53–65.
- Que, T. et al., 2015. Decreased miRNA-637 is an unfavorable prognosis marker and promotes glioma cell growth, migration and invasion via direct targeting Akt1. *Oncogene*.
- Quelle, D.E. et al., 1995. Alternative reading frames of the INK4a tumor suppressor gene encode two unrelated proteins capable of inducing cell cycle arrest. *Cell*, 83(6), pp.993–1000.
- De Raedt, T. et al., 2003. Elevated risk for MPNST in NF1 microdeletion patients. *American journal of human genetics*, 72(5), pp.1288–1292.
- De Raedt, T. et al., 2014. PRC2 loss amplifies Ras-driven transcription and confers sensitivity to BRD4-based therapies. *Nature*, 514(7521), pp.247–51.

- 
- Rahrman, E.P. et al., 2013. Forward genetic screen for malignant peripheral nerve sheath tumor formation identifies new genes and pathways driving tumorigenesis. *Nature genetics*, 45(7), pp.756–66.
- Ramaswamy, S. et al., 2003. A molecular signature of metastasis in primary solid tumors. *Nature genetics*, 33(1), pp.49–54.
- Ramdas, V. et al., 2013. Canonical transforming growth factor- $\beta$  signaling regulates disintegrin metalloprotease expression in experimental renal fibrosis via miR-29. *The American journal of pathology*, 183(6), pp.1885–96.
- Rauen, K.A., 2007. HRAS and the Costello syndrome. *Clinical genetics*, 71(2), pp.101–8.
- Razzaque, M.A. et al., 2007. Germline gain-of-function mutations in RAF1 cause Noonan syndrome. *Nature genetics*, 39(8), pp.1013–7.
- Reinhart, B.J. et al., 2000. The 21-nucleotide let-7 RNA regulates developmental timing in *Caenorhabditis elegans*. *Nature*, 403(6772), pp.901–906.
- Reynolds, R.M. et al., 2003. Von Recklinghausen's neurofibromatosis: neurofibromatosis type 1. *Lancet*, 361(9368), pp.1552–4.
- Rheinheimer, B. et al., 2013. Epigenetic silencing alters the SLIT2/ROBO1/miR-218-1 signaling axis in pancreatic cancer. *Cancer Research*, 73(13 Supplement), pp.B13–B13.
- Riccardi, V.M., 1981. Cutaneous manifestation of neurofibromatosis: cellular interaction, pigmentation, and mast cells. *Birth defects original article series*, 17(2), pp.129–45.
- Riccardi, V.M., 1982. Neurofibromatosis: clinical heterogeneity. *Current problems in cancer*, 7(2), pp.1–34.

- Riccardi, V.M., 2007. The genetic predisposition to and histogenesis of neurofibromas and neurofibrosarcoma in neurofibromatosis type 1. *Neurosurgical focus*, 22(6), p.E3.
- Robaina, M.C. et al., 2015. Deregulation of DNMT1, DNMT3B and miR-29s in Burkitt lymphoma suggests novel contribution for disease pathogenesis. *Experimental and molecular pathology*, 98(2), pp.200–7.
- Roberts, A.E. et al., 2007. Germline gain-of-function mutations in SOS1 cause Noonan syndrome. *Nature genetics*, 39(1), pp.70–4.
- Robertson, K.D. et al., 1999. The human DNA methyltransferases (DNMTs) 1, 3a and 3b: Coordinate mRNA expression in normal tissues and overexpression in tumors. *Nucleic Acids Research*, 27(11), pp.2291–8.
- Rodriguez, F.J. et al., 2007. Low grade malignant peripheral nerve sheath tumor with smooth muscle differentiation. *Acta neuropathologica*, 113(6), pp.705–9.
- Roll, J.D. et al., 2008. DNMT3b overexpression contributes to a hypermethylator phenotype in human breast cancer cell lines. *Molecular cancer*, 7(c), p.15.
- Romano, A.A. et al., 2010. Noonan syndrome: clinical features, diagnosis, and management guidelines. *Pediatrics*, 126(4), pp.746–59.
- Rosenfeld, N. et al., 2008. MicroRNAs accurately identify cancer tissue origin. *Nature biotechnology*, 26(4), pp.462–9.
- Roth, J. et al., 2003. Phagocyte-specific S100 proteins: a novel group of proinflammatory molecules. *Trends in immunology*, 24(4), pp.155–8.
- Ruggieri, M. & Huson, S.M., 2001. The clinical and diagnostic implications of mosaicism in the neurofibromatoses. *Neurology*, 56(11), pp.1433–43.

- 
- Russo, V.C. et al., 2005. Insulin-like growth factor binding protein-2 binding to extracellular matrix plays a critical role in neuroblastoma cell proliferation, migration, and invasion. *Endocrinology*, 146(10), pp.4445–55.
- Russo, V.E.A., Martienssen, R.A. & Riggs, A.D., 1996. *Epigenetic Mechanisms of Gene Regulation*, Cold Spring Harbor Laboratory Press, Woodbury.
- Rustandi, R.R. et al., 1998. The Ca(2+)-dependent interaction of S100B(beta beta) with a peptide derived from p53. *Biochemistry*, 37(7), pp.1951–60.
- Saito, Y. et al., 2001. Expression of mRNA for DNA methyltransferases and methyl-CpG-binding proteins and DNA methylation status on CpG islands and pericentromeric satellite regions during human hepatocarcinogenesis. *Hepatology (Baltimore, Md.)*, 33(3), pp.561–8.
- Salama, I. et al., 2008. A review of the S100 proteins in cancer. *European journal of surgical oncology*, 34(4), pp.357–64.
- Sandhu, R. et al., 2014. Dysregulation of microRNA expression drives aberrant DNA hypermethylation in basal-like breast cancer. *International journal of oncology*, 44(2), pp.563–72.
- Sandhu, R., Rivenbark, A.G. & Coleman, W.B., 2012. Loss of post-transcriptional regulation of DNMT3b by microRNAs: a possible molecular mechanism for the hypermethylation defect observed in a subset of breast cancer cell lines. *International journal of oncology*, 41(2), pp.721–32.
- Sarkozy, A., Digilio, M.C. & Dallapiccola, B., 2008. Leopard syndrome. *Orphanet journal of rare diseases*, 3, p.13.
- Sato, N. et al., 2004. Identification of maspin and S100P as novel hypomethylation targets in pancreatic cancer using global gene expression profiling. *Oncogene*, 23(8), pp.1531–8.

- 
- Sceusi, E.L., Loose, D.S. & Wray, C.J., 2011. Clinical implications of DNA methylation in hepatocellular carcinoma. *HPB: the official journal of the International Hepato Pancreato Biliary Association*, 13(6), pp.369–76.
- Schickel, R. et al., 2008. MicroRNAs: key players in the immune system, differentiation, tumorigenesis and cell death. *Oncogene*, 27(45), pp.5959–74.
- Schittenhelm, J. et al., 2010. WT1 expression in normal and neoplastic cranial and peripheral nerves is independent of grade of malignancy. *Cancer biomarkers: section A of Disease markers*, 7(2), pp.73–7.
- Schmittgen, T.D. & Livak, K.J., 2008. Analyzing real-time PCR data by the comparative C(T) method. *Nature protocols*, 3(6), pp.1101–1108.
- Schubbert, S. et al., 2006. Germline KRAS mutations cause Noonan syndrome. *Nature genetics*, 38(3), pp.331–6.
- Schwarz, D.S. et al., 2003. Asymmetry in the assembly of the RNAi enzyme complex. *Cell*, 115(2), pp.199–208.
- Scotto, C. et al., 1999. Concerted regulation of wild-type p53 nuclear accumulation and activation by S100B and calcium-dependent protein kinase C. *Molecular and cellular biology*, 19(10), pp.7168–80.
- Sedani, A., Cooper, D.N. & Upadhyaya, M., 2012. An emerging role for microRNAs in NF1 tumorigenesis. *Human genomics*, 6, p.23.
- Sengupta, S. et al., 2008. MicroRNA 29c is down-regulated in nasopharyngeal carcinomas, up-regulating mRNAs encoding extracellular matrix proteins. *Proceedings of the National Academy of Sciences of the United States of America*, 105(15), pp.5874–8.

- Shah, M.Y. et al., 2010. DNMT3B7, a truncated DNMT3B isoform expressed in human tumors, disrupts embryonic development and accelerates lymphomagenesis. *Cancer research*, 70(14), pp.5840–50.
- Shanmuganathan, R. et al., 2013. Conventional and nanotechniques for DNA methylation profiling. *The Journal of molecular diagnostics: JMD*, 15(1), pp.17–26.
- Shen, H. et al., 2002. A novel polymorphism in human cytosine DNA-methyltransferase-3B promoter is associated with an increased risk of lung cancer. *Cancer research*, 62(17), pp.4992–5.
- Sherman, L.S. et al., 2000. Single cell Ras-GTP analysis reveals altered Ras activity in a subpopulation of neurofibroma Schwann cells but not fibroblasts. *The Journal of biological chemistry*, 275(39), pp.30740–5.
- Shimada, H. et al., 1988. Pathologic features of extraosseous Ewing's sarcoma: a report from the Intergroup Rhabdomyosarcoma Study. *Human pathology*, 19(4), pp.442–53.
- Shimozaki, K. et al., 2005. Stage- and site-specific DNA demethylation during neural cell development from embryonic stem cells. *Journal of neurochemistry*, 93(2), pp.432–9.
- Shintani, Y. et al., 2006. Collagen I promotes metastasis in pancreatic cancer by activating c-Jun NH(2)-terminal kinase 1 and up-regulating N-cadherin expression. *Cancer research*, 66(24), pp.11745–53.
- Shiraishi, M. et al., 2002. A comprehensive catalog of CpG islands methylated in human lung adenocarcinomas for the identification of tumor suppressor genes. *Oncogene*, 21(23), pp.3804–3813.
- Siegel, P.M. et al., 2003. Transforming growth factor beta signaling impairs Neu-induced mammary tumorigenesis while promoting pulmonary metastasis.

---

*Proceedings of the National Academy of Sciences of the United States of America*, 100(14), pp.8430–5.

Singal, R. et al., 2005. Polymorphisms in the DNA methyltransferase 3b gene and prostate cancer risk. *Oncology reports*, 14(2), pp.569–73.

Singer-Sam, J. et al., 1990. A quantitative HpaII-PCR assay to measure methylation of DNA from a small number of cells. *Nucleic acids research*, 18(3), p.687.

Singh, A. et al., 2012. Wilms tumor-1, claudin-1 and ezrin are useful immunohistochemical markers that help to distinguish schwannoma from fibroblastic meningioma. *Pathology oncology research : POR*, 18(2), pp.383–9.

Smit, L.H.M. et al., Value of serum S-100B for prediction of distant relapse and survival in stage III B/C melanoma. *Anticancer research*, 28(4C), pp.2297–302.

Smith, R.W., 1989. A treatise on the pathology, diagnosis and treatment of neuroma. 1849. *Clinical orthopaedics and related research*, (245), pp.3–9.

Smith, S.I. et al., 2000. Expression of the Wilms' tumor suppressor gene, WT1, reduces the tumorigenicity of the leukemic cell line M1 in C.B-17 scid/scid mice. *Cancer research*, 60(4), pp.808–14.

Stamatopoulos, B. et al., 2009. microRNA-29c and microRNA-223 down-regulation has in vivo significance in chronic lymphocytic leukemia and improves disease risk stratification. *Blood*, 113(21), pp.5237–45.

Steele, R., Mott, J.L. & Ray, R.B., 2010. MBP-1 upregulates miR-29b that represses Mcl-1, collagens, and matrix-metalloproteinase-2 in prostate cancer cells. *Genes & cancer*, 1(4), pp.381–387.

Stein, G.H. et al., 1999. Differential roles for cyclin-dependent kinase inhibitors p21 and p16 in the mechanisms of senescence and differentiation in human fibroblasts. *Molecular and cellular biology*, 19(3), pp.2109–17.

- 
- Stott, F.J. et al., 1998. The alternative product from the human CDKN2A locus, p14(ARF), participates in a regulatory feedback loop with p53 and MDM2. *The EMBO journal*, 17(17), pp.5001–14.
- Stowe, I.B. et al., 2012. A shared molecular mechanism underlies the human rasopathies Legius syndrome and Neurofibromatosis-1. *Genes & development*, 26(13), pp.1421–6.
- Stumpf, D., Alksne, J. & Annegers, J., 1988. National Institutes of Health consensus development statement on neurofibromatosis. *Arch Neurol*, 45, pp.575–578.
- Subramanian, S. et al., 2010. Genome-wide transcriptome analyses reveal p53 inactivation mediated loss of miR-34a expression in malignant peripheral nerve sheath tumours. *Journal of Pathology*, The, (October 2009), pp.58–70.
- Sugiyama, D., Kulkeaw, K. & Mizuochi, C., 2013. TGF-beta-1 up-regulates extracellular matrix production in mouse hepatoblasts. *Mechanisms of development*, 130(2-3), pp.195–206.
- Swarbrick, A. et al., 2010. miR-380-5p represses p53 to control cellular survival and is associated with poor outcome in MYCN-amplified neuroblastoma. *Nature medicine*, 16(10), pp.1134–1140.
- Takamizawa, J. et al., 2004. Reduced expression of the let-7 microRNAs in human lung cancers in association with shortened postoperative survival. *Cancer research*, 64(11), pp.3753–6.
- Tang, B. et al., 2003. TGF-beta switches from tumor suppressor to prometastatic factor in a model of breast cancer progression. *The Journal of clinical investigation*, 112(7), pp.1116–24.
- Tarhini, A.A. et al., 2009. Prognostic significance of serum S100B protein in high-risk surgically resected melanoma patients participating in Intergroup Trial

- ECOG 1694. *Journal of clinical oncology: official journal of the American Society of Clinical Oncology*, 27(1), pp.38–44.
- Tartaglia, M. et al., 2007. Gain-of-function SOS1 mutations cause a distinctive form of Noonan syndrome. *Nature genetics*, 39(1), pp.75–9.
- Tartaglia, M. et al., 2001. Mutations in PTPN11, encoding the protein tyrosine phosphatase SHP-2, cause Noonan syndrome. *Nature genetics*, 29(4), pp.465–8.
- Tidyman, W.E. & Rauen, K.A., 2009. The RASopathies: developmental syndromes of Ras/MAPK pathway dysregulation. *Current opinion in genetics & development*, 19(3), pp.230–6.
- Tie, J. et al., 2010. MiR-218 inhibits invasion and metastasis of gastric cancer by targeting the Robo1 receptor. *PLoS Genetics*, 6(3), p.e1000879.
- Tost, J. & Gut, I.G., 2007. DNA methylation analysis by pyrosequencing. *Nature Protocols*, 2(9), pp.2265–75.
- Trevisson, E. et al., 2013. Neurofibromatosis type 1 in two siblings due to maternal germline mosaicism. *Clinical genetics*.
- Tripathy, K. et al., 2010. A Rare Malignant Triton Tumor. *Case reports in neurology*, 2(2), pp.69–73.
- Trojani, M. et al., 1984. Soft-tissue sarcomas of adults; study of pathological prognostic variables and definition of a histopathological grading system. *International journal of cancer. Journal international du cancer*, 33(1), pp.37–42.
- Tsang, E., Birch, P. & Friedman, J.M., 2012. Valuing gene testing in children with possible neurofibromatosis 1. *Clinical genetics*, 82(6), pp.591–3.

- Tucker, T. et al., 2005. Association between benign and malignant peripheral nerve sheath tumors in NF1. *Neurology*, 65(2), pp.205–11.
- Tulchinsky, E. et al., 1995. Transcriptional regulation of the mts1 gene in human lymphoma cells: the role of DNA-methylation. *Biochimica et biophysica acta*, 1261(2), pp.243–8.
- Ueda, T. et al., 2003. Overexpression of the Wilms' tumor gene WT1 in human bone and soft-tissue sarcomas. *Cancer science*, 94(3), pp.271–6.
- Upadhyaya, M., 2011. Genetic basis of tumorigenesis in NF1 malignant peripheral nerve sheath tumors. *Frontiers in bioscience (Landmark edition)*, 16, pp.937–51.
- Upadhyaya, M. et al., 2008. Germline and somatic NF1 gene mutation spectrum in NF1-associated malignant peripheral nerve sheath tumors (MPNSTs). *Human mutation*, 29(1), pp.74–82.
- Upadhyaya, M., 2008. NF1 Gene Structure and NF1 Genotype / Phenotype Correlations. *Structure*, 16, pp.162200–162200.
- Upadhyaya, M. et al., 2003. Three different pathological lesions in the NF1 gene originating de novo in a family with neurofibromatosis type 1. *Human genetics*, 112(1), pp.12–7.
- Vaissière, T. et al., 2010. Quantitative analysis of DNA methylation profiles in lung cancer identifies aberrant DNA methylation of specific genes and its association with gender and cancer risk factors. *Cancer*, 69(1), pp.243–252.
- Valeri, N. et al., 2010. Modulation of mismatch repair and genomic stability by miR-155. *Proceedings of the National Academy of Sciences of the United States of America*, 107(15), pp.6982–7.

- Veeck, J. & Esteller, M., 2010. Breast cancer epigenetics: from DNA methylation to microRNAs. *Journal of mammary gland biology and neoplasia*, 15(1), pp.5–17.
- Verdijk, R.M. et al., 2010. TP53 Mutation Analysis of Malignant Peripheral Nerve Sheath Tumors. *Experimental Neurology*, 69(1), pp.16–26.
- Vivarelli, R. et al., 2003. Epilepsy in neurofibromatosis 1. *Journal of child neurology*, 18(5), pp.338–342.
- Wagner, N. et al., 2008. The Wilms' tumor suppressor WT1 is associated with melanoma proliferation. *Pflügers Archiv: European journal of physiology*, 455(5), pp.839–47.
- Wakefield, L.M. & Roberts, A.B., 2002. TGF-beta signaling: positive and negative effects on tumorigenesis. *Current opinion in genetics & development*, 12(1), pp.22–9.
- Wakioka, T. et al., 2001. Spred is a Sprouty-related suppressor of Ras signalling. *Nature*, 412(6847), pp.647–51.
- Wallace, M.R. et al., 1990. Type 1 neurofibromatosis gene: identification of a large transcript disrupted in three NF1 patients. *Science (New York, N.Y.)*, 249(4965), pp.181–6.
- Walter, M.J. et al., 2011. Recurrent DNMT3A mutations in patients with myelodysplastic syndromes. *Leukemia*, 25(7), pp.1153–8.
- Wang, B. et al., 2015. MiR-194, commonly repressed in colorectal cancer, suppresses tumor growth by regulating the MAP4K4/c-Jun/MDM2 signaling pathway. *Cell cycle (Georgetown, Tex.)*.
- Wang, C.-M. et al., 2011. miR-29c targets TNFAIP3, inhibits cell proliferation and induces apoptosis in hepatitis B virus-related hepatocellular carcinoma. *Biochemical and biophysical research communications*, 411(3), pp.586–92.

- Wang, Q. et al., 2007. Hypomethylation of WNT5A, CRIP1 and S100P in prostate cancer. *Oncogene*, 26(45), pp.6560–5.
- Wang, X. et al., 2013. Wilms' tumour suppressor gene 1 (WT1) is involved in the carcinogenesis of Lung cancer through interaction with PI3K/Akt pathway. *Cancer cell international*, 13(1), p.114.
- Wang, Y. et al., 2006. Functional CpG methylation system in a social insect. *Science (New York, N.Y.)*, 314(5799), pp.645–7.
- Wang, Y. et al., 2013. Tumor-suppressive effects of miR-29c on gliomas. *Neuroreport*, 24(12), pp.637–45.
- Wang, Z. et al., 2013. MicroRNA-210 promotes proliferation and invasion of peripheral nerve sheath tumor cells targeting EFNA3. *Oncology research*, 21(3), pp.145–54.
- Watabe, T. & Miyazono, K., 2009. Roles of TGF-beta family signaling in stem cell renewal and differentiation. *Cell research*, 19(1), pp.103–15.
- Watanabe, T. et al., 2001. Malignant peripheral nerve sheath tumour arising within neurofibroma. An immunohistochemical analysis in the comparison between benign and malignant components. *Journal of clinical pathology*, 54(8), pp.631–6.
- Weber, M. et al., 2005. Chromosome-wide and promoter-specific analyses identify sites of differential DNA methylation in normal and transformed human cells. *Nature Genetics*, 37(8), pp.853–862.
- Weemaes, C.M.R. et al., 2013. Heterogeneous clinical presentation in ICF syndrome: correlation with underlying gene defects. *European journal of human genetics : EJHG*, 21(11), pp.1219–25.

- Weiss, S.W. & Goldblum, J.R., 2007. *Enzinger and Weiss's Soft Tissue Tumors* 5th ed., St. Louis, Mo. ; London : Mosby, 2007.
- Weiss, S.W., Langloss, J.M. & Enzinger, F.M., 1983. Value of S-100 protein in the diagnosis of soft tissue tumors with particular reference to benign and malignant Schwann cell tumors. *Laboratory investigation; a journal of technical methods and pathology*, 49(3), pp.299–308.
- Weiss, S.W. & Nickoloff, B.J., 1993. CD-34 is expressed by a distinctive cell population in peripheral nerve, nerve sheath tumors, and related lesions. *The American journal of surgical pathology*, 17(10), pp.1039–45.
- Wicki, R. et al., 1997. Repression of the candidate tumor suppressor gene S100A2 in breast cancer is mediated by site-specific hypermethylation. *Cell calcium*, 22(4), pp.243–54.
- Wiercinska, E. et al., 2010. The TGF- $\beta$ /Smad pathway induces breast cancer cell invasion through the up-regulation of matrix metalloproteinase 2 and 9 in a spheroid invasion model system. *Breast Cancer Research and Treatment*, 128, pp.657–666.
- Wild, L. & Flanagan, J.M., 2010. Genome-wide hypomethylation in cancer may be a passive consequence of transformation. *Biochimica et biophysica acta*, 1806(1), pp.50–7.
- Wilson, A.J., Maddox, P.H. & Jenkins, D., 1991. CD1a and S100 antigen expression in skin Langerhans cells in patients with breast cancer. *The Journal of pathology*, 163(1), pp.25–30.
- Wilson, A.S., Power, B.E. & Molloy, P.L., 2007. DNA hypomethylation and human diseases. *Biochimica et biophysica acta*, 1775(1), pp.138–62.

- Winbanks, C.E. et al., 2011. TGF-beta regulates miR-206 and miR-29 to control myogenic differentiation through regulation of HDAC4. *The Journal of biological chemistry*, 286(16), pp.13805–14.
- Wojtkowiak, J.W. et al., 2008. Induction of apoptosis in neurofibromatosis type 1 malignant peripheral nerve sheath tumor cell lines by a combination of novel farnesyl transferase inhibitors and lovastatin. *The Journal of pharmacology and experimental therapeutics*, 326(1), pp.1–11.
- Woodruff, J.M. & Christensen, W.N., 1993. Glandular peripheral nerve sheath tumors. *Cancer*, 72(12), pp.3618–28.
- Wu, J.Y. et al., 2001. The neuronal repellent Slit inhibits leukocyte chemotaxis induced by chemotactic factors. *Nature*, 410(6831), pp.948–52.
- Wu, M.Y. & Hill, C.S., 2009. Tgf-beta superfamily signaling in embryonic development and homeostasis. *Developmental cell*, 16(3), pp.329–43.
- Xiong, Y. et al., 2010. Effects of microRNA-29 on apoptosis, tumorigenicity, and prognosis of hepatocellular carcinoma. *Hepatology (Baltimore, Md.)*, 51(3), pp.836–45.
- Xu, G.L. et al., 1999. Chromosome instability and immunodeficiency syndrome caused by mutations in a DNA methyltransferase gene. *Nature*, 402(6758), pp.187–91.
- Xu, X. et al., 2005. Matrix metalloproteinase-2 contributes to cancer cell migration on collagen. *Cancer research*, 65(1), pp.130–6.
- Yakulis, R., Manack, L. & Murphy, A.I., 1996. Postradiation malignant triton tumor. A case report and review of the literature. *Archives of pathology & laboratory medicine*, 120(6), pp.541–8.

- Yamaguchi, U. et al., 2003. Low grade malignant peripheral nerve sheath tumour: varied cytological and histological patterns. *Journal of clinical pathology*, 56(11), pp.826–30.
- Yanaihara, N. et al., 2006. Unique microRNA molecular profiles in lung cancer diagnosis and prognosis. *Cancer cell*, 9(3), pp.189–98.
- Yang, J.C. et al., 1998. Randomized prospective study of the benefit of adjuvant radiation therapy in the treatment of soft tissue sarcomas of the extremity. *Journal of clinical oncology: official journal of the American Society of Clinical Oncology*, 16(1), pp.197–203.
- Yeh, M.L. et al., 2014. Robo1 modulates proliferation and neurogenesis in the developing neocortex. *The Journal of neuroscience: the official journal of the Society for Neuroscience*, 34(16), pp.5717–31.
- Yilmaz, K. et al., 2007. Bone mineral density in children with neurofibromatosis 1. *Acta paediatrica (Oslo, Norway: 1992)*, 96(8), pp.1220–2.
- Yu, F. et al., 2007. Let-7 Regulates Self Renewal and Tumorigenicity of Breast Cancer Cells. *Cell*, 131(6), pp.1109–23.
- Zamora-Avila, D.E. et al., 2007. RNAi silencing of the WT1 gene inhibits cell proliferation and induces apoptosis in the B16F10 murine melanoma cell line. *Melanoma research*, 17(6), pp.341–8.
- Zapata-Benavides, P. et al., 2002. Downregulation of Wilms' tumor 1 protein inhibits breast cancer proliferation. *Biochemical and biophysical research communications*, 295(4), pp.784–90.
- Zenker, M., 2011. Clinical manifestations of mutations in RAS and related intracellular signal transduction factors. *Current opinion in pediatrics*, 23(4), pp.443–51.

- 
- Zhang, M. et al., 2014. Somatic mutations of SUZ12 in malignant peripheral nerve sheath tumors. *Nature genetics*, 46(11), pp.1170–2.
- Zhang, Y. et al., 2014. miR-29b as a therapeutic agent for angiotensin II-induced cardiac fibrosis by targeting TGF- $\beta$ /Smad3 signaling. *Molecular therapy : the journal of the American Society of Gene Therapy*, 22(5), pp.974–85.
- Zhang, Y.-J. et al., 2012. Global hypomethylation in hepatocellular carcinoma and its relationship to aflatoxin B(1) exposure. *World journal of hepatology*, 4(5), pp.169–75.
- Zhao, J.-J. et al., 2010. microRNA expression profile and identification of miR-29 as a prognostic marker and pathogenetic factor by targeting CDK6 in mantle cell lymphoma. *Blood*, 115(13), pp.2630–9.
- Zheng, P.-P. et al., 2009. Cell proliferation and migration are mutually exclusive cellular phenomena in vivo: implications for cancer therapeutic strategies. *Cell cycle (Georgetown, Tex.)*, 8(6), pp.950–1.
- Zimmer, D.B. et al., 2013. Evolution of the S100 family of calcium sensor proteins. *Cell calcium*, 53(3), pp.170–9.
- Zitzmann, F. et al., 2014. Frequent hypermethylation of a CTCF binding site influences Wilms tumor 1 expression in Wilms tumors. *Oncology Reports*, 31(4), pp.1871–1876.